



Ollscoil Chathair
Bhaile Átha Cliath
Dublin City University

**Developing Approaches to Skin Volatile Biodiagnostics
Using Non-Invasive Techniques**

**A thesis submitted to Dublin City University in fulfilment of the
requirements for the award of the degree of Doctor of Philosophy**

By

Melissa Finnegan, BSc

**Dublin City University,
School of Chemical Sciences**

Supervisor:

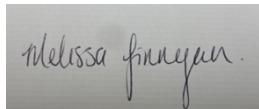
Dr Aoife Morrin

Submitted: November 2023

Declaration

I hereby certify that this material, which I now submit for assessment on the programme of study leading to the award of PhD, is entirely my own work, that I have exercised reasonable care to ensure that the work is original, and does not to the best of my knowledge breach any law of copyright, and has not been taken from the work of others save and to the extent that such work has been cited and acknowledged within the text of my work.

Signed:

A rectangular box containing a handwritten signature in cursive script that reads "Melissa Finnyan".

(Candidate) ID No.: 15386446

Date: 31/10/23

Acknowledgements

Firstly, I would like to give a huge thanks to my supervisor Dr. Aoife Morrin. Thank you for your unwavering support, guidance and encouragement throughout the last few years. The knowledge I have gained from you is invaluable and I will forever be grateful.

Secondly, I'd like to thank Dr. Naomi Walsh and her research group NICB for all their help with Chapter 4 of this thesis. Thank you for all the cell culture knowledge, for answering my many questions and the use of the fantastic facilities in the NICB.

Thanks to the technical team in DCU, Veronica, Ambrose, Catherine, John and Damien. Thanks for always being there for anything I needed and for the amazing technical support you provide. A huge thank you to Mary Ross who is always there for any GC-MS issues, you have saved me countless times and I can't thank you enough!!

Thanks to all my postgraduate friends in DCU, Roberta, Aicha and Shirin. Thanks for all your constant support and for being there for all the highs and the lows.

A huge thanks to my friends from AS + AC² who were always there for constant support. I definitely missed you in DCU the last four years.

A big thank you to my partner, Mick, who has there been through all the highs and low of this journey. Thank you for always giving me confidence in myself.

Finally, a massive thanks to my family, Mam, Dad, Ciara and Granda for you constant love and support over my years in college. Lastly, I'd like to say a special thanks to my Granny who is no longer with us but always shared many words of encouragement. I hope that I'm making you proud!

Dedication

For Granny

List of publications and presentations

Publications

- Shetewi T, Finnegan M, Fitzgerald S, Xu S, Duffy E and Morrin A, 2021, Investigation of the relationship between skin-emitted volatile fatty acids and skin surface acidity in healthy participants – a pilot study, *J. Breath Res.* **15**, 037101.
- Finnegan M, Duffy E and Morrin A 2022 The determination of skin surface pH via the skin volatile emission using wearable colorimetric sensors, *Sensing and Bio-Sensing Research*, **35**, 100473.

Oral presentations

- *Developing Approaches to Biodiagnostics via Wearable Platforms: Investigating Skin Volatile Emissions using Colorimetric Sensors*, 6th Insight Student Conference, University of Galway, Galway, Ireland, 2019.
- *Wearable Biodiagnostics via Skin Volatile Emission Detection Using Colorimetric Sensors*, Virtual MRS Spring/Fall Meeting & Exhibit, 2020.
- *Wearable Colorimetric Sensors for Biodiagnostic Applications*, Virtual 6th Annual DCU Chemical Research Symposium, Dublin City University, 2021.
- *Wearable Colorimetric Sensors for Biodiagnostic Applications*, Virtual 72nd Irish Chemistry Research Colloquium, 2021.
- *Monitoring oxidative stress on skin via the volatile aldehyde emission*, 7th Annual DCU Chemical Research Symposium, Dublin City University, 2022.

Poster presentations

- *Investigating Skin Volatile Emissions using Colorimetric Sensors*, 2nd Annual Conference on Chemical Sensors for Wearable Devices, Technion, Israel, 2020.
- *Wearable Colorimetric Sensors for Biodiagnostic Applications*, RSC Analytical Research Forum, Burlington House, London, 2022.
- *Wearable Colorimetric Sensors for Biodiagnostic Applications*, NCSR Research Day, Dublin City University, 2022.

Table of Contents

Developing Approaches to Skin Volatile Biodiagnostics Using Non-Invasive Techniques ..8

Chapter 1: Optical sensors in wearable biodiagnostics9

Abstract	10
1.1. Introduction	11
1.2. Skin composition and function	11
1.2.1. Physical structure	11
1.2.2. Stratum corneum	12
1.2.2.1. Glands	13
1.2.2.2. Microbiome	15
1.2.2.3. pH	17
1.3. Potential sources of novel skin-based biomarkers	18
1.3.1. Interstitial fluid	19
1.3.2. Sweat	20
1.3.3. Volatiles	21
1.4. Chemical sensing	22
1.4.1. Electrochemical sensing	22
1.4.2. Optical sensing	23
1.4.2.1. Fluorometric sensing	24
1.4.2.2. Colorimetric sensing	24
1.5. Current state of the art in wearable optical biochemical sensors	25
1.5.1. Extraction and generation of skin biofluids and volatiles	26
1.5.2. Fabrication of optical sensors for wearable applications	30
1.5.2.1. Fluid handling, materials consideration and integration	31
1.5.2.2. Optical sensing chemistry formulations and encapsulation	36
1.5.2.3. Integration of sensor chemistry into sensor platform	42
1.5.3. Transduction in optical wearable sensors	44
1.5.3.1. Imaging	44
1.5.3.2. Image analysis techniques	46
1.6. Conclusion	50
1.7. References	51

Thesis Outline66

Chapter 2: Assessing diurnal and site-associated differences in the skin volatile emission, skin surface pH and tissue dielectric constant in healthy skin70

Abstract	71
2.1. Introduction	72
2.2. Materials and methods	73
2.2.1. Participant profile and skin volatile emission sampling	73
2.2.2. Gas chromatography-mass spectrometry analysis	74
2.2.3. Data analysis	75
2.2.4. Skin surface pH and tissue dielectric constant measurements	76
2.3. Results and discussion	76
2.3.1. Stability of the skin volatile profile, skin surface pH and TDC across a day	76
2.3.2. Site variation of the skin volatile profile, skin surface pH and TDC	83
2.4. Conclusion	90
2.5. References	91

Chapter 3: Skin volatile emission profiling of healthy participants – influence of gender and age	96
Abstract	97
3.1. Introduction	98
3.2. Materials and methods.....	100
3.2.1. Participant profile and skin volatile emission sampling.....	100
3.2.2. Standard calibration curves	101
3.2.3. Gas chromatography-mass spectrometry analysis	101
3.2.4. Data analysis	102
3.2.5. Skin surface pH and tissue dielectric constant measurements	102
3.3. Results and discussion	102
3.3.1. Characterising the skin volatile profile in healthy participants.....	102
3.3.2. Gender influences on the skin volatile emission	105
3.3.3. Correlation of age with skin surface pH, TDC and the skin volatile emission.....	109
3.4. Conclusion	115
3.5. References	115
Chapter 4: The impact of skin-derived volatile compounds on host skin cells' signalling pathways.....	122
Abstract	123
4.1. Introduction	124
4.2. Materials and methods.....	127
4.2.1. Cell lines and culture conditions	127
4.2.2. Cell cytotoxicity assay	127
4.2.3. Reactive oxygen species (ROS) assay	128
4.2.3.1. Liquid phase	128
4.2.3.2. Volatile phase.....	129
4.2.4. Immunofluorescence	130
4.2.4.1. Slide preparation	130
4.2.4.2. Immunofluorescence staining.....	130
4.2.4.3. Confocal imaging	131
4.2.5. Statistical analysis	131
4.3. Results and discussion.....	131
4.3.1. Morphology of NHEKs.....	131
4.3.2. Cytotoxicity assay	132
4.3.3. Nrf2 translocation to the nucleus	134
4.3.4. Elucidation of the mechanism of Nrf2 induction.....	139
4.3.4.1. Investigation of ROS generation induced by compounds in liquid phase	139
4.3.4.2. Investigation of ROS generation induced by nonanal in gas phase	141
4.4. Conclusion	145
4.5. References	146
Chapter 5: The determination of skin surface pH via skin volatile emission using colorimetric sensors	149
Abstract	150
5.1. Introduction	151
5.2 Materials and Methods	154
5.2.1. Preparation of colorimetric sol-gel	154
5.2.2. Solution-based pH study	154
5.2.3. Preparation of colorimetric sensor spots	154

5.2.4. Indirect colorimetric sensing of skin volatiles	155
5.2.4.1 Control for indirect study	155
5.2.5. Colorimetric sensor response to ammonia	156
5.2.6. Direct colorimetric sensing of skin volatiles - preparation of wearable platform	156
5.2.7. Direct colorimetric sensing of skin volatiles (using a wearable sensor)	156
5.2.7.1. Control for wearable colorimetric sensor study	157
5.2.8. Skin treatment study	159
5.2.9. Image analysis	159
5.2.10. Data analysis	159
5.3. Results and discussion	159
5.3.1. Solution-based response of BCG sol-gel solution	159
5.3.2. Indirect sensing of skin volatiles	160
5.3.3. Effect of substrate on BCG sol-gel solution	162
5.3.4. Colorimetric response to volatile fatty acids and ammonia	163
5.3.5. Direct sensing of skin volatiles using a wearable sensor platform	164
5.4. Conclusion	172
5.5. References	173
Chapter 6: Conclusions and future work	178
6.1. Conclusions and future work	179
6.2. References	185
Appendix	186

Keywords:

Skin volatile emission

Non-invasive

Gland secretions

Skin microbiome

Headspace solid-phase microextraction (HS-SPME)

Gas-chromatography mass-spectrometry (GC-MS)

Wearable

Colorimetric sensor

Skin surface pH

Developing Approaches to Skin Volatile Biodiagnostics Using Non-Invasive Techniques

Melissa Finnegan

Wearable sensors have become popular in recent years with many types being available on the commercial market. These wearable sensors allow the monitoring of physiological parameters such as heart rate but give limited insights into the body's biochemistry and lack the ability to characterize important metabolic processes. While blood is the "gold standard" for monitoring the body's biochemistry, it is known that various components of skin, including interstitial fluid (ISF) and sweat offer alternative, non-invasive "windows" into the health of the individual via the tracking of biomarkers present within these matrices. This has prompted the innovative development of new types of wearable biodiagnostic platforms capable of in-situ extraction and analysis of these various skin matrices.

Wearable sensor development for biofluids such as ISF and sweat have thrown up many challenges with respect to generating and collecting sufficient volumes of such biofluids for reliable analyte detection. This thesis seeks to overcome the specific requirement for biofluid collection and manipulation by investigating the volatile emission from skin, a matrix that is continuously emitted from skin and which contains biomarkers of metabolic and cellular processes within the body. The work seeks to establish the volatile profile for healthy skin using a headspace solid-phase microextraction (HS-SPME) gas-chromatography (GC-MS) workflow to better understand factors that impact the emission including circadian rhythm, skin sampling site, gender and age. Mammalian cell culture studies were undertaken to investigate the response of human keratinocytes to frequently emitted skin volatiles to further understand and establish the contribution of such skin-derived compounds to the induction of cutaneous protective pathways. Finally, a move toward the use of a simple, cost-effective, wearable colorimetric sensor platform to monitor volatile emissions from skin was also explored with the feasibility of measuring skin surface pH, through the volatile ammonia emission from skin.

Overall, this work seeks to understand the robustness of the healthy skin volatile profile across a population and to demonstrate novel, simple approaches to tracking volatiles of interest to health via HS-SPME GC-MS workflows and wearable colorimetric-based biodiagnostics while also outlining their challenges and limitations. Exploiting the skin volatile emission to monitor skin physiology without the need for microneedles or the requirement to harvest fluid from skin is enticing. The understanding of this emission and its exploitation for wearable biodiagnostics has great potential for personalised monitoring of general health and self-management of chronic diseases shown to be associated with volatile biomarkers in the future.

Chapter 1: Optical sensors in wearable biodiagnostics

Abstract

Wearable sensing technology has recently and rapidly moved towards the development of many commercially available sensing devices that focus on physical measurements such as heart rate and blood oxygen levels. Such physical measurements give a limited insight into an individual's health status. While being described as barrier to our surrounding environment, the skin is a unique organ that has great biodiagnostic potential and can offer insight into metabolic processes within the body through the analysis of matrices produced within the skin such as biofluid and volatile emissions. Such biodiagnostic potential has led to the innovative development wearable sensors capable of detecting biomarkers from skin. While many sensors employ electrochemical transduction of biomarker response, wearable sensors utilising optical transduction are gaining traction owing to their simplicity and low-cost. This review aims to outline recent advancements in the development of wearable optical sensors for the detection of biomarkers in ISF and sweat as well as the skin volatile emission while also outlining practical challenges in their use, along with possible opportunities ahead for personalised monitoring of general health and self-management of chronic diseases.

1.1. Introduction

Skin is the largest organ of the body and while complex [1], has tremendous biodiagnostic potential. Acting as a barrier to the external environment around us, it prevents the invasion of pathogens that may cause infection and also regulates the loss of water and solutes [2]. Various skin biofluids and volatile emissions from skin offer a “window” into the metabolic processes of the body and give insight into the health of an individual by means of biomarkers present in such matrices [3]. Biofluids and volatile emissions are easily accessible and can be sampled in minimally- and non-invasive manners therefore overcoming the need for invasive methods of sampling such as biopsies and blood-sampling, which can prove uncomfortable for patients. Glucose, for example, can be detected in both ISF and sweat, in good correlation with blood-glucose concentration, thus offering a non-invasive means of assessment for diabetic patients [4]. Other studies have correlated biomarkers such as sodium and potassium in sweat as biomarkers of dehydration in athletes [5]. Such studies highlight the potential of detecting such biomarkers for human health, well-being and physical performance.

These findings have prompted the innovative development of various types of wearable epidermal sensors capable of sampling and detecting such biomarkers of interest. To date, electrochemical transduction has been employed for the analysis of biofluids and volatile emissions from skin but recently optical transduction through fluorometric and colorimetric sensors has gained traction and shows exciting possibility. This review will focus on the latest in wearable optical sensors outlining sampling techniques, sampler and sensor materials, sensing chemistries and their integration within the platform along with the challenges and opportunities for wearable optical sensors.

1.2. Skin composition and function

1.2.1. Physical structure

The skin is the largest organ of the human body and has a surface area of 1.5-2 m² [6]. It is a complex organ that is comprised of three main layers, the epidermis, dermis and subcutaneous tissue or hypodermis [7] (Figure 1.1). Each layer of the skin varies in structure, function and composition. The main function of the skin is as a barrier against the external environment around us [8]. It prevents the invasion of pathogens into the body that might cause infection and helps to regulate loss of water and solutes [1]. Another key role of the skin is thermoregulation, a homeostasis process which regulates body temperature [9].

The hypodermis layer is found deep within the skin and binds the skin organ to the skeletal frame of the body. Located above this is the dermis and this layer protects the skin against mechanical damage. The outermost layer of the skin is the epidermis, which is comprised of sublayers including the stratum basale, stratum spinosum, stratum granulosum and the final layer, exposed to the environment around us, the stratum corneum (SC) [7].

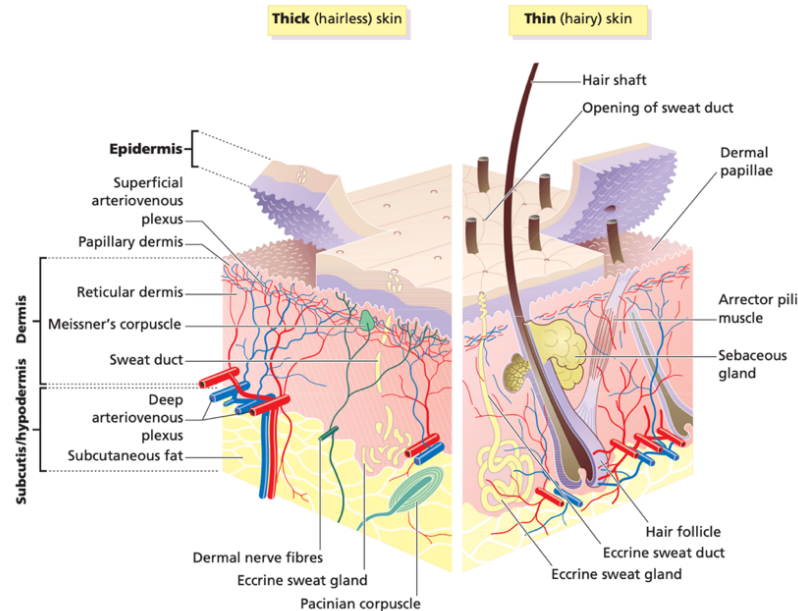


Figure 1.1. Diagram of the skin structure showing the three main layers, the epidermis, dermis and subcutaneous layer. All components of each layer are labelled including each gland present in the skin [10].

1.2.2. Stratum corneum

The SC is the outermost layer of the skin and is the first line of defence between the body and the external environment. It is a region of high metabolic activity where secretion of a rich variety of biochemical markers occurs, including lipids, peptides, proteins, cytokines, nucleic acids and volatile compounds. The structure of the SC can be described as a “brick and mortar” configuration (Fig 1.2) [6]. The epidermis is known to regenerate over a period of 28 days via a terminal differentiation process called keratinization or cornification [11,12]. This process results in a cornified envelope known as the “bricks” which is surrounded by a lipid rich lamellae described as the “mortar” [13]. Corneocytes are flat elongated cells (composed primarily of keratin (70%-80%) and lipids (20%)) surrounded by a cornified cell envelope. The cornified cell envelope is a polymeric protein/lipid envelope formed just below the cytoplasmic membrane found on the exterior of corneocytes. It consists of two parts; lipid envelope and a protein envelope [2]. The protein envelope dictates the biomechanical properties of the cells

by crosslinked structural proteins (filaggrin, involucrin, loricrin, elafin, cystatin A, and desmosomal proteins) through amide and sulfide bonds. The lipid envelope comprises N- ω -hydroxyceramides (OH-Cer) covalently bound to the protein envelope [2]. The lipid matrix helps regulate permeability of the epidermal barrier and is mainly comprised of cholesterol, free fatty acids (FFAs) and ceramides.

Proper development and maintenance of this “brick and mortar” type structure is crucial to protecting the body against chemical and microbial attacks from the external environment. The maintenance of the SC is also key to hydration of skin and regulating water loss. If the skin barrier is compromised or impaired then microbes or irritants will easily penetrate this skin barrier and may cause disease and infection in the body/skin such as atopic dermatitis (AD) [14,15]. Researchers have moved towards monitoring the skin of individuals who are prone to these diseases in order to detect biomarkers or early signs of disease onset. The water content [16], pH of skin surface [17] and volatile skin emission [18] are all parameters investigated in order to further understand these types of skin conditions.

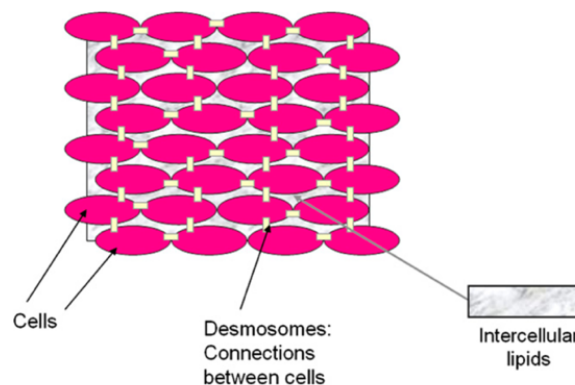


Figure 1.2. Structure of the SC showing cornified cells (bricks) and lipid lamellae (mortar) [13].

1.2.2.1. Glands

Glands are skin appendages that allow the excretion for sweat and sebum to the skins surface. There are three main types of glands present in skin: eccrine, apocrine and sebaceous glands which are illustrated in Figure 1.3 below [19]. Gland density is not uniform across the body and varies across different skin sites [20]. Eccrine and apocrine glands are characterised as sweat glands and contribute to overall sweat production [19].

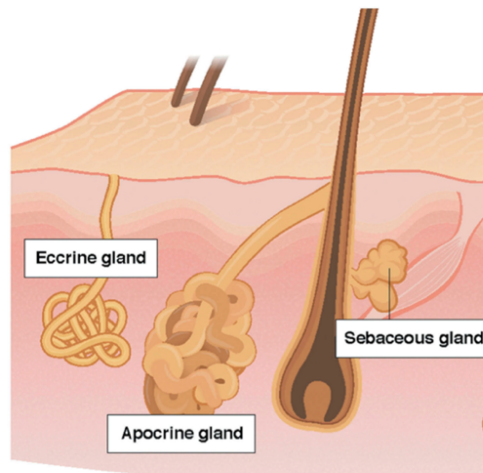


Figure 1.3. Structure of eccrine, apocrine and sebaceous glands in human skin [19].

Eccrine glands are the most numerous glands, distributed across the entire body surface area and are responsible for the highest volume of sweat excretion. They are coiled tube-like structures that have two domains; the secretory and the ductal portions. The secretory portion consists of a single layer of cells while the duct consists of two layers of cells and is covered internally with a material called the cuticle. As a consequence, the duct has a slightly smaller diameter than the secretory portion. Eccrine sweat is released directly onto the skins surface from these glands [21] and its composition is governed by factors such as diet, metabolic rate and drug administration [19]. Eccrine glands are mainly responsible for thermoregulation of the body, which helps keep the body cool [22]. This homeostasis process is crucial to maintaining a constant environment within the body. These glands can be located on both glabrous and non-glabrous skin, with the highest density being found on the palms and soles (~250-550 glands/cm²) [23]. Gland density on glabrous skin such as the face, arms and legs is ~2-5-fold lower compared to the palm and soles [23]. Eccrine sweat secretion is mostly comprised of water but also has a rich composition of electrolytes such as chloride [24], potassium [5] and sodium [25], metabolites such as lactate [26], glucose [27] and urea [28] and other components including amino acids [19].

Apocrine glands are the second type of sweat gland located in human skin. These glands differ from eccrine glands in that they are larger and open into hair follicles rather than directly onto the skin surface [29]. They comprise a coiled secretory portion and a straight duct portion. The coiled secretory portion is the gland itself and is found in the lower dermis of the skin. It's walls are composed of cells known as granules. Small granules are round while the large granules are fine, electron-dense and rich in iron. Glands terminate in the duct region and lead

directly into hair follicles [30]. Apocrine glands are primarily located in the axillae, breasts and genital regions and are responsible for odour and lipid-rich sweat which is comprised of proteins and sugars [31]. Their secretory function does not begin until puberty [32].

Sebaceous glands are another type of gland that are present over much of the body surface but are densely located on the forehead, face, upper back and scalp. Sebaceous glands are found midway down the dermis layer, almost always adjacent to a hair follicle with a duct emptying into the follicular canal. Sebaceous glands are absent from non-glabrous skin such as the palm and soles [31]. These glands secrete a viscous, lipid rich sebum that contains triglycerides, cholesterol, wax esters, and squalene [19]. Maximum secretion of sebum from these glands is achieved only after puberty [33]. Sebum produced contributes to the physical barrier of the SC by preventing evaporation of excess water from skin and it also serves a chemical function as it is a nutrient rich medium that promotes the growth of skin bacteria [34]. Over production of this lipid-rich fluid has also been linked to the development of skin diseases such as acne [35,36].

1.2.2.2. Microbiome

The skin acts as a physical barrier to prevent the invasion of pathogens as discussed above. It's surface is host to millions of bacteria, fungi, viruses and mites that form the skin microbiota (Fig 1.4) [37].

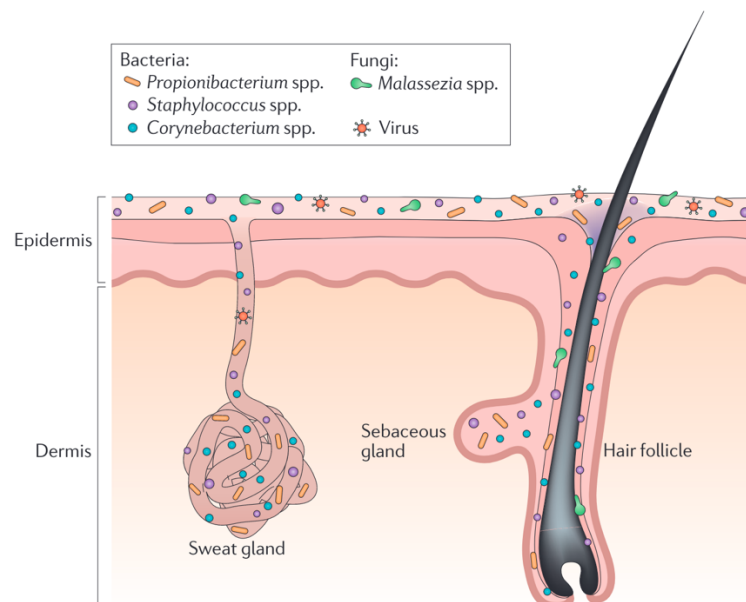


Figure 1.4. Structure of skin with various microorganisms living on skin surface labelled [38].

Skin's microorganisms play an important role in defence against invading pathogens, education of our immune system and the breakdown of natural products. Eccrine, apocrine and sebaceous gland density as well as the microorganisms present within the skin gland duct itself can contribute to the microbiota composition on the skin's surface at specific body sites [37]. Sites can be categorised as sebaceous, moist or dry. Sebaceous sites, such as the forehead, are known to be dominated by lipophilic *Propionibacterium* species. Bacteria such as *Staphylococcus* and *Corynebacterium* are abundant in moist sites such as the bends of the elbows, axillae region and feet. Dry sites of the body, such as the arms and the legs, are mainly populated by *Staphylococcus* and *Micrococci* species [39]. These bacteria species interact with the various gland secretions produced at the various sites. For example, sebaceous glands are relatively anoxic and can support the growth of anaerobes such as *Propionibacterium acnes*, which is a common skin commensal bacterium [40]. *P. acnes* is known to hydrolyse triglycerides present in sebum to release free fatty acids (FFAs) onto the skin surface. Bacterium can then adhere to these FFAs and aid in the colonisation of the sebaceous gland. Production of these FFAs also contribute to the acidic pH of the skins surface which will be discussed in more detail in section 1.2.2.3. Bacteria helps maintain and support the natural microbial balance of the skin, however it can also cause disease such as acne vulgaris under certain conditions [41].

While bacteria are known to be the most abundant kingdom across skin sites, other non-bacterial microorganisms including fungal species and viruses have also been isolated from skin. In contrast to bacterial communities, fungal community composition is similar across the entire body and less diverse with *Malassezia* being the main genus of fungi that predominates across the skin. The foot has the most diversity in terms of fungal communities where *Malassezia*, *Aspergillus*, *Cryptococcus*, *Rhodotorula*, *Epicoccum* and *Candida* were all species of fungi recovered [39,42]. Moreover, viruses such as Bacteriophages are also present in the skin's surface and play a role in the skin microbiome by modulating the physiology and composition of the microbiome's microbial community. However, due to low phage biomass

in skin samples and a lack of sequencing data, there are few studies on the impact of phages on the skin microbiome [37,43].

Overall, the diverse skin microbiome is mainly comprised of bacteria, fungi and viruses which all play an important role in the defence against the invasion of pathogens, preservation of skin homeostasis and modulation of the immune system [37,38,42].

1.2.2.3. pH

The hydrogen ion concentration or skin surface pH of skin can provide valuable information about an individual's health. An acidic pH of between 4.2 and 6.1 is observed in healthy human skin [6]. Cutaneous pH plays an important role in maintaining the normal bacterial flora of the skin and prevents invasion of pathogens, as discussed above. Skin surface pH measurements are typically performed using ion selective electrodes that measure the concentration of the hydrogen ion and convert it into an electrical signal [44]. Endogenous and exogenous factors such as eccrine and sebaceous secretions, anatomic sites, proton pumps, age, gender and genetic predisposition can affect the skin surface pH [45,46]. Figure 1.5 illustrates the sources that modulate skin surface pH.

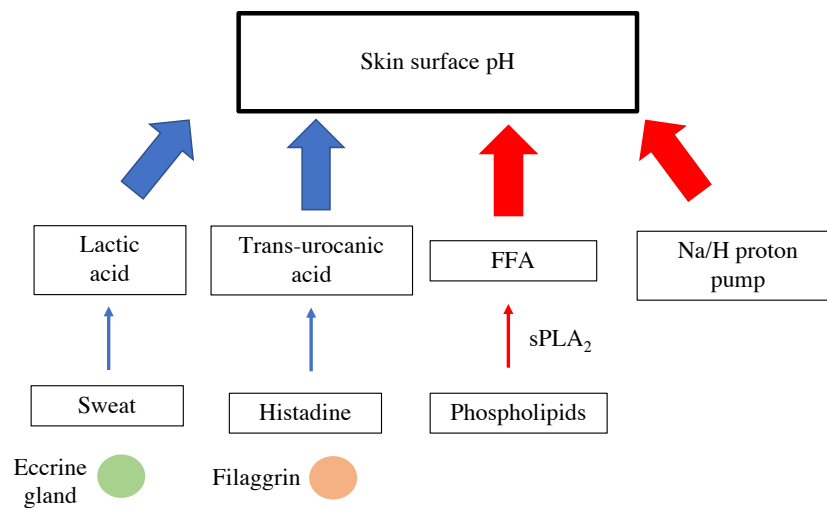


Figure 1.5. Contributors to skin surface pH. Exogenous sources highlighted by blue arrows; endogenous sources indicated by red arrows.

A hydrolipidic film covers the outer surface of the SC and plays an important role in the functioning of the epidermal barrier. The hydrolipidic layer is comprised of two fractions including the aqueous fraction derived typically from eccrine sweat gland excretions and the

lipidic fraction called the skin surface lipid (SSL) fraction. SSL fraction composition is derived from endogenous epidermal lipids within the cornified layer of the SC and in the case of sites containing sebaceous glands, secreted sebum. The composition and thickness of this SSL depends on the number of sebaceous glands present at a site [47]. Sebum contains triglycerides, wax esters, free fatty acids (FFAs) and squalene as the main components of the SSL. Essential fatty acids of carbon chain length C16 and C18 dominate the FFAs present in the hydrophilic film [48]. The generation of FFAs can be driven by the hydrolysis of sebum-derived triglycerides by lipases of bacteria whose activity is known to be modulated by pH [49].

In general, acidity of the skin surface is important for both antimicrobial defence and permeability barrier formation. Several mechanisms have been associated with the acidic pH of skin, these include exogenous and endogenous mechanisms [46]. The exogenous mechanism of FFA generation by microbial hydrolysis of components of sebum in hydrophilic film described above. Another exogenous pH modulation source is the generation of lactic acid and ammonia as eccrine-derived sweat products [50,51]. Endogenously, FFA production arises from the hydrolysis of phospholipids catalysed by a secretory phospholipase enzyme (sPLA₂) in the SC [46]. Furthermore, sodium proton pumps which actively pump protons to are also thought to contribute to the acidity of the SC [50].

While there are several mechanisms that contribute to skin surface acidity, FFA generation from certain pathways is clearly an important contributor. Recently, our group has examined a correlation between the skin surface pH and the emission of volatile fatty acids from skin of healthy participants [52]. Volatile fatty acid (VFA) emissions from the skin were sampled and analysed by gas-chromatography mass-spectrometry (GC-MS). Strong correlations were observed between recovered VFA abundances and skin surface pH for specific body sites. Such research supports the premise that skin surface pH is linked with FFA production.

1.3. Potential sources of novel skin-based biomarkers

While the skin has been described as an information barrier [3,53], various skin matrices such as ISF, sweat and also the volatile skin arising from volatile glandular and microbial emissions contain metabolites that are potential biomarkers of health [3]. Exploiting these gives interesting opportunities for the development of new biodiagnostics in the form of epidermal-based devices capable of sampling and the in-situ detection of biomarkers expressed in skin biofluids and the volatile emission.

1.3.1. Interstitial fluid

ISF is a body fluid that fills extracellular space in tissues. The main function of ISF is to transport metabolites and electrolytes to tissues, muscle cells, cartilage, bone cells, organs and groups of cells [54]. Small molecules including cortisol [55], glucose [56], lactate [57], sodium [58] and potassium [59] are readily exchanged by diffusion from blood and surrounding vascular tissue into the ISF thus offering an alternative to blood sampling of these molecules.

Molecules enter dermal ISF from blood in various ways such as by transcellular diffusion where molecules, such as small uncharged molecule like cortisol, diffuse through the plasma membrane of capillary endothelial cells [60]. Paracellular diffusion can also occur where molecules are transported through the space between cells. Finally, transcytosis can occur which is the vesicular transport of molecules through the cell. High capillary density, low flow rate, force produced by blood pressure and ability of large molecules all contribute to the facile exchange of fluid and analytes between blood and ISF [53]. Net fluid flow from the blood is driven by hydrostatic pressure and this results in similar or equal analyte concentrations between blood and ISF, highlighting ISF as an alternative, more easily accessible matrix comparable to blood. For example, small charged analytes including Na^+ , K^+ , and other compounds such as glucose pass through the cell membrane via paracellular diffusion or transcytosis and have similar ISF and blood concentrations [61].

ISF glucose (3.9 – 6.6 mM [62]) concentrations have frequently been shown to correlate with concentrations in blood (4.9-6.9 mM [63]) with a lag time of 5-10 minutes [4,64–66] thus offering a less invasive means of monitoring compared to blood finger prick. This has led to the innovation of the commercially available continuous glucose monitors (CGMs) such as the Abbott Freestyle Libre and the Dexcom sensor, that are capable of continuous sampling and monitoring of glucose concentrations for diabetes patients with high accuracy [67]. Other small charged molecules such as sodium and potassium ions has also been shown to also similar ISF concentrations compared to blood [61] while lactate, originally thought to have strong correlation with blood was shown to have weak correlation [68].

Despite these innovative advancements in the use of ISF as a proxy for blood, there are still many challenges associated with its extraction and biomarker detection, which be discussed in section 1.5.

1.3.2. Sweat

Sweat is mainly generated by eccrine and apocrine sweat glands which were discussed in section 1.2.3 [19]. The primary function of sweating is body temperature regulation [19,69]. Sweat is also thought to play a role in epidermal barrier homeostasis through its delivery of water, natural moisturising factors and antimicrobial peptides to the surface of the skin [70]. Furthermore, sweat plays a minor role in eliminating waste products and toxicants from the body [71]. Biomarkers in sweat include glucose [72], lactate [73], sodium [25], potassium [74], urea [75], cortisol [76] and hydrogen [77].

Similar to ISF, molecules found in the blood are secreted into sweat via 3 main routes, transcellular diffusion through the plasma membrane of capillary endothelial cells, paracellular diffusion between cells and finally through vesicular transport through the cell known as transcytosis [78]. Here, net fluid flow from blood and ISF, driven by osmotic pressure combined with greater cellular barriers for analyte transfer causes dilution of the biomarkers detected in sweat compared to blood [53] thus increasing difficulty in the detection of biomarkers. Furthermore, skin surface contamination may prove an issue and previously excreted sweat residing on skin may mix with newly excreted sweat thus hindering accurate analyte detection [79]. Sodium and chloride concentration in sweat are shown to have no correlation with blood concentrations and this is likely due to the reabsorption of these ions in the sweat glands thus making their concentrations independent of blood [53]. Similarly, lactate is produced within the sweat gland itself and during high exertion periods a spike in lactate concentration in sweat dominates diffusion from the blood and correlates well with exercise intensity but does not show representation of the anaerobic state of the body [26,28,73,80,81].

Monitoring changes in the concentrations of some these electrolytes can potentially act as indicators for clinical conditions or hydration status in athletes [28]. For example, cystic fibrosis (CF) is a disease that has been linked to changes in the transport of sodium and chloride ions which can lead to a build-up of mucus in various organs such as the lungs and intestines [82,83], thus monitoring their concentrations in sweat can prove useful in CF diagnosis. Moreover, sodium and chloride concentration determination in sweat, along with whole body sweat loss has been linked to the hydration status of athletes [84]. Monitoring these may aid in detection of certain conditions such as hyponatremia (low sodium content) and can also assist in optimising approaches to re-hydration to help enhance athletic performance and general health [85,86].

In general, sweat has a rich diagnostic potential however there are still many challenges faced including sufficient sweat generation, fluid handling and manipulation that will be discussed in the further sections.

1.3.3. Volatiles

Exploiting volatile biomarkers emanating from the skin as a source of information to probe the body's biochemistry has been of great interest recently as the volatile profile from skin contains information on cellular processes within the body and thus can offer insight into the metabolic condition of an individual. Skin volatile profiles reflect metabolites of the dermal and epidermal cellular layers, compounds carried to the skin via the bloodstream as well as volatile metabolites that are derived from symbiotic bacteria that live on the skin and from metabolization and transformation of secreted compounds in sweat and sebum [87].

Different regions of skin emit different volatile profiles comprised of a diverse groups of compounds which are volatile at skin temperature. Literature has reported over 600 volatile compounds previously isolated from human skin extracts [88]. Emitted compound classes include alkanes, alkenes, aldehydes, acids, ketones, alcohols, sulphur-containing compounds and nitrogen-containing compounds, from both endogenous and exogenous sources [88] with compounds each having different emission flux ranges from skin, for example the aldehyde nonanal shows an emission flux range of 18.1-119 fmol/cm²/min while the ketone, acetone is emitted is at a much higher rate of 493-3680 fmol/cm²/min [89]. Acetone is a component of ketone bodies that has frequently been detected in human breath as a potential means of monitoring diabetes [90]. Acetone is also emitted from skin [91] and significant correlation between ketone bodies detected in the blood and skin acetone emission have also been established [92].

Skin volatiles sampling techniques can be categorised into surface-contact and headspace sampling modes [93]. Typically, surface-contact modes often employ the use of an adsorbent such as glass beads [94], gauze [95–97], poly(2,6-diphenylphenylene oxide) (Tenax) patches [98] or polydimethylsiloxane (PDMS) membranes [99,100]. Samples obtained using these sampling techniques typically require solvent extraction or the employment of pre-concentration techniques due to the trace quantities emitted from skin. Recently, however, direct headspace solid-phase microextraction (HS-SPME), a headspace-based sampling mode, has emerged as the gold standard for the analysis of trace volatile emissions from skin as it allows sensitive extraction and pre-concentration in one step thus omitting the need for extra

pre-concentration steps [18,52,101,102]. Furthermore, gas-chromatography mass-spectrometry (GC-MS) is the gold standard for analysis of trace volatiles and so has been employed frequently to detect analytes in skin volatile emissions [52,89,96,102].

Volatile emissions from skin are emitted from skin continuously and passively and offer an exciting alternative to the analysis of biofluids such as ISF and sweat. Their potential, along with challenges faced in fabrication and biomarker detection will be outlined in more detail in section 1.5.

1.4. Chemical sensing

Chemical sensing involves the transforming of relevant chemical or physical properties of a molecular or ionic species into analytically useful outputs that can be used to detect subtle changes in a chemical environment [103]. Typically, a chemical or biochemical sensor is comprised of two elements, a receptor, and a transducer. In the receptor element, chemical information such as the concentration of a compound, pH or temperature is converted into a useful analytical signal; electrochemical, optical, or electronic, that can be measured by a transducer (Fig 1.6). These biochemical sensors typically have selectivity for a single analyte, with some sensors having the ability to detect multiple analytes by utilizing several different receptor elements within a single platform. Biomarker detection from skin is commonly carried out using electrochemical or optical transduction [104]. Electrochemical sensors has frequently been employed for detection of skin biofluid and volatile biomarkers due to their high sensitivity, high selectivity and fast response times [105]. Optical chemical sensing, however, has been used less frequently but is recently finding its niche for the detection of biomarkers in skin biofluids and volatiles and offers an exciting alternative to electrochemical transduction.

1.4.1. Electrochemical sensing

Electrochemical sensing employs the use of electrodes to measure the electrochemical changes that are generated upon the interaction of a target molecule with an immobilized sensing surface using amperometric, potentiometric or impedimetric techniques [106]. Electrochemical sensing has, to date, been the main transduction method used for the analysis of biofluids such as ISF [57,107–110] and sweat for wearable devices. Metal oxide (MOx) sensors [111–113] have been developed for the detection of skin volatiles utilizing electrochemical transduction as an emerging alternative to the typically used gold standard

headspace solid-phase microextraction (HS-SPME) sampling coupled with gas-chromatography mass spectrometry (GC-MS) analysis [18,52,89,101].

Despite the integration of highly innovative electrochemical detection techniques there are still some challenges associated with such sensor platforms. For example, electrochemical noise, signal drift and fouling remains to pose challenges for wearable electrochemical sensors [114]. Efficiency of the electrochemical response may be affected by intrinsic body noise, skin-electrode interface noise and environment noise [3]. Signal drift is another challenge that is associated with electrochemical sensors. For example, commercialised CGMs suffer from signal drift related to sensor aging and frequently require calibration by the user using the finger-prick method. Fouling of the electrodes can also occur which can limit sensor stability thus reducing the wear-time of the sensor.

Moreover, there are demanding energy requirements for adequate power and memory capacity to allow for continuous monitoring. While self-powered wearable electrochemical sensors such as the use of triboelectric nanogenerators (TENGs) [115], piezoelectric nanogenerators (PENGs) [116] and biofuel-powered sensors which utilise biofluids as sustainable bioenergy sources [117,118], have been developed there is still continued research required to preserve simplicity of operation and maintenance of the miniaturization required for wearable biosensors.

These flaws have prompted revisiting to the pre-electronic era of analytical chemistry by the use of optical sensors. The lack of electrical components, simplicity in design, ease of use and low-cost has made optical sensors an attractive alternative to electrochemical sensors.

1.4.2. Optical sensing

Optical chemical sensors use visible, infrared or ultraviolet light to probe chemical reactions at liquid or solid interfaces. Such sensors can be further subdivided based on the type of optical property used for sensing, for example, absorbance, reflectance, fluorescence, luminescence, refractive index, optothermal effect or light scattering [119]. Different optical transduction methods utilise various regions of the electromagnetic spectrum and measure a wide range of parameters including intensity of light, lifetime and polarization. Detection mechanisms of optical sensors rely on two fundamental requirements: a chemical reaction between the analyte of interest and a chromogenic/fluorogenic substance and a production of a quantifiable change under the excitation or irradiation of light [120]. Absorbance, reflectance and fluorescent detection are commonly employed in wearable optical sensors.

1.4.2.1. Fluorometric sensing

One of the most commonly used spectroscopic methods is fluorescence detection and exhibits high sensitivity compared to other optical methods. Fluorescence is a type of luminescence that occurs when photons in the singlet ground state are promoted to the singlet excited state. The spin of the excited electron is still paired with the ground state electron. Return to the ground state is spin allowed and occurs rapidly with the emission of a photon [121]. Fluorescent measurements take advantage of a wide variety of parameters including fluorescence intensity, emission lifetime and fluorescence decay. There are three types of fluorophores: intrinsic probes where the sensor itself is fluorescent, extrinsic probes where the fluorophore is attached to the sensor binding site and the fluorescent property is modulated by analyte binding and differential/displacement probes where the analyte of interest binds competitively to a receptor that already has a fluorophore bound already and the release of the fluorophore allows a change in the fluorescence signal [120]. Biomarkers in skin biofluids and volatile emission have recently been sensed using both intrinsic and extrinsic fluorescent probes with their sensing chemistry and integration into wearable sensors being discussed in further in the following sections [122–124].

1.4.2.2. Colorimetric sensing

Colorimetry is a quantitative measurement of UV-vis absorbance or reflectance. The underlying principle involves the generation of colour by a chemical or biochemical reaction between an analyte and a colorimetric sensing reagent. Intensity of the resulting colour can be distinguished using the naked-eye and further quantified by measuring absorbance using a spectrophotometer/colorimeter. Further image analysis is done using softwares such as ImageJ and MATLAB. Colour spaces, which are abstract mathematical representations that define the range of perceivable colours in human vision, have been used to accurately quantify colorimetric sensor responses upon interaction with analytes. These colour spaces include red, green and blue (RGB), hue, saturation and brightness (HSB), Y'UV and L*a*b (L defines the whiteness of blackness of a pixel and A and B are colour difference channels) [125].

Many colorimetric sensors are on the commercial market for different applications such as pregnancy tests and COVID tests which both work on a lateral flow principle where capillary action is employed to move the sample toward a detection antibody and a line appears only if the target molecule is present in the sample indicating a positive test [126].

Colorimetric sensors offer a low cost, instrument-free alternative to the more costly electrochemical sensors as they do not require complex electronics and power supply. Recent advancements, along with challenges and opportunities for the use of colorimetric sensing in the analysis of skin biofluids and volatile emission will be discussed in-depth in the following sections.

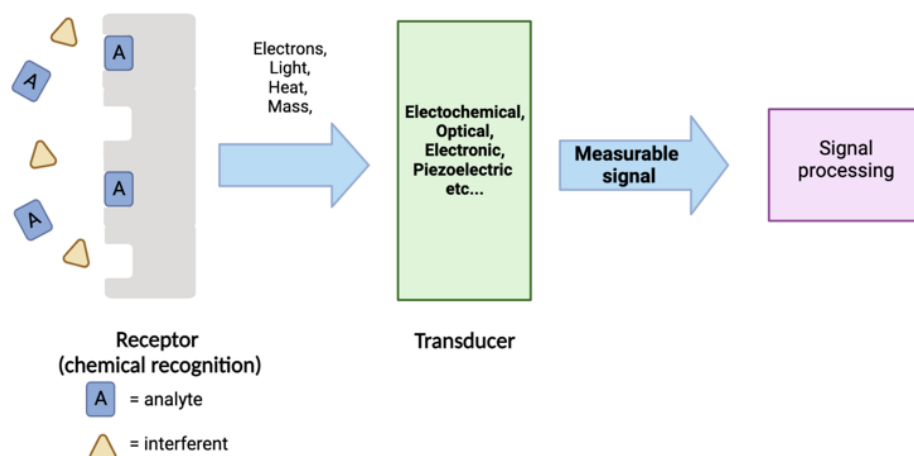


Figure 1.6. Schematic of a chemical sensor with selectivity for a single analyte.

1.5. Current state of the art in wearable optical biochemical sensors

The broad wearable sensor market is currently dominated by commercial watch brands, eg Apple Watch and the Fitbit [127]. These watches house sensor technology to monitor physiological parameters such as heart rate and blood oxygen levels through the use of optical sensing technique called photoplethysmography (PPG). PPG involves the detection of changes in the light intensity with respect to the changes in blood flow of the tissue to configure a heart rate [128]. These physiological sensors only monitor physical activity and can give only limited insight into an individual’s health status. As previously mentioned, sensing biomarkers in skin biofluids and volatiles has the potential to give insight into the metabolic processes of the body [129]. This has prompted research into the innovative development of various types of wearable devices capable of extracting, sampling and analysing biomarkers in skin matrices such as ISF, sweat and skin volatiles.

1.5.1. Extraction and generation of skin biofluids and volatiles

One of the main challenges faced with wearable optical sensors is the extraction, generation and sampling of a sufficient volume of a biofluid of interest for biomarker detection. Extraction of ISF requires drawing ISF from the dermis layer to the SC using techniques involving suction blister [130], reverse iontophoresis [108–110,131], microneedles (MNs) [59,107,132–134] and more recently magnetohydrodynamics [135,136] all of which are minimally invasive. Sweat, derived from sweat glands, is excreted directly onto the SC therefore making it readily accessible and available for non-invasive sampling. Sufficient volumes of sweat can be easily generated for collection through exercise [137,138], thermal [24,139,140] or by chemical stimulation [141–143]. Volatiles however, are continually and passively emitted from skin and this obviates the need for extraction or generation associated with ISF and sweat [89,144,145]. Biofluid extraction or generation techniques commonly employed in wearable optical sensors are outlined here along with a discussion around challenges faced and possible opportunities for improved extraction and generation.

Polymeric-based MNs, such as methacrylated hyaluronic acid (MeHA), polyvinyl alcohol (PVA), polyethylene glycol diacrylate (PEGDA), polystyrene (PS) and hyaluronic acid (HA) have frequently been employed for ISF extraction within wearable optical sensing platforms [146–150]. MNs need to penetrate the skin in order to recover biofluid and typically employ capillary action to drive the extraction of ISF from the dermis thus making biocompatibility of the MN with skin paramount [151]. Nicholas et al. utilised a hollow MN geometry, fabricated using a photopolymer mix and a silicone mould to produce a sharp bevelled-edged MN (400 μm in length), to extract ISF via capillary action [149]. Other hollow MNs using PEGDA were fabricated by a photolithographic technique to extract ISF for colorimetric detection. This 13 x 13 MN sensor array (MN height: 600 μm) had the ability to extract ISF successfully for glucose detection. Solid polymeric-based MNs, have also been employed [146–148]. Wang et al employed solid polyvinyl alcohol (PVA)-based MNs capable of ISF extraction for the colorimetric detection of glucose in mice [147]. This 5 x 5 MN array had a length of 1500 μm and swelling-driven capillary flow allowed for the rapid extraction of ISF within 10 min of insertion, albeit slower than reported hollow MN extraction techniques [149,152].

While many of these MNs allow for the extraction of ISF volume ranges of 1-10 μl which is a sufficient volume for reliable detection of biomarkers within the biofluid [60], disruption of the skin using MN sampling may elicit an immune response that drives the

composition of ISF away from homeostasis. Such a response may distort the concentrations of analytes of interest in the ISF thus giving unreliable quantification [153]. Furthermore, continuous extraction of ISF will cause dilution of biomarkers in the extraction fluid [60].

Tattooing into the dermis of the skin using responsive inks has allowed the direct sensing of biomarkers in ISF and has recently emerged as alternative to extraction of ISF to the skin's surface. Yetisen et al has been at the forefront of this tattoo sensor field and uses a conventional tattoo gun to inject both colorimetric (Fig 1.7 (a)) [154] and fluorescent (Fig 1.7 (b)) sensing reagents into the dermis [123] capable of sensing biomarkers in ISF. In this work, the sensing chemistry formulation ink is dispensed onto the skin surface and a tattoo needle punctures the skin over this area. When the needle is removed, the resulting vacuum drives the ink into the skin. Penetration depth is critical as shallow injections rapidly fade whereas deeper penetration can damage the subcutaneous tissue. The group have shown that the density, position, depth and angle of the inks can be accurately controlled. Work by He et al. uses hyaluronic acid (HA)-based MN patch to deliver colorimetric sensing tattoo reagents into the skin via the dissolution of MN tips into the dermis for multiplexed detection of ISF pH, glucose, uric acid and also body temperature (Fig 1.7 (c-d)). This HA-MN patch supports the injection of multiple sensing reagents in a single insertion to the dermis whereas injection with a tattoo gun only facilitates insertion of one single sensing reagent at a time. Moreover, consistency and accuracy of the penetration depth of the dermal tattoo sensing inks is improved in comparison to injection with a tattoo gun [155]. Currently, these optical tattoo inks have only been assessed in ex vivo [123,154,156] and in vivo skin [155] however, further in vivo studies in animals and humans must be carried out to further understand immunogenicity and foreign body response to their insertion into skin.

To date, minimally invasive techniques such as the use of MNs described above have been employed in the extraction of ISF for optical detection however there is opportunity there for the integration of less-invasive extraction techniques such as iontophoresis [108] and magnetohydrodynamics [135,136] to extract ISF in wearable optical sensors.

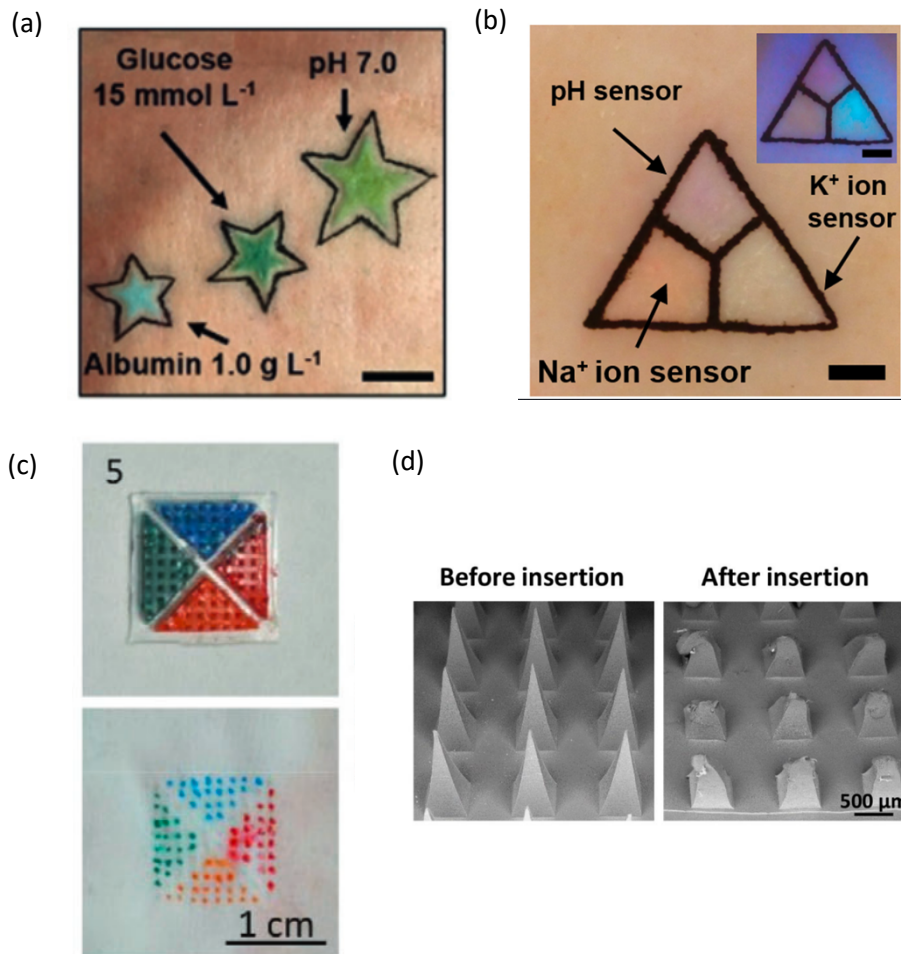


Figure 1.7. (a) Dermal tattoo for colorimetric metabolite detection in porcine skin [154], (b) dermal tattoo for fluorometric electrolyte detection in porcine skin [123], (c) dermal tattoo fabricated by MN patch [155] and (d) HA-based MNs before and after insertion into skin [155].

As previously outlined, sweat is a more accessible skin biofluid than ISF and its sampling allows us to move away from the invasive or minimally-invasive methods associated with ISF and also blood sampling. In order to achieve a reliable detection of sweat analytes, a sufficient volume of sweat must be generated for biochemical sensing through an increased sweat rate [157]. Due to the limitations of low secretion and high evaporation rates [158], many wearable optical sweat sensors have focused on using exercise [122,159–161] or thermal [162,163] stimulation to produce a sufficient volume of sweat for analysis. These methods allow a facile way generate the sufficient volume of sweat needed for biomarker analysis but also have their drawbacks. An increased sweat rate associated with prolonged exercise or thermal induction of perspiration can induce the dehydration and variation of electrolyte and

metabolite concentration in sweat, which is not ideal for diagnosis of disease but may be useful for athletes to assess hydration status during performance [164,165].

Sampling thermoregulatory sweat, natural sweat generated while doing sedentary tasks, may offer a more promising method of assessing biomarkers in sweat without the need for the active stimulation methods outlined above. Elevated or inhibited sweat secretion rate at rest has been known to reflect underlying health conditions such as diabetes [166] and Parkinson's disease [167]. In addition to this, cytokine levels in sweat are known to be biomarkers of an infection/inflammatory event and need to be measured in passively emitted sweat as sweat stimulation methods may lead to inaccurate cytokine levels influenced by local inflammation of the stimulated site rather than actual inflammatory response of infection [168]. Moreover, the lower sweat rate reduces the dilution of the biomarkers of interest in sweat which preserves equilibrium and gives more accurate correlations between blood and sweat. This highlights the potential of sampling thermoregulatory sweat which has been extracted and used for electrochemical sensing [168,169] and opens up possibilities for these mechanisms to be integrated with optical sensors which have not yet been realised

Compared to sweat and ISF, volatile emissions are a more accessible skin matrix as volatiles are passively and continuously emitted, eliminating the need for generation or extraction of fluid. Optical sensors are typically placed in an enclosed headspace above the skin (approx. cm^3 volumes) where volatiles are collected and biomarkers detected [91,124,170–172]. Headspace enclosure is required to exclude ambient volatile inferences from the surrounding environment. Yu et al [91] have developed a gradient-based colorimetric array sensor (GCAS) in both an offline (sensor imaged using a smartphone, ambient light not controlled) (Fig 1.8 (a)) and online (sensor imaged continuously throughout wear using a webcam, ambient light is controlled) (Fig 1.8 (b)) format which detects skin emissions such as acetone, ammonia and CO_2 . For the offline studies, where influences of ambient light were not controlled, the sensor was worn for 6 h enclosed in a small headspace defined by a petri-dish. The evolution to the online study allowed real-time imaging monitoring of skin-emitted acetone in a small gas chamber with dimensions of 14 x 14 x 1.3 mm. Toma et al [124] recently developed an interesting approach to collecting volatile emissions from the body using an over-ear gas collection cell equipped with a biochemical gas sensor for the fluorescent detection of ethanol. Here, commercial earmuffs were modified to have an inlet which allowed filtered air (carrier gas) into the 151 mL headspace and an outlet which was used to collect sample volatile gas from the headspace ((Fig 1.8 (c)). Our group has also recently developed a wearable

colorimetric sensor platform comprising an enclosed headspace containing pH indicator dye sensor spots on cellulose. This planar device comprises a stainless steel woven mesh as spacer layer, cellulose layer comprising sensor spots and a transparent polyethylene terephthalate (PET) film (5 x 4 cm) covering the sensor spots to enclose the device (Fig 1.8 (d)) [172].

Another colorimetric sensing approach was employed to detect early onset of infection in wounds [173,174] through the detection of CO₂ emissions from the wound bed. Again, an enclosed headspace was used to protect from possible ambient interferents and so these CO₂ sensors were incorporated into occlusive wound dressings (6 x 7 cm).

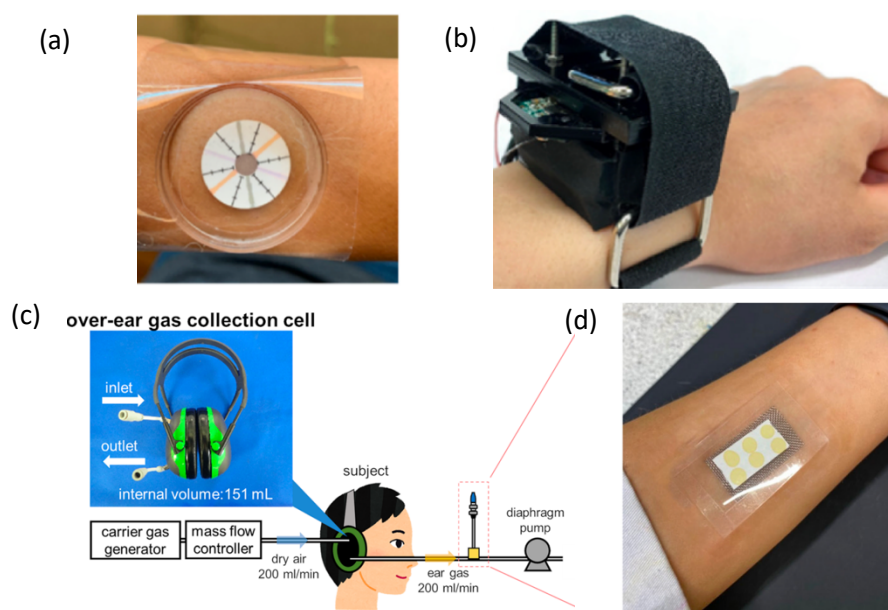


Figure 1.8. (a) “Offline” GCAS attached to the forearm for in-situ detection of transdermal gases with a transparent chamber on top to block possible ambient interferences, (b) “Online” GCAS for real-time monitoring of the emission of acetone from skin [91], (c) schematic of Toma et al’s external ears for detection of ethanol from skin gas [124] and (d) image of a wearable ammonia sensing platform worn on the forearm [172].

1.5.2. Fabrication of optical sensors for wearable applications

Following extraction of ISF, generation of sweat or passive emission of skin volatiles, the next challenge faced by wearable optical sensors is transport of the biofluid or volatiles to the optical sensing element within the platform. Materials of which the wearable sensing platform are fabricated from are also important with biocompatibility and conformability with skin being paramount. Some optical sensing platforms employ different materials for the

extraction/sampling and sensing elements and integration of these materials is required. Section 1.5.2.1 will discuss the materials commonly used for the fabrication of wearable optical sensor and how these materials facilitate guidance of the biofluid to the sensing element. Optical sensing chemistries, along with their encapsulation and integration or housing in wearable platforms will be discussed in section 1.5.2.2 and 1.5.2.3, along with the main challenges associated with the use of these chemistries.

1.5.2.1. Fluid handling, materials consideration and integration

The human epidermis is soft, curvilinear and deformable which means that substrates used for wearable optical sensors must be thin, have high flexibility, stretchability and be able to conform to skin and its geometry. Substrates used require biocompatibility, need to be able to endure stress by daily human motion and moreover, must be comfortable to wear in order to minimise interferences with the wearer's daily life [105,151]. Furthermore, these substrates must be able to collect the biofluids either from the dermis (ISF) or from the skin's surface (sweat and volatiles) and guide them efficiently toward the optical sensing element for biomarker detection.

As discussed above polymer-based solid and hollow MNs have been employed for the extraction of ISF from the dermis. Techniques such as photopolymerisation [149,175], crosslinking [146] and vacuum- or centrifugation-based mould casting [147] are typically employed in MN fabrication. Fabricated MNs are also responsible for the transport of ISF, through capillary action, from the dermis to the optical sensing element. For optical ISF biomarker detection, different materials have frequently been used for the fabrication of extracting/sampling MNs and the optical sensing element with PVA and paper-based materials typically being employed [146–149,175,176]. For example, an MeHA solid MN-array for ISF extraction through capillary action were fabricated through UV initiated crosslinking. A nitrocellulose membrane immobilised with different colorimetric sensing reagents was employed for biomarker detection in extracted ISF [146]. In order to integrate the sensing elements with the MNs, a thin layer of MeHA was applied to the sensing membrane before application to the MNs followed by drying and UV-crosslinking, to allow adhesion directly on top of the MN extraction material (Fig 1.9 (a)) which allowed transport of the ISF via capillary action from the MNs to the sensing elements. Similarly, Nicholas et al (Fig 1.9 (b)) used a hollow MN for ISF extraction and a cellulose-based sensing material immobilised with

colorimetric sensing dyes for ISF glucose detection. Again, capillary action allowed the extraction of ISF from the dermis through the MN to cellulose sensing material [149].

Moving away from paper-based sensing material, Zhang et al's wearable sensor for uric acid comprised two components, a PVA-MN array for ISF extraction and transport embedded with an enzyme for selective oxidation and a PVA sensing layer immobilised with colorimetric detection reagents for uric acid detection in ISF using a mould-fabrication technique (Fig 1.9 (c)) [148]. Similarly, other studies have employed PVA-MN-arrays with a PVA-based sensing element immobilised with colorimetric detection reagents for ISF glucose sensing [147].

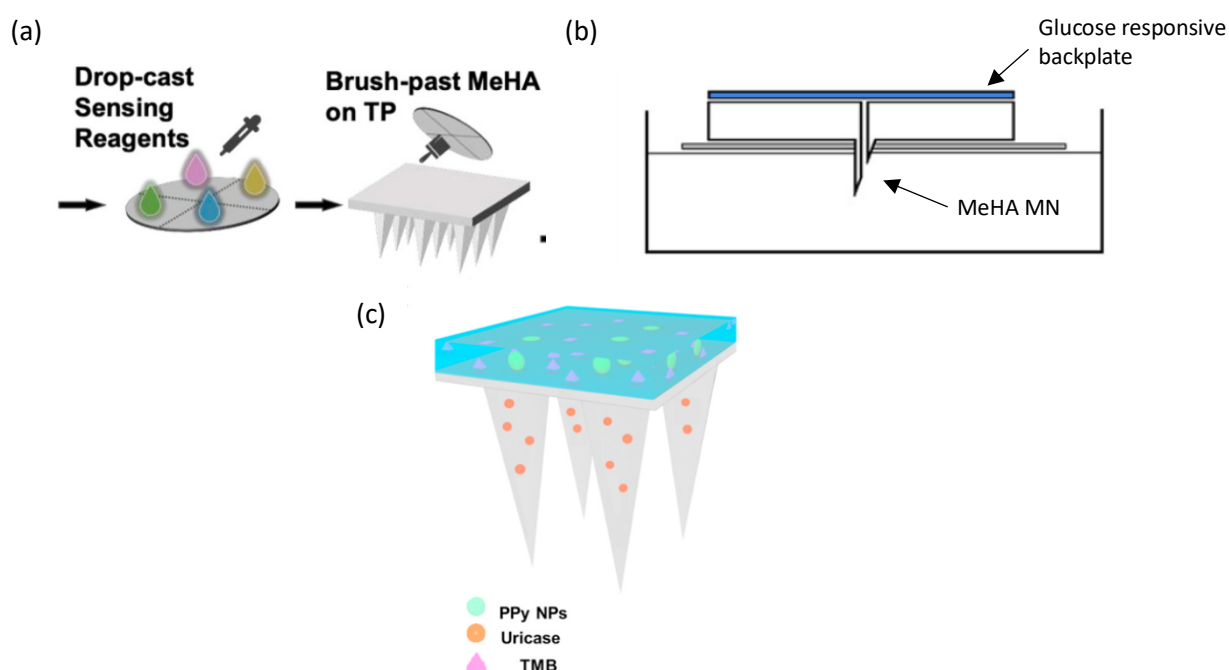


Figure 1.9. Schematics of (a) the integration of cellulose-based sensing material with a MN patch [146], (b) a single, hollow-MN integrated with a glucose cellulose-based glucose sensor [149], and (c) an immobilised PVA colorimetric uric acid sensor integrated with a PVA MN-array [148].

In order to ensure continuous and robust sweat collection for analysis and routing to the optical sensing element, the sampler for a wearable sensor must establish and maintain a conformal, intimate interface with the epidermis. Flexible materials such as polydimethylsiloxane (PDMS), polyethylene terephthalate (PET), PMMA and other hydrogel-based materials such as PVA have been employed in wearable optical sweat sensors. Wearable optical sweat sensors frequently employ the use of soft, microfluidic architecture to capture

and transport generated sweat toward reservoirs that contain fluorometric or colorimetric sensors in-solution [159,162,164,177–179] or immobilised on paper substrates [179].

Rogers' group has been at the forefront of the sweat-based optical transduction with their published devices being highly conformable with skin through innovations in the materials and geometries used. Their wearable devices are comprised of several layers including skin-compatible adhesives, microfluidic channels and valve structures that route extracted sweat to microreservoirs via capillary force, colorimetric or fluorometric reagents and sealing layers [117,139,162,164,177,178,180]. Capillary force-based sweat fluids, involves the movement of secreted sweat through a very thin channel where natural eccrine gland sweat pressure allows transportation of the sweat toward sensing reservoirs. Such designs allow the sensor platforms to have both on-board sampling and sensing capabilities. Sweat capture for on-board analysis is enabled by inlets present on the skin-interfaced surface of the sensor system. A serpentine channel, with thicknesses of μm in width, routes extracted sweat toward reservoirs that contain optical sensing reagents either in-solution or immobilised on a paper substrate [181,182].

Soft lithographic techniques are employed as a fabrication methods whereby PDMS, or other soft flexible materials such as PMMA are cast and cured against lithographically prepared moulds to yield solid elastomers with specific features on their surfaces for microfluidic channels, valves and reservoirs. A corona treatment process is typically employed to bond layers within the devices [117,139,162,164,177,178,180].

Rogers' group have recently commercialised the Gx Sweat Patch which is a wearable optical sweat that use PDMS microfluidic architecture, fabricated using soft-lithographic techniques, to guide generated sweat to the colorimetric sensing reservoirs for the detection of sweat loss, sweating rate and chloride concentrations in athletes (Fig 1.10 (a)) [84,183]. Microchannel diameter ranges from 4 – 7 μm with capability for collection of 30-130 μl of sweat. Sweat rate could be calculated from the rate at which the fluid travelled through the microchannel during on-field sports and was found to be $\sim 1.99 \text{ mg/cm}^2/\text{min}$ [84]. While this Gx sweat patch is innovative it only offers single-one time use and then needs to be disposed of. This is mainly due to the irreversibility of the sensing chemistries used.

The ever-growing concern of proper environmentally friendly waste management and the current capability of wearable optical sweat sensor to be single-use has led to the fabrication of environmentally degradable wearable microfluidic devices using thermoplastic copolymer elastomers (TPCs) such as APINAT BIO biodegradable compounds and cellulose-based top

sealing layers (Fig 1.10 (b)). Such TPCs offer the same skin conformable properties thus making them a viable alternative to PDMS based optical sweat sensors. A lithographic technique is again used to create a PDMS mould which is then used to create a TPC-based microfluidic device [177]. This device exploits the use of microchannels/microreservoirs and microvalves with depth of $\sim 330 \mu\text{m}$ for movement of sweat toward sensing reservoirs and the middle serpentine channel also allows the monitoring of sweat rate and loss up to a total volume of $\sim 20 \mu\text{l}$.

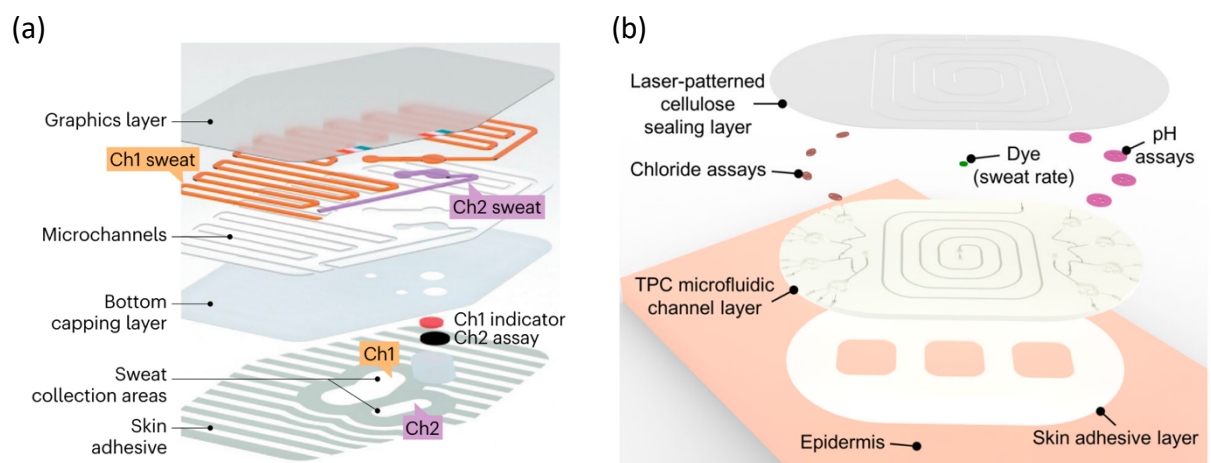


Figure 1.10. (a) Schematic of the microfluidic-based Gx Sweat Patch [183] and (b) schematic of an environmentally degradable microfluidic colorimetric sweat sensor [177].

Similar to ISF extraction and sensing substrates, owing to its biocompatibility, PVA-based hydrogels, have been used to house wearable colorimetric sweat sensor chemistries thus obviating the need for microfluidic channels to guide sweat toward optical sensing elements. A self-healable hydrogel patch, with a thickness of 5 mm, was fabricated by cross-linking PVA and sucrose where the self-healable properties are attributed to the hydrogen bonds formed between the two compounds [161]. Patterned micropores (9 mm in diameter) were manually produced in these hydrogels using a puncher followed by solvent displacement to embed colorimetric detection elements for glucose, pH, chloride and calcium. Such methods of immobilisation inhibits leaching of the colorimetric dyes while also does not compromise the self-healable nature of the hydrogel. Following this, a colorimetric hydrogel was selected and filled into the pores of the main substrate platform. The self-healable nature of the hydrogel allowed a single layer wearable colorimetric hydrogel patch be formed. Moreover, this hydrogel can directly attach and conformally come into contact with skin and so obviates the need for any skin adhesive (Fig 1.11 (a)) [161].

Textiles have been used as wearable optical sweat sensor substrates. Chitosan-coated cotton patches [184], cotton-thread/paper based microfluidic devices [160,185,186] and Janus fabrics facilitate adequate sweat sampling while ensuring no backflow of colorimetric reagent toward the skin. Janus fabrics are fabricated by electrospinning hydrophobic polyurethane nanofiber arrays onto hydrophilic gauze. Colorimetric dye leaching can be an issue for wearable sensors. Janus fabrics can overcome this issue as they have asymmetric wettability, where sweat travels from the hydrophobic side close to skin to the hydrophilic area where the detection agents are present, thus allowing for unidirectional sweat collection. Xi et al. recently developed a Janus fabric-based wearable colorimetric sweat sensor capable of chloride, pH and urea content in sweat, with detection reagents being drop-cast on nitrocellulose filter membranes (Fig 1.11 (b)) [187].

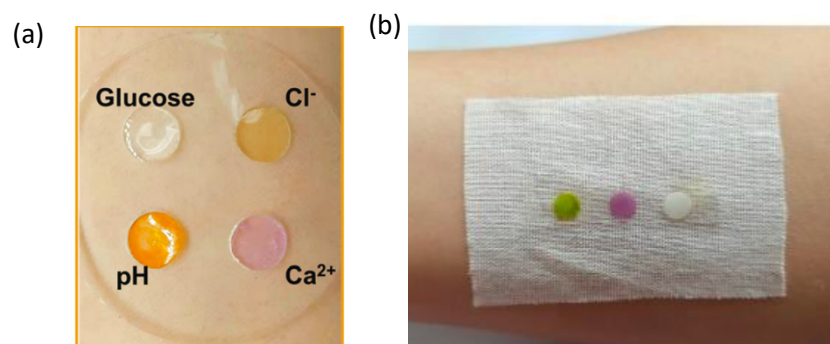


Figure 1.11. (a) A flexible, self-healable hydrogel patch for colorimetric sweat detection on skin [161] and (b) Smart Janus fabric-based colorimetric sensors for the detection of pH, chloride and urea in sweat [187].

Wearable optical sensors developed for volatile biomarker detection from skin can be fabricated on flexible, reasonably thin substrates (to minimise mass transport effects) such as silica-gel thin layer chromatography (TLC) plates, cellulose TLC plates, cellulose filter and polytetrafluoroethylene membranes. As discussed above, Yu et al. developed a GCAS in both offline and online (wearable with continuous imaging) formats to detect acetone, ammonia and CO₂. Here, silica gel TLC plates were cut into specific shapes using a laser cutter. For the offline sensor chip, the sensing chemistries in water/methanol solvent were drawn onto the TLC plate using a fountain pen or dropcast and vacuum dried. These sensors were covered with transparent scotch tape to protect sensing chemistries from ambient air and to enable easy imaging of the sensor. Polyethylene double-coated tape was used to adhere the offline sensor (Fig 1.8 (a)) to the skin while the online sensor was fixed in the wearable device and so did not

need direct adhesion to skin [91]. Ikeda et al developed an ammonia sensing wearable comprised of a watch-like device housing a planar ammonia sensor fabricated by drop-casting alizarin red dissolved in a glycerol/methanol on filter paper [171]. Similarly, our recently developed ammonia sensor also has such a planar format and is comprised of BCG dye encapsulated in an organically modified silicate (ormosil) sol-gel and drop-cast to an acetylated cellulose TLC plate. Arakawa et al developed a wearable sensor that could fluorometrically sense ethanol gas through an enzymatic reaction involving alcohol dehydrogenase (ADH). For this, ADH was immobilised on a commercially available hydrophilic form of polytetrafluoroethylene (H-PTFE) membrane using a polymer for entrapping the ADH which was synthesised in-house [124,170]. A bifurcated optical fibre probe, with one fibre for fluorescence detection surrounded by 35 fibres for ultraviolet excitation was also incorporated to enable continuous monitoring of ethanol over a 20 minute time period.

1.5.2.2. Optical sensing chemistry formulations and encapsulation

Many of the sensing chemistries employed in wearable optical biosensors for ISF, sweat and volatile emission from skin are simple pH indicator dyes, enzymes together with colorimetric substrates as well as intrinsic and extrinsic fluorescent dyes. Such dyes have been used to detect biomarkers in the different skin matrices including pH, potassium, chloride, sodium, lactate, glucose, uric acid, acetone, ammonia, ethanol, zinc, vitamin C, calcium and CO₂.

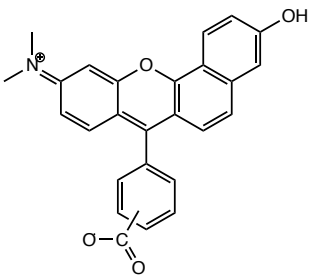
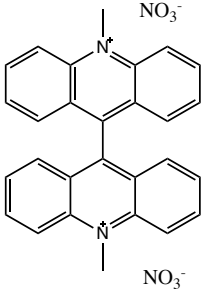
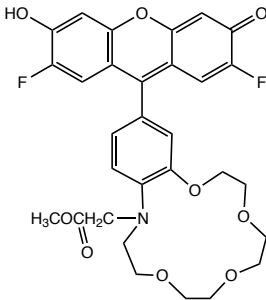
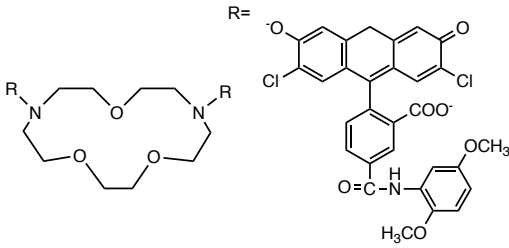
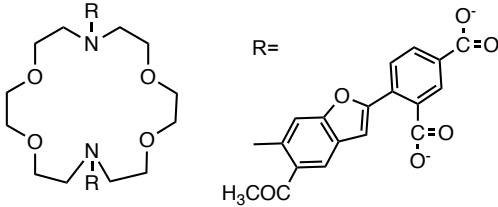
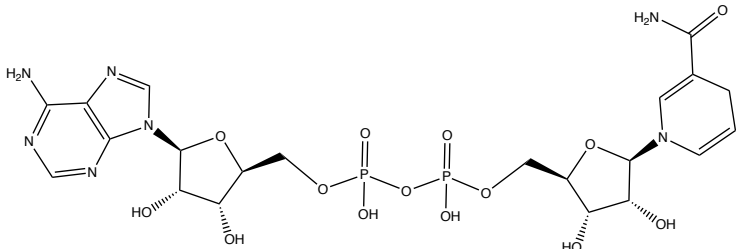
Both intrinsic and extrinsic fluorescent dyes have been used to sense biomarkers such as pH, sodium, potassium, chloride, zinc and ethanol. The normal physiological range for ISF pH is quite narrow, between 6.6-7.6 [188]. Reduced or increased ISF pH values can lead to metabolic acidosis or alkalosis, respectively. An intrinsic fluorophore, seminaphthorhodafluor, was used to measure ISF pH and has a pK_a of 7.5 and can sense pH changes between pH 7 and 8 which exhibit as pH-dependent emission shift from yellow/orange fluorescence under acidic conditions and deep red fluorescence under basic conditions. Selectivity of seminaphthorhodafluor dissolved in DI water for H⁺ ions was examined and results showed the emission intensity level was high in response to H⁺ ions compared to other ions. Responses were also noted for Zn²⁺ however, such ions are known to be in a concentration lower than 1 mM compared to H⁺ ions in ISF which are present in the μM range [189]. Other intrinsic fluorophores used include lucigenin for the detection of chloride in sweat and a fluorometric probe to sense zinc in sweat [122]. Normal physiological chloride sweat concentration ranges

from 20-60 mM [190] and here, the fluorescent intensity of lucigenin in response to 5-100 mM concentrations of chloride in an artificial sweat mix. High selectivity of the lucigenin sensor for chloride was demonstrated through exposure to a complex artificial sweat mix. Recently, a naturally intrinsic fluorescent probe, nicotinamide adenine dinucleotide (NADH), which emits fluorescence at 490 nm [124,170], was used to sense volatile ethanol emission from the ear using an over-ear gas collection cell and a gas-phase biosensor and showed the ability to sense within a wide dynamic range of 26 ppb-554 ppm which spans the typical physiological emission of ethanol after consuming alcohol which is ~148 ppb. An enzymatic reaction was employed where alcohol dehydrogenase (ADH) was used to catalyse the oxidation of ethanol to produce acetaldehyde while simultaneously an oxidized form of β -nicotinamide adenine dinucleotide (NAD^+), accepts the electron to become reduced (NADH), exhibiting autofluorescence, proportional to ethanol emission. This solution-based NADH intrinsic fluorescent probe showed high selectivity for ethanol compared to other VOCs that are released from skin such as acetone and acetaldehyde.

Extrinsic fluorescent probes in wearable sensors to date are more limited, however recent work shows their use within novel tattoo inks injected into the dermis for ISF sensing. Functionalised crown ethers are sensitive to monovalent electrolytes such as sodium and potassium and have been used for the detection of sodium and potassium in ISF [123]. Two fluorescein derivatives were linked to a crown ether to form a fluorescent diaza-15-crown-5 ether (cavity size:0.17-0.22 nm), capable of sodium detection within a physiological relevant range (132-142 mM). A high binding affinity of the sensor was observed for sodium compared to other ions commonly present in ISF such as Fe^{2+} and Fe^{3+} . Varying pH, however, modulated the emission, and therefore required measurement before processing the sensors response. For potassium sensing, two benzofuran isophthalate fluorophores connected to a diaza 18-crown-6 ether, which has a cavity size of 0.26-0.32 nm were used to bind potassium within a physiological relevant range from 2-6 mM. Similar to the sodium probe, other ions commonly present in ISF did not show any interference with potassium affinity, however, pH again showed interference.

Another extrinsic fluorescent probe for sodium sensing within a physiological relevant range (20-60 mM) [190], this time in sweat, is CoroNa green, comprised of fluorescein molecule linked to a crown ether with a specific cavity size that confers selectivity for the sodium ion.

Table 1.1. Structures of fluorescent dyes applied in wearable sensors.

<p>Seminaphthorhodafluor [123]</p> 	<p>Lucigenin [122]</p> 	<p>CoroNa Green [122]</p> 
<p>Fluorescent diaza-15-crown-5 ether [123]</p> 	<p>Fluorescent diaza-18-crown-6 ether [123]</p> 	
<p>Reduced nicotinamide adenine dinucleotide [124,170]</p> 		

Simple Brønsted acid/base dyes have also been employed for the detection of various biomarkers in skin biofluids and volatile emissions such as pH [146,154,172], calcium [191], ammonia [91,171,172], acetone [91] and CO₂ [91,192]. Brønsted acids or bases are pH dependent with protonation or deprotonation occurring as the pH environment changes, resulting in a change in the UV-Vis absorption spectra. A wide range of synthetically made organic chromophores have been used in wearable sensors including azo dyes, triphenylmethane dyes, phthalein and sulfophthalein dyes. For instance, the triphenylmethane dye, BCG has been used for pH sensing in ISF both in vitro in an artificial ISF solution and in vivo in mice, where BCG was dissolved in de-ionised water (DI) followed by drop-casting on

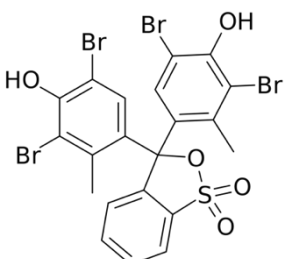
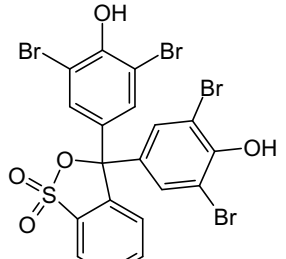
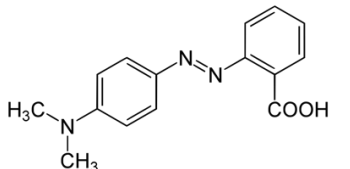
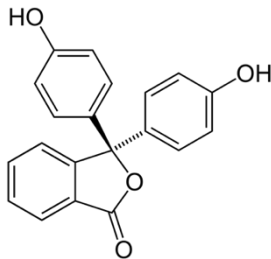
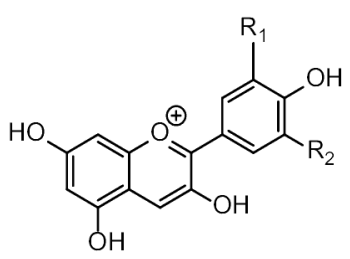
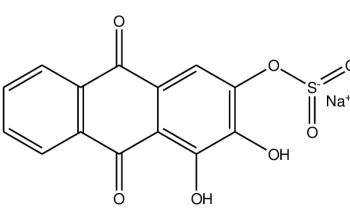
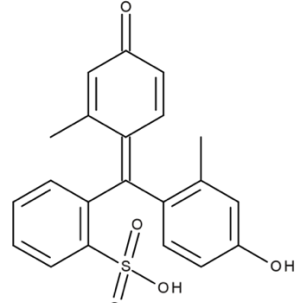
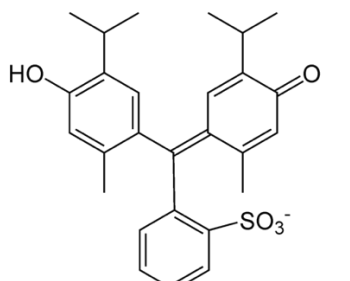
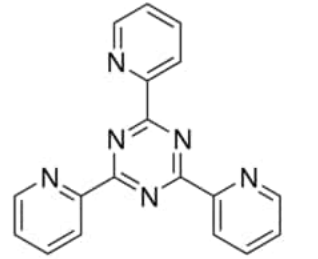
a nitrocellulose membrane [146]. ISF pH values from 5 to 8 can be sensed using BCG which spans the normal physiological pH range of ISF. Other groups have employed the use of a cocktail of azo-, sulfophthalein- and phthalein-based dyes dissolved in a DMSO/water solution for ISF pH sensing. Dye solutions were loaded onto a MN array and injected into the dermis via the MNs for ISF pH sensing with response being tracked in vitro artificial ISF solutions and also in vivo in rabbits using smartphone imaging and extraction of hue values to track colour changes of the dermis-entrapped dyes [136]. Yetisen et al also prepared a dye cocktail for the pH sensing of ISF for injection in the dermis using a tattoo gun. The formulation comprised chromogenic dyes dissolved in DI water [154]. 3',3'',5',5''-tetrachlorophenol-3,4,5,6-tetrabromosulfophthalein, a sulfophthalein-based dye was also employed to sense albumin. This albumin sensor was based on protein error of pH where functional groups form associates with the sulfophthalein-based dye and induce protonation or deprotonation in a colour shift from yellow to green [154,193]. Natural pH indicators such as anthocyanin, dissolved in water have also been used to monitor the pH of sweat [177] within the physiological range of 4.6-6.6 [194]. Although innovative, the use of these natural indicators is at an early stage but shows promise to move away from pH assays that use non-biocompatible reagents [139].

Triphenylmethane and sulfophthalein dyes have also been used in sensing of volatile emissions from the skin. For example, BCG encapsulated in an ormosil sol-gel as a sensor spot on acetylated cellulose substrate was employed for the determination of skin surface pH via the volatile ammonia emission from skin with a limit of detection (LOD) of 0.092 mg [172]. Sol-gel encapsulation promoted hydrophobicity which limited leaching of the dye and also limited the effects of humidity and sweating from the skin [195], a common challenge faced by wearable optical sensors for sensing skin volatiles in particular [91,170–172]. Another triphenylmethane dye, bromophenol blue [91] has also been used to sense the volatile ammonia emission from skin in a GCAS format. Similarly, alizarin red, an electroactive anthraquinone dye was used to sense volatile ammonia emission. This dye was dissolved in glycerol/methanol and drop-cast to cellulose filter paper. Similar to the ormosil sol-gel, owing to glycerol's hygroscopic properties, the glycerol/methanol solution was used to attempt to moderate any variation in humidity and sweating that might occur [171]. Acetone sensing has also been demonstrated in wearables using a hydroxylamine sulphate and thymol blue, a sulfophthalein dye, as a drop-cast film on a silica TLC plate. Acetone selectively reacts with hydroxylamine sulphate and the protons produced cause a colour change from yellow to pink in thymol blue.

In the same study, cresol purple was used for CO₂ sensing whereby interaction with CO₂ drives a change in the pH of the sensing environment giving rise to a colour change [91,196]. This study dissolved these dyes in water/methanol and water/ethanol which do not promote hydrophobicity. However a humidity sensor, cobalt chloride hexahydrate, was included on the array and is used to correct for the humidity effect and also used to detect skin hydration and perspiration [91]. This sensor shows that the humidity level in the headspace of the sensors above the skin becomes saturated and constant after being placed on the skin for 6 h. While sweating was not observed in this study due to the controlled laboratory environment, including controlled temperature and humidity, sweat is an issue for volatile analyte detection in real-world wear where these parameters cannot be controlled and so may interfere with sensor response. Response time is another challenge faced by wearable colorimetric sensors for sensing volatile emission mainly due to low concentrations (ppb) being emitted from skin [89]. Many colorimetric sensors require wear-times of up to 2 h to observe interaction between the analyte of interest and the sensor [91,172]. Further work needs to be carried out in order to increase sensitivity of these volatile sensors to reduce wear-time before they can become practically viable.

Chloride sensing in ISF and sweat using wearable optical sensors has been demonstrated and in one example has involved the use of silver chloranilate which complexes with chloride ions to generate a distinct purple colour [197]. The commercially available Gx Sweat Patch also uses silver chloranilate dye for the real-time monitoring of sweat Cl⁻ [84]. Silver chloranilate has also been employed in another microfluidic-based wearable for cystic fibrosis diagnosis based on sweat chloride concentration [197] where concentrations below 20 mM represent normal physiological concentration of chloride in sweat. Other detection mechanisms for chloride including the competitive binding of Hg²⁺ and Fe²⁺ with 2,4,6-tris(2-pyridyl)-s-triazine (TPTZ) where in the presence of chloride ions, Fe²⁺ binds with TPTZ and Hg²⁺ precipitates out and gives a colour change from transparent to blue [178,191].

Table 1.2. Structures of colorimetric dyes typically employed in wearable colorimetric sensors.

<p>Bromocresol green [52,146,172,191,198]</p> 	<p>Bromophenol blue [91,185,198]</p> 	<p>Methyl red [155]</p> 
<p>Phenolphthalein [155]</p> 	<p>Anthocyanin [177]</p> 	<p>Alizarin Red [171]</p> 
<p>Cresol purple [91]</p> 	<p>Thymol blue [91,155]</p> 	<p>TPTZ [178,191]</p> 

Many wearable optical sensors employ bio-catalysed reaction systems whereby an enzyme is used to catalyse a reaction which typically produces hydrogen peroxide (H_2O_2) which is then reduced using a peroxidase such as horseradish peroxidase (HRP) or more recently, via conducting polymer materials (polypyrrole nanoparticles) [148]. This redox product can then be optically detected through the use of colorimetric or fluorescent dyes which can be immobilised onto substrates or housed in reservoirs in bulk solution, such as TMB [147,149,154], 2,2'-azino-bis(3-ethylbenzothiazoline-6-sulfonic acid) (ABTS)[146], o-phenylenediamine (OPD) [146] and diazoaminobenzene (DAB). Dual enzyme sensing mechanisms have typically been used to detect glucose in both ISF [146,148,149,154,155] and sweat [159,161,178] in wearables. Glucose is oxidised by glucose oxidase to produce gluconic

acid and hydrogen peroxide and HRP is used to catalyse a reaction between H_2O_2 and a chromogen/fluorogen to give a visible colorimetric/fluorometric change. Many researchers [147,149,154] have utilised this dual enzyme based mechanism to detect glucose in ISF using TMB. TMB acts here as a hydrogen donor for the reduction of H_2O_2 to water by HRP. Koh et al used iodide (yellow) which is oxidized to iodine (brown) to detect the concentration of glucose in sweat following the oxidation of glucose to H_2O_2 by glucose oxidase, however this system has low sensitivity for low concentrations of glucose in sweat which could be associated with the reducing property of I^- which is easily oxidized when exposed to oxygen. A GOx-HRP-*o*-dianisidine system was employed by Xiao et al in order to detect glucose in sweat [159]. *o*-dianisidine is a redox indicator dye which is pH independent meaning changes in the sensing environments pH will not affect its response (Fig 1.12)). The *o*-dianisidine system allowed for detection of sweat glucose at concentrations below 0.1 mM. Similar dual sensing mechanisms have been employed for the sensing of lactate [146,160], uric acid [148,155] and cholesterol [146] using lactate oxidase, cholesterol oxidase and uricase, respectively. While enzymatic-based colorimetric sensors are frequently used in wearables, there are challenges including denaturation of enzymes during storage or long-term use and high sensitivity toward variations in pH and temperature. Some studies have employed mechanisms such as the biomineralization of HRP with a calcium phosphate shell to add a pH responsive feature which improves sensitivity and selectivity of the sensor [147].

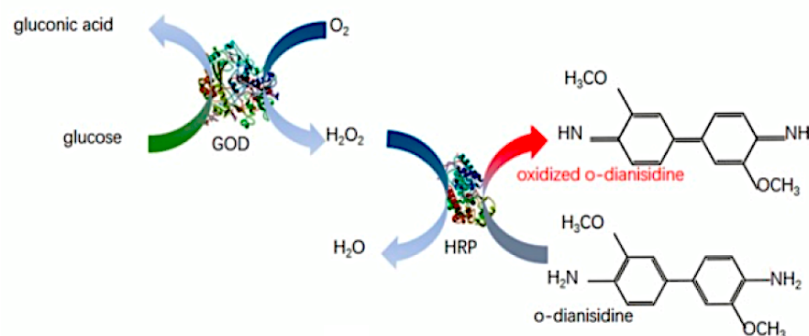


Figure 1.12. Schematic of Xiao et al's GOD-HRP-*o*-dianisidine system [159], which is typical of many dual enzyme sensing mechanisms employed in wearable optical sensors.

1.5.2.3. Integration of sensor chemistry into sensor platform

An important element of a wearable optical sensor is the integration of the sensing chemistry within the sensor platform. Typically, for biofluids such as ISF and sweat a wearable

optical sensor is comprised of a sampler that guides the biofluid toward an optical sensor capable of transducing a response to an analyte.

For ISF, MNs which are inserted into the dermis of the skin to extract ISF via capillary action are frequently employed as a sampler [146,147]. Extracted ISF is then transported through the MNs to the sensing material, which is typically paper or PVA-based and is immobilised with a colorimetric sensing reagent (Fig 1.9) [146,147,149]. Recently, dermal tattoo sensing mechanisms have also been employed where fluorometric or colorimetric dyes were injected directly into the dermis for ISF sensing using a tattoo gun [123,154,156] or MN arrays [155]. By injecting the sensing dye directly into the dermis it eliminates the need for extraction of ISF from the skin, thus simplifying the optical sensing process.

As discussed above, wearable optical sweat sensors frequently employ the use of soft, microfluidic architecture to capture and transport generated sweat toward reservoirs that contain fluorometric or colorimetric sensors in-solution [159,162,164,177–179] or immobilised on paper substrates [179] (Fig 1.10). Valving within microchannels been employed within these microfluidic sweat sensors in order to allow for time-sequenced analysis and to reduce assay-assay cross contamination in sensors with more than one sensing assay [181]. While bio-fouling from the skin or environmental contaminants poses a potential issue for these microfluidic-based optical sweat sensing platforms, their multi-layer construction and encapsulations of sensing dyes within these layers limit such a problem (Fig 1.10) [181]. Microfluidic thread/paper-based optical sensor have also been used to quantitatively monitor sweat glucose for example [160,185,186]. Here, plasma-treated hydrophilic cotton was used as a microchannel to transport generated sweat toward a paper-based colorimetric sensor to detect glucose through an enzymatic reaction discussed in section 1.5.2.1.

Other groups have moved away from microfluidic channels and have employed the use of other materials such as hydrogels [161,199,200] and Janus fabrics/paper-based platforms [187] to sample and sense biomarker in sweat from skin. Hydrogels have great hygroscopicity and can absorb sweat present on the skin's surface [201]. Colorimetric dyes are embedded with the hydrogel through solvent displacement thus obviating the need for microfluidic channels to route the sweat to particular reservoirs (Fig 1.11 (a)) [161]. Janus fabrics allow sweat sampling with no backflow as discussed in section 1.5.2.1. This allows the transfer of sweat to paper sensors where colorimetric sensing dyes are drop-cast on nitrocellulose membranes that have been attached to the surface of the Janus fabric using adhesive tape.

Sensing chemistries typically used for sensing volatile emissions from skin are frequently dissolved in DI water or other solutions that promote hydrophobicity such as sol-gels or glycerol/methanol solutions. Such solutions are then drop-cast on paper-based substrates such as silica or cellulose TLC plates [91,171,172]. The nature of volatile emissions from skin obviates the need MN extraction of microfluidic manipulation associated with ISF and sweat.

As volatile emissions are passively, continuously emitted from skin and optical volatile sensors typically incorporate a chamber which allows volatiles to accumulate and reach the sensor (Fig 1.8). One of the main challenges associated with volatile emission is their trace emission from skin thus accumulation in the sensor headspace is required for effective sensing. Typically, preconcentration of volatile emissions is employed during sampling prior to analysis, however this has proved challenging in the optical volatile sensing space. GCAS was developed in an attempt to overcome this. Porous GCAS sensing channels serve as a preconcentrating column to accumulate volatile emission over time. Here, transdermal volatile biomarkers diffuse into each gradient channel from the opening, causing localised colour development thus improving the sensitivity of the sensor (Fig 1.13) [91].

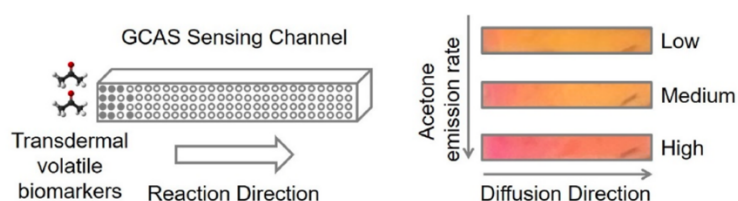


Figure 1.13. Schematic illustrating how volatile emissions enter and diffuse through the GCAS sensing channels and how different emission rates cause different localised colour development [91].

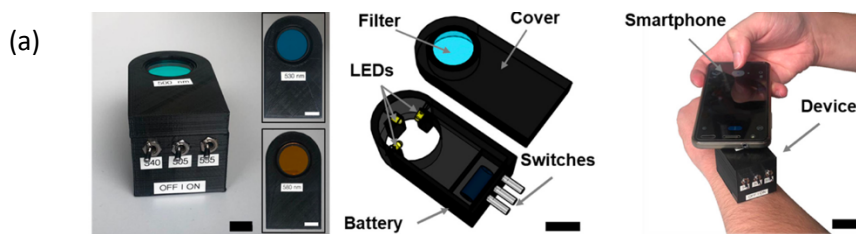
1.5.3. Transduction in optical wearable sensors

1.5.3.1. Imaging

Taking advantage of the rapid development in digital imaging technology, many methods have been employed for the imaging of wearable optical sensors including the use of flatbed scanners, digital cameras and smartphone cameras. The imaging method should provide high resolution images that can be analysed easily. One of the main challenges to overcome is changes in lighting during imaging which distort colour and hence analytical responses. Imaging of wearable fluorometric sensor spots requires excitation and emission filters to allow a standard camera/smartphone take fluorescence images, which adds complexity but has been

demonstrated [122,123]. Flatbed scanners allow for high resolution images with constant illumination to be obtained and eliminates ambient light. Our group have employed a scanner to obtain images of colorimetric sensor spots before and after wearing for measuring ammonia fluxes from skin [52,172]. Other studies have also employed scanners to image colour changes for transdermal ISF glucose sensing MN patch [147]. However, this scanner-based imaging modality is offline and does not offer continuous, real-time imaging. Currently, we are striving toward the development of a wearable device, that will incorporate an ESP-Wi-Fi enabled camera, capable of real-time imaging while on skin which will further enhance the sensors deployability and potential use.

Continuous, real-time imaging of sensor response throughout wear on the skin is highly desirable, with some studies having realised this using smartphone cameras. For example, wearable fluorescent sensors have been imaged using smartphones and portable readout devices [122,123], which block out ambient light to minimise photobleaching and are comprised of an excitation light source for excitation of the fluorescent dye coupled with bandpass emission filters that allow specific wavelength bands of interest to pass while blocking others. For example, Jiang et al's fluorescent dermal tattoo biosensors sense pH, Na⁺ and K⁺ ions in ISF [123], using a smartphone coupled with a portable readout device employing LEDs with specific excitation wavelengths and bandpass optical filters to allow for continuous, real-time imaging. For pH sensing, an LED with a wavelength of 505 nm for excitation coupled with a bandpass filter with a centre wavelength of 580 nm was fitted into a dark-light-shielded box and a smartphone was used to capture images of the fluorescent sensor. Sekine et al used a similar imaging modality to obtain images of their fluorescent sensors to detect sweat chloride, sodium and zinc. A smartphone fitted with an optical module consisted of excitation LED and excitation filters (excitation wavelength range = 400-530 nm) and emission filters fitted within a dark box was worn on skin to obtain fluorescence images [122].



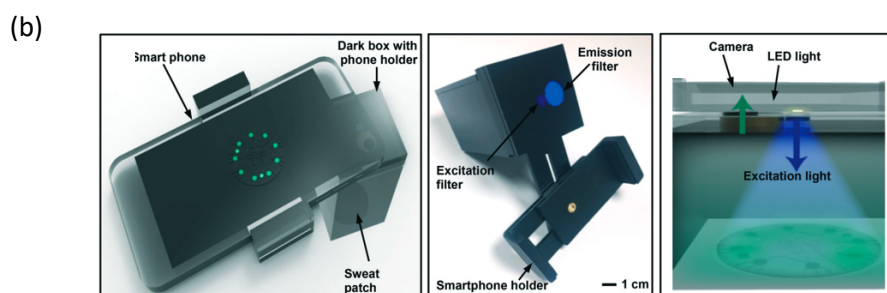


Figure 1.14. (a) Jiang et al.’s portable readout device in combination with a smartphone for obtaining fluorescence images [123] and (b) Sekine et al’s smartphone fitted optical module consisting of excitation and emission filters [122].

Many of the colorimetric sensors for ISF, sweat and volatile emission from skin utilise digital cameras [171] or smartphone cameras in order to take continuous, real-time images [187]. He et al used a smartphone camera to take images of the colorimetric reagents present in the dermis of the skin for further semi-qualitative analysis after insertion using their microneedle patch [155]. You et al also used a smartphone to obtain images of the glucose paper sensor on their MN/paper based glucose sensor after insertion into the skin of mice [175]. Again, a smartphone was used to capture images every few minutes of Liu et al’s soft, degradable microfluidic device capable of sensing pH and chloride concentration in sweat [177]. The now commercially available Gx Sweat Patch also employs a smartphone to image the sensor for real-time assessment of total sweat loss and chloride concentration in sweat [183]. In terms of sensing the volatile emission from skin, Yu et al have developed both “offline” and “online” imaging modalities for the detection of transdermal gases from skin. The “offline” method (Fig 1.8 (a)) employs the use of a smartphone to image the acetone, ammonia and CO₂ sensor. This “offline” method of imaging can be sensitive to changes in light conditions and so an “online” imaging device (Fig 1.8 (b)) was devised where the sensor chamber was fitted with a white LED in order to illuminate the GCAS sensor chip and webcam to allow for continuous, real-time imaging of the GCAS [91].

1.5.3.2. Image analysis techniques

While optical sensor responses at visible wavelengths can be clearly distinguished by the naked eye, there are many deficiencies with this technique including poor ambient light and person-to-person perceptual differences. Therefore, following the acquisition of images of optical sensors after exposure to skin, it is paramount that a suitable image analysis techniques are used to ensure robust and reproducible quantification of sensor response. To do so a visible

colour space, which is an abstract mathematical representation that defines the spectrum of colours that can be perceived by the human eye, can be used. Software such as ImageJ, Python and MATLAB are commonly used [125]. Moreover, bespoke smartphone apps, with custom-written algorithms for the analysis of specific optical sensors have been developed [123,178], e.g. for the Gx Sweat Patch [84,183].

For image analysis, the red, green and blue (RGB) colour scheme is the most widely used. A tuple is used to represent each distinct colour in RGB models, which are additive tristimulus systems. More specifically, the RGB colour space is made up of three colours: red, green, and blue. You et al obtained an image of their ISF glucose sensor before and after exposure to ISF and analysed the images in Python [175]. Here, RGB values were determined before and after exposure and the response was quantified in terms of a change in colour intensity between the before and after images. Many other studies analysing biomarkers in ISF have employed the use of imaging processing software such as ImageJ to extract the RGB values from their sensor response images [146,149]. Xi et al also recorded images of their smart Janus fabric sensors capable of detecting pH, chloride and urea in sweat using a smartphone and employed an open-source analytical app to extract the RGB colours from each image. Percentage of each colour channel was then calculated and this was used to quantify the response from the sensors [187]. Wang et al also analysed RGB values of their hydrogel-based sweat patch using a commercially available smartphone application called Colour Recogniser. Similar to Xi et al, the percentage R, G and B values were calculated and standard calibration curves were constructed here for physiological concentrations of sweat pH, glucose, chloride and calcium and were used as references for specific responses observed when worn on skin [161]. Our group have also employed the RGB colour space for the analysis of our volatile skin surface pH/ammonia sensor. Absolute R, G and B values were measured before and after sensor exposure to the skin. The sensor spot response was then quantified using the colour distance measurement Euclidean Distance (ED) [172].

Other studies employ different colour spaces such as HSB and $L^*a^*b^*$. The hue component of the HSB colour space is frequently employed and is commonly used for bitonal transitions and is robust against small changes in lighting which can affect image analysis [125]. He et al employed the use of hue for the analysis of colour changes in their dermal tattoo biosensors which senses glucose, uric acid, pH and temperature in ISF [155].

In 1976, the international commission on illumination (CIE) converted the RGB colour model to a new model that better captures the numerical relationship between wavelengths and

the human physiological reaction to observed colour or colour changes. This new colour space, called $L^*a^*b^*$, is now regarded as the most accurate representation of human colour perception. $L^*a^*b^*$ divides the image into a single luminescence channel and two colour difference channels, where L defines the whiteness or blackness of a pixel and A and B are colour difference channels that specify the chrominance of each pixel [125]. Many wearable optical sensors have employed the use of $L^*a^*b^*$ to analyse sensor response. Most recently, Liu et al employed $L^*a^*b^*$ to quantify the sensor response from their sweat pH and chloride sensor [177]. In comparison to the RGB colour space, the $L^*a^*b^*$ colour model provides enhanced reliability in real-world scenarios where lighting intensity cannot be well controlled. In contrast to other studies where only the chromatic colours, a^* and b^* were only assessed [197], here, the pure white background of the sensor serves as a reference background to account for the effect of overall lightness (L^*) which can affect colour associated with different biomarkers. Similar to our study, a distance measurement allowed capturing of the change in both the chromatic colours and lightness. Moreover, the use of $L^*a^*b^*$ can also allow for device-independent analysis [197]. Ikeda et al also used the $L^*a^*b^*$ colour model for quantification of sensor spot response on their volatile ammonia sensor [171]. This colorimetric sensor changes from yellow to red upon interaction with ammonia emission from skin and here, $L^*a^*b^*$ values of uncoloured (yellow) and coloured (red) parts of the sensor were obtained using a ColorMeter RGB colorimeter as the analysis software. Again, a distance measurement was employed to quantify the change between before and after exposure to ammonia. A pre-calculated calibration curve was also constructed here and assists with the calculation of ammonia emission flux from the skin, similar to Wang et al's hydrogel-based sweat sensor study.

Much of the research in this field employs the use of a calibration curve in order to be able to accurately compare and quantify sensor response after wear on the body. Typically, for sweat analysis the sensor is exposed to artificial sweat comprised of differing concentrations of biomarkers of interest and the response quantified and constructed as a calibration curve. For volatile optical sensors, the sensor is exposed to a headspace of known volume with a known concentration of the analyte present, the response is quantified and a calibration curve constructed [171,172].

In order to further improve interferences from changes in ambient lighting and further improve accurate analysis of responses, many studies have employed the use of integrated references into the optical sensor platform. For example, Sekine et al integrated a stable

fluorescence dye reference, rhodamine chloride, which has an excitation wavelength close the fluoroprobes used, into their fluorescent, microfluidic sweat chloride, sodium and zinc detection platform. Here, the fluorescent intensity of each reservoir was analysed using ImageJ software and was then normalised by the intensity of the reference probe (Fig 1.15 (a)) [122]. Kim et al also integrated colour reference markers on their microfluidic device for nutrient detection in sweat which further reduce the interferences from ambient light. These colour reference markers were constructed by exposing the sensors to standard nutrients and artificial sweat solutions, imaging the sensors and then laser-printing the reference markers on polyester adhesive films (Fig 1.15 (b)) [162]. Similarly, Yu et al incorporates black marker lines onto their GCAS for volatile sensing of transdermal gases. The black marker again is employed in order to compensate any variation that can arise due to variable lighting conditions when taking an image with a smartphone (Fig 1.15 (c)) [91].

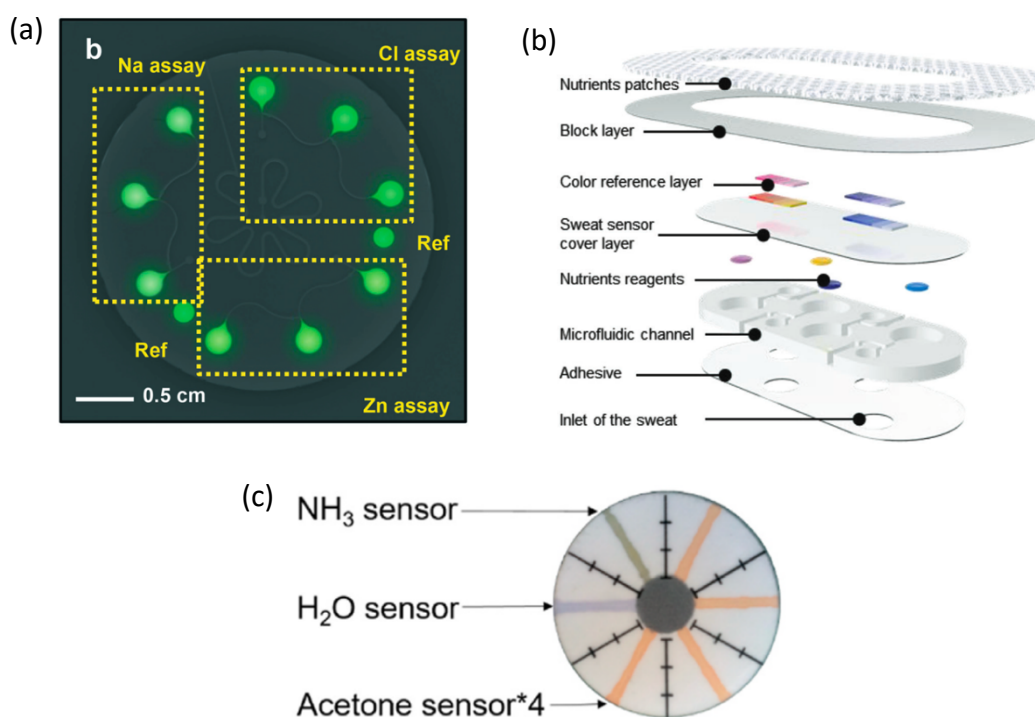


Figure 1.15. (a) Fluorescent sensor showing the fluorescent signal associated with chloride, sodium, zinc probes along with a rhodamine chloride reference [122], (b) schematic showing the different components of a miniaturized sweat microfluidic device with colour reference markers [162] and (c) CGAS with printed marker lines for improving image analysis [91].

1.6. Conclusion

With the skin being the largest organ of the body, it has great biodiagnostic potential. Skin matrices such as ISF, sweat and the volatile emission can potentially give insight into subcutaneous and systemic biochemistry. These matrices offer an alternative, less invasive means of monitoring human health and well-being compared to the traditional methods such as biopsies and intravenous blood sampling. Accessibility of such matrices have given rise to the development and fabrication of many wearable sensors capable of detecting and monitoring biomarkers in skin matrices. Sensors capable of optical transduction through fluorometric or colorimetric sensing have recently gained traction as an alternative to wearable sensors that utilise electrochemical transduction. ISF optical sensing typically employ the use of MNs and capillary force to extract ISF followed by sensing using a paper or PVA detection layer immobilised with various sensing chemistries. Tattoo sensing mechanisms whereby the sensing chemistry is directly injected into the dermis have also emerged as an innovative method for biomarker detection in ISF, however are at an early stage. Fluorometric and colorimetric-based sensors have also frequently been employed for the detection of biomarkers in sweat, typically using microfluidic architecture to guide sweat toward the sensing chemistries with the Gx Sweat Patch being the first of its kind to be commercialised. Volatile emission from skin has recently gained traction in the scientific community due to its ability to be passively sampled unlike ISF which needs to be extracted and sweat which needs to be generated, typically through exercise. Development of optical sensor for the detection of biomarkers in this volatile emission have been limited with ammonia, acetone and ethanol sensors recently been demonstrated. Sampling time and sensitivity are the main challenges facing wearable optical volatile sensors owing to the trace quantities of volatiles emitted from skin and enhanced sensitivity is required in order to reduce wear-time.

Overall, great strides have recently been made in the biofluids and volatile emission wearable optical sensor field recently, however, there are still many challenges that need to be met in order to develop robust, reliable wearables that can be easily extract or sample and reliably sense biomarkers in ISF, sweat and volatile emission. Despite these challenges, there is still great potential for the use of wearable optical sensors for personalised monitoring of general health and self-management of chronic diseases associated with biomarkers in ISF, sweat and volatile emission.

1.7. References

- [1] Kolarsick P A J, Kolarsick M A and Goodwin C Anatomy and Physiology of the Skin *SKIN CANCER* 12
- [2] Benson H A E 2011 Skin Structure, Function, and Permeation *Topical and Transdermal Drug Delivery* (John Wiley & Sons, Ltd) pp 1–22
- [3] Heikenfeld J, Jajack A, Rogers J, Gutruf P, Tian L, Pan T, Li R, Khine M, Kim J, Wang J and Kim J 2018 Wearable sensors: modalities, challenges, and prospects *Lab Chip* **18** 217–48
- [4] Jina A, Tierney M J, Tamada J A, McGill S, Desai S, Chua B, Chang A and Christiansen M 2014 Design, development, and evaluation of a novel microneedle array-based continuous glucose monitor *J Diabetes Sci Technol* **8** 483–7
- [5] Baker L B, Stofan J R, Hamilton A A and Horswill C A 2009 Comparison of regional patch collection vs. whole body washdown for measuring sweat sodium and potassium loss during exercise *Journal of Applied Physiology* **107** 887–95
- [6] Drislane C and Irvine A D 2020 The role of filaggrin in atopic dermatitis and allergic disease *Annals of Allergy, Asthma & Immunology* **124** 36–43
- [7] Honari G and Maibach H 2014 Chapter 1 - Skin Structure and Function *Applied Dermatotoxicology* ed H Maibach and G Honari (Boston: Academic Press) pp 1–10
- [8] Proksch E, Brandner J M and Jensen J-M 2008 The skin: an indispensable barrier *Experimental Dermatology* **17** 1063–72
- [9] Arens E A and Zhang H The Skin's Role in Human Thermoregulation and Comfort 51
- [10] Weller R P J B, Hunter H J A and Mann M W 2015 *Clinical dermatology* (Chichester, West Sussex ; Hoboken, NJ: John Wiley & Sons Inc)
- [11] Ishitsuka Y, Ogawa T and Roop D 2020 The KEAP1/NRF2 Signaling Pathway in Keratinization *Antioxidants (Basel)* **9** 751
- [12] Webb A, Li A and Kaur P 2004 Location and phenotype of human adult keratinocyte stem cells of the skin *Differentiation* **72** 387–95
- [13] Wickett R R and Visscher M O 2006 Structure and function of the epidermal barrier *American Journal of Infection Control* **34** S98–110
- [14] Cork M J, Danby S G, Vasilopoulos Y, Hadgraft J, Lane M E, Moustafa M, Guy R H, MacGowan A L, Tazi-Ahnini R and Ward S J 2009 Epidermal Barrier Dysfunction in Atopic Dermatitis *Journal of Investigative Dermatology* **129** 1892–908
- [15] T K, A M-F and A M 2011 Stratum corneum hydration and skin surface pH in patients with atopic dermatitis. *Acta Dermatovenerol Croat* **19** 242–7
- [16] Tagami H 2014 Electrical measurement of the hydration state of the skin surface in vivo *British Journal of Dermatology* **171** 29–33

- [17] Danby S G and Cork M J 2018 pH in Atopic Dermatitis *pH of the Skin: Issues and Challenges* **54** 95–107
- [18] Duffy E, Jacobs M R, Kirby B and Morrin A 2017 Probing skin physiology through the volatile footprint: Discriminating volatile emissions before and after acute barrier disruption *Experimental Dermatology* **26** 919–25
- [19] Baker L B 2019 Physiology of sweat gland function: The roles of sweating and sweat composition in human health *Temperature (Austin)* **6** 211–59
- [20] Tagami H 2008 Location-related differences in structure and function of the stratum corneum with special emphasis on those of the facial skin *International Journal of Cosmetic Science* **30** 413–34
- [21] Sato K 1977 The physiology, pharmacology, and biochemistry of the eccrine sweat gland *Rev Physiol Biochem Pharmacol* **79** 51–131
- [22] Cui C-Y and Schlessinger D 2015 Eccrine sweat gland development and sweat secretion *Exp Dermatol* **24** 644–50
- [23] Taylor N A and Machado-Moreira C A 2013 Regional variations in transepidermal water loss, eccrine sweat gland density, sweat secretion rates and electrolyte composition in resting and exercising humans *Extrem Physiol Med* **2** 4
- [24] Baker L B, Ungaro C T, Sopena B C, Nuccio R P, Reimel A J, Carter J M, Stofan J R and Barnes K A 2018 Body map of regional vs. whole body sweating rate and sweat electrolyte concentrations in men and women during moderate exercise-heat stress *J Appl Physiol (1985)* **124** 1304–18
- [25] Baker L B, Barnes K A, Anderson M L, Passe D H and Stofan J R 2016 Normative data for regional sweat sodium concentration and whole-body sweating rate in athletes *J Sports Sci* **34** 358–68
- [26] Buono M J, Lee N V L and Miller P W 2010 The relationship between exercise intensity and the sweat lactate excretion rate *J Physiol Sci* **60** 103–7
- [27] Moyer J, Wilson D, Finkelshtein I, Wong B and Potts R 2012 Correlation Between Sweat Glucose and Blood Glucose in Subjects with Diabetes *Diabetes Technology & Therapeutics* **14** 398–402
- [28] Alvear-Ordenes I, García-López D, de paz jose antonio and González-Gallego J 2005 Sweat Lactate, Ammonia, and Urea in Rugby Players *International journal of sports medicine* **26** 632–7
- [29] Weiner J S and Hellmann K 1960 The Sweat Glands *Biological Reviews* **35** 141–86
- [30] Murphrey M B, Safadi A O and Vaidya T 2021 *Histology, Apocrine Gland* (StatPearls Publishing)
- [31] Montagna W and Parakkal P F 1974 *The structure and function of skin* (New York: Academic Press)

- [32] Sato K, Leidal R and Sato F 1987 Morphology and development of an apoeccrine sweat gland in human axillae *American Journal of Physiology-Regulatory, Integrative and Comparative Physiology* **252** R166–80
- [33] Hoover E, Aslam S and Krishnamurthy K 2021 *Physiology, Sebaceous Glands* (StatPearls Publishing)
- [34] Shamloul G and Khachemoune A 2021 An updated review of the sebaceous gland and its role in health and diseases Part 1: Embryology, evolution, structure, and function of sebaceous glands *Dermatologic Therapy* **34** e14695
- [35] Pappas A, Johnsen S, Liu J-C and Eisinger M 2009 Sebum analysis of individuals with and without acne *Dermatoendocrinol* **1** 157–61
- [36] Zouboulis C C 2004 Acne and sebaceous gland function *Clinics in Dermatology* **22** 360–6
- [37] Grice E A and Segre J A 2011 The skin microbiome *Nature Reviews Microbiology* **9** 244–53
- [38] Byrd A L, Belkaid Y and Segre J A 2018 The human skin microbiome *Nature Reviews Microbiology* **16** 143–55
- [39] Grice E A, Kong H H, Conlan S, Deming C B, Davis J, Young A C, Bouffard G G, Blakesley R W, Murray P R, Green E D, Turner M L and Segre J A 2009 Topographical and Temporal Diversity of the Human Skin Microbiome *Science* **324** 1190–2
- [40] Schommer N N and Gallo R L 2013 Structure and function of the human skin microbiome *Trends in Microbiology* **21** 660–8
- [41] Lomholt H B and Kilian M 2010 Population Genetic Analysis of Propionibacterium acnes Identifies a Subpopulation and Epidemic Clones Associated with Acne *PLOS ONE* **5** e12277
- [42] Boxberger M, Cenizo V, Cassir N and La Scola B 2021 Challenges in exploring and manipulating the human skin microbiome *Microbiome* **9** 125
- [43] Verbanic S, Kim C Y, Deacon J M and Chen I A 2019 Improved single-swab sample preparation for recovering bacterial and phage DNA from human skin and wound microbiomes *BMC Microbiology* **19** 214
- [44] du Plessis J L, Stefaniak A B and Wilhelm K-P 2018 Measurement of Skin Surface pH *Current Problems in Dermatology* vol 54, ed C Surber, C Abels and H Maibach (S. Karger AG) pp 19–25
- [45] Rippke F, Schreiner V and Schwanitz H-J 2002 The Acidic Milieu of the Horny Layer *American Journal of Clinical Dermatology* **3** 261–72
- [46] Fluhr J W, Kao J, Ahn S K, Feingold K R, Elias P M and Jain M 2001 Generation of Free Fatty Acids from Phospholipids Regulates Stratum Corneum Acidification and Integrity *Journal of Investigative Dermatology* **117** 44–51

- [47] Boer M, Duchnik E, Maleszka R and Marchlewicz M 2016 Structural and biophysical characteristics of human skin in maintaining proper epidermal barrier function *Postepy Dermatol Alergol* **33** 1–5
- [48] Ludovici M, Kozul N, Materazzi S, Risoluti R, Picardo M and Camera E 2018 Influence of the sebaceous gland density on the stratum corneum lipidome *Scientific Reports* **8** 11500
- [49] Freinkel R K and Shen Y 1969 The origin of free fatty acids in sebum. II. Assay of the lipases of the cutaneous bacteria and effects of pH *Journal of Investigative Dermatology* **53** 422–7
- [50] Elias P M 2015 Stratum corneum acidification: how and why? *Exp Dermatol* **24** 179–80
- [51] Proksch E 2018 pH in nature, humans and skin *The Journal of Dermatology* **45** 1044–52
- [52] Shetewi T, Finnegan M, Fitzgerald S, Xu S, Duffy E and Morrin A 2021 Investigation of the relationship between skin-emitted volatile fatty acids and skin surface acidity in healthy participants – a pilot study *Journal of Breath Research* **15** 037101
- [53] Heikenfeld J, Jajack A, Feldman B, Granger S W, Gaitonde S, Begtrup G and Katchman B A 2019 Accessing analytes in biofluids for peripheral biochemical monitoring *Nat Biotechnol* **37** 407–19
- [54] Aukland K and Nicolaysen G 1981 Interstitial fluid volume: local regulatory mechanisms. *Physiological Reviews* **61** 556–643
- [55] Venugopal M, Arya S K, Chornokur G and Bhansali S 2011 A realtime and continuous assessment of cortisol in ISF using electrochemical impedance spectroscopy *Sensors and Actuators A: Physical* **172** 154–60
- [56] Bollella P, Sharma S, Cass A E G and Antiochia R 2019 Minimally-invasive Microneedle-based Biosensor Array for Simultaneous Lactate and Glucose Monitoring in Artificial Interstitial Fluid *Electroanalysis* **31** 374–82
- [57] Bollella P, Sharma S, Cass A E G and Antiochia R 2019 Microneedle-based biosensor for minimally-invasive lactate detection *Biosensors and Bioelectronics* **123** 152–9
- [58] Samant P P, Niedzwiecki M M, Raviele N, Tran V, Mena-Lapaix J, Walker D I, Felner E I, Jones D P, Miller G W and Prausnitz M R 2020 Sampling interstitial fluid from human skin using a microneedle patch *Science Translational Medicine* **12**
- [59] Parrilla M, Cuartero M, Padrell Sánchez S, Rajabi M, Roxhed N, Niklaus F and Crespo G A 2019 Wearable All-Solid-State Potentiometric Microneedle Patch for Intradermal Potassium Detection *Anal. Chem.* **91** 1578–86
- [60] Friedel M, Thompson I A P, Kasting G, Polsky R, Cunningham D, Soh H T and Heikenfeld J 2023 Opportunities and challenges in the diagnostic utility of dermal interstitial fluid *Nat. Biomed. Eng* 1–15

- [61] Fogh-Andersen N, Altura B M, Altura B T and Siggaard-Andersen O 1995 Composition of interstitial fluid *Clin Chem* **41** 1522–5
- [62] Juvenile Diabetes Research Foundation Continuous Glucose Monitoring Study Group 2010 Variation of Interstitial Glucose Measurements Assessed by Continuous Glucose Monitors in Healthy, Nondiabetic Individuals *Diabetes Care* **33** 1297–9
- [63] Bruen D, Delaney C, Florea L and Diamond D 2017 Glucose Sensing for Diabetes Monitoring: Recent Developments *Sensors* **17** 1866
- [64] Hakala T A, Zschaechner L K, Vänskä R T, Nurminen T A, Wardale M, Morina J, Boeva Z A, Saukkonen R, Alakoskela J-M, Pettersson-Fernholm K, Hægström E, Bobacka J and García Pérez A 2022 Pilot study in human healthy volunteers on the use of magnetohydrodynamics in needle-free continuous glucose monitoring *Sci Rep* **12** 18318
- [65] Cengiz E and Tamborlane W V 2009 A Tale of Two Compartments: Interstitial Versus Blood Glucose Monitoring *Diabetes Technology & Therapeutics* **11** S-11
- [66] Dye L, Mansfield M, Lasikiewicz N, Mahawish L, Schnell R, Talbot D, Chauhan H, Croden F and Lawton C 2010 Correspondence of continuous interstitial glucose measurement against arterialised and capillary glucose following an oral glucose tolerance test in healthy volunteers *British Journal of Nutrition* **103** 134–40
- [67] Al Hayek A A, Robert A A and Al Dawish M A 2019 Differences of FreeStyle Libre Flash Glucose Monitoring System and Finger Pricks on Clinical Characteristics and Glucose Monitoring Satisfactions in Type 1 Diabetes Using Insulin Pump *Clin Med Insights Endocrinol Diabetes* **12** 1179551419861102
- [68] Spehar-Délèze A-M, Anastasova S and Vadgama P 2021 Monitoring of Lactate in Interstitial Fluid, Saliva and Sweat by Electrochemical Biosensor: The Uncertainties of Biological Interpretation *Chemosensors* **9** 195
- [69] Casa D J, Chevront S N, Galloway S D and Shirreffs S M 2019 Fluid Needs for Training, Competition, and Recovery in Track-and-Field Athletes *International Journal of Sport Nutrition and Exercise Metabolism* **29** 175–80
- [70] Watabe A, Sugawara T, Kikuchi K, Yamasaki K, Sakai S and Aiba S 2013 Sweat constitutes several natural moisturizing factors, lactate, urea, sodium, and potassium *Journal of Dermatological Science* **72** 177–82
- [71] Crinnion W J 2011 Sauna as a valuable clinical tool for cardiovascular, autoimmune, toxicant- induced and other chronic health problems *Altern Med Rev* **16** 215–25
- [72] J M, D W, I F, B W and R P 2012 Correlation between sweat glucose and blood glucose in subjects with diabetes *Diabetes technology & therapeutics* **14**
- [73] Derbyshire P J, Barr H, Davis F and Higson S P J 2012 Lactate in human sweat: a critical review of research to the present day *J Physiol Sci* **62** 429–40

- [74] Pirovano P, Dorrian M, Shinde A, Donohoe A, Brady A J, Moyna N M, Wallace G, Diamond D and McCaul M 2020 A wearable sensor for the detection of sodium and potassium in human sweat during exercise *Talanta* **219** 121145
- [75] Yoon J, Lee D, Lee E, Sim M, Oh T-S, Yoon Y S and Kim D-J 2019 Noninvasive Urea Monitoring Using a Flexible Electrochemical Sweat Based Sensor *Meet. Abstr.* **MA2019-02** 2241
- [76] Cheng C, Li X, Xu G, Lu Y, Low S S, Liu G, Zhu L, Li C and Liu Q 2021 Battery-free, wireless, and flexible electrochemical patch for in situ analysis of sweat cortisol via near field communication *Biosensors and Bioelectronics* **172** 112782
- [77] Curto V F, Coyle S, Byrne R, Diamond D and Benito-Lopez F 2011 Real-Time Sweat Analysis: Concept and Development of an Autonomous Wearable Micro-Fluidic Platform *Procedia Engineering* **25** 1561–4
- [78] Yuan X, Li C, Yin X, Yang Y, Ji B, Niu Y and Ren L 2023 Epidermal Wearable Biosensors for Monitoring Biomarkers of Chronic Disease in Sweat *Biosensors* **13** 313
- [79] Heikenfeld J 2016 Non-invasive Analyte Access and Sensing through Eccrine Sweat: Challenges and Outlook circa 2016 *Electroanalysis* **28** 1242–9
- [80] Sato K, Kang W H, Saga K and Sato K T 1989 Biology of sweat glands and their disorders. I. Normal sweat gland function *Journal of the American Academy of Dermatology* **20** 537–63
- [81] Green J M, Bishop P A, Muir I H, Jr J R M and Heath H E 2000 Effects of High and Low Blood Lactate Concentrations on Sweat Lactate Response *Int J Sports Med* **21** 556–60
- [82] Di Sant'agnese P A, Darling R C, Perera G A and Shea E 1953 Abnormal electrolyte composition of sweat in cystic fibrosis of the pancreas; clinical significance and relationship to the disease *Pediatrics* **12** 549–63
- [83] Gahm N and Shwachman H 1956 Studies in cystic fibrosis of the pancreas; a simple test for the detection of excessive chloride on the skin *N Engl J Med* **255** 999–1001
- [84] Baker L B, Model J B, Barnes K A, Anderson M L, Lee S P, Lee K A, Brown S D, Reimel A J, Roberts T J, Nuccio R P, Bonsignore J L, Ungaro C T, Carter J M, Li W, Seib M S, Reeder J T, Aranyosi A J, Rogers J A and Ghaffari R 2020 Skin-interfaced microfluidic system with personalized sweating rate and sweat chloride analytics for sports science applications *Science Advances* **6** eabe3929
- [85] Gonzalez R R, Chevront S N, Montain S J, Goodman D A, Blanchard L A, Berglund L G and Sawka M N 2009 Expanded prediction equations of human sweat loss and water needs *Journal of Applied Physiology* **107** 379–88
- [86] Maughan R J and Shirreffs S M 2010 Dehydration and rehydration in competitive sport *Scandinavian Journal of Medicine & Science in Sports* **20** 40–7
- [87] Shirasu M and Touhara K 2011 The scent of disease: volatile organic compounds of the human body related to disease and disorder *J Biochem* **150** 257–66

- [88] Drabińska N, Flynn C, Ratcliffe N, Belluomo I, Myridakis A, Gould O, Fois M, Smart A, Devine T and Costello B D L 2021 A literature survey of all volatiles from healthy human breath and bodily fluids: the human volatilome *Journal of Breath Research* **15** 034001
- [89] Mochalski P, King J, Unterkofler K, Hinterhuber H and Amann A 2014 Emission rates of selected volatile organic compounds from skin of healthy volunteers *Journal of Chromatography B* **959** 62–70
- [90] Saasa V, Beukes M, Lemmer Y and Mwakikunga B 2019 Blood Ketone Bodies and Breath Acetone Analysis and Their Correlations in Type 2 Diabetes Mellitus *Diagnostics (Basel)* **9** 224
- [91] Yu J, Wang D, Tipparaju V V, Jung W and Xian X 2022 Detection of transdermal biomarkers using gradient-based colorimetric array sensor *Biosensors and Bioelectronics* **195** 113650
- [92] Yokokawa T, Sato T, Suzuki S, Oikawa M, Yoshihisa A, Kobayashi A, Yamaki T, Kunii H, Nakazato K, Ishida T and Takeishi Y 2018 Feasibility of skin acetone analysis in patients with cardiovascular diseases *Fukushima Journal of Medical Science* **64** 60–3
- [93] Peters R, Veenstra R, Heutinck K, Baas A, Munniks S and Knotter J 2023 Human scent characterization: A review *Forensic Science International* 111743
- [94] Bernier U R, Kline D L, Barnard D R, Schreck C E and Yost R A 2000 Analysis of Human Skin Emanations by Gas Chromatography/Mass Spectrometry. 2. Identification of Volatile Compounds That Are Candidate Attractants for the Yellow Fever Mosquito (*Aedes aegypti*) *Anal. Chem.* **72** 747–56
- [95] Trivedi D K, Sinclair E, Xu Y, Sarkar D, Walton-Doyle C, Liscio C, Banks P, Milne J, Silverdale M, Kunath T, Goodacre R and Barran P 2019 Discovery of Volatile Biomarkers of Parkinson's Disease from Sebum *ACS Central Science* **5** 599–606
- [96] Curran A M, Rabin S I, Prada P A and Furton K G 2005 Comparison of the Volatile Organic Compounds Present in Human Odor Using Spme-GC/MS *Journal of Chemical Ecology* **31** 1607–19
- [97] Haertl T, Owsienko D, Schwinn L, Hirsch C, Eskofier B M, Lang R, Wirtz S and Loos H M 2023 Exploring the interrelationship between the skin microbiome and skin volatiles: A pilot study *Frontiers in Ecology and Evolution* **11**
- [98] Vishinkin R, Busool R, Mansour E, Fish F, Esmail A, Kumar P, Gharaa A, Cancilla J C, Torrecilla J S, Skenders G, Leja M, Dheda K, Singh S and Haick H 2021 Profiles of Volatile Biomarkers Detect Tuberculosis from Skin (Adv. Sci. 15/2021) *Advanced Science* **8** 2170093
- [99] Roodt A P, Naudé Y, Stoltz A and Rohwer E 2018 Human skin volatiles: Passive sampling and GC × GC-ToFMS analysis as a tool to investigate the skin microbiome and interactions with anthropophilic mosquito disease vectors *Journal of Chromatography B* **1097–1098** 83–93

- [100] Jiang R, Cudjoe E, Bojko B, Abaffy T and Pawliszyn J 2013 A non-invasive method for in vivo skin volatile compounds sampling *Analytica Chimica Acta* **804** 111–9
- [101] Gallagher M, Wysocki C J, Leyden J J, Spielman A I, Sun X and Preti G 2008 Analyses of volatile organic compounds from human skin *British Journal of Dermatology* **159** 780–91
- [102] Duffy E, Guzman K D, Wallace R, Murphy R and Morrin A 2017 Non-Invasive Assessment of Skin Barrier Properties: Investigating Emerging Tools for In Vitro and In Vivo Applications *Cosmetics* **4** 44
- [103] Spichiger-Keller U E 1998 *Chemical Sensors and Biosensors for Medical and Biological Applications* (Wiley)
- [104] Coyle S, Curto V F, Benito-Lopez F, Florea L and Diamond D 2014 Chapter 2.1 - Wearable Bio and Chemical Sensors *Wearable Sensors* ed E Sazonov and M R Neuman (Oxford: Academic Press) pp 65–83
- [105] Chung M, Fortunato G and Radacsi N 2019 Wearable flexible sweat sensors for healthcare monitoring: a review *Journal of The Royal Society Interface* **16** 20190217
- [106] Baranwal J, Barse B, Gatto G, Broncova G and Kumar A 2022 Electrochemical Sensors and Their Applications: A Review *Chemosensors* **10** 363
- [107] Goud K Y, Moonla C, Mishra R K, Yu C, Narayan R, Litvan I and Wang J 2019 Wearable Electrochemical Microneedle Sensor for Continuous Monitoring of Levodopa: Toward Parkinson Management *ACS Sens.* **4** 2196–204
- [108] Kim J, Sempionatto J R, Imani S, Hartel M C, Barfidokht A, Tang G, Campbell A S, Mercier P P and Wang J 2018 Simultaneous Monitoring of Sweat and Interstitial Fluid Using a Single Wearable Biosensor Platform *Adv Sci (Weinh)* **5**
- [109] Bandodkar A J, Jia W, Yardımcı C, Wang X, Ramirez J and Wang J 2015 Tattoo-Based Noninvasive Glucose Monitoring: A Proof-of-Concept Study *Anal. Chem.* **87** 394–8
- [110] Yao Y, Chen J, Guo Y, Lv T, Chen Z, Li N, Cao S, Chen B and Chen T 2021 Integration of interstitial fluid extraction and glucose detection in one device for wearable non-invasive blood glucose sensors *Biosensors and Bioelectronics* **179** 113078
- [111] Lawson B, Aguir K, Tomas F, Laithier V, Bouchakour R, Reynard-Carette C and Bendahan M M 2018 Skin Alcohol perspiration Measurements Using MOX Sensors *Sensors and Actuators B Chemical*
- [112] Güntner A T, Pineau N J, Mochalski P, Wiesenhofer H, Agapiou A, Mayhew C A and Pratsinis S E 2018 Sniffing Entrapped Humans with Sensor Arrays *Anal. Chem.* **90** 4940–5
- [113] Carmona E N, Sberveglieri V, Ponzoni A, Galstyan V, Zappa D, Pulvirenti A and Comini E 2017 Detection of food and skin pathogen microbiota by means of an electronic nose based on metal oxide chemiresistors *Sensors and Actuators B: Chemical* **C** 1224–30

- [114] dos Santos C C, Lucena G N, Pinto G C, Júnior M J and Marques R F C 2021 Advances and current challenges in non-invasive wearable sensors and wearable biosensors—A mini-review *MEDICAL DEVICES & SENSORS* **4** e10130
- [115] Song Y, Min J, Yu Y, Wang H, Yang Y, Zhang H and Gao W 2020 Wireless battery-free wearable sweat sensor powered by human motion *Science Advances* **6** eaay9842
- [116] Han W, He H, Zhang L, Dong C, Zeng H, Dai Y, Xing L, Zhang Y and Xue X 2017 A Self-Powered Wearable Noninvasive Electronic-Skin for Perspiration Analysis Based on Piezo-Biosensing Unit Matrix of Enzyme/ZnO Nanoarrays *ACS Appl. Mater. Interfaces* **9** 29526–37
- [117] Bandodkar A J, Gutruf P, Choi J, Lee K, Sekine Y, Reeder J T, Jeang W J, Aranyosi A J, Lee S P, Model J B, Ghaffari R, Su C-J, Leshock J P, Ray T, Verrillo A, Thomas K, Krishnamurthi V, Han S, Kim J, Krishnan S, Hang T and Rogers J A 2019 Battery-free, skin-interfaced microfluidic/electronic systems for simultaneous electrochemical, colorimetric, and volumetric analysis of sweat *Science Advances* **5** eaav3294
- [118] Yu Y, Nassar J, Xu C, Min J, Yang Y, Dai A, Doshi R, Huang A, Song Y, Gehlhar R, Ames A D and Gao W 2020 Biofuel-powered soft electronic skin with multiplexed and wireless sensing for human-machine interfaces *Science Robotics* **5**
- [119] Ebralidze I I, Laschuk N O, Poisson J and Zenkina O V 2019 Chapter 1 - Colorimetric Sensors and Sensor Arrays *Nanomaterials Design for Sensing Applications Micro and Nano Technologies* ed O V Zenkina (Elsevier) pp 1–39
- [120] Li Z, Askim J R and Suslick K S 2019 The Optoelectronic Nose: Colorimetric and Fluorometric Sensor Arrays *Chem. Rev.* **119** 231–92
- [121] Albrecht C 2008 Joseph R. Lakowicz: Principles of fluorescence spectroscopy, 3rd Edition *Anal Bioanal Chem* **390** 1223–4
- [122] Sekine Y, Kim S B, Zhang Y, Bandodkar A J, Xu S, Choi J, Irie M, Ray T R, Kohli P, Kozai N, Sugita T, Wu Y, Lee K, Lee K-T, Ghaffari R and Rogers J A 2018 A fluorometric skin-interfaced microfluidic device and smartphone imaging module for *in situ* quantitative analysis of sweat chemistry *Lab Chip* **18** 2178–86
- [123] Jiang N, Yetisen A K, Linhart N, Flisikowski K, Dong J, Dong X, Butt H, Jakobi M, Schnieke A and Koch A W 2020 Fluorescent dermal tattoo biosensors for electrolyte analysis *Sensors and Actuators B: Chemical* **320** 128378
- [124] Toma K, Suzuki S, Arakawa T, Iwasaki Y and Mitsubayashi K 2021 External ears for non-invasive and stable monitoring of volatile organic compounds in human blood *Sci Rep* **11** 10415
- [125] Woolf M S, Dignan L M, Scott A T and Landers J P 2021 Digital postprocessing and image segmentation for objective analysis of colorimetric reactions *Nat Protoc* **16** 218–38
- [126] Bahadır E B and Sezgentürk M K 2016 Lateral flow assays: Principles, designs and labels *TrAC Trends in Analytical Chemistry* **82** 286–306

- [127] Bai Y, Hibbing P, Mantis C and Welk G J 2018 Comparative evaluation of heart rate-based monitors: Apple Watch vs Fitbit Charge HR *Journal of Sports Sciences* **36** 1734–41
- [128] Madhan Mohan P, Nagarajan V and Vignesh J C 2017 Spot measurement of heart rate based on morphology of PhotoPlethysmoGraphic (PPG) signals *Journal of Medical Engineering & Technology* **41** 87–96
- [129] Paliwal S, Hwang B H, Tsai K Y and Mitragotri S 2013 Diagnostic opportunities based on skin biomarkers *European Journal of Pharmaceutical Sciences* **50** 546–56
- [130] Kiistala U 1968 Suction Blister Device for Separation of Viable Epidermis from Dermis* *Journal of Investigative Dermatology* **50** 129–37
- [131] Tierney M J, Tamada J A, Potts R O, Jovanovic L and Garg S 2001 Clinical evaluation of the GlucoWatch® biographer: a continual, non-invasive glucose monitor for patients with diabetes *Biosensors and Bioelectronics* **16** 621–9
- [132] Miller P R, Skoog S A, Edwards T L, Lopez D M, Wheeler D R, Arango D C, Xiao X, Brozik S M, Wang J, Polsky R and Narayan R J 2012 Multiplexed microneedle-based biosensor array for characterization of metabolic acidosis *Talanta* **88** 739–42
- [133] Li H, Wu G, Weng Z, Sun H, Nistala R and Zhang Y 2021 Microneedle-Based Potentiometric Sensing System for Continuous Monitoring of Multiple Electrolytes in Skin Interstitial Fluids *ACS Sens.* **6** 2181–90
- [134] Dervisevic M, Dervisevic E, Esser L, Easton C D, Cadarso V J and Voelcker N H 2023 Wearable microneedle array-based sensor for transdermal monitoring of pH levels in interstitial fluid *Biosensors and Bioelectronics* **222** 114955
- [135] Hakala T A, García Pérez A, Wardale M, Ruuth I A, Vänskä R T, Nurminen T A, Kemp E, Boeva Z A, Alakoskela J-M, Pettersson-Fernholm K, Hæggström E and Bobacka J 2021 Sampling of fluid through skin with magnetohydrodynamics for noninvasive glucose monitoring *Sci Rep* **11** 7609
- [136] Kemp E, Palomäki T, Ruuth I A, Boeva Z A, Nurminen T A, Vänskä R T, Zschaechner L K, Pérez A G, Hakala T A, Wardale M, Haeggström E and Bobacka J 2022 Influence of enzyme immobilization and skin-sensor interface on non-invasive glucose determination from interstitial fluid obtained by magnetohydrodynamic extraction *Biosensors and Bioelectronics* **206** 114123
- [137] Zhao Z, Li Q, Chen L, Zhao Y, Gong J, Li Z and Zhang J 2021 A thread/fabric-based band as a flexible and wearable microfluidic device for sweat sensing and monitoring *Lab on a Chip* **21** 916–32
- [138] Glennon T, O’Quigley C, McCaul M, Matzeu G, Beirne S, Wallace G G, Stroiescu F, O’Mahoney N, White P and Diamond D 2016 ‘SWEATCH’: A Wearable Platform for Harvesting and Analysing Sweat Sodium Content *Electroanalysis* **28** 1283–9
- [139] Zhang Y, Guo H, Kim S B, Wu Y, Ostojich D, Park S H, Wang X, Weng Z, Li R, Bandodkar A J, Sekine Y, Choi J, Xu S, Quaggin S, Ghaffari R and Rogers J A 2019

- Passive sweat collection and colorimetric analysis of biomarkers relevant to kidney disorders using a soft microfluidic system *Lab Chip* **19** 1545–55
- [140] Sim J K, Yoon S and Cho Y-H 2018 Wearable Sweat Rate Sensors for Human Thermal Comfort Monitoring *Sci Rep* **8** 1181
- [141] Emaminejad S, Gao W, Wu E, Davies Z A, Nyein H Y Y, Challa S, Ryan S P, Fahad H M, Chen K, Shahpar Z, Talebi S, Milla C, Javey A and Davis R W 2017 Autonomous sweat extraction and analysis applied to cystic fibrosis and glucose monitoring using a fully integrated wearable platform *PNAS* **114** 4625–30
- [142] Tai L-C, Liaw T S, Lin Y, Nyein H Y Y, Bariya M, Ji W, Hettick M, Zhao C, Zhao J, Hou L, Yuan Z, Fan Z and Javey A 2019 Wearable Sweat Band for Noninvasive Levodopa Monitoring *Nano Lett.* **19** 6346–51
- [143] Sonner Z, Wilder E, Gaillard T, Kasting G and Heikenfeld J 2017 Integrated sudomotor axon reflex sweat stimulation for continuous sweat analyte analysis with individuals at rest *Lab Chip* **17** 2550–60
- [144] Duffy E and Morrin A 2019 Endogenous and microbial volatile organic compounds in cutaneous health and disease *TrAC Trends in Analytical Chemistry* **111** 163–72
- [145] Mochalski P, Unterkofler K, Teschl G and Amann A 2015 Potential of volatile organic compounds as markers of entrapped humans for use in urban search-and-rescue operations *TrAC Trends in Analytical Chemistry* **68** 88–106
- [146] Zhu D D, Zheng L W, Duong P K, Cheah R H, Liu X Y, Wong J R, Wang W J, Tien Guan S T, Zheng X T and Chen P 2022 Colorimetric microneedle patches for multiplexed transdermal detection of metabolites *Biosensors and Bioelectronics* **212** 114412
- [147] Wang Z, Li H, Wang J, Chen Z, Chen G, Wen D, Chan A and Gu Z 2020 Transdermal colorimetric patch for hyperglycemia sensing in diabetic mice *Biomaterials* **237** 119782
- [148] Zhang P, Wu X, Xue H, Wang Y, Luo X and Wang L 2022 Wearable transdermal colorimetric microneedle patch for Uric acid monitoring based on peroxidase-like polypyrrole nanoparticles *Analytica Chimica Acta* **1212** 339911
- [149] Nicholas D, Logan K A, Sheng Y, Gao J, Farrell S, Dixon D, Callan B, McHale A P and Callan J F 2018 Rapid paper based colorimetric detection of glucose using a hollow microneedle device *International Journal of Pharmaceutics* **547** 244–9
- [150] Zeng Q, Xu M, Hu W, Cao W, Zhan Y, Zhang Y, Wang Q and Ma T 2023 Porous Colorimetric Microneedles for Minimally Invasive Rapid Glucose Sampling and Sensing in Skin Interstitial Fluid *Biosensors* **13** 537
- [151] Liu G-S, Kong Y, Wang Y, Luo Y, Fan X, Xie X, Yang B-R and Wu M X 2020 Microneedles for transdermal diagnostics: Recent advances and new horizons *Biomaterials* **232** 119740

- [152] Wu T, You X and Chen Z 2022 Hollow Microneedles on a Paper Fabricated by Standard Photolithography for the Screening Test of Prediabetes *Sensors* **22** 4253
- [153] Liebl H and Kloth L C 2012 Skin Cell Proliferation Stimulated by Microneedles *Journal of the American College of Clinical Wound Specialists* **4** 2–6
- [154] Yetisen A K, Moreddu R, Seifi S, Jiang N, Vega K, Dong X, Dong J, Butt H, Jakobi M, Elsner M and Koch A W 2019 Dermal Tattoo Biosensors for Colorimetric Metabolite Detection *Angewandte Chemie International Edition* **58** 10506–13
- [155] He R, Liu H, Fang T, Niu Y, Zhang H, Han F, Gao B, Li F and Xu F 2021 A Colorimetric Dermal Tattoo Biosensor Fabricated by Microneedle Patch for Multiplexed Detection of Health-Related Biomarkers *Advanced Science* **8** 2103030
- [156] Pazos M D, Hu Y, Elani Y, Browning K L, Jiang N and Yetisen A K 2021 Tattoo Inks for Optical Biosensing in Interstitial Fluid *Advanced Healthcare Materials* **10** 2101238
- [157] Qiao L, Benzigar M R, Subramony J A, Lovell N H and Liu G 2020 Advances in Sweat Wearables: Sample Extraction, Real-Time Biosensing, and Flexible Platforms *ACS Appl. Mater. Interfaces* **12** 34337–61
- [158] Lin P-H, Sheu S-C, Chen C-W, Huang S-C and Li B-R 2022 Wearable hydrogel patch with noninvasive, electrochemical glucose sensor for natural sweat detection *Talanta* **241** 123187
- [159] Xiao J, Liu Y, Su L, Zhao D, Zhao L and Zhang X 2019 Microfluidic Chip-Based Wearable Colorimetric Sensor for Simple and Facile Detection of Sweat Glucose *Anal. Chem.* **91** 14803–7
- [160] Xiao G, He J, Qiao Y, Wang F, Xia Q, Wang X, Yu L, Lu Z and Li C-M 2020 Facile and Low-Cost Fabrication of a Thread/Paper-Based Wearable System for Simultaneous Detection of Lactate and pH in Human Sweat *Adv. Fiber Mater.* **2** 265–78
- [161] Wang L, Xu T, He X and Zhang X 2021 Flexible, self-healable, adhesive and wearable hydrogel patch for colorimetric sweat detection *J. Mater. Chem. C* **9** 14938–45
- [162] Kim J, Wu Y, Luan H, Yang D S, Cho D, Kwak S S, Liu S, Ryu H, Ghaffari R and Rogers J A 2022 A Skin-Interfaced, Miniaturized Microfluidic Analysis and Delivery System for Colorimetric Measurements of Nutrients in Sweat and Supply of Vitamins Through the Skin *Advanced Science* **9** 2103331
- [163] Bong Kim S, Koo J, Yoon J, Hourlier-Fargette A, Lee B, Chen S, Jo S, Choi J, Suk Oh Y, Lee G, Min Won S, J. Aranyosi A, P. Lee S, B. Model J, V. Braun P, Ghaffari R, Park C and A. Rogers J 2020 Soft, skin-interfaced microfluidic systems with integrated enzymatic assays for measuring the concentration of ammonia and ethanol in sweat *Lab on a Chip* **20** 84–92
- [164] Baker L B, Seib M S, Barnes K A, Brown S D, King M A, De Chavez P J D, Qu S, Archer J, Wolfe A S, Stofan J R, Carter J M, Wright D E, Wallace J, Yang D S, Liu S, Anderson J, Fort T, Li W, Wright J A, Lee S P, Model J B, Rogers J A, Aranyosi A J

- and Ghaffari R 2022 Skin-Interfaced Microfluidic System with Machine Learning-Enabled Image Processing of Sweat Biomarkers in Remote Settings *Advanced Materials Technologies* **7** 2200249
- [165] Morris D, Schazmann B, Wu Y, Coyle S, Brady S, Hayes J, Slater C, Fay C, Lau K T, Wallace G and Diamond D 2008 Wearable sensors for monitoring sports performance and training 2008 5th International Summer School and Symposium on Medical Devices and Biosensors 2008 5th International Summer School and Symposium on Medical Devices and Biosensors pp 121–4
- [166] Cheshire W P and Freeman R 2003 Disorders of Sweating *Semin Neurol* **23** 399–406
- [167] Micieli G, Tosi P, Marcheselli S and Cavallini A 2003 Autonomic dysfunction in Parkinson's disease *Neurol Sci* **24** s32–4
- [168] Jagannath B, Lin K-C, Pali M, Sankhala D, Muthukumar S and Prasad S 2021 Temporal profiling of cytokines in passively expressed sweat for detection of infection using wearable device *Bioengineering & Translational Medicine* **6** e10220
- [169] Nyein H Y Y, Tai L-C, Ngo Q P, Chao M, Zhang G B, Gao W, Bariya M, Bullock J, Kim H, Fahad H M and Javey A 2018 A Wearable Microfluidic Sensing Patch for Dynamic Sweat Secretion Analysis *ACS Sens.* **3** 944–52
- [170] Arakawa T, Suzuki T, Tsujii M, Iitani K, Chien P-J, Ye M, Toma K, Iwasaki Y and Mitsubayashi K 2019 Real-time monitoring of skin ethanol gas by a high-sensitivity gas phase biosensor (bio-sniffer) for the non-invasive evaluation of volatile blood compounds *Biosensors and Bioelectronics* **129** 245–53
- [171] Ikeda S, Asai S, Umezawa K, Miyachi H, Nakamura A, Kaifuku Y and Sekine Y 2022 Development of a wristband-type wearable device for the colorimetric detection of ammonia emanating from the human skin surface *Results in Chemistry* **4** 100502
- [172] Finnegan M, Duffy E and Morrin A 2022 The determination of skin surface pH via the skin volatile emission using wearable colorimetric sensors *Sensing and Bio-Sensing Research* **35** 100473
- [173] Yusufu D, Magee E, Gilmore B and Mills A 2022 Non-invasive, 3D printed, colourimetric, early wound-infection indicator *Chem. Commun.* **58** 439–42
- [174] Mirani B, Hadisi Z, Pagan E, Dabiri S M H, van Rijt A, Almutairi L, Noshadi I, Armstrong D G and Akbari M Smart Dual-Sensor Wound Dressing for Monitoring Cutaneous Wounds *Advanced Healthcare Materials* **n/a** 2203233
- [175] You X-Q, He Q-Y, Wu T-W, Huang D-Y, Peng Z-Z, Chen D-Y, Chen Z and Liu J 2023 Multi-groove microneedles based wearable colorimetric sensor for simple and facile glucose detection *Microchemical Journal* **190** 108570
- [176] Yang H, Jiang X, Zeng Y, Zhang W, Yuan Q, Yin M, Wu G and Li W 2023 A swellable bilateral microneedle patch with core-shell structure for rapid lactate analysis and early melanoma diagnosis *Chemical Engineering Journal* **455** 140730

- [177] Liu S, Yang D S, Wang S, Luan H, Sekine Y, Model J B, Aranyosi A J, Ghaffari R and Rogers J A Soft, environmentally degradable microfluidic devices for measurement of sweat rate and total sweat loss and for colorimetric analysis of sweat biomarkers *EcoMat* **n/a** e12270
- [178] Koh A, Kang D, Xue Y, Lee S, Pielak R M, Kim J, Hwang T, Min S, Banks A, Bastien P, Manco M C, Wang L, Ammann K R, Jang K-I, Won P, Han S, Ghaffari R, Paik U, Slepian M J, Balooch G, Huang Y and Rogers J A 2016 A soft, wearable microfluidic device for the capture, storage, and colorimetric sensing of sweat *Sci. Transl. Med.* **8**
- [179] Liu D, Liu Z, Feng S, Gao Z, Chen R, Cai G and Bian S 2023 Wearable Microfluidic Sweat Chip for Detection of Sweat Glucose and pH in Long-Distance Running Exercise *Biosensors* **13** 157
- [180] Choi J, Kang D, Han S, Kim S B and Rogers J A 2017 Thin, Soft, Skin-Mounted Microfluidic Networks with Capillary Bursting Valves for Chrono-Sampling of Sweat *Advanced Healthcare Materials* **6** 1601355
- [181] Bandodkar A J, Jeang W J, Ghaffari R and Rogers J A 2019 Wearable Sensors for Biochemical Sweat Analysis *Annual Review of Analytical Chemistry* **12** 1–22
- [182] Jo S, Sung D, Kim S and Koo J 2021 A review of wearable biosensors for sweat analysis *Biomed. Eng. Lett.* **11** 117–29
- [183] Ghaffari R, Aranyosi A J, Lee S P, Model J B and Baker L B 2023 The Gx Sweat Patch for personalized hydration management *Nat Rev Bioeng* **1** 5–7
- [184] Promphet N, Rattanawaleedirojn P, Siralertmukul K, Soatthiyanon N, Potiyaraj P, Thanawattano C, Hinestroza J P and Rodthongkum N 2019 Non-invasive textile based colorimetric sensor for the simultaneous detection of sweat pH and lactate *Talanta* **192** 424–30
- [185] Cheng Y, Feng S, Ning Q, Li T, Xu H, Sun Q, Cui D and Wang K 2023 Dual-signal readout paper-based wearable biosensor with a 3D origami structure for multiplexed analyte detection in sweat *Microsyst Nanoeng* **9** 1–10
- [186] Xiao G, He J, Chen X, Qiao Y, Wang F, Xia Q, Yu L and Lu Z 2019 A wearable, cotton thread/paper-based microfluidic device coupled with smartphone for sweat glucose sensing *Cellulose* **26** 4553–62
- [187] Xi P, He X, Fan C, Zhu Q, Li Z, Yang Y, Du X and Xu T 2023 Smart Janus fabrics for one-way sweat sampling and skin-friendly colorimetric detection *Talanta* 124507
- [188] Marunaka Y 2015 Roles of interstitial fluid pH in diabetes mellitus: Glycolysis and mitochondrial function *World J Diabetes* **6** 125–35
- [189] Michaëlsson G, Ljunghall K and Danielson B 1980 Zinc in epidermis and dermis in healthy subjects *Acta Dermato-Venereologica* **60** 295–9
- [190] Patterson M J, Galloway S D R and Nimmo M A 2000 Variations in Regional Sweat Composition in Normal Human Males *Experimental Physiology* **85** 869–75

- [191] Zhang K, Zhang J, Wang F and Kong D 2021 Stretchable and Superwetable Colorimetric Sensing Patch for Epidermal Collection and Analysis of Sweat *ACS Sens.* **6** 2261–9
- [192] Yusufu D and Mills A 2018 Spectrophotometric and Digital Colour Colourimetric (DCC) analysis of colour-based indicators *Sensors and Actuators B: Chemical* **273** 1187–94
- [193] Suzuki Y 2007 Protein Error of pH Indicators in the Presence of Detergents *Analytical Sciences* **23** 733–8
- [194] Possanzini L, Decataldo F, Mariani F, Gualandi I, Tessarolo M, Scavetta E and Fraboni B 2020 Textile sensors platform for the selective and simultaneous detection of chloride ion and pH in sweat *Sci Rep* **10** 17180
- [195] Suslick K S, Rakow N A and Sen A 2004 Colorimetric sensor arrays for molecular recognition
- [196] Bridgeman D T A Portable Colorimetric Sensing Platform for the Evaluation of Carbon Dioxide in Breath
- [197] Ray T R, Ivanovic M, Curtis P M, Franklin D, Guventurk K, Jeang W J, Chafetz J, Gaertner H, Young G, Rebollo S, Model J B, Lee S P, Ciraldo J, Reeder J T, Hourlier-Fargette A, Bandodkar A J, Choi J, Aranyosi A J, Ghaffari R, McColley S A, Haymond S and Rogers J A 2021 Soft, skin-interfaced sweat stickers for cystic fibrosis diagnosis and management *Science Translational Medicine* **13**
- [198] Curto V F, Fay C, Coyle S, Byrne R, O’Toole C, Barry C, Hughes S, Moyna N, Diamond D and Benito-Lopez F 2012 Real-time sweat pH monitoring based on a wearable chemical barcode micro-fluidic platform incorporating ionic liquids *Sensors and Actuators B: Chemical* **171–172** 1327–34
- [199] Lee T, Kim C, Kim J, Seong J B, Lee Y, Roh S, Cheong D Y, Lee W, Park J, Hong Y and Lee G 2022 Colorimetric Nanoparticle-Embedded Hydrogels for a Biosensing Platform *Nanomaterials (Basel)* **12** 1150
- [200] Siripongpreda T, Somchob B, Rodthongkum N and Hoven V P 2021 Bacterial cellulose-based re-swelling hydrogel: Facile preparation and its potential application as colorimetric sensor of sweat pH and glucose *Carbohydrate Polymers* **256** 117506
- [201] Zhou P, Zhang Z, Mo F and Wang Y A Review of Functional Hydrogels for Flexible Chemical Sensors *Advanced Sensor Research* **n/a** 2300021

Thesis Outline

The main aim of this work is to overcome the specific requirement for biofluid collection and manipulation outlined here in Chapter 1 by investigating the volatile emission from skin, a matrix that is passively and continuously emitted from skin and which contains biomarkers of metabolic and cellular processes within the body. The work seeks to establish the volatile profile for healthy skin using a headspace solid-phase microextraction (HS-SPME) gas-chromatography (GC-MS) workflow to better understand factors that impact the emission including circadian rhythm, skin sampling site, gender and age. Assessment of the ability of frequently emitted skin-derived compounds to impact host cells' signalling pathways was also assessed in cell culture. Finally, a move toward the use of a simple, cost-effective, wearable colorimetric sensor platform to monitor volatile emissions from skin was also explored. The feasibility of measuring skin surface pH, via the volatile ammonia emission from skin using this wearable colorimetric sensor was investigated and offers great potential for easy personalised monitoring of general health.

Chapter 2 reports the use of a non-invasive, HS-SPME GC-MS workflow to initially characterise the skin volatile emission from the volar forearm of a single healthy participant. Following identification of a variety of compound classes emanating from human skin, including frequently reported compounds, origins of each of the compounds recovered were discussed. Diurnal- and site-associated changes in the human skin volatilome were then investigated. Other parameters associated with skin including skin surface pH and tissue dielectric constant (TDC) were also assessed for diurnal and skin site differences and their correlation with the skin volatile profile. Results confirm significant diurnal- and site-associated changes in the skin volatile emission as well significant as differences in skin surface pH and TDC across different skin sites, while diurnal variation was only observed for skin surface pH but not TDC. All experimental elements of this chapter were carried out by the candidate.

Chapter 3 involves the characterization of the skin volatile emissions from the volar forearm of a large healthy participant cohort (n=60) comprised of male and female participants ranging in age from 18-80 years old, again, employing the same HS-SPME GC-MS workflow as in Chapter 2. A wide variety of compounds classes were again detected with variability in recovery and abundance observed. Gender and age associated changes in the skin volatile emission from the volar was assessed across the participant cohort. Results confirm significant gender influences on the skin volatile emission indicating that male and female data should be treated individually when investigating age-related changes in the skin volatile emission. Statistical analysis of the volatile profile with age showed that there were compound

abundances that significantly changed with age (acetic acid, hexanal, nonanal, undecanal, benzyl alcohol and 2-ethyl-1-hexanol). Age-related changes in skin surface pH and TDC were also observed. All experimental elements of this chapter were carried out by the candidate.

Chapter 4 aims to understand the impact of skin-derived compounds on host skin cells' signalling pathway, specifically the Nrf2-Keap1 cellular defence mechanism. Chapter 2 and 3 showed that nonanal, decanal and 6-methyl-5-hepten-2-one are frequently recovered from the headspace of skin. The ability of these compounds to trigger activation of the Nrf2-pathway in primary human keratinocytes was investigated showing that the aldehydes, nonanal and decanal activate translocation of the Nrf2 protein to the nucleus to afford protection against oxidative stress whereas the ketone, and 6-methyl-5-hepten-2-one does not elicit activation. Elucidation of the mechanism by which the Nrf2-Keap1 pathway was triggered was also investigated and reactive oxygen species (ROS) generation was shown to increase when cells were treated with nonanal and decanal but not 6-methyl-5-hepten-2-one indicating indirect activation of the mechanism. A proof of concept study also showed an increase in ROS production when cells were exposed to varying concentrations of nonanal in gas phase. To the best of our knowledge, this is the first study that investigates the effect of treatment of cells with nonanal in the volatile phase and hypothesises that nonanal in gas phase produced by the skin may induce ROS generation in cells and neighbouring cells which in turn may lead to the activation of the Nrf2-Keap1 pathway through indirect activation. All experimental elements of this chapter were carried out by the candidate.

Chapter 5 investigates the use of a simple wearable colorimetric sensing platform incorporating sensor spots comprising encapsulated bromocresol green pH indicator dye in an enclosed headspace above the skin. The sensor spots change from yellow to blue as a response to basic volatile nitrogen compounds such as ammonia and volatile amines being emitted from skin. By deploying this wearable in a healthy participant study, a strong correlation between sensor Euclidean Distance (ED) response and skin surface pH was demonstrated, despite a high inter-individual variability being noted. Sensor response was observed to be highly dependent on gender as well as body site, and attributed to factors such as gland and microbial composition differences. Finally, skin surface pH and wearable sensor responses were measured following various skin treatments and showed the wearable's ability to detect changes in skin surface pH in response to topical skin treatments. All experimental elements of this chapter were carried out by the candidate.

Chapter 6 outlines conclusions from this work and discusses future work that is currently on-going.

Chapter 2: Assessing diurnal and site-associated differences in the skin volatile emission, skin surface pH and tissue dielectric constant in healthy skin

Abstract

The skin is the largest organ of the body and has tremendous biodiagnostic potential through the analysis of biofluids such as ISF and sweat. Assessment of biomarkers in biofluids typically require generation or extraction which can add complexity to analysis. Exploiting the skin volatile emission has recently gained traction as it is passively and continuously emitted from skin thus obviating the need for generation or extraction. In this work, a headspace solid-phase microextraction (SPME) gas-chromatography (GC-MS) workflow was employed to investigate diurnal and site-associated variations in the healthy skin volatile profile. Other parameters including skin surface pH and tissue dielectric constant (TDC) were also assessed for diurnal and site differences. A total of 21 compounds comprising of acids, aldehydes, ketones, alcohols, hydrocarbons and esters were recovered from the skin across a day and from different skin sites. Significant diurnal variations were observed in the acid, ketone and ester emission from skin across a day. Significant diurnal variation was noted for skin surface pH while no variation in TDC was observed. Skin site variation in the volatile profile was observed where the palm showed the highest emission of almost all volatile emitted across the sites. Furthermore, ketone emission was also up-regulated on the forehead compared to all other sites. Significant variations in skin surface pH and TDC measurements for different skin sites were also observed with the forehead exhibiting the lowest skin surface pH coupled with the highest TDC measurement. Overall, this work provides a comprehensive analysis of the diurnal and site-associated changes in the skin volatile profile, skin surface pH and TDC in a healthy participant. Characterising these changes in a healthy participant and understanding the healthy- baseline volatile profile across a day and across different skin sites may allow for easier diagnosis of disease. Furthermore, such studies may prove useful in the development of treatments within the cosmetic industry.

2.1. Introduction

The skin is a unique organ that has great biodiagnostic potential and has the ability to offer insights into metabolic processes within the body through the analysis of matrices produced within the skin such as biofluids including interstitial fluid (ISF) and other recently investigated matrices such as skin volatile emissions [1–3]. Exploiting volatile biomarker emission from skin has recently gained lots of traction as volatiles are continuously and passively emitted from skin thus obviating the need for generation and extraction that is associated with the sampling of ISF and sweat [4,5]. Volatile emissions are derived from eccrine, apocrine and sebaceous gland secretions and from the interaction of these secreted compounds with microorganisms present on the skin's surface [6] with a variety of compounds classes being emitted including alkanes, alkenes, aldehydes, acids, ketones, alcohols, sulphur-containing compounds and nitrogen-containing compounds from both endogenous and exogenous sources [2,7]. Work has shown changes in the volatile emission composition from skin related to specific pathologies that have altered cellular metabolism [6]. For example characteristic profiles have been reported for patients with chronic wounds [8], Parkinson's disease [9], melanoma [10] and skin associated diseases such as atopic dermatitis [11].

The body exhibits circadian rhythms, or 24-hour oscillations in metabolic processes, which serve to maximize cellular functions and adapt to the environmental demands of the day such as UV radiation for example [12,13]. Studies have shown circadian variations in various skin parameters such as skin capacitance, sebum excretion, transepidermal water loss (TEWL), skin surface pH, skin thickness and temperature [14–16]. Furthermore, diurnal-associated changes have been shown in the skin microbiome with the time of the day contributing to variances at the community level, however studies are limited to date [17–19]. For example, in one study, the relative abundance of *Propionibacterium* was significantly higher during the evening compared to morning [20]. Another study, however, has shown no temporal difference in the microbial communities on skin despite constant exposure to external environment [21]. This leaves diurnal changes in the skin microbiome up for debate and indicates further work is needed to truly understand diurnal changes, if there are any. Many studies have investigated the impact of the circadian clock on breath volatiles with studies showing changes in the volatile profile depending on the time of the day [22–25] with some also assessing the diurnal nature of the volatile ammonia [26] and hydrogen cyanide [27] emission from skin. Other studies have assessed the diurnal emission of acetone following the consumption of a keto- or carb-rich diet [28].

As mentioned above, volatile emissions from skin are derived from secretions produced by the skin glands and from further metabolization of these secretions by the skin microbiome [29]. Gland density and distribution is not uniform across the body and varies at different skin sites [30] with eccrine glands being found in a high density on the palms and foot [31], apocrine glands most dense in the axillae [32] and sebaceous glands densely located on the forehead and upper back [33]. Furthermore, the composition of the skin microbiome differs at different skin sites, for example, sebaceous sites such as the forehead are dominated by lipophilic *Propionibacterium* species, the arms and the legs are known as dry areas and are mainly populated by *Staphylococcus* and *Micrococci* species whereas *Staphylococcus* and *Corynebacterium* species are abundant in moist areas such as the bends of the elbows, axillae region and feet [34,35]. Variations in the skin volatile emission at different skin sites have been identified and such differences have been attributed each skin site's unique gland density and microbiome [36–38].

To date, research on diurnal and skin site variation-associated changes in the skin volatile emission is limited [36–38]. This work aims to first characterise the skin volatile emission and then assess changes in the profile across a 6 hour period on 3 separate days. Following this, the volatile emission profile at different skin sites including the palm, foot, lower back, forehead and volar forearm was assessed for differences. Other physiological parameters including tissue dielectric constant (TDC) and skin surface pH and their correlations with the volatile profile were also investigated for diurnal and site specific variations. Overall, this research provides further insight into diurnal and site specific differences in skin which may prove useful for the understanding of healthy base-line skin volatile profile across a day and at different skin sites.

2.2. Materials and methods

2.2.1. Participant profile and skin volatile emission sampling

A healthy volunteer, aged 26 was recruited. No special dietary regimes were applied, however, the participant was asked not to apply perfumes or cosmetics on their arms on the day of sample volatile collection. The participant was informed on the aim and purpose of the study and asked to provide written informed consent alongside filling out a short questionnaire about their gender, age and cosmetic/fragrance use. The local ethics committee (Dublin City University Research Ethics Committee) approved the study on skin volatiles prior to commencement of the work (DCUREC/2016/053), and the study was performed according to

the Declaration of Helsinki. Solid-phase microextraction (SPME) fibres were used for sampling volatiles in a headspace (HS) above the skin using a method described previously [11]. Briefly, SPME fibres were comprised of 50/30/20 μm divinylbenzene/carboxen/polydimethylsiloxane Stableflex (2 cm) assemblies (Supelco Corp., Bellefonte, PA, USA). The SPME fibre was housed within a glass HS affixed to the left volar forearm (Figure 2.1), left palm, left sole of foot, lower back or forehead with Leukosilk surgical tape (BSN Medical GmbH, Hamburg, Germany). This was comprised of a glass funnel (3 mL volume, Pyrex®, Fisher Scientific Ireland, Dublin, Ireland) and two septa (Supelco Thermogreen LB-2 Septa plug, Sigma Aldrich, Arklow, Ireland) where the septa served to hold the exposed SPME fibre in the enclosed HS directly above the skin. SPME fibres were exposed within the HS for 15 min, after which the fibre was transferred into the GC injector for desorption.

Blank air samples were collected with the equivalent glass HS used to sample from above skin. The glass funnel HS was fully enclosed by wrapping in aluminium foil followed by parafilm and was sampled in the same manner, again for 15 min (n=6).

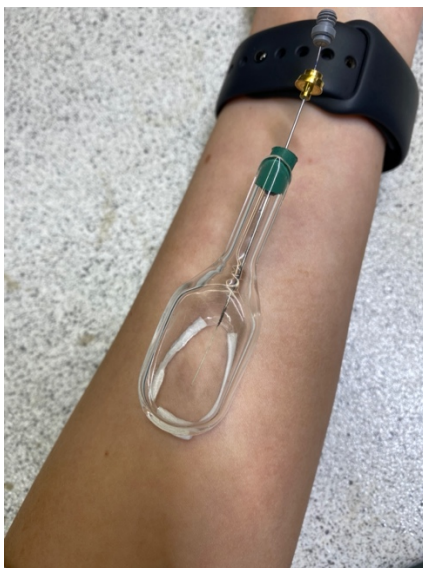


Figure 2.1. HS-SPME housed in a glass HS affixed to the volar forearm.

2.2.2. Gas chromatography-mass spectrometry analysis

An Agilent 7820A gas chromatograph connected to an Agilent 5977B mass selective detector (Agilent Technologies, Inc., Santa Clara, CA, USA) was used for all analyses. Separations were performed on an SLB-5 ms column (30 m \times 0.25 mm \times 0.25 μm df; Supelco).

Helium carrier gas was used throughout this work with a constant flow rate of 1 mL min⁻¹. The system was equipped with a SPME Merlin Microseal (Merlin Instrument Company, Newark, DE, USA), and the inlet was maintained at a temperature of 250°C. Splitless injection was used for all samples, and each SPME fibre was desorbed for 2 min within a SPME inlet liner (Supelco). The initial GC oven temperature was 40°C for 5 minutes after which the oven was programmed at a rate of 10°C min⁻¹ to 270°C. The MS was operated at a scan rate of 3.94 s⁻¹, with a scan range of 35-400 m/z, ion source temperature 230°C and ionising energy of 70 eV.

2.2.3. Data analysis

Agilent MassHunter Qualitative Analysis 10.0 software was used to analyse raw chromatographic data (Figure A2.1). Peak acquisition and the respective peak area data were calculated by employing the chromatogram deconvolution compound mining algorithm. A peak filter of ≥ 10000 counts was set. A Level 2 putative identification of compounds and structures was performed using the National Institute of Standards and Technology (NIST) library, and was supported by a visual comparison of the unknown mass spectra, with previous literature reports and with retention index (RI) matching with a tolerance of ± 15 RI units. A standard mixture of saturated alkanes (C₇–C₃₀), (Sigma Aldrich, Ireland) was used for RI matching. In addition to this, confirmation of the retention time (RT) of compound characteristic to volatile skin emission was carried out using commercially available analytical standards (acetic acid, octanoic acid, nonanoic acid, hexanal, octanal, nonanal, decanal, benzaldehyde, 6-methyl-5-hepten-2-one, geranylacetone and 2-ethyl-1-hexanol) (Merck, Ireland). Furthermore, compounds deemed to be contaminants (e.g. siloxanes likely arising from SPME fibres and column bleed) were excluded from the data set.

RStudio (version 2023.03.0) and Prism (version 9.4.0) were used for all data exploration and visualisation. Wilcoxon testing was used to determine significant difference and p-values < 0.1 were deemed to be statistically significant. Spearman correlation analysis was carried out using R package ‘corrplot’ (version: 0.92). R packages used included: ‘tidyverse’, ‘ggplot2’, ‘ggfortify’. Principal component analysis (PCA) were carried out on the dataset obtained using the R packages: ‘FactoMineR’ and ‘factoextra’. Other R packages used included: ‘tidyverse’, ‘ggplot2’, ‘ggfortify’.

2.2.4. Skin surface pH and tissue dielectric constant measurements

Following the sampling of skin volatiles, skin surface pH at the same skin site was obtained using a wireless HALO flat glass probe (HI14142) (Hanna Instruments). All skin surface pH measurements were carried out in triplicate. Delfin MoistureMeter D, a commercial skin hydration probe (Delfin Technologies, Kuopio, Finland), was used to measure tissue dielectric constant (TDC). Each measurement was repeated 3 times using the probe with an effective measuring depth of 0.5 mm.

2.3. Results and discussion

2.3.1. Stability of the skin volatile profile, skin surface pH and TDC across a day

Diurnal stability of the skin volatile emission from the volar forearm of a healthy female participant was investigated with a wide variety of compound classes emitted from human skin including acids, aldehydes, ketones, alcohols, hydrocarbons and esters. In order to assess diurnal stability, a HS-SPME sample was taken from the volar forearm starting at 10:00 a.m., with a sample taken every hour until 3:00 p.m. Figure 2.2 (a) compares the average absolute abundances of each compound class emitted and total emissions identified in the participants skin volatile profile in the morning (10:00 a.m, 11:00 a.m and 12:00 p.m, n=9) and afternoon samples (1:00 p.m, 2:00 p.m and 3:00 p.m, n=9). Significant differences in morning and afternoon abundances were observed for acidic, ketones and ester compounds. Acidic emission was shown to decrease in the afternoon samples ($p= 0.024$), ketone emission was shown to increase ($p= 4.10 \times 10^{-5}$) and ester emission was shown to decrease ($p= 0.007$). A discussion around individual compounds contributing to these changes and hypotheses for such differences are outlined further on. No significant differences were observed in total, aldehyde, hydrocarbon and alcohol emissions.

In total, 21 compounds were reliably identified across all samples taken at different time points analysed using a combination of RI matching and commercially available analytical standards. Among these are frequently reported skin volatile compounds such as acetic acid, octanoic acid, nonanoic acid, geranylacetone, 6-methyl-5-hepten-2-one, hexanal, octanal, nonanal, decanal, benzaldehyde, 2-ethyl-1-hexanol and isopropyl myristate [2,7,11,39]. Acetic acid, a short chain fatty acid (SCFA) was detected in a high frequency across samples and is known to be a primary microbial metabolite with many studies reporting it as a key component of the human skin volatile profile [39–41]. This SCFA is produced via the catabolism of skin lipids into long-chain fatty acids which are then further broken down by bacterial including

Propionibacteria and Staphylococci present on the skin [42]. Longer chain free fatty acids (FFAs) including octanoic, nonanoic and n-decanoic acid were also recovered within this study and are well-established as main components of secreted sebum produced by sebaceous glands [43,44]. Six saturated and one aromatic aldehydes were recovered across all sampling time-points. Volatile aldehyde emissions from skin are considered to be end-products of lipid peroxidation reactions initiated by oxidative stress [45]. Benzaldehyde was recovered from skin and its production within skin has been linked to benzyl alcohol oxidation and it has also been considered as a microbial metabolite [46–48]. The ketones, 6-methyl-5-hepten-2-one and geranylacetone, which are among the most frequently reported volatile compounds [40] were also recovered from the volar forearm. 2-ethyl-1-hexanol is an alcohol reported previously as a skin volatile [36,48], is linked to microbial degradation of plasticizers [49,50]. Hydrocarbons including tridecane and hexadecane were also recovered and their origin is thought to be endogenous through lipid peroxidation [51]. Compounds known to be from exogenous sources such as the esters, isopropyl myristate, isopropyl palmitate and linal (linked to frequent use of fragrance and cosmetics) [37] were also recovered. Despite employing pre-sampling procedures such as the limitation of the use of cosmetics on the day of sampling, it is impractical to exclude such compounds given their pervasive use in cosmetic products [52,53] and their high frequency of occurrence.

Blank HS samples of room air were also collected and analysed within the same HS volume where acetic acid, nonanal, decanal and 2-ethyl-1-hexanol were all detected but in much lower abundances compared to the average abundances recovered from the headspace of skin (Fig 2.2(b)).

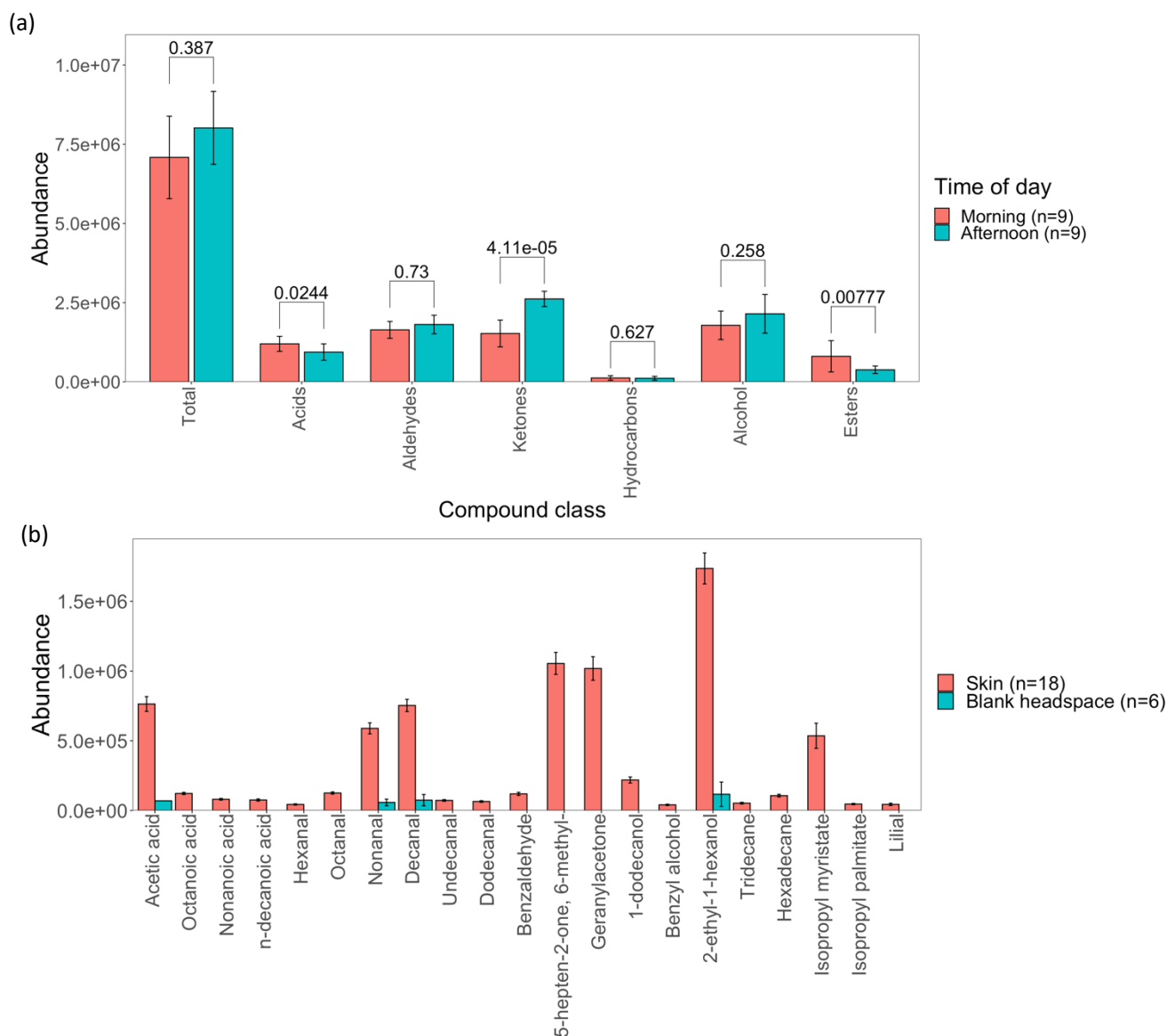


Figure 2.2. (a) Bar chart illustrating differences between the average absolute abundances of each compound class and total emission from the volar of a single participant across morning (10:00 a.m, 11:00 a.m and 12:00 p.m, n=9) and afternoon (1:00 p.m, 2:00 p.m and 3:00 p.m, n=9) samples. Statistical significance was calculated using the Wilcoxon signed rank test. Error bars represent standard deviation in recovered abundances. (b) bar chart illustrating the average emission of each compound from skin (n = 18 samples from a single participant) compared to blank HS samples of indoor air (n=6). Error bars represent standard deviation in abundances recovered.

Following identification of significant differences in the volatile profile of the forearm between morning and afternoon samples in Figure 2.2 (a), correlations between all 21 skin-emitted volatile compounds with time of sampling, skin surface pH and TDC were investigated

(Figure 2.3, Table 2.1). Skin surface pH and TDC were initially assessed for diurnal changes. Some studies have shown changes in the skin surface pH of axillary skin with a significant decrease shown between the morning and evening [54]. Others have shown circadian rhythms of skin surface pH on the shin and forearm with a peak in pH shown around mid-day for both sites [14]. TDC assesses local tissue hydration levels through an impedance measurement [55]. Similarly, diurnal changes in TDC have been observed [55,56]. In this study, skin surface pH was shown to increase significantly across a day ($p = 0.006$) while no significant differences were observed for TDC ($p = 0.726$).

As shown in Fig 2.2 (a) the acidic emission from skin was shown to decrease in the afternoon compared to the morning. Correlation results from Fig 2.3 show that the longer chains VFAs such as nonanoic acid ($p = 0.060$) and n-decanoic (0.061) were significantly decreased across a day and showed negative correlation with skin surface pH ($p=0.056$, $p=0.025$, respectively). This suggests that skin surface pH is linked to the emission of VFAs across a day and is supported by previous work from our group [38]. Other acids emitted from skin including acetic acid ($p = 0.146$) and octanoic acid (0.112) showed no significant change with time or pH.

Most notably, the abundances of the ketones, 6-methyl-5-hepten-2-one and geranylacetone were shown to significantly increase across the day ($p = 0.077$ and $p = 0.042$, respectively). As discussed above, sebum excretion has been shown to increase diurnally with excretion peaking in the mid-afternoon [12,16,57]. Squalene is a key component of sebum and 6-methyl-5-hepten-2-one and geranylacetone emission are volatile metabolites of its lipid peroxidation [39,58] which may explain their up-regulation across a day. Furthermore, the breakdown of squalene is triggered by extrinsic factors such as UV light and ozone and increased exposure to these throughout the day may also explain the increased emission [59]. Moreover, it was noted that the participant showered on the morning of sampling which may have washed/removed sebum from the skin which may lead to the lower abundances of ketones recovered in the morning samples.

In terms of aldehyde emission, it could be hypothesised that emissions would increase throughout the day in a similar way to ketones as they are end-products of lipid peroxidation processes initiated by oxidative stress [60] which may increase with increased exposure to UV light and ozone which are both exogenous sources of reactive oxygen species (ROS) [61]. This work shows a significant diurnal increase for dodecanal ($p = 0.062$) while in contrast, octanal

shows a significant diurnal decrease over the course of day ($p=0.012$) while no other aldehydes recovered showed any diurnal variation significance.

In contrast, the abundance of ester compounds, specifically isopropyl myristate ($p=0.055$) were shown to down-regulated across a day. Ester compounds are typically linked to the frequent use of fragrance and cosmetic products. Despite employing pre-sampling procedures these compounds persist to reside on the skin [7,37]. A decrease in the relative abundance of these ester compounds was observed throughout the day. It could be speculated that higher abundances observed in the morning samples may be related to showering in the morning and cosmetic use from the previous days (fragrance use etc...) and the decline in abundance may indicate metabolization of these compounds by the skin microbiota. For example, isopropyl myristate may be hydrolysed on the skin to myristic acid and its corresponding alcohol, isopropyl alcohol [62]. Furthermore, these esters reside in the stratum corneum (SC) as opposed to sebum. As discussed above, showering on the morning of sampling could have led to the removal of sebum from the skin which may allow for higher volatile emissions of isopropyl myristate to be recovered from the skin. Diurnal changes in sebum production have been noted in many studies causing sebum accumulation throughout the day. Such sebum accumulation could be hypothesised to block the emission of ester products from the SC.

Finally, it could be hypothesised that as hydrophobic sebum on the skin increases throughout the day, TDC might also change, however, no significant difference in TDC across a day was observed for any of the recovered compounds or total volatile emissions. TDC is not a surface measurement and instead measures skin-to-fat tissue water and measures at a depth of 0.5 mm [56,63]. TEWL may be a better measurement for assessing changes in skin surface hydration throughout the day.

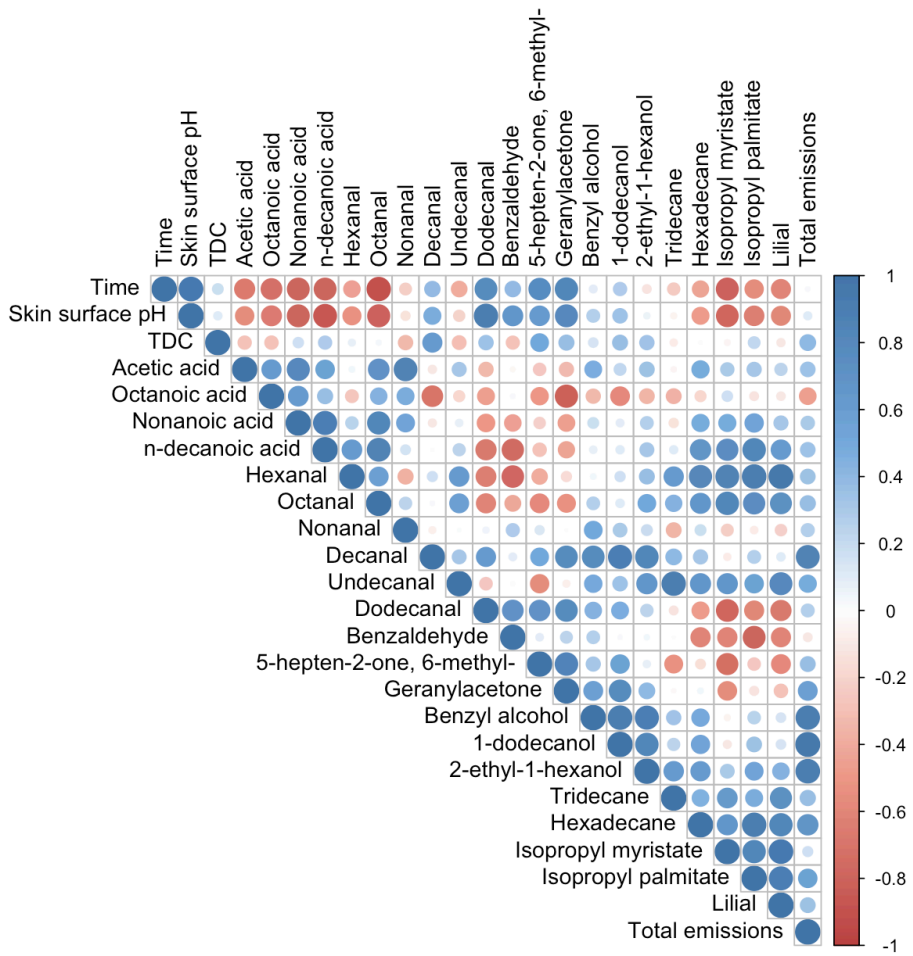


Figure 2.3. Spearman correlation plot of average abundances (n=3) of identified volatile compounds at each sampling point with time of sampling, skin surface pH and TDC for a single female participant. Blue indicates a positive correlation and red indicates a negative correlation.

Table 2.1. Results of Spearman correlation (Fig 2.2) of skin volatile emissions as a function of time of sampling, skin surface pH and TDC for a single female participant (n=1). Significant change ($p < 0.1$) with time, skin surface pH or TDC are bolded and arrows represent up-regulation (\uparrow) or down-regulation (\downarrow).

Compound	Correlation (coefficient <i>r</i> , <i>p</i> -value)		
	Time	Skin surface pH	TDC
Acetic acid	-0.668, 0.146	-0.558, 0.250	-0.287, 0.581
Octanoic acid	-0.712, 0.112	-0.656, 0.157	-0.291, 0.576
Nonanoic acid	-0.792, 0.060 \downarrow	-0.799, 0.056 \downarrow	0.174, 0.742
n-decanoic acid	-0.790, 0.061 \downarrow	-0.867, 0.025 \downarrow	0.286, 0.582
Hexanal	-0.446, 0.375	-0.536, 0.273	0.076, 0.886
Octanal	-0.909, 0.012 \downarrow	-0.810, 0.050 \downarrow	0.037, 0.944
Nonanal	-0.228, 0.663	-0.134, 0.800	-0.336, 0.515
Decanal	0.386, 0.449	0.476, 0.339	0.603, 0.205
Undecanal	-0.400, 0.432	-0.205, 0.697	-0.310, 0.550
Dodecanal	0.788, 0.062 \uparrow	0.908, 0.012 \uparrow	0.341, 0.508
Benzaldehyde	0.393, 0.441	0.656, 0.157	-0.282, 0.588
6-methyl-5-hepten-2-one	0.763, 0.0773 \uparrow	0.631, 0.178	0.516, 0.294
Geranylacetone	0.827, 0.0422 \uparrow	0.803, 0.054 \uparrow	0.372, 0.467
Benzyl alcohol	0.098, 0.854	0.272, 0.602	0.147, 0.781
1-dodecanol	0.288, 0.579	0.344, 0.504	0.366, 0.475
2-ethyl-1-hexanol	-0.121, 0.819	0.061, 0.908	0.335, 0.516
Tridecane	-0.245, 0.639	-0.053, 0.920	-0.082, 0.877
Hexadecane	-0.433, 0.391	-0.473, 0.343	-0.012, 0.981
Isopropyl myristate	-0.801, 0.055 \downarrow	-0.782, 0.065 \downarrow	-0.048, 0.922
Isopropyl palmitate	-0.555, 0.253	-0.632, 0.177	-0.224, 0.669
Lilial	-0.602, 0.206	-0.595, 0.212	-0.107, 0.840
Total emissions	0.029, 0.956	0.103, 0.845	0.406, 0.423

2.3.2. Site variation of the skin volatile profile, skin surface pH and TDC

Stability of the volatile profile from different sites including the volar forearm, lower back, sole of foot, palm and forehead was then investigated. Again, a wide variety of compound classes were emitted from each site including acid, aldehydes, ketones, hydrocarbons, alcohols and esters. Here, in order to assess any variation in the volatilome of each skin site, a 15 min HS-SPME sample was taken from each skin site across 3 days (n=6 hourly measurements per day). Figure 2.4 compares the absolute abundance of each compound class emitted and total emissions across each skin site samples. In terms of total emissions, the palm showed a significantly higher abundance of recovered compounds compared to all other sites sampled. Moreover, the emission of acids, aldehydes and alcohols were found to be highest from the palm. Ketone emission was found to be slightly higher on the forehead compared to the palm, while hydrocarbon emission was observed to be increased at the sole of the foot and the forearm. Ester emission was highest at both the palm and forearm compared to all other sites sampled.

Again, as in section 2.3.1, the same 21 compounds were reliably identified across all samples taken at different body sites using a combination of RI matching and commercially available analytical standards. The origin of these volatile compounds was discussed in section 2.3.1.

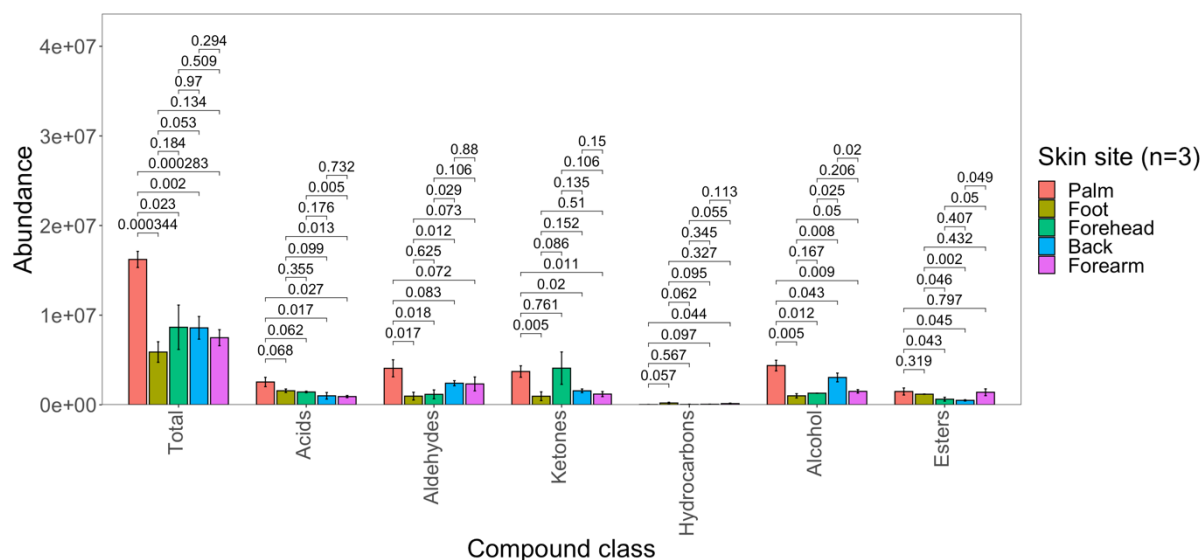


Figure 2.4. Bar chart illustrating differences between the average absolute abundances of each compound class and total emission from each skin site sampled (n=3) (palm, foot, forehead, back and forearm). Statistical significance was calculated for pairwise comparisons of each site

using the Wilcoxon signed rank test and p-values are shown. Error bars represent standard deviation in recovered abundances.

Principal component analysis (PCA) was also carried out in order to further understand dissimilarities in the skin volatile at each site. PCA reduces the dimensionality of the data by identifying characteristic volatiles and uses these to construct new linear variables called principal components (PCs), along which variation is maximised [64]. The principal components are then visualised by scores and loading plots which characterise the dataset. Figure 2.5 (a) shows the PCA scores plot where each sample is coloured to its respective site. Variation between the palm and all other sites is summarised by PC1 (Dim1) while the variation between all other sites sampled is summarised across PC2 (Dim2).

Figure 2.5 (b) shows the loadings plot which summarises the contribution of all the volatiles to the discrimination between skin sites. This shows dodecanal, undecanal, decanal, octanal, octanoic acid and nonanoic acid contribute the greatest to the discrimination of the palm from the other skin sites. It is known that the palm and foot have similar gland distributions with a high density of eccrine glands [31,65] which may suggest that their volatile emission might be similar however there is clear separation between their volatile signatures along PC1. Furthermore, the back and forehead are both sites with a high density of sebaceous glands which may indicate similar emission, however PCA analysis shows clear separation between the two sites along PC2.

Furthermore, the back, foot and the forearm are all clustered quite closely indicating that their volatile profile may be of a similar composition despite differences in their gland distributions whereby hexadecane, tridecane and benzaldehyde all seem to be contributing to their separation from the palm and forehead. Overall, this PCA analysis highlights the ability of the skin volatile profile to discriminate, to some degree, between skin sites.

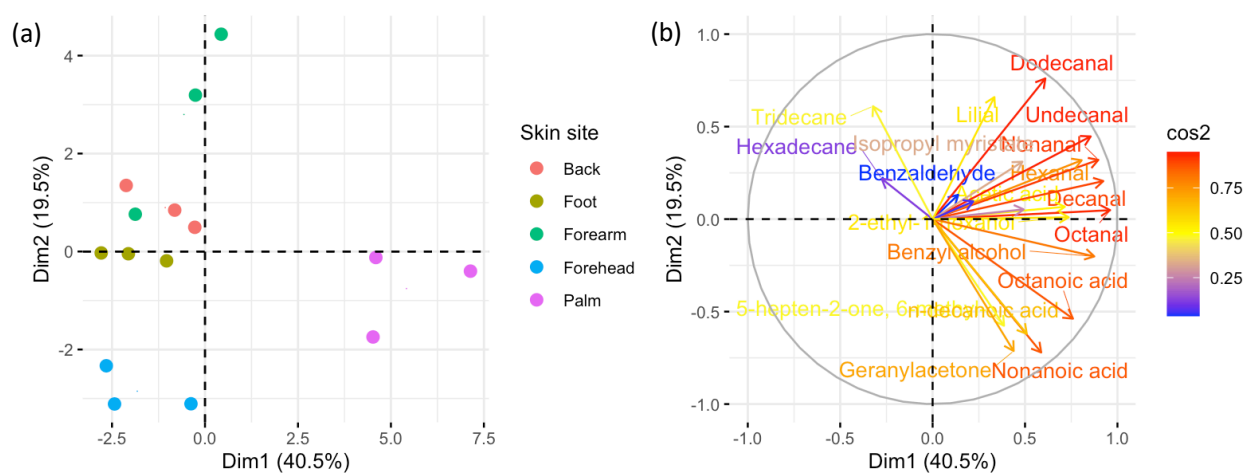


Figure 2.5. (a) Score plot representation from the PCA of the volatile emission from different skin sites sampled across n=3 days (n=1 measurement from each site per day). PC1 and PC2 summarised 60% of the variance of the overall dataset, with 40.5% being summarised by PC1 and 19.5% being summarised by PC2 and (b) loadings plot from the PCA analysis showing the contribution of each compound recovered to the site discrimination. The length and colour of the arrows represent the contribution of each sensor to principal components 1 and 2.

Following identification of variations in site volatile emission (Figure 2.4 and 2.5), differences in the volatile emissions with respect to the 21 individual compounds recovered was then investigated (Figure 2.6, Table 2.2). Each site was categorised based on gland distribution and differences in the volatile profile, skin surface pH and TDC between them were assessed. The palm and the foot are known to have similar gland distribution with a high density of eccrine glands at each site [66], however, the palm has been shown to have a higher number of activated sweat glands compared to the foot [31]. Interestingly, similar skin surface pH measurements were obtained from the palm (4.72 ± 0.01) and foot (4.71 ± 0.02) and similar TDC measurements were also recorded (palm: 40.81 ± 2.54 and foot: 39.42 ± 0.433) indicating that both sites have a similar skin-to-fat water content. Despite these similarities, significant differences in the volatile profile of the sites were observed. For example, all acidic and aldehyde emissions were shown to be higher from the palm compared to the foot. Volatile aldehyde emissions are lipid peroxidation end products and are considered a marker of oxidative stress on the skin. These volatiles result from increased production of reactive oxygen species (ROS) either by endogenous (mitochondria) or exogenous sources (UV light and ozone) [60]. Increased emission from the palm compared to the foot may indicate increased oxidative stress at these sites. For example, the palm is typically exposed to the surrounding environment whereas the foot is not and increased exposure to UV light and ozone may initiate lipid peroxidation thus increasing volatile aldehyde emission. Similarly, the ketones, 5-hepten-2-on, 6-methyl- ($p= 0.093$) and geranylactone ($p= 0.015$) were increased in emission from the palm compared to the forearm and again as they are products of oxidative squalene breakdown and increased exposure to UV light and ozone may cause increased emission due to increased squalene breakdown. In contrast, emission of the hydrocarbon hexadecane was increased in the foot compared to the back and recent studies have found correlation between *Corynebacterium* and *Staphylococcus* bacteria with alkanes such as hexadecane and heptadecane [36]. This correlates with abundances of these bacteria at specific sites, for example the foot possess a high abundance of *Staphylococcus* bacteria in its microbiome which may explain hexadecane's

increased emission at the foot compared to the palm [34]. This highlights that differences in the skin microbiome in both sites may also drive the variation in the volatile profile seen between the palm and the foot. The foot is a moist skin site mainly by Staphylococcaceae bacteria while the palm is a dry skin site populated mainly by Proteobacteria [34]. Such differences may suggest that the volatiles profile of the palm and foot may differ based on their different microbiome composition, however further work is needed to investigate and understand correlations between the two.

Sebaceous glands are mainly found on the face, scalp, chest and back [67] and so the back and forehead volatile emissions, skin surface pH and TDC were examined for site-specific variations. Recently, our group have shown differences between the acidic profile of skin between the forearm, forehead and back of the hand where increased acidic abundance was recovered from the forehead compared to the other sites and these changes were shown to correlate with skin surface pH [38]. Here, increased abundances of the medium-chain VFAs, nonanoic acid and n-decanoic acid, were recovered on the forehead compared to the back (nonanoic acid, $p=0.014$; n-decanoic acid, $p=0.015$). Increased abundances of VFA emission on the forehead may be attributed to a higher density of sebaceous glands on the forehead compared to the back [38,68] or may be linked to the differences in the skin microbiome at each site, whereby the back is mainly populated by Propionibacterium and the forehead is populated mainly by Corynebacterium [34]. Interestingly, skin surface pH of the forehead (4.53 ± 0.02) was found to be significantly lower than that of the back (4.80 ± 0.02) which may be modulated by the increased emission of VFAs on the forehead [38]. Similarly, TDC was significantly increased on the forehead (42.78 ± 1.56) compared to the back (36.5 ± 0.96) indicating an increased skin-to-fat tissue water content in the forehead. Similar to the palm, it could be hypothesised that aldehyde and ketone emissions would be increased on the forehead compared to the back given that it is in contact with UV light and ozone which trigger lipid peroxidation and the breakdown of squalene. Here, an increase in geranylacetone abundance was reported in the forehead compared to the back but a significant decrease in nonanal, undecanal, dodecanal and benzaldehyde was observed. Endogenous production of ROS [69,70] may contribute to the increased aldehyde emission on the back given that the back is not typically exposed to UV light or ozone, although further work would be needed to understand this increased emission.

The forearm is a mixed gland site with the presence of both sebaceous and eccrine glands. Sebaceous gland density is much lower on the forearm compared to forehead and back

along with a decreased eccrine gland density compared to the palm and the foot. The highest skin surface pH (4.85 ± 0.04) and the lowest TDC (34.6 ± 1.15) was observed for the forearm compared to all other skin sites. Interestingly, the lowest abundance of octanoic acid and nonanoic acid were recovered from the volar forearm and their lower abundance may have modulated a lower skin surface pH measurement at the forearm. Aldehydes emission, specifically hexanal, octanal, nonanal and undecanal were found to be increased in emission from the forearm compared to all other body sites, except for the palm, and may be linked to increased UV and ozone exposure at that site.

Furthermore, studies have shown differences in the emission of exogenous compounds across different sites with Gallagher et al. for example showing variations in abundance of the exogenous compounds dimethylsulfone, hexyl salicylate and α -hexyl cinnamaldehyde between the upper back and the volar forearm [37]. Here, the emission of isopropyl myristate, an emollient commonly employed in cosmetic formulations [53], varied across skin sites with increased abundances on the foot, forearm and palm. Differences in the abundances of these exogenous compounds can prove useful in site discrimination and can further understand the use of fragrances and cosmetics across different sites of the body.

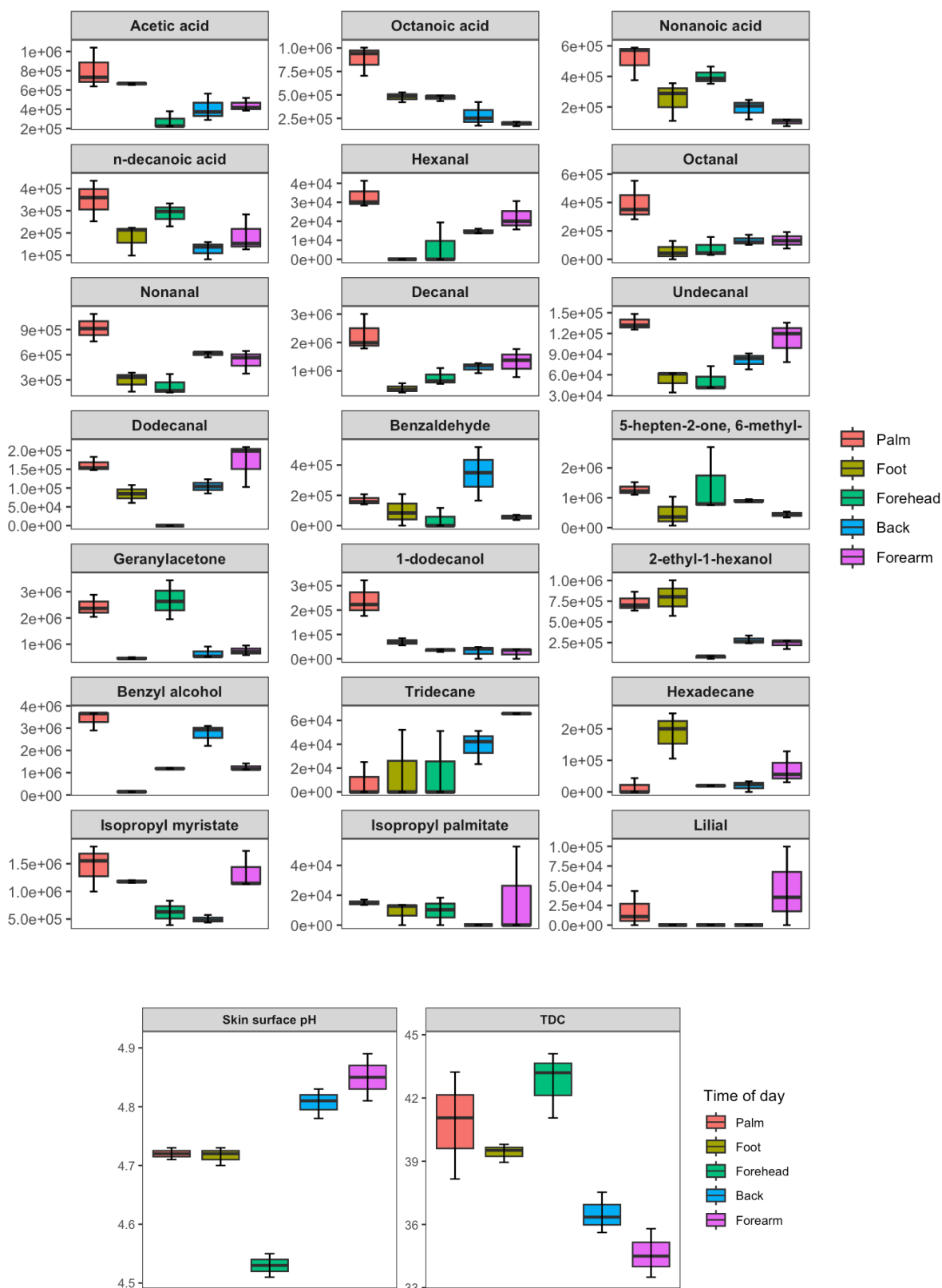


Figure 2.6. (a) Grouped boxplots comparing the abundances of compounds emitted each skin site. Y-axis labels are displayed in scientific notation where $a \times 10^b = a \times 10^b$ and (b) grouped boxplots comparing the skin surface pH and TDC of the different skin sites. Statistical significance was calculated using the Wilcoxon signed rank test. Boxes represent the

interquartile range: the line running across each box represents the 50th percentile (median), the top of the box represents the 75th percentile, and the bottom of the box represents the 25th percentile. The whiskers (error bars) represent either the smallest or largest value within 1.5 times the interquartile range above the 75th percentile or below the 25th percentile.

Table 2.2 Comparisons of the emission of compounds and skin surface pH and TDC measurements from different skin sites (Figure 2.6) where significant p-values are listed ($p < 0.1$). Arrows represent up-regulation (\uparrow) or down-regulation (\downarrow) and n.s = not significant. (For example, \downarrow arrow is shown for acetic acid emission from foot vs back indicating that the abundance emitted is lower in the back compared to the foot.)

Compound	p-value									
	Foot vs. back	Foot vs. palm	Foot vs. Forearm	Foot vs. forehead	Back vs. palm	Back vs. forearm	Back vs. forehead	Palm vs. forearm	Palm vs. forehead	Forearm vs. forehead
Skin surface pH	0.010 \uparrow	n.s.	0.018 \uparrow	0.0003 \downarrow	0.016 \downarrow	n.s.	0.0001 \downarrow	0.025 \uparrow	0.0007 \downarrow	0.001 \downarrow
TDC	0.021 \downarrow	n.s.	0.011 \downarrow	0.056 \uparrow	0.084 \uparrow	n.s.	0.007 \uparrow	0.035 \downarrow	n.s.	0.002 \uparrow
Acetic acid	0.087 \downarrow	n.s.	0.029 \uparrow	0.016 \downarrow	0.062 \uparrow	n.s.	n.s.	0.084 \downarrow	0.034 \downarrow	0.069 \downarrow
Octanoic acid	n.s.	0.036 \uparrow	0.004 \downarrow	n.s.	0.008 \uparrow	n.s.	n.s.	0.015 \downarrow	n.s.	4.0×10^{-4} \uparrow
Nonanoic acid	n.s.	0.061 \uparrow	n.s.	n.s.	0.024 \uparrow	n.s.	0.014 \uparrow	0.023 \downarrow	n.s.	0.006 \uparrow
n-Decanoic acid	n.s.	0.067 \uparrow	n.s.	0.100 \uparrow	0.036 \uparrow	n.s.	0.015 \uparrow	0.088 \downarrow	n.s.	n.s.
Hexanal	0.002 \uparrow	0.015 \uparrow	0.038 \uparrow	n.s.	0.041 \uparrow	n.s.	n.s.	n.s.	n.s.	n.s.
Octanal	n.s.	0.036 \uparrow	n.s.	n.s.	0.075 \uparrow	n.s.	n.s.	0.068 \downarrow	n.s.	n.s.
Nonanal	0.035 \uparrow	0.008 \uparrow	0.089 \uparrow	n.s.	0.076 \uparrow	n.s.	0.026 \downarrow	0.036 \downarrow	n.s.	0.050 \downarrow
Decanal	0.007 \uparrow	0.031 \uparrow	0.072 \uparrow	n.s.	0.085 \uparrow	n.s.	n.s.	n.s.	n.s.	n.s.
Undecanal	0.073 \uparrow	0.003 \uparrow	0.055 \uparrow	n.s.	0.005 \uparrow	n.s.	0.090 \downarrow	n.s.	n.s.	0.052 \downarrow
Dodecanal	0.048 \uparrow	n.s.	0.039 \downarrow	0.028 \downarrow	0.012 \uparrow	n.s.	0.012 \downarrow	0.008 \downarrow	0.009 \downarrow	0.029 \downarrow
Benzaldehyde	n.s.	n.s.	n.s.	n.s.	n.s.	0.100 \downarrow	0.081 \downarrow	0.016 \downarrow	0.060 \downarrow	n.s.
5-hepten-2-one, 6-methyl-	n.s.	0.093 \uparrow	n.s.	n.s.	0.088 \uparrow	0.007 \downarrow	n.s.	0.011 \downarrow	n.s.	n.s.
Geranylacetone	n.s.	0.015 \uparrow	n.s.	0.036 \uparrow	0.008 \uparrow	n.s.	0.034 \uparrow	0.011 \downarrow	n.s.	0.040 \uparrow
Benzyl alcohol	0.100 \downarrow	0.053	0.047 \downarrow	0.039 \downarrow	0.029 \uparrow	n.s.	n.s.	0.030 \downarrow	n.s.	n.s.
1-dodecanol	0.048 \downarrow	n.s.	0.039 \downarrow	0.028 \downarrow	0.012 \uparrow	n.s.	0.012 \downarrow	0.008 \downarrow	0.009 \downarrow	0.029 \downarrow
2-ethyl-1-hexanol	0.011 \uparrow	0.006 \uparrow	0.006 \uparrow	6.5×10^{-5} \uparrow	0.152 \uparrow	0.023 \downarrow	0.029 \downarrow	0.008 \downarrow	0.013 \downarrow	n.s.
Tridecane	n.s.	n.s.	n.s.	n.s.	0.060 \downarrow	0.083 \uparrow	n.s.	0.021 \uparrow	n.s.	0.100 \downarrow
Hexadecane	0.052 \downarrow	0.044 \downarrow	0.100 \downarrow	0.059 \downarrow	n.s.	n.s.	n.s.	n.s.	n.s.	n.s.
Isopropyl myristate	0.002 \downarrow	n.s.	n.s.	0.046 \downarrow	0.054 \uparrow	0.046 \uparrow	n.s.	n.s.	n.s.	0.046 \downarrow
Isopropyl palmitate	n.s.	n.s.	n.s.	n.s.	0.005 \uparrow	n.s.	n.s.	n.s.	n.s.	n.s.
Lilial	n.s.	n.s.	n.s.	n.s.	n.s.	n.s.	n.s.	n.s.	n.s.	n.s.

2.4. Conclusion

The main aim of this study was to investigate diurnal- and site-associated variations in skin volatile emissions, skin surface pH and TDC measurements. A variety of compounds classes including acids, aldehydes, ketones, alcohols, hydrocarbons and esters were recovered from the skin with a total of 21 compounds being emitted.

Initially, diurnal variation in the volatile profile of the volar forearm was assessed. The ketone and ester emission from skin were shown to have the most variation across a day. Emission of the ketones, 6-methyl-5-hepten-2-one and geranylacetone were shown to increase significantly across the day while a decrease in the emission of ester compounds such as isopropyl myristate and palmitate was observed. Significant diurnal-variation was also noted for skin surface pH and correlation between the acidic profile of skin was established. No variations in TDC measurements on the volar forearm were observed.

Following this, site variation of the skin volatile profile was assessed where HS-SPME samples were taken from the palm, foot, forearm, forehead and lower back. Overall, the palm showed the highest emission of most volatile and this may be attributed to dense population of eccrine glands at that site which may induce sweating. Interestingly, an increased emission of acidic compounds was observed from the forehead compared to all other sites except the palm. Furthermore, ketone emission was also up-regulated at the forehead compared to all other sites and this may be linked to the increased sebaceous gland density at this site. Significant changes in skin surface pH and TDC across sites were also noted.

Overall, these results obtained using a comprehensive HS-SPME GC-MS workflow show proof of concept for diurnal and site variation in the skin volatile profile, skin surface pH and TDC. While these findings provide evidence for diurnal and site variation, they are limited by the small sample size. Further work would need to be carried out to assess these changes in larger participant cohorts. Moreover, in terms of the diurnal study, abundances of compounds at only six time points during the daylight cycle were investigated. Investigating changes in the volatile profile between daylight and night-time cycles may prove more interesting. Understanding diurnal and site variation of these parameters in healthy participants can allow for characterisation of a healthy profile which can then be used to help in the diagnosis of disease. Furthermore, this work may prove useful in the development of treatments in the cosmetic industry.

2.5. References

- [1] Heikenfeld J, Jajack A, Rogers J, Gutruf P, Tian L, Pan T, Li R, Khine M, Kim J, Wang J and Kim J 2018 Wearable sensors: modalities, challenges, and prospects *Lab Chip* **18** 217–48
- [2] Drabińska N, Flynn C, Ratcliffe N, Belluomo I, Myridakis A, Gould O, Fois M, Smart A, Devine T and Costello B D L 2021 A literature survey of all volatiles from healthy human breath and bodily fluids: the human volatilome *Journal of Breath Research* **15** 034001
- [3] Peters R, Veenstra R, Heutinck K, Baas A, Munniks S and Knotter J 2023 Human scent characterization: A review *Forensic Science International* 111743
- [4] Yetisen A K, Moreddu R, Seifi S, Jiang N, Vega K, Dong X, Dong J, Butt H, Jakobi M, Elsner M and Koch A W 2019 Dermal Tattoo Biosensors for Colorimetric Metabolite Detection *Angewandte Chemie International Edition* **58** 10506–13
- [5] Ghaffari R, Aranyosi A J, Lee S P, Model J B and Baker L B 2023 The Gx Sweat Patch for personalized hydration management *Nat Rev Bioeng* **1** 5–7
- [6] Shirasu M and Touhara K 2011 The scent of disease: volatile organic compounds of the human body related to disease and disorder *The Journal of Biochemistry* **150** 257–66
- [7] Dormont L, Bessièrè J-M and Cohuet A 2013 Human Skin Volatiles: A Review *Journal of Chemical Ecology* **39** 569–78
- [8] Thomas A N, Riazanskaia S, Cheung W, Xu Y, Goodacre R, Thomas C L P, Baguneid M S and Bayat A 2010 Novel noninvasive identification of biomarkers by analytical profiling of chronic wounds using volatile organic compounds *Wound Repair Regen* **18** 391–400
- [9] Trivedi D K, Sinclair E, Xu Y, Sarkar D, Walton-Doyle C, Liscio C, Banks P, Milne J, Silverdale M, Kunath T, Goodacre R and Barran P 2019 Discovery of Volatile Biomarkers of Parkinson’s Disease from Sebum *ACS Central Science* **5** 599–606
- [10] Kwak J, Gallagher M, Ozdener M H, Wysocki C J, Goldsmith B R, Isamah A, Faranda A, Fakharzadeh S S, Herlyn M, Johnson A T C and Preti G 2013 Volatile biomarkers from human melanoma cells *J Chromatogr B Analyt Technol Biomed Life Sci* **931** 90–6
- [11] Duffy E, Jacobs M R, Kirby B and Morrin A 2017 Probing skin physiology through the volatile footprint: Discriminating volatile emissions before and after acute barrier disruption *Experimental Dermatology* **26** 919–25
- [12] Matsui M S, Pelle E, Dong K and Pernodet N 2016 Biological Rhythms in the Skin *Int J Mol Sci* **17** 801
- [13] Lyons A B, Moy L, Moy R and Tung R 2019 Circadian Rhythm and the Skin: A Review of the Literature *J Clin Aesthet Dermatol* **12** 42–5
- [14] Yosipovitch G, Xiong G L, Haus E, Sackett-Lundeen L, Ashkenazi I and Maibach H I 1998 Time-Dependent Variations of the Skin Barrier Function in Humans:

- Transepidermal Water Loss, Stratum Corneum Hydration, Skin Surface pH, and Skin Temperature *Journal of Investigative Dermatology* **110** 20–3
- [15] Tsukahara K, Takema Y, Moriwaki S, Fujimura T and Imokawa G 2001 Diurnal variation affects age-related profile in skin thickness *J Cosmet Sci* **52** 391–7
- [16] Fur I L, Reinberg A, Lopez S, Morizot F, Mechkouri M and Tschachler E 2001 Analysis of Circadian and Ultradian Rhythms of Skin Surface Properties of Face and Forearm of Healthy Women *J Invest Dermatol* **117** 718–24
- [17] Nobs S P, Tuganbaev T and Elinav E 2019 Microbiome diurnal rhythmicity and its impact on host physiology and disease risk *EMBO reports* **20** e47129
- [18] Pearson J A, Wong F S and Wen L 2020 Crosstalk between circadian rhythms and the microbiota *Immunology* **161** 278–90
- [19] Hoisington A J, Stamper C E, Bates K L, Stanislawski M A, Flux M C, Postolache T T, Lowry C A and Brenner L A 2023 Human microbiome transfer in the built environment differs based on occupants, objects, and buildings *Sci Rep* **13** 6446
- [20] Wilkins D, Tong X, Leung M H Y, Mason C E and Lee P K H 2021 Diurnal variation in the human skin microbiome affects accuracy of forensic microbiome matching *Microbiome* **9** 129
- [21] Oh J, Byrd A L, Park M, Kong H H and Segre J A 2016 Temporal Stability of the Human Skin Microbiome *Cell* **165** 854–66
- [22] Martinez-Lozano Sinues P, Tarokh L, Li X, Kohler M, Brown S A, Zenobi R and Dallmann R 2014 Circadian Variation of the Human Metabolome Captured by Real-Time Breath Analysis *PLoS One* **9** e114422
- [23] Liotino V, Dragonieri S, Quaranta V N, Carratu P, Ranieri T and Resta O 2018 Influence of circadian rhythm on exhaled breath profiling by electronic nose *J Biol Regul Homeost Agents* **32** 1261–5
- [24] Berna A Z, McCarthy J S, Wang X R, Michie M, Bravo F G, Cassells J and Trowell S C 2018 Diurnal variation in expired breath volatiles in malaria-infected and healthy volunteers *J. Breath Res.* **12** 046014
- [25] Sinues P M-L, Kohler M and Zenobi R 2013 Monitoring Diurnal Changes in Exhaled Human Breath *Anal. Chem.* **85** 369–73
- [26] Schmidt F M, Vaittinen O, Metsälä M, Lehto M, Forsblom C, Groop P-H and Halonen L 2013 Ammonia in breath and emitted from skin *J. Breath Res.* **7** 017109
- [27] Schmidt F M, Metsälä M, Vaittinen O and Halonen L 2011 Background levels and diurnal variations of hydrogen cyanide in breath and emitted from skin *J. Breath Res.* **5** 046004
- [28] Yu J, Wang D, Tipparaju V V, Jung W and Xian X 2022 Detection of transdermal biomarkers using gradient-based colorimetric array sensor *Biosensors and Bioelectronics* **195** 113650

- [29] Duffy E and Morrin A 2019 Endogenous and microbial volatile organic compounds in cutaneous health and disease *TrAC Trends in Analytical Chemistry* **111** 163–72
- [30] Tagami H 2008 Location-related differences in structure and function of the stratum corneum with special emphasis on those of the facial skin *International Journal of Cosmetic Science* **30** 413–34
- [31] Taylor N A and Machado-Moreira C A 2013 Regional variations in transepidermal water loss, eccrine sweat gland density, sweat secretion rates and electrolyte composition in resting and exercising humans *Extrem Physiol Med* **2** 4
- [32] Murphrey M B, Safadi A O and Vaidya T 2021 *Histology, Apocrine Gland* (StatPearls Publishing)
- [33] Montagna W and Parakkal P F 1974 *The structure and function of skin* (New York: Academic Press)
- [34] Grice E A and Segre J A 2011 The skin microbiome *Nat Rev Microbiol* **9** 244–53
- [35] Grice E A, Kong H H, Conlan S, Deming C B, Davis J, Young A C, Bouffard G G, Blakesley R W, Murray P R, Green E D, Turner M L and Segre J A 2009 Topographical and Temporal Diversity of the Human Skin Microbiome *Science* **324** 1190–2
- [36] Haertl T, Owsienko D, Schwinn L, Hirsch C, Eskofier B M, Lang R, Wirtz S and Loos H M 2023 Exploring the interrelationship between the skin microbiome and skin volatiles: A pilot study *Frontiers in Ecology and Evolution* **11**
- [37] Gallagher M, Wysocki C J, Leyden J J, Spielman A I, Sun X and Preti G 2008 Analyses of volatile organic compounds from human skin *British Journal of Dermatology* **159** 780–91
- [38] Shetewi T, Finnegan M, Fitzgerald S, Xu S, Duffy E and Morrin A 2021 Investigation of the relationship between skin-emitted volatile fatty acids and skin surface acidity in healthy participants – a pilot study *Journal of Breath Research* **15** 037101
- [39] Rankin-Turner S and McMeniman C 2022 A headspace collection chamber for whole body volatilomics
- [40] Drabińska N, Flynn C, Ratcliffe N, Belluomo I, Myridakis A, Gould O, Fois M, Smart A, Devine T and Costello B D L 2021 A literature survey of all volatiles from healthy human breath and bodily fluids: the human volatilome *Journal of Breath Research* **15** 034001
- [41] Wang N, Ernle L, Bekö G, Wargocki P and Williams J 2022 Emission Rates of Volatile Organic Compounds from Humans *Environmental Science & Technology* **56** 4838–48
- [42] James A G, Hyliands D and Johnston H 2004 Generation of volatile fatty acids by axillary bacteria *International Journal of Cosmetic Science* **26** 149–56
- [43] Ludovici M, Kozul N, Materazzi S, Risoluti R, Picardo M and Camera E 2018 Influence of the sebaceous gland density on the stratum corneum lipidome *Scientific Reports* **8** 11500

- [44] Girod A, Ramotowski R and Weyermann C 2012 Composition of fingermark residue: A qualitative and quantitative review *Forensic Science International* **223** 10–24
- [45] Mochalski P, Wiesenhofer H, Allers M, Zimmermann S, Güntner A T, Pineau N J, Lederer W, Agapiou A, Mayhew C A and Ruzsanyi V 2018 Monitoring of selected skin- and breath-borne volatile organic compounds emitted from the human body using gas chromatography ion mobility spectrometry (GC-IMS) *Journal of Chromatography B* **1076** 29–34
- [46] Jenkins C L and Bean H D 2020 Dependence of the Staphylococcal Volatilome Composition on Microbial Nutrition *Metabolites* **10** 347
- [47] Timm C M, Lloyd E P, Egan A, Mariner R and Karig D 2018 Direct Growth of Bacteria in Headspace Vials Allows for Screening of Volatiles by Gas Chromatography Mass Spectrometry *Frontiers in Microbiology* **9** 491
- [48] Acevedo C A, Sánchez E Y, Reyes J G and Young M E 2007 Volatile Organic Compounds Produced by Human Skin Cells *Biological Research* **40**
- [49] Wakayama T, Ito Y, Sakai K, Miyake M, Shibata E, Ohno H and Kamijima M 2019 Comprehensive review of 2-ethyl-1-hexanol as an indoor air pollutant *Journal of Occupational Health* **61** 19–35
- [50] Nalli S, Horn O J, Grochowalski A R, Cooper D G and Nicell J A 2006 Origin of 2-ethylhexanol as a VOC *Environmental Pollution* **140** 181–5
- [51] Van Gossum A and Decuyper J 1989 Breath alkanes as an index of lipid peroxidation *Eur Respir J* **2** 787–91
- [52] McGinty D, Scognamiglio J, Letizia C S and Api A M 2010 Fragrance material review on 2-ethyl-1-hexanol *Food and Chemical Toxicology* **48** S115–29
- [53] Draelos Z D and DiNardo J C 2006 A re-evaluation of the comedogenicity concept *Journal of the American Academy of Dermatology* **54** 507–12
- [54] Burry J, Coulson H F and Roberts G 2001 Circadian rhythms in axillary skin surface pH *Int J Cosmet Sci* **23** 207–10
- [55] Mayrovitz H N 2017 Diurnal changes in local skin water assessed via tissue dielectric constant at 300 MHz *Biomed. Phys. Eng. Express* **3** 047001
- [56] Mayrovitz H N Tissue Dielectric Constant of the Lower Leg as an Index of Skin Water: Temporal Variations *Cureus* **14** e26506
- [57] Mayrovitz H N and Berthin T Assessing Potential Circadian, Diurnal, and Ultradian Variations in Skin Biophysical Properties *Cureus* **13** e17665
- [58] Mochalski P, King J, Unterkofler K, Hinterhuber H and Amann A 2014 Emission rates of selected volatile organic compounds from skin of healthy volunteers *Journal of Chromatography B* **959** 62–70

- [59] Coffaro B and Weisel C P 2022 Reactions and Products of Squalene and Ozone: A Review *Environ. Sci. Technol.* **56** 7396–411
- [60] Ron-Doitch S and Kohen R 2020 The Cutaneous Physiological Redox: Essential to Maintain but Difficult to Define *Antioxidants (Basel)* **9** 942
- [61] Chen J, Liu Y, Zhao Z and Qiu J 2021 Oxidative stress in the skin: Impact and related protection *International Journal of Cosmetic Science* **43** 495–509
- [62] Anon 1982 Final Report on the Safety Assessment of Myristyl Myristate and Isopropyl Myristate *Journal of the American College of Toxicology* **1** 55–80
- [63] Mayrovitz H N, Carson S and Luis M 2010 Male–female differences in forearm skin tissue dielectric constant *Clinical Physiology and Functional Imaging* **30** 328–32
- [64] Ringnér M 2008 What is principal component analysis? *Nat Biotechnol* **26** 303–4
- [65] Harker M 2013 Psychological Sweating: A Systematic Review Focused on Aetiology and Cutaneous Response *SPP* **26** 92–100
- [66] Baker L B 2019 Physiology of sweat gland function: The roles of sweating and sweat composition in human health *Temperature (Austin)* **6** 211–59
- [67] SanMiguel A and Grice E A 2015 Interactions between host factors and the skin microbiome *Cell. Mol. Life Sci.* **72** 1499–515
- [68] Samaras S and Hoptroff M 2020 The Microbiome of Healthy Skin *Skin Microbiome Handbook* (John Wiley & Sons, Ltd) pp 1–32
- [69] Li J-M and Shah A M 2003 ROS generation by nonphagocytic NADPH oxidase: potential relevance in diabetic nephropathy *J Am Soc Nephrol* **14** S221–226
- [70] Sabharwal S S and Schumacker P T 2014 Mitochondrial ROS in cancer: initiators, amplifiers or an Achilles' heel? *Nat Rev Cancer* **14** 709–21

Chapter 3: Skin volatile emission profiling of healthy participants – influence of gender and age

Abstract

The skin is the largest organ of the body, is complex, and has tremendous potential for non- or minimally-invasive diagnostics in part due to its waste secretion function. Acting as a barrier to the surrounding external environment, it prevents invasion by pathogenic microbes and regulates water and solute loss. Gender-linked physiological differences in skin are well known and it is also well-established that structural, physical and biochemical changes occur in healthy skin during the aging process. The volatile emission from human skin is of great interest as it contains a variety of biomarkers that can provide information on the metabolic activity underway in the body and can be sampled in a wholly non-invasive manner. Previous research has shown that the skin volatile profile changes with age but is limited. This work aims to further characterise the volatile emission profile from the skin (volar forearm) in a healthy participant cohort (n=60) and assess changes with gender and age, via headspace-solid phase microextraction (HS-SPME) with analysis via gas chromatography-mass spectrometry (GC-MS). Characterisation of the skin volatile of the participant cohort showed there was a variety of compound classes emitted from skin, such as acids, aldehydes, ketones, alcohols, hydrocarbons and esters, being recovered with variability in recovery and relative abundance. A total of 18 compounds were deemed eligible for the investigation of the influence of gender and age on the skin volatile emission study based on a frequency detection threshold. Origins of each of the compounds included in the study were also discussed.

Gender influences on the skin volatile emission were observed. The acidic, aldehyde and ester emissions of male and female participants showed significant differences indicating that both data sets should be treated individually when assessing changes in VOC emissions with age. Statistical analysis of the volatile profile with age showed that there were 6 volatile compounds (acetic acid, hexanal, nonanal, undecanal, benzyl alcohol and 2-ethyl-1-hexanol) that changed in abundance with increasing participant age. Finally, MLR models showed that skin surface pH, TDC, gender and age-significant volatile compounds allowed for improved prediction of age compared to a model only containing age-significant compounds. Overall, this study provides a comprehensive analysis of observed changes in skin volatile profiles with age and gender. This non-invasive analysis of skin volatiles allows us to assess age-related changes in skin barrier function and cutaneous microbial defence which may manifest into disease and may also prove useful for the development of anti-aging treatments in the cosmetic industry.

3.1. Introduction

The skin is the largest organ of the human body and has a surface area of 1.5-2 m² [1]. It is a complex organ that is comprised of three main layers, the epidermis, dermis and subcutaneous tissue or hypodermis [2]. Each layer of the skin varies in structure, function and composition. The main function of the skin is as a barrier against the external environment around us [3,4]. It prevents the invasion of pathogens into the body that might cause infection and helps to regulate loss of water and solutes [5]. The hypodermis layer is found deep within the skin and binds the skin organ to the skeletal frame of the body. Located above this is the dermis and this layer protects the skin against mechanical damage. The outermost layer of the skin is the epidermis, which is comprised of sublayers including the stratum basale, stratum spinosum, stratum granulosum and the final layer, exposed to the external environment, the stratum corneum (SC) [2].

Gender-linked differences in the skin's structural, physical and biochemical properties have been well-reported and are mainly linked to differences in the metabolism of sex hormones [6–8]. Male skin is known to be thicker than female skin along with an increased collagen density, which is a major component in skin thickness [9] and may be linked to increased testosterone stimulation in males. Moreover, the biochemical composition, specifically the microbiome of skin [10,11], has been shown to differ between genders with increased relative abundances of *Propionibacterium* and *Corynebacterium* in males compared to females [12]. Other differences include an increased skin surface pH in females and higher transepidermal water loss (TEWL) compared to males [13]. Rates of sweating and sebum production also differ between genders with males exhibiting increased sweating and sebum content on skin [14].

In addition to this, it is well-known that aging of the skin can also induce profound changes in the skin's biochemical, structural and physical properties that can lead to impaired biological function and even disease. In general, the aging of human skin is driven by two basic processes: intrinsic aging, also known as chronological aging which occurs due to inherent genetics and extrinsic aging, attributed to environmental and lifestyle factors, including sunlight exposure and diet [15]. Phenotypic changes in cutaneous cells occur through these aging processes as well as functional and structural changes in extracellular matrix components such as collagen, elastin and proteoglycans which support strength, elasticity and hydration of the skin [16].

One of the main mechanisms through which aging of the structural and physical properties of skin occurs is via oxidative damage, caused by an increased production of reactive oxygen species (ROS) in the skin [17–20]. Endogenous sources of ROS include by-products of the

mitochondrial aerobic metabolism electron transport chain [21,22], while exogenous sources include ultraviolet (UV) light and ozone (O₃). ROS activate a myriad of signalling pathways that result in reduced collagen production, synthesis and activation of matrix metalloproteinases (MMPs) for degrading connective tissue, secretion of senescence-associated secretory phenotype (SASP), all of which ultimately promote aging of skin.

Other physiological skin changes also occur during aging, including an increase in skin surface pH [23–27], decreases in skin tissue hydration and transepidermal water loss (TEWL) [24] and changes in the composition of the skin microbiome [28]. This increase in pH is linked to a decreased sodium-hydrogen antiporter 1 (NHE1) expression [29], slowed breakdown of filaggrin [30] and reduced/delayed breakdown of phospholipids into free fatty acids [23]. Rates of sweat and sebum production are also known to decrease with age, leading to a decreased buffering capacity of the skin [31].

Age-associated changes in the skin microbiome have been established [32,33]. Howard et al for example recently demonstrated increased bacterial diversity across several skin sites with increasing age. It was also noted that *Lactobacillus* and *Cutibacterium* demonstrated a significant change (decrease) in abundance at all sampled skin sites with increasing age [28]. These changes correlated with aging-associated alterations in several host factors, including decreased sebum and increased lipids/natural moisturising factors (NMFs). Other researchers have also demonstrated age-related changes in the microbiome including changes in the relative abundances of *Propionibacterium* and *Corynebacterium* [28,34].

The volatile emission from human skin, originating from glandular secretions and their interaction with microorganism on the skins surface [35], contains a variety of biomarkers that can provide information on endogenous metabolic activities as well as the microbial nature [36]. Over 600 volatile compounds have been detected in human skin extracts and comprise of a variety of compound classes including alkanes, alkenes, aldehydes, acids, ketones, alcohols, sulphur-containing compounds and nitrogen-containing compounds [37].

Specific compounds, including long chain fatty acids (FAs) such as pentadecanoic acid and hexadecenoic acid have been shown to be linked to gender with males having an increased abundance [38,39]. This increased abundances of FAs has been linked to a decreased skin surface pH observed in males [13]. Furthermore, aldehydes and ketone emission has been shown to be increased in male vs female participants [38]. Other studies however have shown no change in skin volatile emission with gender [40].

Certain volatile compounds including specific aldehydes have been noted as characteristic of aging. Haze et al [41] identified the unsaturated aldehyde 2-nonenal as a characteristic odour of aging in male participants over 40 years. The increase in emission of 2-nonenal is linked to oxidative stress and an increased rate of lipid peroxidation of the unsaturated fatty acid, palmitoleic acid, known to increase with age. However, other studies have also detected 2-nonenal in younger participants, weakening the case for it as a marker of age [42]. Gallagher et al [40] observed increased abundances of the saturated aldehyde nonanal, and also benzothiazole and dimethylsulfone within the skin volatile emission with age that were statistically significant. In general, the volatile aldehyde emission from the body is considered a marker of oxidative stress [43] resulting from an increased production of ROS. Fatty acids [44,45] are present in sebum [46,47] and ROS from the outlined sources induce peroxidation of these fatty acids. This involves the β -scission of alkoxy radicals formed by the homolytic cleavage of fatty acid hydroperoxides, subsequently producing volatile aldehydes thus making these compounds reflect oxidative stress on the skin. Interestingly, these volatile aldehydes [48,49] have been investigated as activators of the Nrf-2-keap1 pathway [20,50] in human keratinocytes which is a principle protective response to oxidative and electrophilic stressors [49].

To date, research on gender and age-associated [40,41] changes in the skin volatile profile are limited. This work aims to further understand changes in the volatile profile with gender and age in healthy skin using a direct HS-SPME sampling coupled with GC-MS analysis in a participant study (n=60). Here, we focus on skin characteristic compounds recovered, identifying 18 compounds as being emitted from the volar forearm. Other physiological parameters of skin including skin surface pH and tissue dielectric constant (TDC) was also measured to investigate their correlation with participant gender, age and volatile profile. Assessment of changes in the human skin volatilome with age may prove useful when diagnosing disease in elderly patients and also to the development of anti-aging treatments in the cosmetic industry.

3.2. Materials and methods

3.2.1. Participant profile and skin volatile emission sampling

60 healthy volunteers, aged 18-78 (39 female, aged 18-71, median age = 32, mean age = 36; 21 male, aged 19-78, median age = 47, mean age = 43), were recruited (Figure 3.1). No special dietary regimes were applied, however, participants were asked not to apply perfumes or cosmetics on their arms on the day of sample volatile collection. Participants were informed

on the aim and purpose of the study and asked to provide written informed consent alongside filling out a short questionnaire about their gender, age and cosmetic/fragrance use. The local ethics committee (Dublin City University Research Ethics Committee) approved the study on skin volatiles prior to commencement of the work (DCUREC/2016/053), and the study was performed according to the Declaration of Helsinki. Solid-phase microextraction (SPME) fibres were used for sampling volatiles in a headspace (HS) above the skin using a method described previously [51]. Briefly, SPME fibres comprised of 50/30/20 μm divinylbenzene/carboxen/polydimethylsiloxane Stableflex (2 cm) assemblies (Supelco Corp., Bellefonte, PA, USA). The SPME fibre was housed within a glass HS affixed to the volar forearm with Leukosilk surgical tape (BSN Medical GmbH, Hamburg, Germany). This comprised of a glass funnel (3 mL volume, Pyrex®, Fisher Scientific Ireland, Dublin, Ireland) and two septa (Supelco Thermogreen LB-2 Septa plug, Sigma Aldrich, Arklow, Ireland) where the septa served to hold the exposed SPME fibre in the enclosed HS directly above the skin. SPME fibres were exposed within the HS for 15 min, after which the fibre was transferred into the GC injector for desorption. All samples were collected during November 2021-February 2022.

3.2.2. Standard calibration curves

Specified concentrations of nonanal (CAS: 124-19-6, purity: 95%) and decanal (CAS: 112-31-2, purity: >98%) standards (Sigma-Aldrich, Ireland), were prepared individually in n-hexane and 1 μl volumes of these solutions were pipetted into separate 20 mL glass vials. Glass vials were sealed and the solutions were allowed to evaporate at 37°C for 10 min. Complete evaporation was assumed, and using the Ideal Gas Law [52], the HS concentrations of both nonanal and decanal in separate vials were recorded as 0.625, 1.25, 2.5, 5, 10 and 20 ppb. Finally, the HS of the vials were sampled using a 50/30/20 μm divinylbenzene/carboxen/polydimethylsiloxane Stableflex (2 cm) SPME fibre for 15 min at 37°C. The SPME fibre was then removed and transferred to the GC injector for desorption. All standard preparation and analysis were performed in triplicate.

3.2.3. Gas chromatography-mass spectrometry analysis

GC-MS analysis has been described previously in Chapter 2, section 2.2.2.

3.2.4. Data analysis

All techniques used for analysis of raw chromatographic data are outlined in Chapter 2, section 2.2.3. RStudio (version 2023.03.0) and Prism (version 9.4.0) were used for all data exploration and visualisation. A Shapiro-Wilk's test was first carried out in order to determine if the data had a normal or non-normal distribution using the R package 'ggpubr'. Results of this test show that the data set has a non-normal distribution thus non-parametric data analysis techniques were employed for data exploration. Wilcoxon testing was used to determine significant difference and p-values < 0.1 were deemed to be statistically significant. Spearman correlation analysis was carried out using R package 'corrplot' (version: 0.92). Canonical correlation analysis (CCA) was carried out using 'cca' (version: 1.2.1) and 'ccp' (version: 1.2). Multiple linear regression (MLR) was carried out on data using 'MASS' (version 7.3). Other R packages used included: 'tidyverse', 'ggplot2', 'ggfortify'.

3.2.5. Skin surface pH and tissue dielectric constant measurements

Procedures for the measurement of skin surface pH and tissue dielectric constant (TDC) are outlined in Chapter 2, section 2.2.4.

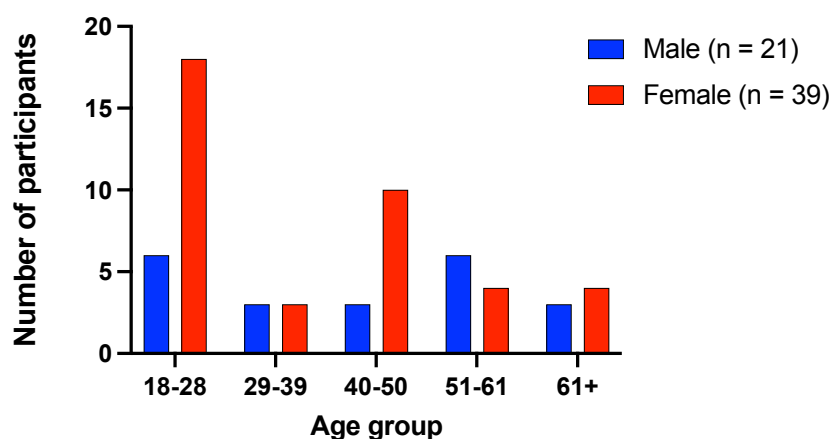


Figure 3.1. Number of male and female participants recruited, categorised into age ranges of 10 years.

3.3. Results and discussion

3.3.1. Characterising the skin volatile profile in healthy participants

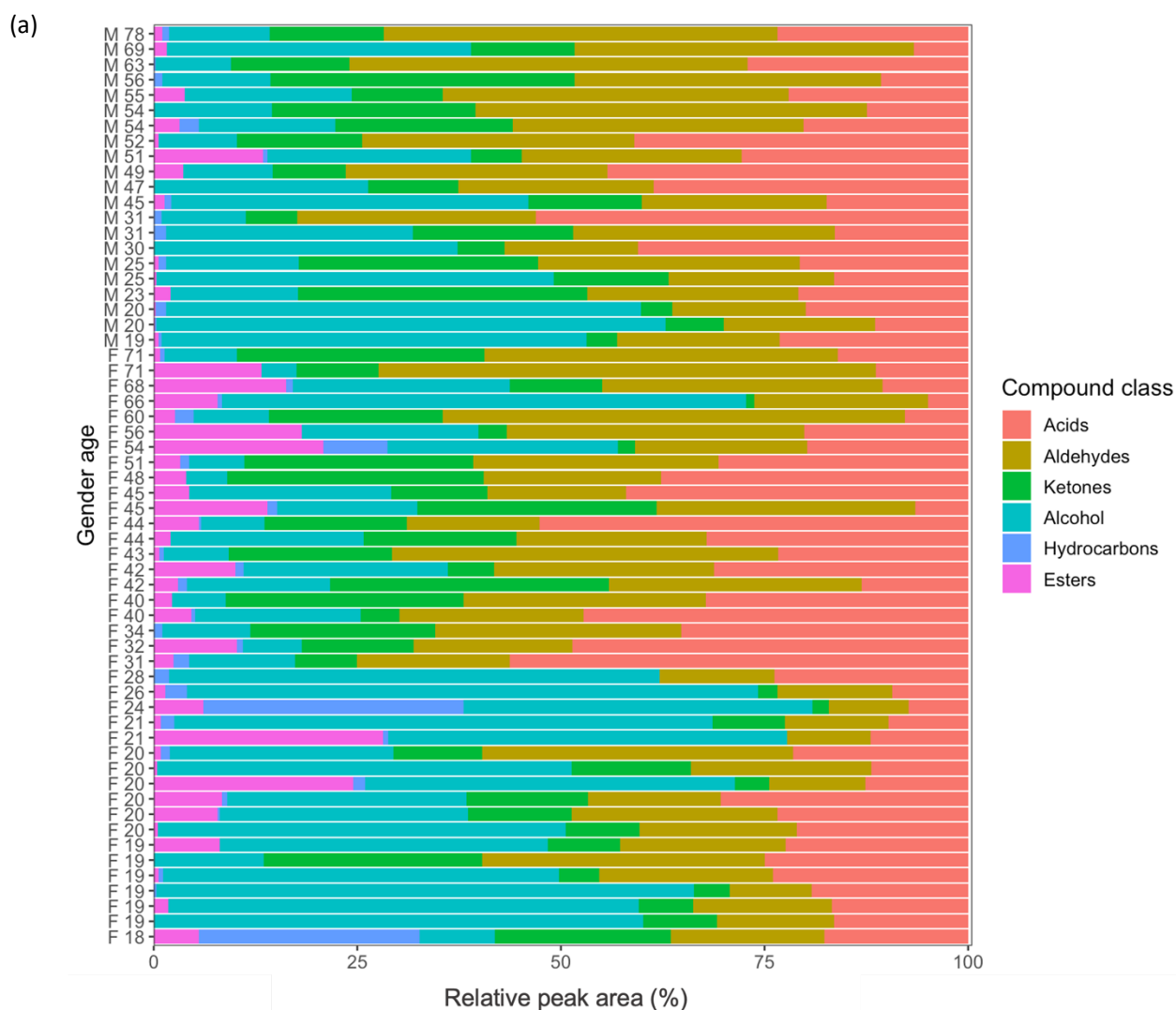
Skin volatile emissions from the volar forearm of 60 participants and characterisation of the VOCs showed there to be a variety of compound classes emitted from human skin, with acids, aldehydes, ketones, alcohols, hydrocarbons and esters being recovered. Figure 3.2 (a)

shows a representative distribution of the relative abundance of compound classes identified in each individual participant's skin volatile profile. Variability in the recovery and relative abundances of compound classes from the skin across participants highlights the variance in inter-participant sampling. For example, the relative acid composition ranges from 5-56%. The main aim of this work is to assess how physiological factors including gender and age impact the chemical composition in the headspace of the skin.

21 compounds were reliably identified across all samples analysed using a combination of RI matching and analytical standards. Figure 3.2 (b) shows the % frequency detected for each compound across male and female participants. Among these are frequently reported skin volatile compounds acetic acid, octanoic acid, nonanoic acid, geranylacetone, 6-methyl-5-hepten-2-one, nonanal and decanal [51,53–55] which were detected in >80% of both male and female participants and so can be considered as omnipresent for both genders. Acetic acid, a short chain fatty acid (SCFA) was detected in a high frequency across samples and is known to be a primary microbial metabolite with many studies reporting it as a key component of the human skin volatile profile [37,55,56]. This SCFA is produced via the catabolism of skin lipids into long-chain fatty acids which are then further broken down by bacterial including Propionibacteria and Staphylococci present on the skin [57]. Longer chain free fatty acids (FFAs) including octanoic, nonanoic and n-decanoic acid were also recovered within this study and are well-established as main components of secreted sebum produced by sebaceous glands [47,58]. Six saturated and one aromatic aldehyde were recovered across both male and female participants. As discussed earlier, volatile aldehyde emissions from skin are considered to be end-products of lipid peroxidation reactions initiated by oxidative stress [59]. Benzaldehyde was recovered in approx. 75% of male and female participants and its production within skin has been linked to benzyl alcohol oxidation and it has also been considered as a microbial metabolite [60–62]. The ketones, 6-methyl-5-hepten-2-one and geranylacetone, which are among the most frequently reported volatile compounds [37], were recovered in approx. 85-100% of all participants. 2-ethyl-1-hexanol is an alcohol reported previously as a skin volatile [36,48], is linked to microbial degradation of plasticizers, and was detected in >80% of male and female samples thus deeming it omnipresent [63,64]. Compounds known to be from exogenous sources including esters such as isopropyl myristate, isopropyl palmitate and linal (linked to frequent use of fragrance and cosmetics) [65] were also recovered. Despite employing pre-sampling procedures such as the limitation of the use of cosmetics on the day of sampling, it is impractical to exclude such compounds given their pervasive use in cosmetic

products [66,67] and their high frequency of occurrence. A frequency of detection threshold of 30% for both male and female participants was employed and thus excluded tridecane, isopropyl palmitate and linal from the final data for further analysis. The final dataset consisting of 18 compounds was used for further data analysis.

Given that nonanal and decanal were the most frequently recovered compounds in this study (97-100%), their emission fluxes were estimated using standard calibration curves (Figure A3.1 in Appendix) as outlined in the Methods Section. Emission fluxes were calculated based on the sampling time and area of skin sampled and are reported in fmoles $\text{cm}^{-2} \text{min}^{-1}$. The calculated emission flux range for nonanal was 105 – 1130 fmoles $\text{cm}^{-2} \text{min}^{-1}$ and for decanal was 85 – 1333 fmoles $\text{cm}^{-2} \text{min}^{-1}$. These emission fluxes are higher than others previously reported [43,68,69]. The highest emission flux calculated for nonanal was for a participant aged 78 and the increased emission flux compared to literature is likely linked to increased age which will be discussed in further detail in section 3.3.



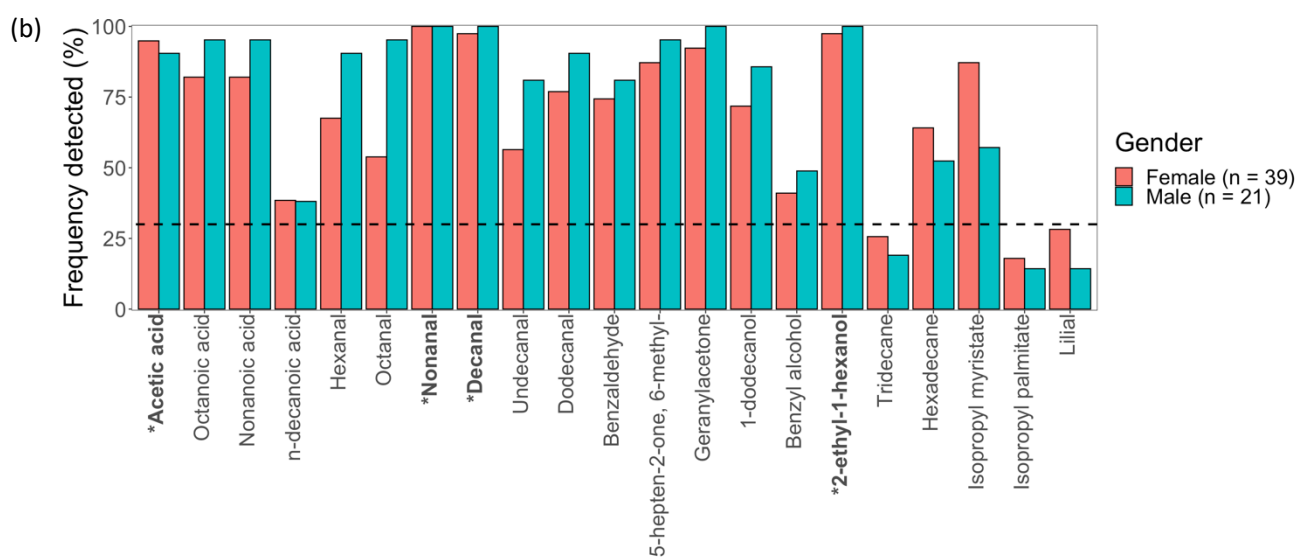


Figure 3.2. (a) Distribution of compound classes recovered from individual skin volatile samples (Gender Age) according to chemical class and based on relative chromatographic peak area and (b) % frequency recovered for male (n=21) and female (n=39) participants (bolded compounds indicate omnipresence across male and female participants) (Dashed line = 30% frequency detection threshold and asterisks indicates compound omnipresence).

3.3.2. Gender influences on the skin volatile emission

Studies have shown that the human skin volatilome is influenced by gender. Our group [38], along with others [39] have shown a significant difference in the recovered abundances of long-chain volatile fatty acids (FAs) such as pentadecanoic and hexadecenoic acid between male and female participants. Similarly, increased abundances of both aldehydes and ketones in male participants has been reported compared to females [38]. Thus, differences between the volatile emission profiles across all male and female participants were investigated here. Male and female participants were categorised into two groups according to age; young (aged 18-40; male: n=9 and female: n=21) (Fig 3.3 (a)) and old (aged 40-80; male: n=12 and female n=18) (Fig 3.3 (b)), similar to Gallagher et al's study [65]. Comparative boxplots in Figure 3.3 show compounds with significant differences in emissions between young and old male and female participants. A p-value threshold of 0.1 was applied in order to test for statistical significance. A significantly higher recovered abundance of aldehydes, hexanal (p=0.071), octanal (p=0.037), decanal (p=0.017), undecanal (p=0.0082) and dodecanal (p=0.077) was observed in young males compared to young females. Acetic acid was also significantly higher in young males (p=0.07). Skin surface pH across participants was also measured in this study

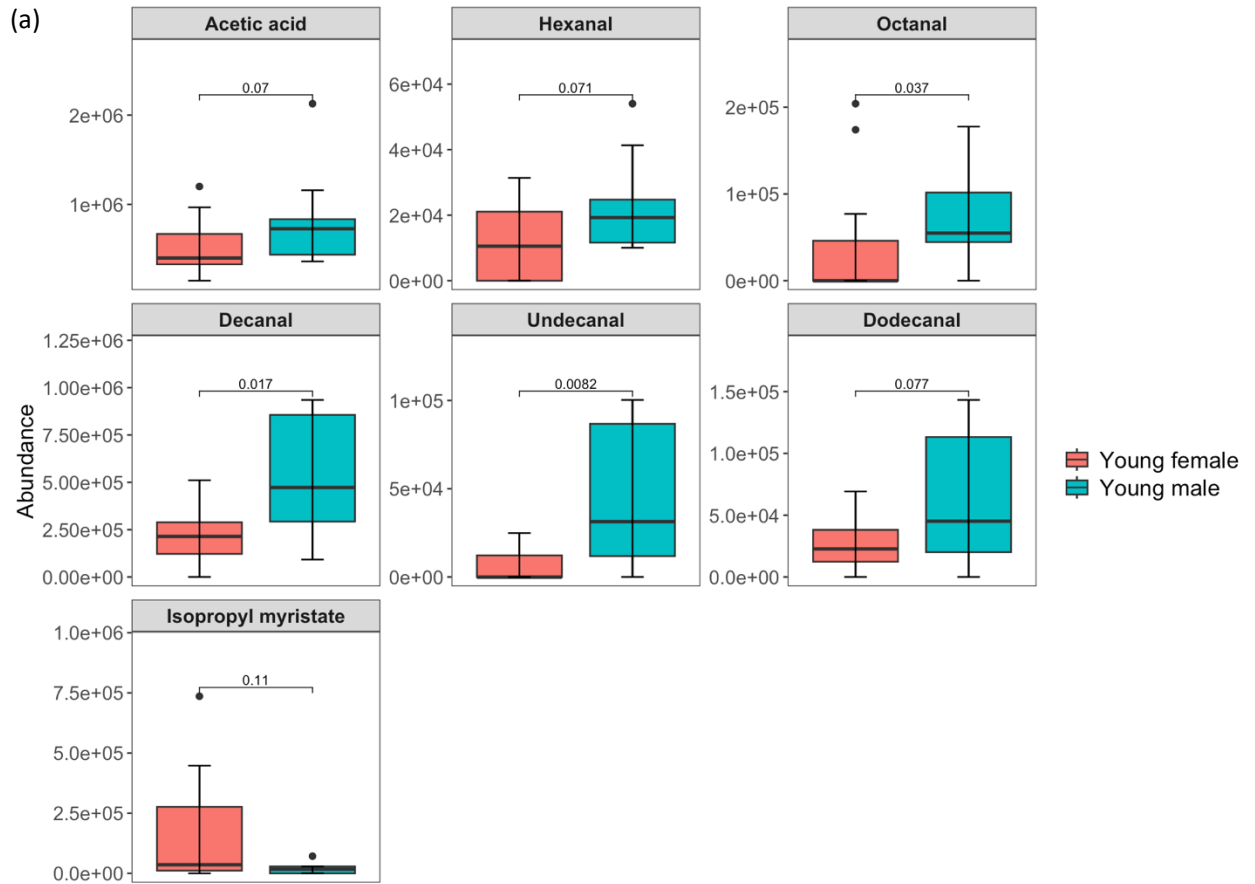
and the greater acetic acid abundance in younger males compared with younger females is correlated with a lower skin surface pH ($p= 0.081$). No significance in the recovered abundances of longer chain VFAs were observed between young male and females. No significant differences between young male and female emissions of ketones, alcohols or esters were observed.

Old males also had significantly increased abundances of four of the aldehydes, i.e., octanal ($p= 0.058$), nonanal ($p= 0.0089$), undecanal ($p= 0.063$), dodecanal ($p= 0.097$) compared to old females. Old females were observed to have a greater recovered abundances of isopropyl myristate compared to old males, where isopropyl myristate is an emollient commonly employed in cosmetic formulations [67].

Canonical correspondence analysis (CCPA), a constrained ordination multivariate analysis technique used to model relationships between a quantitative set of variables and a qualitative/categorical set of variables, was also employed. CCPA attempts to maximise correlation within the dataset and understand what quantitative variables (recovered abundances of VOCs, skin surface pH, TDC) are most associated with a range of categorical variables (male, female, old, young). (Figure 3.3 (c)). The direction and length of the arrow indicates the quantitative variable's correlation to the categorical variable lying in that direction/quadrant. CCPA analysis supports the results shown in Figure 3.3 (a-b) where the aldehydes, decanal, undecanal and dodecanal are increased in abundance in male participants in general. Similarly, isopropyl myristate correlates most strongly with female participants here and supports the data in Figure 3.3 (a-b).

In terms of initial assessment of the VOC variables correlation with age, we can note the following from Figure 3.3 (c): 2-ethyl-1-hexanol and acetic acid correlate most strongly with young participants and nonanal, hexanal and benzyl alcohol correlate most strongly with old participants.

Both analyses highlighted significant differences between age-grouped male and female volatile profiles suggesting that the volatile profiles of male and females in this sample set differ based on the acidic, aldehyde and ester emission thus when investigating the effect of age on volatile emissions both genders must be examined individually.



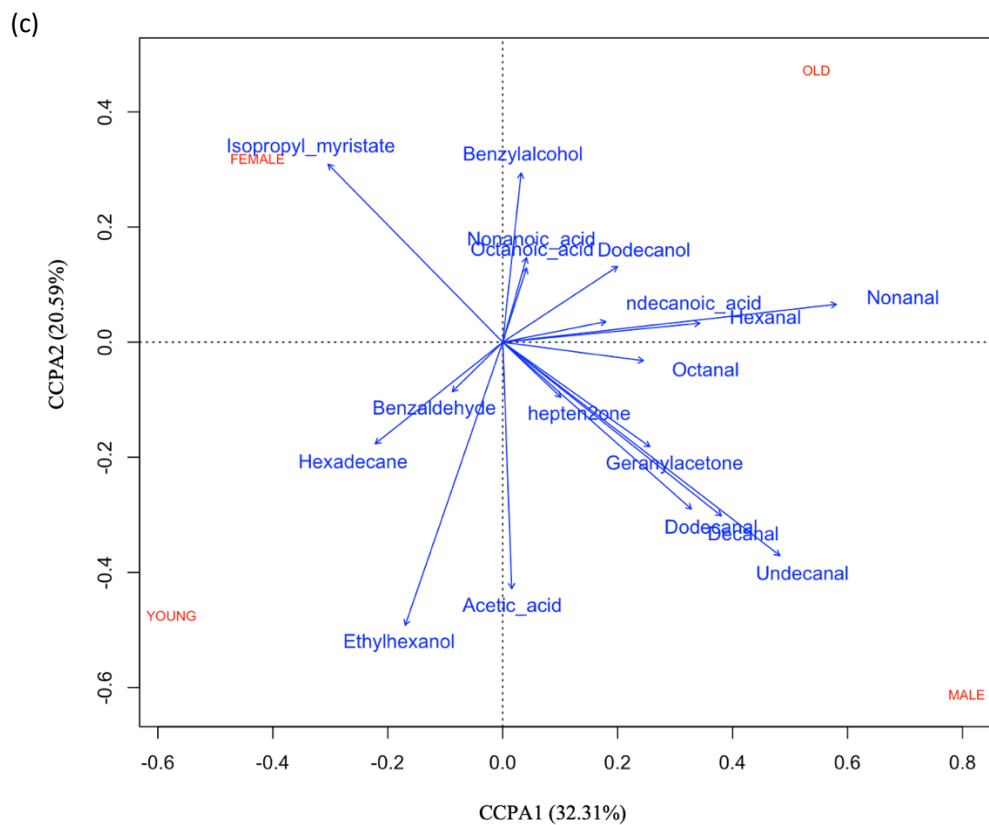
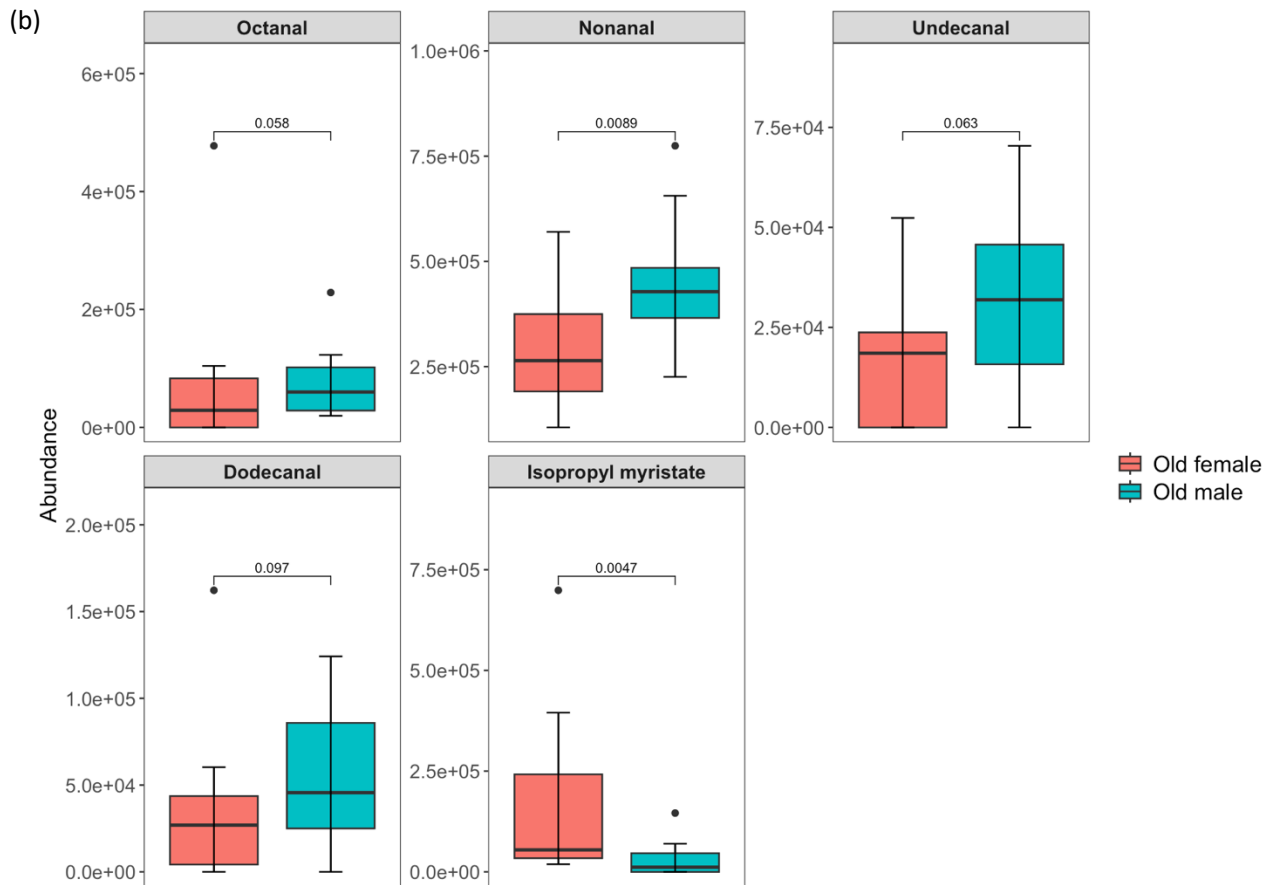


Figure 3.3. Grouped boxplots comparing the abundances of compounds emitted with significant differences by (a) young males (n = 9) and females (n = 21) aged 18-40, (b) older males (n = 12) and females (n = 18) aged 40-80. Y-axis labels are displayed in scientific notation where $a \times 10^b = a \times 10^b$. Statistical significance was calculated using the Wilcoxon signed rank test. Boxes represent the interquartile range: the line running across each box represents the 50th percentile (median), the top of the box represents the 75th percentile, and the bottom of the box represents the 25th percentile. The whiskers (error bars) represent either the smallest or largest value within 1.5 times the interquartile range above the 75th percentile or below the 25th percentile. Black dots above or below the boxes represent outliers that are greater than 1.5 times the interquartile range beyond either end of the box. (c) CCPA ordination of skin volatile emissions in relation to categorical variables describing age and gender (n=60 participants; male n=21, female n=39).

3.3.3. Correlation of age with skin surface pH, TDC and the skin volatile emission

Correlations between skin surface pH, TDC and all selected volatile compounds with age for both male and female participants were investigated (Figure 3.4 (a-b) and results summarised in Table 3.1. Skin surface pH and TDC both significantly increase with age for males (skin surface pH: $p = 0.045$; TDC: $p = 0.029$) and females (skin surface pH: $p = 0.002$; TDC: $p = 0.033$), consistent with earlier literature [27,70] and links with various mechanisms [71,72] which are responsible for the acidification of skin that are thought to be disturbed in older skin [23–25,27]. These include a decreased sodium-hydrogen antiporter 1 (NHE1) expression [23], a reduced rate of breakdown of phospholipids into FFAs [71] and a reduced rate of breakdown of the filaggrin gene [73]. TDC is also known to increase with age and this is thought to be related to changes in the skin where water states shift from mostly bound to protein but as skin ages, this changes to a free state where water binds to itself in a tetrahedron confirmation due to altered protein folding [74–76].

In terms of VOCs, both males and females showed a down-regulation of recovered acetic acid abundance with age. As discussed previously, acetic acid is the product the breakdown of long-chain fatty acids by Propionibacteria and Staphylococci which are present on the skin. These bacteria, have been shown to decrease in abundance with aging [28,34,77] which may be linked to the decrease in acetic acid with age observed here. Moreover, this down-regulation of acetic acid abundance with age correlates with an increased skin surface pH (M: $p = 0.044$; F: $p = 0.038$). However, no significant age effects were noted for octanoic,

nonanoic and n-decanoic acid as the longer chain VFAs which are likely linked to endogenous production [58,78].

The saturated aldehyde, nonanal, is a lipid peroxidation end-product of oleic acid, a major monounsaturated fatty acid component of sebum. It was observed to be significantly up-regulated with age in both male ($p = 0.030$) and female ($p = 0.024$) participants. This may be linked to increased oxidative stress in skin with age likely through both intrinsic and extrinsic aging [65]. Other saturated aldehydes, hexanal and undecanal were significantly upregulated in older females ($p = 0.046$, $p = 0.073$, respectively) but not in older males ($p = 0.530$, $p = 0.611$, respectively). Hexanal, again, is a lipid peroxidation end-product that arises from the breakdown of linoleic and palmitoleic acids and is triggered by an increase in reactive oxygen species (ROS) such as ozone [79]. Undecanal is an end-product of the lipid peroxidation of the less abundant *cis*-heptadec-6-enoic acid in skin owing to its lower abundance recovered from skin [80].

The alcohol, 2-ethyl-1-hexanol showed a significant decrease in abundance for both male ($p = 0.0005$) and female ($p = 0.00002$) participants with age. While this compound is known not to be derived from endogenous sources, it is known to be produced by microbial degradation of plasticisers such as diethyl phthalate (DEP), typically present in room air. Such plasticisers are also commonly used in fragrances and cosmetic products [81,82]. There is good evidence to show that these plasticisers could be metabolised by bacteria present on skin to produce 2-ethyl-1-hexanol [64], however no skin commensal(s) have been elucidated as being responsible for driving this metabolic process to our knowledge. It could be speculated that there are changes in the skin microbiome that occur with increased age [11] which may lead to a decreased ability of the microbiome to metabolise phthalates to produce 2-ethyl-1-hexanol. Furthermore, 2-ethyl-1-hexanol itself has been reported as a component of fragrances and so it also could be speculated that its higher abundances in younger participants may be linked to a more frequent use of fragrances compared to older participants [66]. However, in contrast to other fragrance-derived VOCs such as isopropyl myristate, no significance across genders was noted.

Benzyl alcohol was up-regulated in older females ($p = 0.085$) but not in older males ($p = 0.256$). Benzyl alcohol is a frequently reported skin emission [55,83,84] which has been detected in the headspace of cultured *S. epidermidis* indicating that it may be a microbial metabolite produced on the skin [55]. Furthermore, there is evidence that benzyl alcohol can be oxidised at the skins surface via microbes to produce benzaldehyde [60,62]. It is

hypothesised here that alterations in the skin microbiome with age may reduce the efficiency of this process of oxidation of benzyl alcohol to benzaldehyde, however no significant change in benzaldehyde's abundance was noted with age in this study.

Finally, no significant change in abundance with age for either gender was observed for any of the ketones, hydrocarbons or esters recovered.

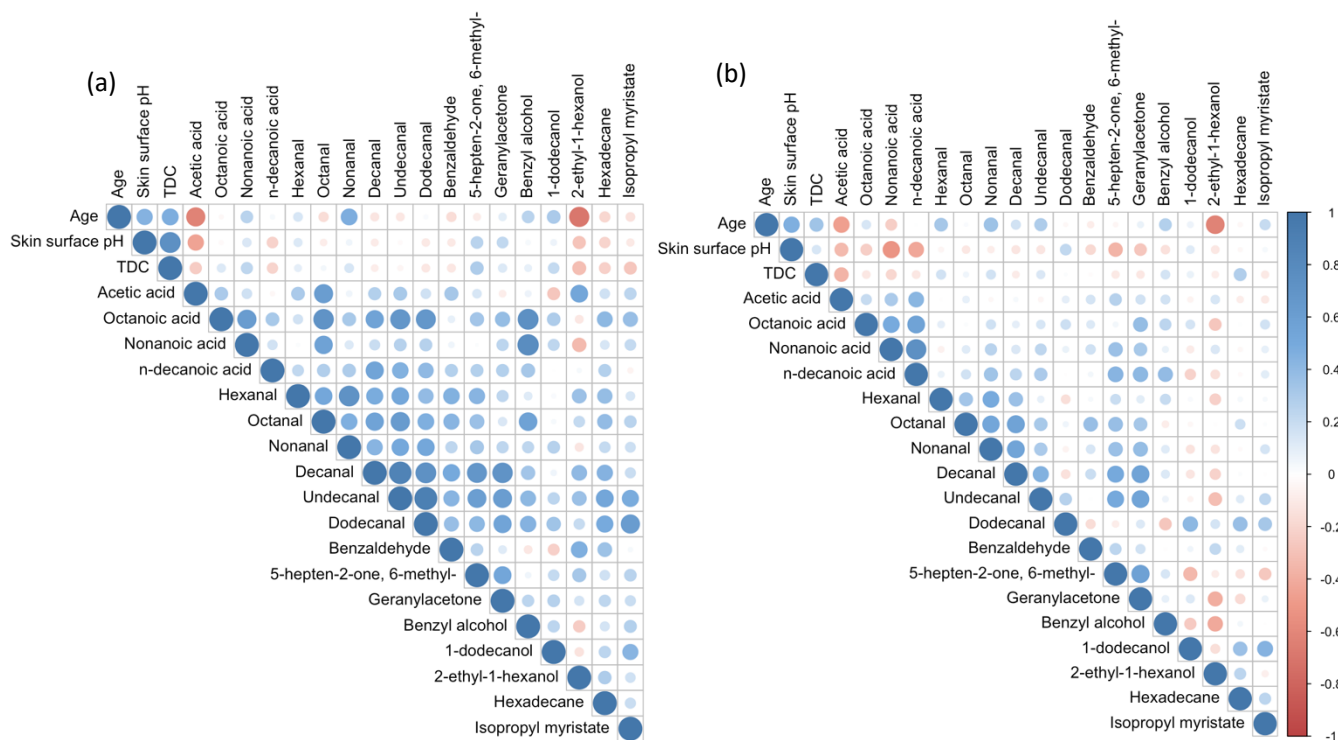


Figure 3.4. Spearman correlation plot of identified volatile compounds with skin surface pH, TDC and age for (a) male (n=21) and (b) female (n=39) participants. Blue indicates a positive correlation and red indicates a negative correlation.

Table 3.1. Results of Spearman correlation for male and female participants of skin surface pH, TDC and selected VOCs as a function of age. Variables which show significant change ($p < 0.1$) with age are bolded and arrows represent up-regulation (\uparrow) or down-regulation (\downarrow).

Variable	Correlation (coefficient r , p-value)	
	Age	
	Male	Female
Skin surface pH	0.440, 0.045 \uparrow	0.465, 0.002 \uparrow
TDC	0.476, 0.029 \uparrow	0.342, 0.033 \uparrow
Acetic acid	-0.622, 0.002 \downarrow	-0.469, 0.002 \downarrow
Octanoic acid	-0.031, 0.895	0.146, 0.375
Nonanoic acid	0.259, 0.256	-0.237, 0.146
n-decanoic acid	0.033, 0.885	0.006, 0.969
Hexanal	0.145, 0.530	0.320, 0.046 \uparrow
Octanal	-0.166, 0.472	0.024, 0.888
Nonanal	0.473, 0.030 \uparrow	0.359, 0.024 \uparrow
Decanal	-0.124, 0.591	0.166, 0.313
Undecanal	-0.118, 0.611	0.290, 0.073 \uparrow
Dodecanal	0.028, 0.904	-0.031, 0.852
Benzaldehyde	-0.165, 0.475	-0.081, 0.622
6-methyl-5-hepten-2-one	-0.094, 0.684	-0.042, 0.800
Geranylacetone	0.107, 0.645	0.074, 0.653
Benzyl alcohol	0.259, 0.256	0.279, 0.085 \uparrow
1-dodecanol	0.307, 0.176	0.070, 0.673
2-ethyl-1-hexanol	-0.692, 0.0005 \downarrow	-0.621, 0.00002 \downarrow
Hexadecane	-0.196, 0.393	-0.039, 0.815
Isopropyl myristate	-0.143, 0.536	0.206, 0.208

CCA is a multivariate technique that identifies relationships between two sets of variables measured for the same sets of samples and can be considered as extension of the bivariate correlations shown by the Spearman correlation analysis. CCA analysis involves creating linear combinations of variables from each set of variables that maximises correlation between them and these are described as the canonical variates. Here, one canonical variate is comprised of the parameters age, skin surface pH and TDC (y-axis) and the other is comprised

of the age significant volatiles (Table 3.1) including acetic acid, hexanal, nonanal, undecanal, benzyl alcohol and 2-ethyl-1-hexanol (x-axis). Figure 3.5 shows the CCA scores plots for both males (Fig 6 (a)) and females (Fig 6 (b)). In each score plot, each point corresponds to the combined data of age, skin surface pH, TDC and volatile profile from the same participant. Results show correlations of 0.936 between the components for male participants and 0.831 between the components for female participants. A higher correlation between components was observed for male participants and may be linked to the increased variability in younger female samples that was not observed in younger male samples. This higher correlation observed in males compared to females may also be linked to sample size. For example, there were fewer male samples ($n=21$) collected compared to female samples ($n=39$) and the lower sample number for males may explain the increased correlation observed. In order to further understand sample size effects equal sample numbers for both male and female should be collected.

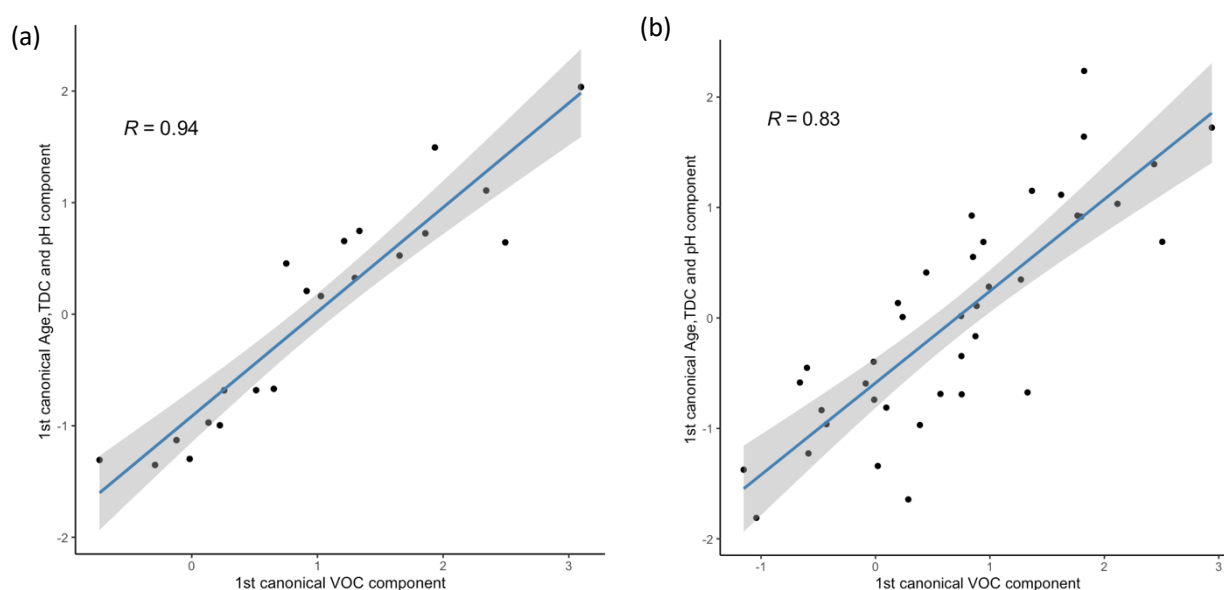


Figure 3.5. CCA score plots between the selected VOCs (x-axis) and the parameters age, skin surface pH and TDC (y-axis) using the first canonical components for (a) male ($n=21$) and (b) female ($n=39$) participants. Grey area show the 95% confidence intervals of the CCA scores plots.

Finally, multiple linear regression (MLR), a statistical approach that uses several variables to predict the outcome of a response variable, was employed to determine if age can be predicted for a participant based on the data collected in this study. Initially, a model

comprising of the 6 compounds that change significantly with age (Table 3.1) was built where it explained 68% of the variance in the data with an approximate error rate of 26%. Following this skin surface pH, TDC and gender were included in the model in order to see if they improve its capability to predict age.

Figure 3.6 shows a plot generated where calculated age, obtained from the MLR model including skin surface pH, TDC, gender and skin volatiles is plotted against the actual age of participants. The inclusion of skin surface pH, TDC and gender improved the MLR predictive models capability of predicting age where approximately 75% of the variance in the male and female data is explained with an approximate 24% error rate. Such a MLR model could have the capability to predict the age of a participant based on skin surface pH, TDC, gender and the 6 age significant volatile compounds.

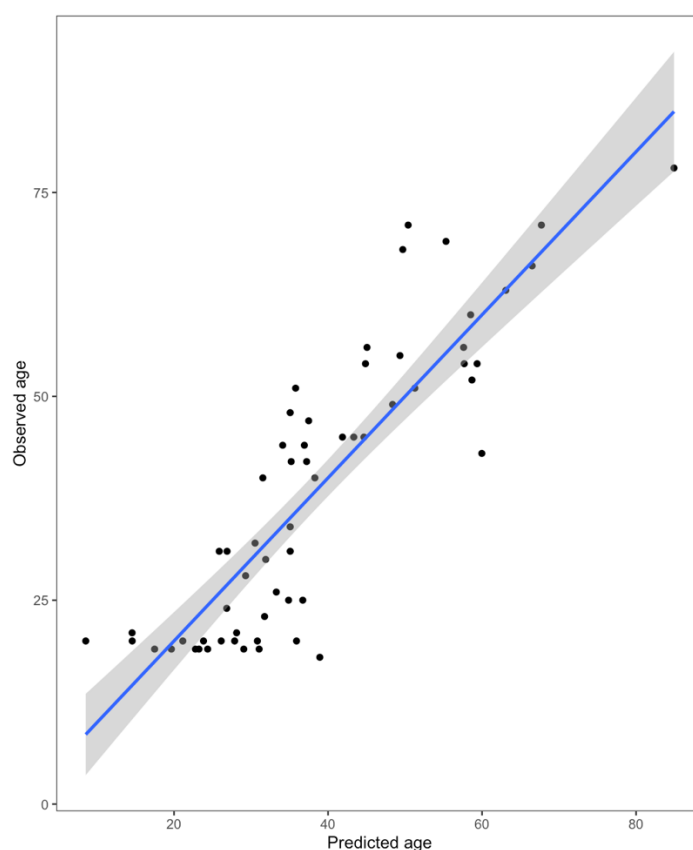


Figure 3.6. MLR predictive model for age using skin surface pH, TDC, gender and age significant volatile compounds as predictors for n= 60 participants (male; n=21, female; n=39). Grey area show the 95% confidence intervals of the MLR regression model.

3.4. Conclusion

Overall, this work provides a comprehensive analysis of the volatile profile emitted by skin and establishes differences related to gender and age via HS-SPME sampling coupled with GC-MS analysis. The main objectives of this study were: (1) to characterise the skin volatile emission profile; (2) assess gender influences on the skin volatile emission; and (3) investigate changes in the skin volatile emission, skin surface pH and TDC with respect to age.

The observed human volatilome was comprised of a variety of compound classes including acids, aldehydes, ketones, alcohols, hydrocarbons and esters with variability in recovery and relative abundances across each participant. Gender influences on the skin volatile emission were observed. The acidic, aldehyde and ester emissions of male and female participants showed significant differences indicating that both data sets should be treated individually when assessing changes in VOC emissions with age. Statistical analysis of the volatile profile with age showed that there were 6 volatile compounds (acetic acid, hexanal, nonanal, undecanal, benzyl alcohol and 2-ethyl-1-hexanol) that changed in abundance with increasing participant age. Finally, MLR models showed that skin surface pH, TDC, gender and age-significant volatile compounds allowed for improved prediction of age compared to a model only containing age-significant compounds.

This work allows us to understand the volatile profile for healthy skin across gender and age. Changes in the volatile profile with age may prove useful when diagnosing disease in elderly patients. Furthermore, assessment of these changes may also prove useful in the development of anti-aging treatments in the cosmetic industry.

3.5. References

- [1] Drislane C and Irvine A D 2020 The role of filaggrin in atopic dermatitis and allergic disease *Annals of Allergy, Asthma & Immunology* **124** 36–43
- [2] Honari G and Maibach H 2014 Chapter 1 - Skin Structure and Function *Applied Dermatotoxicology* ed H Maibach and G Honari (Boston: Academic Press) pp 1–10
- [3] Proksch E, Brandner J M and Jensen J-M 2008 The skin: an indispensable barrier *Experimental Dermatology* **17** 1063–72
- [4] Proksch E 2018 pH in nature, humans and skin *The Journal of Dermatology* **45** 1044–52
- [5] Kolarsick P A J, Kolarsick M A and Goodwin C Anatomy and Physiology of the Skin *SKIN CANCER* 12

- [6] Choi E H 2018 Gender, Age, and Ethnicity as Factors That Can Influence Skin pH *pH of the Skin: Issues and Challenges* **54** 48–53
- [7] Dao H and Kazin R A 2007 Gender differences in skin: A review of the literature *Gender Medicine* **4** 308–28
- [8] Fitzmaurice S and Maibach H I 2010 Gender Differences in Skin *Textbook of Aging Skin* ed M A Farage, K W Miller and H I Maibach (Berlin, Heidelberg: Springer) pp 999–1017
- [9] Firooz A, Rajabi-Estarabadi A, Zartab H, Pazhoji N, Fanian F and Janani L 2017 The influence of gender and age on the thickness and echo-density of skin *Skin Research and Technology* **23** 13–20
- [10] Grice E A and Segre J A 2011 The skin microbiome *Nat Rev Microbiol* **9** 244–53
- [11] Ratanapokasatit Y, Laisuan W, Rattananukrom T, Petchlorlian A, Thaipsisuttikul I and Sompornrattanaphan M 2022 How Microbiomes Affect Skin Aging: The Updated Evidence and Current Perspectives *Life (Basel)* **12** 936
- [12] Ying S, Zeng D-N, Chi L, Tan Y, Galzote C, Cardona C, Lax S, Gilbert J and Quan Z-X 2015 The Influence of Age and Gender on Skin-Associated Microbial Communities in Urban and Rural Human Populations *PLOS ONE* **10** e0141842
- [13] Luebberding S, Krueger N and Kerscher M 2013 Skin physiology in men and women: in vivo evaluation of 300 people including TEWL, SC hydration, sebum content and skin surface pH *International Journal of Cosmetic Science* **35** 477–83
- [14] Giacomoni P U, Mammone T and Teri M 2009 Gender-linked differences in human skin *Journal of Dermatological Science* **55** 144–9
- [15] Farage M A, Miller K W, Elsner P and Maibach H I 2008 Intrinsic and extrinsic factors in skin ageing: a review *International Journal of Cosmetic Science* **30** 87–95
- [16] Mora Huertas A C, Schmelzer C E H, Hoehenwarter W, Heyroth F and Heinz A 2016 Molecular-level insights into aging processes of skin elastin *Biochimie* **128–129** 163–73
- [17] Kohen R 1999 Skin antioxidants: their role in aging and in oxidative stress--new approaches for their evaluation *Biomed Pharmacother* **53** 181–92
- [18] Ron-Doitch S and Kohen R 2020 The Cutaneous Physiological Redox: Essential to Maintain but Difficult to Define *Antioxidants (Basel)* **9** 942
- [19] Tsuchida K and Kobayashi M 2020 Oxidative stress in human facial skin observed by ultraweak photon emission imaging and its correlation with biophysical properties of skin *Sci Rep* **10** 9626
- [20] Halliwell B 1989 Free radicals, reactive oxygen species and human disease: a critical evaluation with special reference to atherosclerosis. *Br J Exp Pathol* **70** 737–57
- [21] Li J-M and Shah A M 2003 ROS generation by nonphagocytic NADPH oxidase: potential relevance in diabetic nephropathy *J Am Soc Nephrol* **14** S221-226

- [22] Sabharwal S S and Schumacker P T 2014 Mitochondrial ROS in cancer: initiators, amplifiers or an Achilles' heel? *Nat Rev Cancer* **14** 709–21
- [23] Choi E-H, Man M-Q, Xu P, Xin S, Liu Z, Crumrine D A, Jiang Y J, Fluhr J W, Feingold K R, Elias P M and Mauro T M 2007 Stratum corneum acidification is impaired in moderately aged human and murine skin *J Invest Dermatol* **127** 2847–56
- [24] Wilhelm K-P, Cua A B and Maibach H I 1991 Skin Aging: Effect on Transepidermal Water Loss, Stratum Corneum Hydration, Skin Surface pH, and Casual Sebum Content *Archives of Dermatology* **127** 1806–9
- [25] Zlotogorski A 1987 Distribution of skin surface pH on the forehead and cheek of adults *Arch Dermatol Res* **279** 398–401
- [26] Sato N, Kitahara T and Fujimura T 2014 Age-Related Changes of Stratum Corneum Functions of Skin on the Trunk and the Limbs *SPP* **27** 181–181
- [27] Man M Q, Xin S J, Song S P, Cho S Y, Zhang X J, Tu C X, Feingold K R and Elias P M 2009 Variation of Skin Surface pH, Sebum Content and Stratum Corneum Hydration with Age and Gender in a Large Chinese Population *Skin Pharmacol Physiol* **22** 190–9
- [28] Howard B, Bascom C C, Hu P, Binder R L, Fadayel G, Huggins T G, Jarrold B B, Osborne R, Rocchetta H L, Swift D, Tiesman J P, Song Y, Wang Y, Wehmeyer K, Kimball A B and Isfort R J 2021 Aging-Associated Changes in the Adult Human Skin Microbiome and the Host Factors that Affect Skin Microbiome Composition *Journal of Investigative Dermatology*
- [29] Behne M J, Meyer J W, Hanson K M, Barry N P, Murata S, Crumrine D, Clegg R W, Gratton E, Holleran W M, Elias P M and Mauro T M 2002 NHE1 regulates the stratum corneum permeability barrier homeostasis. Microenvironment acidification assessed with fluorescence lifetime imaging *J Biol Chem* **277** 47399–406
- [30] Takahashi M and Tezuka T 2004 The content of free amino acids in the stratum corneum is increased in senile xerosis *Arch Dermatol Res* **295** 448–52
- [31] Schreml S, Kemper M and Abels C 2014 SKIN pH IN THE ELDERLY AND APPROPRIATE SKIN CARE 9
- [32] Roux P-F, Oddos T and Stamatias G 2021 Deciphering the Role of Skin Surface Microbiome in Skin Health: An Integrative Multiomics Approach Reveals Three Distinct Metabolite–Microbe Clusters *Journal of Investigative Dermatology*
- [33] Byrd A L, Belkaid Y and Segre J A 2018 The human skin microbiome *Nat Rev Microbiol* **16** 143–55
- [34] Jugé R, Rouaud-Tinguely P, Breugnot J, Servaes K, Grimaldi C, Roth M-P, Coppin H and Closs B 2018 Shift in skin microbiota of Western European women across aging *Journal of Applied Microbiology* **125** 907–16
- [35] Shirasu M and Touhara K 2011 The scent of disease: volatile organic compounds of the human body related to disease and disorder *The Journal of Biochemistry* **150** 257–66

- [36] Duffy E and Morrin A 2019 Endogenous and microbial volatile organic compounds in cutaneous health and disease *TrAC Trends in Analytical Chemistry* **111** 163–72
- [37] Drabińska N, Flynn C, Ratcliffe N, Belluomo I, Myridakis A, Gould O, Fois M, Smart A, Devine T and Costello B D L 2021 A literature survey of all volatiles from healthy human breath and bodily fluids: the human volatilome *J. Breath Res.* **15** 034001
- [38] Shetewi T, Finnegan M, Fitzgerald S, Xu S, Duffy E and Morrin A 2021 Investigation of the relationship between skin-emitted volatile fatty acids and skin surface acidity in healthy participants—a pilot study *J. Breath Res.* **15** 037101
- [39] Penn D J, Oberzaucher E, Grammer K, Fischer G, Soini H A, Wiesler D, Novotny M V, Dixon S J, Xu Y and Brereton R G 2007 Individual and gender fingerprints in human body odour *J R Soc Interface* **4** 331–40
- [40] Gallagher M, Wysocki C J, Leyden J J, Spielman A I, Sun X and Preti G 2008 Analyses of volatile organic compounds from human skin *Br J Dermatol* **159** 780–91
- [41] Haze S, Gozu Y, Nakamura S, Kohno Y, Sawano K, Ohta H and Yamazaki K 2001 2-Nonenal Newly Found in Human Body Odor Tends to Increase with Aging *Journal of Investigative Dermatology* **116** 520–4
- [42] Curran A M, Rabin S I, Prada P A and Furton K G 2005 Comparison of the volatile organic compounds present in human odor using SPME-GC/MS *J. Chem. Ecol.* **31** 1607–19
- [43] Mochalski P, King J, Unterkofler K, Hinterhuber H and Amann A 2014 Emission rates of selected volatile organic compounds from skin of healthy volunteers *J Chromatogr B Analyt Technol Biomed Life Sci* **959** 62–70
- [44] Nicolaides N 1974 Skin Lipids: Their Biochemical Uniqueness *Science* **186** 19–26
- [45] De Luca C and Valacchi G 2010 Surface lipids as multifunctional mediators of skin responses to environmental stimuli *Mediators Inflamm* **2010** 321494
- [46] Freinkel R K and Shen Y 1969 The origin of free fatty acids in sebum. II. Assay of the lipases of the cutaneous bacteria and effects of pH *J Invest Dermatol* **53** 422–7
- [47] Ludovici M, Kozul N, Materazzi S, Risoluti R, Picardo M and Camera E 2018 Influence of the sebaceous gland density on the stratum corneum lipidome *Sci Rep* **8** 11500
- [48] Forman H J 2010 Reactive oxygen species and α,β -unsaturated aldehydes as second messengers in signal transduction *Annals of the New York Academy of Sciences* **1203** 35–44
- [49] Ron-Doitch S, Soroka Y, Frusic-Zlotkin M, Barasch D, Steinberg D and Kohen R 2021 Saturated and aromatic aldehydes originating from skin and cutaneous bacteria activate the Nrf2-keap1 pathway in human keratinocytes *Experimental Dermatology* **30** 1381–7
- [50] Motohashi H and Yamamoto M 2004 Nrf2-Keap1 defines a physiologically important stress response mechanism *Trends Mol Med* **10** 549–57

- [51] Duffy E, Jacobs M R, Kirby B and Morrin A 2017 Probing skin physiology through the volatile footprint: Discriminating volatile emissions before and after acute barrier disruption *Exp. Dermatol.* **26** 919–25
- [52] Müller-Wirtz L M, Kiefer D, Ruffing S, Brausch T, Hüppe T, Sessler D I, Volk T, Fink T, Kreuer S and Maurer F 2021 Quantification of Volatile Aldehydes Deriving from In Vitro Lipid Peroxidation in the Breath of Ventilated Patients *Molecules* **26** 3089
- [53] Dormont L, Bessièrè J-M and Cohuet A 2013 Human Skin Volatiles: A Review *J Chem Ecol* **39** 569–78
- [54] Drabińska N, Flynn C, Ratcliffe N, Belluomo I, Myridakis A, Gould O, Fois M, Smart A, Devine T and Costello B D L 2021 A literature survey of all volatiles from healthy human breath and bodily fluids: the human volatilome *J. Breath Res.* **15** 034001
- [55] Rankin-Turner S and McMeniman C 2022 A headspace collection chamber for whole body volatilomics
- [56] Wang N, Ernle L, Bekö G, Wargocki P and Williams J 2022 Emission Rates of Volatile Organic Compounds from Humans *Environ. Sci. Technol.* **56** 4838–48
- [57] James A G, Hyliands D and Johnston H 2004 Generation of volatile fatty acids by axillary bacteria *International Journal of Cosmetic Science* **26** 149–56
- [58] Girod A, Ramotowski R and Weyermann C 2012 Composition of fingermark residue: A qualitative and quantitative review *Forensic Science International* **223** 10–24
- [59] Mochalski P, Wiesenhofer H, Allers M, Zimmermann S, Güntner A T, Pineau N J, Lederer W, Agapiou A, Mayhew C A and Ruzsanyi V 2018 Monitoring of selected skin- and breath-borne volatile organic compounds emitted from the human body using gas chromatography ion mobility spectrometry (GC-IMS) *Journal of Chromatography B* **1076** 29–34
- [60] Jenkins C L and Bean H D 2020 Dependence of the Staphylococcal Volatilome Composition on Microbial Nutrition *Metabolites* **10** 347
- [61] Timm C M, Lloyd E P, Egan A, Mariner R and Karig D 2018 Direct Growth of Bacteria in Headspace Vials Allows for Screening of Volatiles by Gas Chromatography Mass Spectrometry *Frontiers in Microbiology* **9** 491
- [62] Acevedo C A, Sánchez E Y, Reyes J G and Young M E 2007 Volatile Organic Compounds Produced by Human Skin Cells *Biol. Res.* **40**
- [63] Wakayama T, Ito Y, Sakai K, Miyake M, Shibata E, Ohno H and Kamijima M 2019 Comprehensive review of 2-ethyl-1-hexanol as an indoor air pollutant *J Occup Health* **61** 19–35
- [64] Nalli S, Horn O J, Grochowalski A R, Cooper D G and Nicell J A 2006 Origin of 2-ethylhexanol as a VOC *Environ Pollut* **140** 181–5

- [65] Gallagher M, Wysocki C J, Leyden J J, Spielman A I, Sun X and Preti G 2008 Analyses of volatile organic compounds from human skin *British Journal of Dermatology* **159** 780–91
- [66] McGinty D, Scognamiglio J, Letizia C S and Api A M 2010 Fragrance material review on 2-ethyl-1-hexanol *Food and Chemical Toxicology* **48** S115–29
- [67] Draelos Z D and DiNardo J C 2006 A re-evaluation of the comedogenicity concept *Journal of the American Academy of Dermatology* **54** 507–12
- [68] Zou Z and Yang X 2022 Skin volatile organic compound emissions from 14 healthy young adults under controlled conditions *Building and Environment* **222** 109416
- [69] Mochalski P, Unterkofler K, Hinterhuber H and Amann A 2014 Monitoring of Selected Skin-Borne Volatile Markers of Entrapped Humans by Selective Reagent Ionization Time of Flight Mass Spectrometry in NO+ Mode *Anal. Chem.* **86** 3915–23
- [70] Schreml S, Zeller V, Meier R J, Korting H C, Behm B, Landthaler M and Babilas P 2012 Impact of Age and Body Site on Adult Female Skin Surface pH *DRM* **224** 66–71
- [71] Fluhr J W, Kao J, Ahn S K, Feingold K R, Elias P M and Jain M 2001 Generation of Free Fatty Acids from Phospholipids Regulates Stratum Corneum Acidification and Integrity *Journal of Investigative Dermatology* **117** 44–51
- [72] Rippke F, Schreiner V and Schwanitz H-J 2002 The Acidic Milieu of the Horny Layer *Am J Clin Dermatol* **3** 261–72
- [73] Tončić R J, Kezić S, Hadžavdić S L and Marinović B 2018 Skin barrier and dry skin in the mature patient *Clinics in Dermatology* **36** 109–15
- [74] Mayrovitz H 2010 Local tissue water assessed by measuring forearm skin dielectric constant: Dependence on measurement depth, age and body mass index *Skin research and technology : official journal of International Society for Bioengineering and the Skin (ISBS) [and] International Society for Digital Imaging of Skin (ISDIS) [and] International Society for Skin Imaging (ISSI)* **16** 16–22
- [75] Mayrovitz H, Singh A and Akolkar S 2015 Age-related differences in tissue dielectric constant values of female forearm skin measured noninvasively at 300 MHz *Skin Research and Technology* **22**
- [76] Mayrovitz H N, Grammenos A, Corbitt K and Bartos S 2017 Age-related changes in male forearm skin-to-fat tissue dielectric constant at 300 MHz *Clinical Physiology and Functional Imaging* **37** 198–204
- [77] Leyden J J, McGiley K J, Mills O H and Kligman A M 1975 Age-Related Changes In The Resident Bacterial Flora Of The Human Face *Journal of Investigative Dermatology* **65** 379–81
- [78] Croxton R S, Baron M G, Butler D, Kent T and Sears V G 2006 Development of a GC-MS Method for the Simultaneous Analysis of Latent Fingerprint Components* *Journal of Forensic Sciences* **51** 1329–33

- [79] Sutaria S R, Gori S S, Morris J D, Xie Z, Fu X-A and Nantz M H 2022 Lipid Peroxidation Produces a Diverse Mixture of Saturated and Unsaturated Aldehydes in Exhaled Breath That Can Serve as Biomarkers of Lung Cancer—A Review *Metabolites* **12** 561
- [80] Wisthaler A and Weschler C J 2010 Reactions of ozone with human skin lipids: Sources of carbonyls, dicarbonyls, and hydroxycarbonyls in indoor air *PNAS* **107** 6568–75
- [81] Api A M 2001 Toxicological profile of diethyl phthalate: a vehicle for fragrance and cosmetic ingredients *Food and Chemical Toxicology* **39** 97–108
- [82] Mostafa A and Shaaban H 2023 GC-MS Determination of Undeclared Phthalate Esters in Commercial Fragrances: Occurrence, Profiles and Assessment of Carcinogenic and Non-Carcinogenic Risk Associated with Their Consumption among Adult Consumers *Molecules* **28** 1689
- [83] Curran A M, Rabin S I, Prada P A and Furton K G 2005 Comparison of the Volatile Organic Compounds Present in Human Odor Using Spme-GC/MS *J Chem Ecol* **31** 1607–19
- [84] Duffy E, Guzman K D, Wallace R, Murphy R and Morrin A 2017 Non-Invasive Assessment of Skin Barrier Properties: Investigating Emerging Tools for In Vitro and In Vivo Applications *Cosmetics* **4** 44

**Chapter 4: The impact of skin-derived volatile compounds
on host skin cells' signalling pathways**

Abstract

Skin is the largest organ of the body and is in constant contact with the surrounding environment which can affect its homeostasis and delicate redox balance. Nuclear factor erythroid 2-related factor-2-Kelch-like ECH-associated protein 1 (Nrf2-Keap1) pathway is a major cellular defence mechanism which affords protection against environmental insults and contributes to the maintenance of a healthy redox state. As part of normal metabolism, the skin passively and continuously emits volatile compounds which are principally derived from glandular secretions and from their interaction with microorganisms present on the skin's surface. Specific classes of compounds, including α,β -unsaturated and, more recently, saturated volatile aldehydes have been demonstrated as activators of this protective mechanism through either direct or indirect activation. Moreover, most this work to date examines cellular response through the treatment of cells in the liquid phase.

Initially, this works aims to further understand the impact of skin derived compounds on host skin cells' signalling pathway, specifically the Nrf2-Keap1 mechanism. In agreement with previous literature, the saturated aldehydes nonanal and decanal were shown to trigger translocation of the Nrf2 protein to the nucleus. Here, the ability of other frequently emitted skin volatiles, such as the ketone, 6-methyl-5-hepten-2-one, to activate the Nrf2 mechanism was investigated and no activation was observed. Elucidation of the mechanism by which the Nrf2-Keap1 pathway was triggered was also investigated and reactive oxygen species (ROS) generation was shown to increase when cells were treated with nonanal and decanal but 6-methyl-5-hepten-2-one indicating indirect activation of the mechanism. Furthermore, most research to date assesses cellular response through the treatment of cells in the liquid phase and lacks the ability to investigate volatile communication between compounds emitted by skin and cells leading to cellular responses. In order to investigate the volatile communication between nonanal and human keratinocyte cells, a proof of concept study was carried and results showed communication between nonanal in gas phase and the cells by means of increased ROS generation.

Overall, this work aims to give a deeper understanding of how skin-derived volatile compounds can impact the host skin cells' signally pathways, specifically the Nrf2-Keap1 mechanism.

4.1. Introduction

Exploiting volatile biomarkers emanating from the skin as a source of information to probe the body's biochemistry has been of great interest recently. The volatile profile from skin contains information on cellular processes within the body and thus can offer insight into the metabolic condition of an individual. Emitted volatiles are comprised of a variety of different compound classes including alkanes, alkenes, aldehydes, acids, ketones, alcohols, sulphur-containing compounds and nitrogen-containing compounds from both endogenous and exogenous sources [1]. Volatile profiles reflect metabolites of the dermal and epidermal cellular layers where compounds are carried to the skin via the bloodstream, as well as volatile metabolites that are derived from symbiotic bacteria that live on the skin and from metabolization and transformation of secreted compounds in sweat and sebum [2,3]. Skin is inhabited by a wide variety of bacterial species with each site hosting a specific niche [4]. *Staphylococcus aureus* and *Staphylococcus epidermis* are two of the most abundant bacterial species present on the skin and contribute to the production of many volatile metabolites emitted from skin [5].

Skin is the outermost protective barrier and is in constant contact with the environment around us and is exposed to stressors from both endogenous sources, such as oxidative metabolism by-products in the mitochondria and exogenous sources including UV light, and environmental pollution such as ozone [6]. All of these insults trigger a downstream cellular production of reactive oxygen species (ROS), where in high concentrations could have deleterious outcomes for cells and contribute to phenomena such as skin aging where there is augmented ROS production and reduced levels of enzymatic and non-enzymatic protectors [7][8]. This indicates that skin is constantly in a state of alert in order to protect against such insults and maintain its physiological redox homeostasis [9]. Given that the skin is constantly exposed to both endogenous and exogenous insults that can challenge its homeostasis, it doesn't possess a resting state referred to as a baseline state which allows it to have a dynamic equilibrium [10][11].

Nuclear factor erythroid 2-related factor-2-Kelch-like ECH-associated protein 1 (Nrf2-Keap1) pathway is a major cellular defence mechanism within the skin that helps to modulate oxidative stress by inducing phase II enzymes such as glutathione S-transferase (GST), quinone reductase NAD(P)H (NQO1), heme oxygenase-1 (HO-1), thioredoxin reductase (TrxR), catalase (CAT), and superoxide dismutase (SOD) [12] which can resolve oxidative stress and promote cellular survival [12][13][14]. Found in the cytoplasm under normal basal condition,

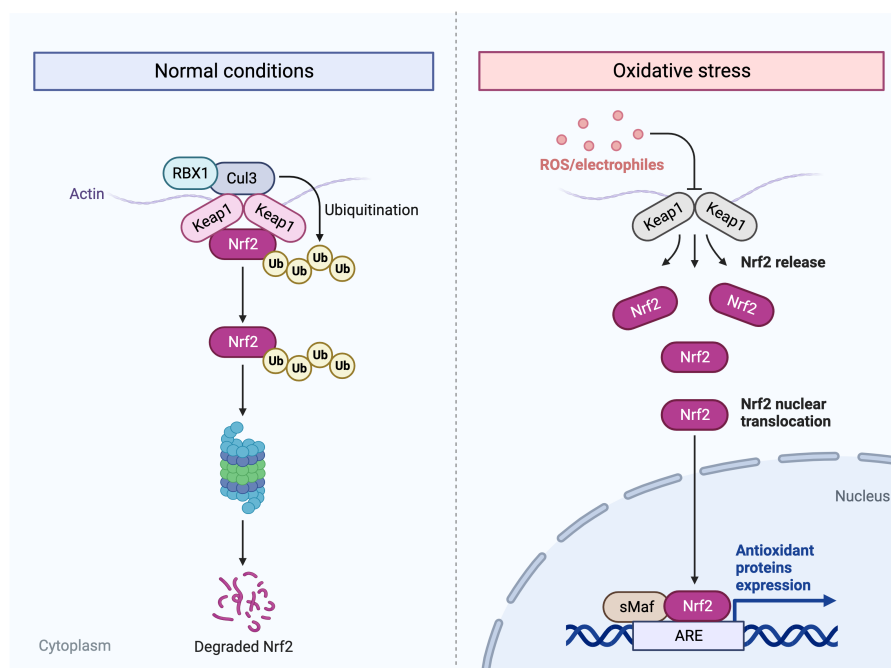
the Nrf2 transcription factor is bound to two molecules of the cysteine rich metalloprotein Keap1 leading to its ubiquitination and consequent proteasomal degradation. The introduction of oxidative stress allows the electrophile to recognise certain cysteine residues on the Keap1 protein and oxidises them thus inhibiting the Keap1 proteasomal degradation of Nrf2, which can be stabilised and translocated to the nucleus [12,15]. After accumulation in the nucleus, Nrf2 forms a complex with Maf proteins which then binds to the antioxidant response element (ARE) and triggers phase II enzymes (Scheme 4.1) [16,17]. Activation of Nrf2-Keap1 signalling pathway can be achieved by either direct or indirect activation. Direct activation is as described above where the electrophile binds to Keap1, and indirect activation occurs when there is increased production of endogenous ROS in low concentrations [18-20]. Direct activation has been shown to be oxygen-independent while the indirect mechanism of activation requires constant activation by endogenously produced compounds of this mechanism. Indirect activation within the skin is beneficial and may help to alleviate any big oxidative stress events which may occur. This has led to the skin being described as having a hormetic mechanism, where low doses of oxidative driving sources is needed and proves beneficial to cells whereas high doses can be toxic to cells and cause cellular damage and death [21-23]. 4-hydroxynonenal (HNE), an α,β -unsaturated advanced lipid peroxidation end product (ALE) and common skin metabolite, was shown to directly activate the Nrf2-Keap1 pathway, acting as a Michael acceptor, by changing the conformation of Keap1 [24-27]. These low concentrations also induce an adaptive response via the induction of thioredoxin, a phase II enzyme, as a result of the activation of the Nrf2 signalling pathway thus protecting cells against forthcoming oxidative stress [23].

Aldehydes and ketones are frequently reported to be emitted from skin in high abundances and comprise a large fraction of the human volatilome [24]. Aldehyde emissions from skin are considered to be ALEs generated from oxidative stress reactions within skin while ketone emissions are oxidative degradation products of squalene [30, 31]. Recent work has shown that cutaneous volatiles such as the saturated aldehydes, nonanal and decanal and the aromatic aldehyde, benzaldehyde, trigger Nrf2-Keap1 activation through an indirect, ROS-dependant mechanism [27]. Mitochondria are the common source of intracellular ROS generation and studies have shown that an augmentation in ROS may be accompanied by mitochondrial depolarization. A significant change in mitochondrial membrane potential was reported for nonanal, decanal and benzaldehyde thus eluding to an augmentation in ROS

entities within the cell. Free radical scavengers as well as anoxia conditions were also employed to further understand this indirect mechanism of activation.

Much of this work has examined cellular response through the treatment of cells in the liquid phase with many different methods developed for assessing cell-to-cell interactions including lab-on-a-chip and 3D microfluidic platforms. While these methods of analysis have great potential to understand cell-signalling pathways in liquid phase metabolites, they are limited in their ability to assess cell-signalling triggered by compounds emitted in the volatile phase [28–30]. Recent studies have shown that compounds emitted in the volatile phase either endogenously from cells themselves [31] or from microbial populations [32] can trigger cellular responses within cells and within neighbouring cells. Human organotypic lung models have been developed which integrate an air-liquid interface (ALI) to assess how volatile emissions from fungal pathogens can trigger an inflammatory, cytokine response within cells [32]. In an ALI culture, culture medium is removed from the top of the cells thus exposing the cells to the surrounding air and the bottom of the cells are in contact with cell culture medium, allowing nutrient supply [33]. The development of such models that integrate ALI cultures attempt to close the *in vitro*-*in vivo* gap to allow for investigation of cell signalling within the volatile phase.

Here, this work aims to further investigate the impact of skin-derived compounds at different concentrations, specifically the aldehydes, nonanal, decanal and the ketone, 6-methyl-5-hepten-2-one, on host skin cells' signalling pathways, specifically the Nrf2-Keap1 mechanism. Further elucidation of the mechanism by which this pathway is activated is investigated by monitoring ROS generation within cells after exposure. Moreover, most studies to date show the response of cells to treatment of compounds, that are typically emitted as volatiles from skin, dissolved in the liquid phase in cell media. Here, we attempt to simulate an enclosed environment where cells are exposed to differing concentrations of nonanal in the volatile phase as a proof of concept that the skin-derived volatile, nonanal, can trigger cell signalling pathways within a skin cell itself and also within neighbouring cells.



Scheme 4.1. Schematic showing Nrf2 bound to Keap1 protein under normal conditions and release of Nrf2 protein under oxidative stress followed by Nrf2 nuclear translocation.

4.2. Materials and methods

4.2.1. Cell lines and culture conditions

Normal human epidermal keratinocytes (adult NHEKs) (Passage 2) were purchased from Lonza Inc. (Belgium) and were cultured in medium comprised of KBM Gold Basal Medium and KGM Gold SingleQuots supplements both supplied by Lonza. The cultures were incubated in 5% CO₂ at 37°C. Upon arrival, cells were thawed in a water bath at 37°C and were seeded in a T75 cm³ flask and allowed to grow for 5 days to ensure 70-80% confluency. Cells were then subcultured (1:3) once 70-80% confluency was reached. Cells at passage 3 or 4 were used for all experiments and cell media was changed every 2-3 days. Cell morphology was examined using a light microscope and images were taken at 10X magnification.

4.2.2. Cell cytotoxicity assay

Cells were trypsinised as per outlined protocol using the ReagentPack from Lonza. 100 µL of a 3x10⁴ cells/ml solution was seeded in a 96-well plates (36 wells seeded) (Greiner CELLSTAR clear 96-well plate, Sigma Aldrich, Ireland). After 24 hours, cells were treated with 2X concentrations of nonanal, decanal and 6-methyl-5-hepten-2-one (Sigma Aldrich, Ireland) in 100 µL of media. In order to prepare the varying concentrations of the compounds, a 2M in dimethyl sulfoxide (DMSO) (Sigma Aldrich, Ireland) stock solution of each compound

was prepared and concentrations ranging from 0.0007 – 7000 μM were prepared by serial dilution in cell media ($n = 4$ for each concentration). DMSO was initially used as it is typically the solvent employed for cytotoxicity assays in the lab where the work was carried out. Cells were also treated with DMSO control whereby the final concentration of DMSO was 0.7%. Cells were exposed to the compounds for 24 h or 72 h in 5% CO_2 at 37°C. 20 μL of the cell viability reagent, PrestoBlue (ThermoFisher Scientific, Ireland) was then added and incubated for a further 5 h in 5% CO_2 at 37°C. A Tecan Infinite F200 microplate reader, in top reading mode, with an excitation wavelength of 560 nm and an emission of 590 nm, was then used to read fluorescence. Background fluorescence was calculated using a blank consisting of cell media only. Percentage viability was calculated relative to untreated controls (cells and media).

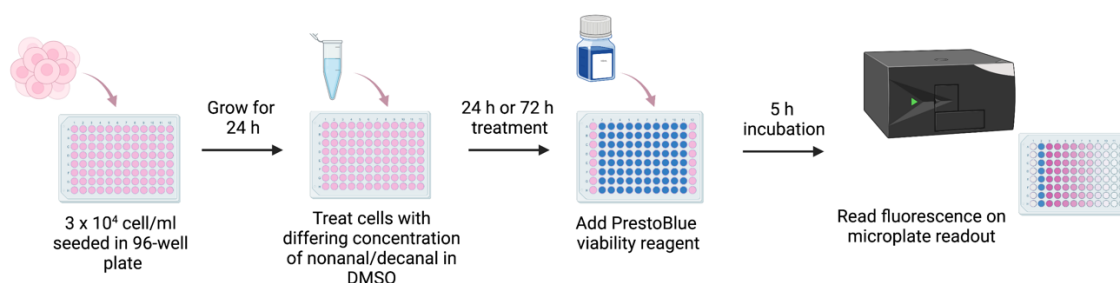


Figure 4.1. Schematic showing the protocol for the cell cytotoxicity assay.

4.2.3. Reactive oxygen species (ROS) assay

Cells were trypsinised and 100 μL of a 3×10^4 cells/ml solution was seeded in a black-walled clear bottom 96-well plates (40 wells seeded) (Corning clear bottom black 96 well plate, Fisher Scientific, Ireland).

4.2.3.1. Liquid phase

After 24 h incubation in 5% CO_2 at 37°C, media was aspirated from cells and cells were simultaneously treated with 100 μL varying 1X concentrations of nonanal, decanal and 6-methyl-5-hepten-2-one in cell media and 100 μL of a dichlorofluorescein diacetate (DCFDA)-based ROS detection agent (ROS-ID Total ROS detection kit, ENZO life Sciences) for both 2 h and 24 h in 5% CO_2 at 37°C. A stock solution of 100 mM of each compounds in *N,N*-dimethylformamide (DMF) was prepared prior to preparation of concentrations ranging from 0.05 – 100 μM diluted in cell media. 100 μL of a positive, ROS-inducing control, pyocyanin

(100 μM), was also used to treat cells. Fluorescence was read using a Tecan Infinite F200, using bottom reading mode and an excitation wavelength of 485 nm and emission of 535 nm.

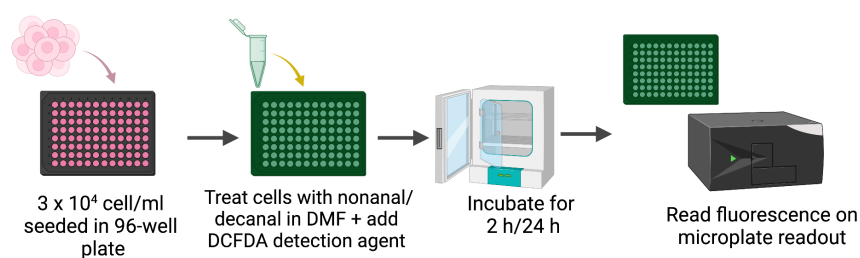


Figure 4.2. Schematic showing the protocol used for ROS assay in the liquid phase.

4.2.3.2. Volatile phase

After 24 h incubation in 5% CO_2 at 37°C , media was aspirated from cells and 20 μL of media was added to half of the wells ($n = 27$ wells) and for the other half of the wells surface media was removed leaving residual media on the cells ($n = 27$ wells). The 96-well plates with the lid on were then carefully placed in a sampling container ('Good For You' 850 ml Borosilicate glass containers, dimensions: 19.3 x 13.6 x 6.7 cm, Amazon UK). Following this, 0.1 μL (16,500 ppbv nonanal in gas phase in 850 ml headspace) or 0.5 μL (82,600 ppbv nonanal in gas phase in 850 ml headspace) of nonanal was pipetted either in the middle of the right hand side (RHS) or left hand side (LHS) of the container. A control was carried out whereby no nonanal was pipetted into the container. The lid was removed from the 96-well plate and the lid of the container was then put on. These containers have a snap-lock silicone seal which enhances sterility. The container containing the 96-well plate was then placed in a static incubator at 37°C for 2 hours. Following this, the 96-well plate was removed from sampling container, all media was aspirated and 100 μL of fresh media was added to all wells followed by the addition of 100 μL of the ROS detection agent. The cells were then incubated in 5% CO_2 at 37°C for 2 h with the detection agent. Again, fluorescence was read using a Tecan Infinite F200, using bottom reading mode and an excitation wavelength of 485 nm and emission of 535 nm.

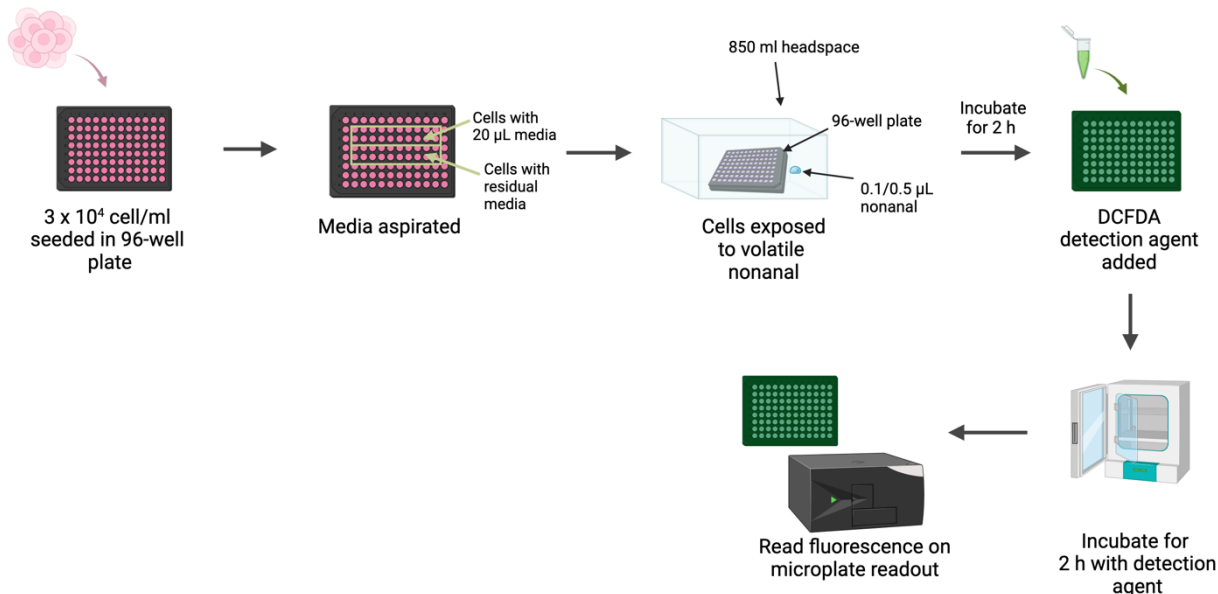


Figure 4.3. Schematic showing protocol used for ROS assay in the volatile phase.

4.2.4. Immunofluorescence

4.2.4.1. Slide preparation

Cells were trypsinised and 200 μ L of a 5×10^4 cells/ml solution was seeded in glass bottomed 8-well plates (Ibidi, 80827) and allowed to grow in 5% CO₂ at 37°C for 24 h. After 24 h the cell media was aspirated and cells were treated with 200 μ L of varying 1X concentrations (0.05 – 100 μ M) of nonanal, decanal and 6-methyl-5-hepten-2-one prepared in cell media for 5 h and 24 h. The effect of different vehicles including DMSO and DMF was also investigated. For this, 100 mM of nonanal, decanal and 6-methyl-5-hepten-2-one in DMSO and DMF were prepared and from these 0.05 – 100 μ M concentrations were prepared by dilution in cell media.

4.2.4.2. Immunofluorescence staining

After 5 h or 24 h, media was removed from cells and the cells were washed three times using a wash buffer (phosphate buffered saline (PBS), 0.1% tween 20 (Sigma-Aldrich, P1379) and 2% bovine serum albumin (BSA)). Cells were then fixed using 4% formaldehyde for 20 min, permeated with 0.5% Triton-X 100 for 45 min (Sigma Aldrich, Ireland) and blocked with 10% foetal bovine serum (FBS) in PBS for 1 h 30 min. The cells were incubated with primary rabbit-antihuman Nrf2 antibody (1:200) (ab62352, Abcam, Cambridge, UK) overnight at 4°C. The next day the cells were further incubated in the primary antibody for 45 min at room

temperature (RT). The primary antibody was removed and then cells were washed three times using the wash buffer solution. The cells were then incubated with a goat anti-rabbit IgG (H+L) cross-adsorbed secondary antibody, AlexaFluor 488 (1:1000) (Invitrogen, ThermoFisher Scientific, Ireland, A11008) for 1 h at RT in the dark. Secondary antibody was removed, and cells were washed three times with the wash buffer solution and then counterstained with DAPI (1:2500) for 3 min and the washed again with wash solution three times before the addition of an antifade mountant.

4.2.4.3. Confocal imaging

The immunofluorescence was observed using a Leica DFC500 microscope equipped with a CCD camera and EBQ 100 power supply. AlexaFluor 488 was excited at 499 nm using a PicoQuant laser unit and the emission was captured between 490 and 566 nm. DAPI was excited at 405 nm and emission was recorded between 387 and 474 nm. Images were taken using 20X magnification.

4.2.5. Statistical analysis

Each experiment was performed with at least 3 or 4 technical replicates and average values are given with standard error of the mean (SEM). Significant differences were tested for using the student's t-test (two tailed with unequal variances).

4.3. Results and discussion

4.3.1. Morphology of NHEKs

Initially, the morphology of the adult NHEK cells was examined at different stages of confluency. These NHEK cells had a doubling time of 24 hours and are guaranteed for 18 population doublings. Figure 4.4 (a) shows NHEK cells 2 days after being thawed back at approximately 20-30% confluency. Cells were allowed to grow for a further 3 days before they reached 60-70% confluency and were subcultured (Fig 4.4 (b)). These cells were subcultured at 60-70% confluency as they can become irreversibly contact-inhibited which may trigger cellular senescence if allowed to grow past 80% confluency.

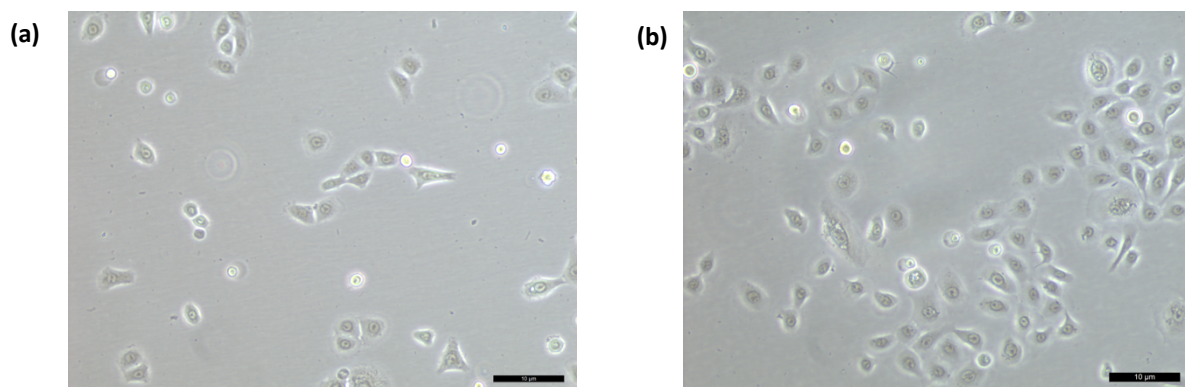


Figure 4.4. NHEK cells images at (a) 20-30% confluency and (b) 60-70% confluency. Images taken at 10X magnification. Scale bars = 100 μm .

4.3.2. Cytotoxicity assay

As discussed in chapter 2, nonanal and decanal and 6-methyl-5-hepten-2-one are compounds common to the skin volatile profile and have been frequently reported in literature. Following assessment of the morphology of NHEK cells, the cytotoxicity of the two aldehydes, nonanal and decanal and the ketone, 6-methyl-5-hepten-2-one, toward the cells was investigated after exposure for 24 h and 72 h. Cells were treated with various concentrations of the compounds ranging from 0.0007 – 7000 μM and the cytotoxicity was determined by using the reazurin-based cell viability reagent, PrestoBlue. Reazurin is a non-toxic, cell-permeable compound that is blue in colour and exhibits no fluorescence. When this dye enters live cells, the reducing environment of viable cells reduces reazurin to resorufin and the compound is red and exhibits high fluorescence. Figure 4.5 shows examples of the visual colour difference observed when cells were treated with various concentrations of nonanal (Fig 4.5 (a)) and decanal (Fig 4.5(b)) for 72 h followed by incubation with the reazurin-based dye for 5 h.

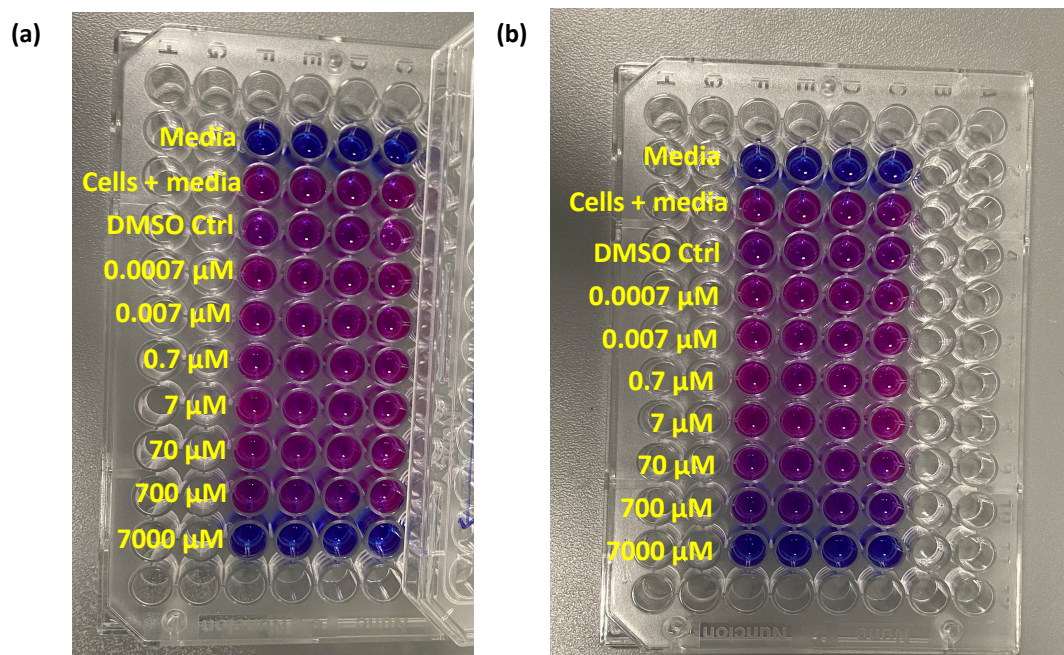


Figure 4.5. NHEK cells after treatment with 0.0007 – 7000 μM concentrations of (a) nonanal and (b) decanal for 72 h followed by incubation with PrestoBlue for 5 h (all solutions contained less than 0.7% DMSO).

The cells were treated with a wide concentration range of each compound to understand if the compounds had cytotoxic effects on the cells and at what concentration the percentage cell viability is decreased. Figure 4.6 shows the % cell viability after exposure to nonanal, decanal and 6-methyl-5-hepten-2-one for 24 h (Fig 4.6 (a)) and 72 h (Fig 4.6 (b)). This data shows that the concentrations of all three compounds between 0.0007 – 7 μM did not have any effect on cell viability for both 24 h and 72 h time-points. Concentrations of compounds from 70 – 7000 μM exhibited some cell death with cytotoxicity being higher after 72 h treatment compared with 24 h treatment. Cell viability was reduced by approx. 2% and 14% after exposure to 70 μM nonanal for 24 h and 72 h, respectively. The ketone, 6-methyl-5-hepten-2-one, exhibited slightly higher cytotoxicity compared to nonanal with a decrease in cell viability by 3% for 24 h and 15% for 72 h exposure to 70 μM 6-methyl-5-hepten-2-one. Decanal exhibited greater cytotoxicity compared with nonanal and 6-methyl-5-hepten-2-one with 7% cell viability reduction following exposure to 70 μM decanal after 24 h and 21% after 72 h treatment. Concentration from 700 – 7000 μM caused significant cell proliferation inhibition with all cells being completely wiped-out following exposure to 7000 μM of each compound.

A vehicle control was also included whereby the final concentration of DMSO was 0.7% and no cytotoxicity for such a concentration was observed.

Based on the results of this cytotoxicity assay, a concentration range of 0.05 – 100 μM of each compound was employed for all subsequent experiments.

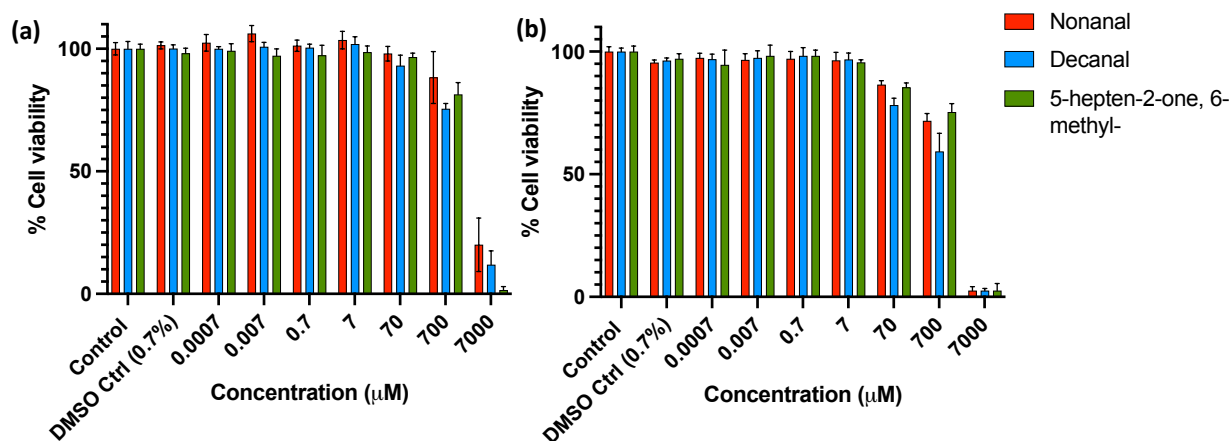


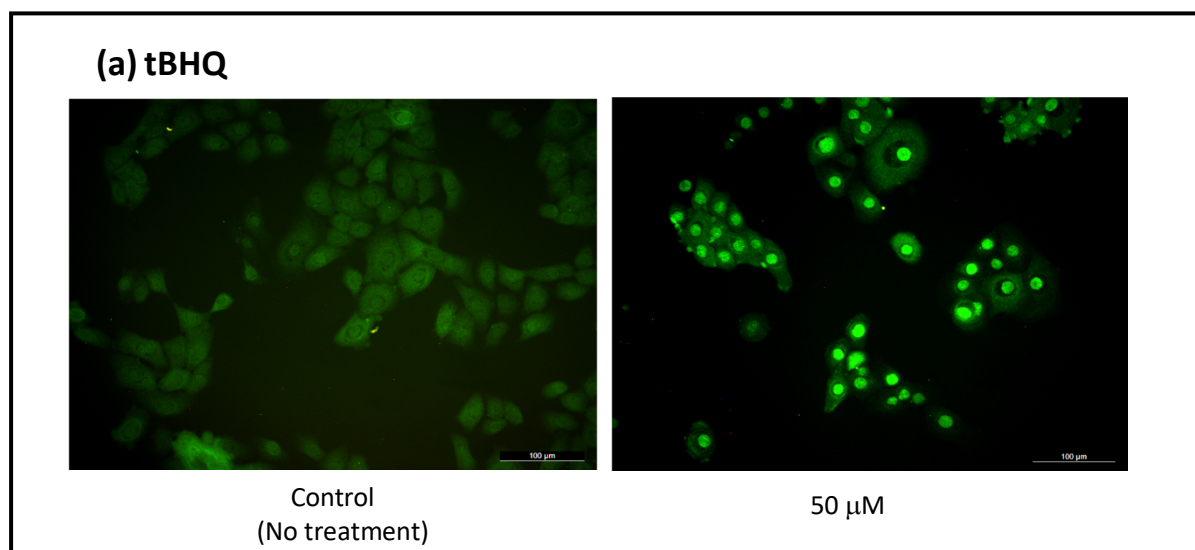
Figure 4.6. Viability of NHEK cells after (a) 24 h and (b) 72 h treatment with nonanal, decanal and 6-methyl-5-hepten-2-one.

4.3.3. Nrf2 translocation to the nucleus

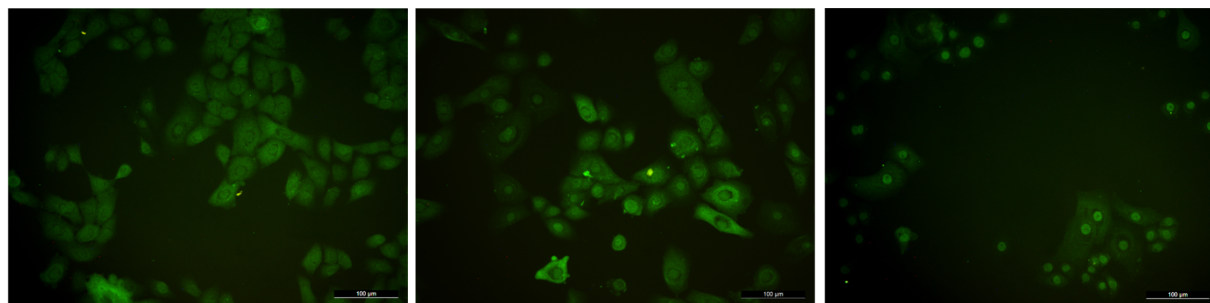
Following the selection of non-toxic concentrations of the compounds, cells were treated with these compounds in varying concentrations in order to investigate if they trigger the translocation of the Nrf2 protein from the cytoplasm to the nucleus. Here, the NHEK cells were stained with an Nrf2 antibody and fluorescent secondary antibody following their exposure to concentrations ranging from 0.05 – 100 μM nonanal, decanal and 6-methyl-5-hepten-2-one to demonstrate Nrf2 intracellular translocation. 50 μM tert-butyl-hydroquinone (tBHQ) served as a positive control (Fig 4.7 (a)). The use of different vehicles, including DMSO and DMF were explored along with differing treatment times including 6 h and 24 h.

The ratio (nuc/cyto) between the fluorescence signals obtained from the cells' nucleus and cells' cytoplasm was used to quantify the nuclear translocation of the protein. This is a commonly used metric for assessing the nucleocytoplasmic distribution of a cell. When this value is less than 1 it means the protein of interest is predominately located in the cytoplasm. Values greater than 1 indicate translocation of the protein to the nucleus and values equal to 1 means the protein is distributed in equal concentration in both the nucleus and cytoplasm. Initially, cells were exposed to VOCs for 6 h (Fig 4.7). The non-treated (NT) control exhibited a nuc/cyto ratio of close to 1, indicating that the Nrf2 protein is evenly distributed between nucleus and cytoplasm.

Translocation of the Nrf2 protein to the nucleus was demonstrated in NHEK cells following exposure to aldehydes including nonanal (Fig 4.7 (b)) and decanal (Fig 4.7 (c)) in cell media and DMF for 6 h. These results of Nrf2 activation by saturated aldehydes common to the skin volatile profile are supported by Ron-Doitch et al's work [27]. Their work examined activation of the pathway using concentrations from 2 – 20 μM whereas this work investigates a wider concentration range of 0.05 – 100 μM , where the lower concentrations investigated are relative to the physiological emission of nonanal and decanal from skin [24,34], as outlined in Chapter 3. A significant increase in nuc/cyto ratio was demonstrated with increasing concentrations of both nonanal and decanal (Fig 4.7 (e)). The highest nuc/cyto ratio was observed for 50 μM of nonanal and decanal followed by a decrease after treatment with 100 μM which may be linked to the cytotoxic effect exhibited by cells treated with higher concentration of the two compounds. In comparison, translocation was not observed for the ketone, 6-methyl-5-hepten-2-one after 6 h of treatment (Fig 4.7 (d) & (e)), this is thought to be linked to the mechanism by which the Nrf2 pathway is induced and will be discussed in section 4.4.3.



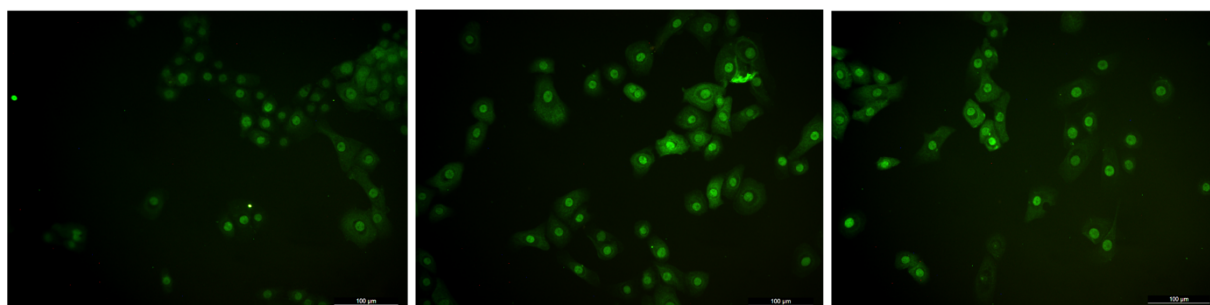
(b) Nonanal



Control
(No treatment)

0.05 μM

0.5 μM

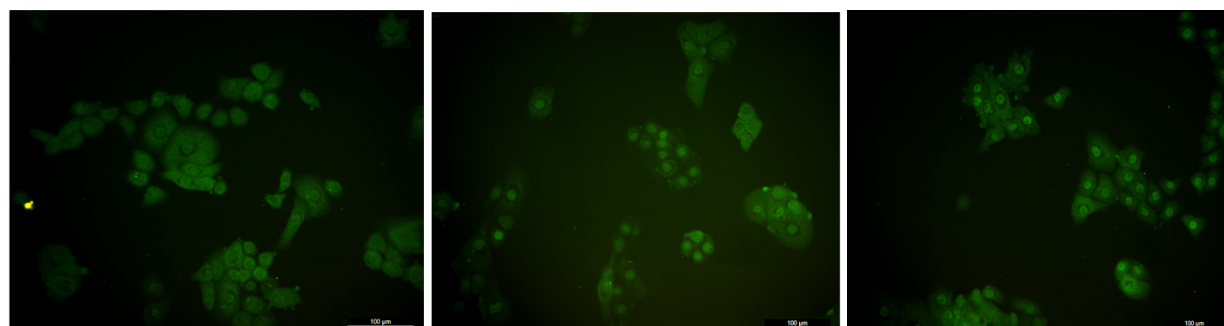


5 μM

50 μM

100 μM

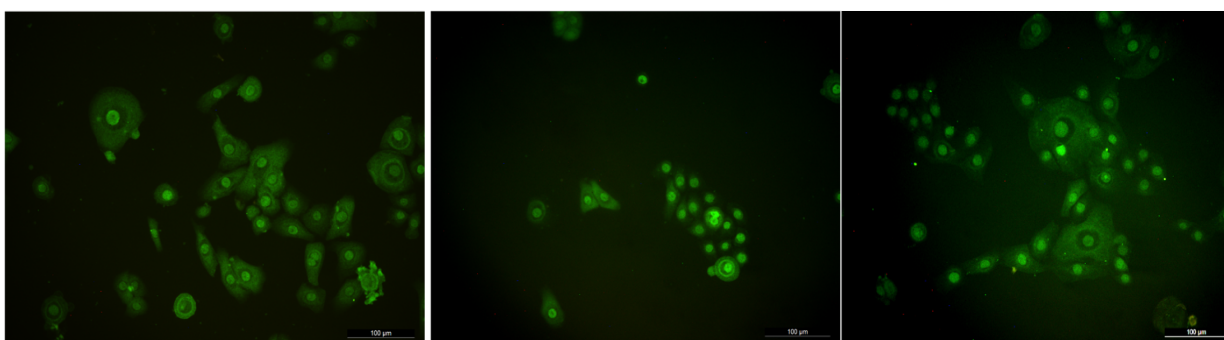
(c) Decanal



Control
(No treatment)

0.05 μM

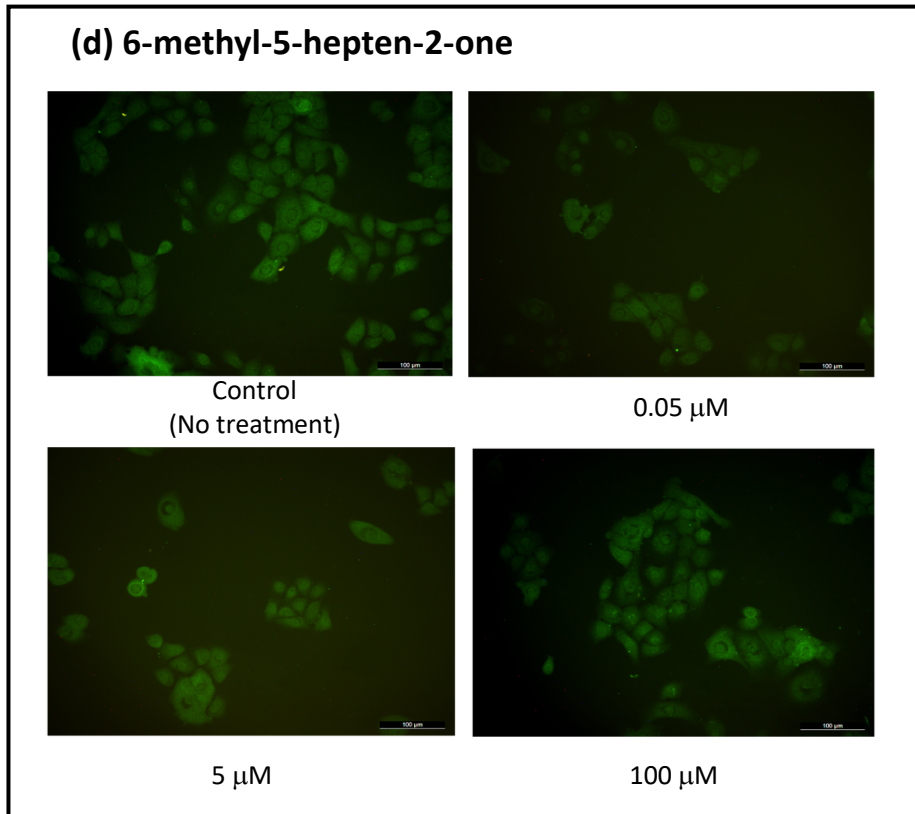
0.5 μM



5 μM

50 μM

100 μM



(e)

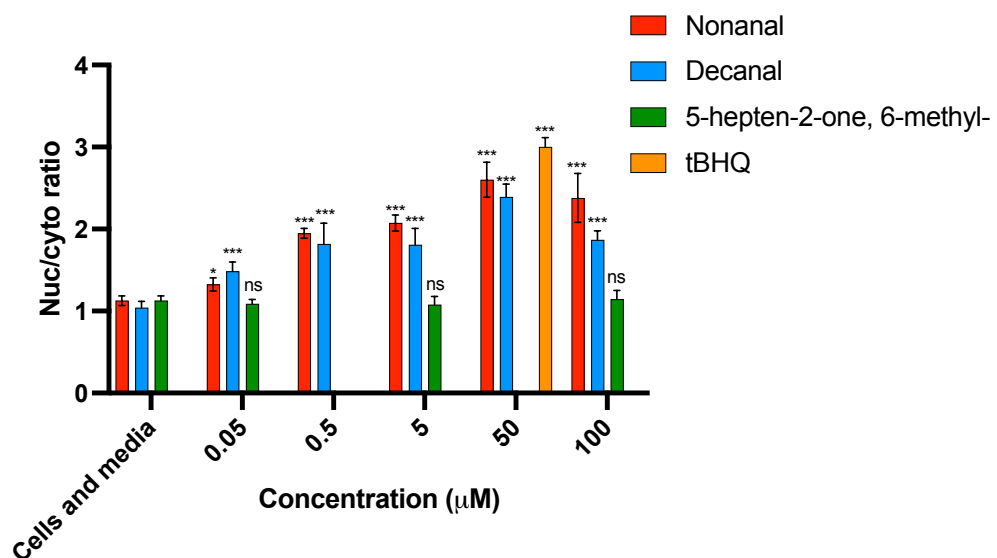


Figure 4.7. Nuclear translocation of Nrf2 protein visualised by immunofluorescent staining after treatment for 6 h with (a) 50 μM tBHQ in cell media and various concentrations of (b) nonanal, (c) decanal and (d) 6-methyl-5-hepten-2-one in cell media and (e) nucleus/cytoplasm fluorescent intensity ratio quantified using ImageJ software. Images taken at 20X magnification. Scale bars = 100 μm . All values shown are the mean nuc/cyto ratio for $n=10$ cells \pm standard error of mean (SEM). Student's t-test (two tailed with unequal variances) was

performed to test significance of nuclear translocation between cells and media (control) and treatments (nonanal, decanal, 6-methyl-5-hepten-2-one and tBHQ), (ns = not significant, * $p < 0.05$, ** = $p < 0.01$ and *** = $p < 0.001$).

Moreover, no translocation of Nrf2 protein was observed when NHEK cells were treated with nonanal and decanal for 24 h indicating that the mechanism by which the translocation is activated by has ceased and keap1, which is a negative regulator of Nrf2, has sequestered the Nrf2 protein in the cytoplasm again (Fig 4.8 (a)).

Furthermore, results also showed that when cells were exposed to varying concentrations of the compounds dissolved in DMSO there was no translocation of the Nrf2 protein to the nucleus. Figure 4.8 (b) also shows the lack of Nrf2 nuclear translocation when NHEK cells were treated with 50 μM nonanal and decanal dissolved in DMSO for 6 h. This is thought, again, to be related to the mechanism by which Nrf2 translocation is induced and also related to the fact that DMSO can act as a free radical scavenger, thus inhibiting hydroxyl radical generation in cells [35].

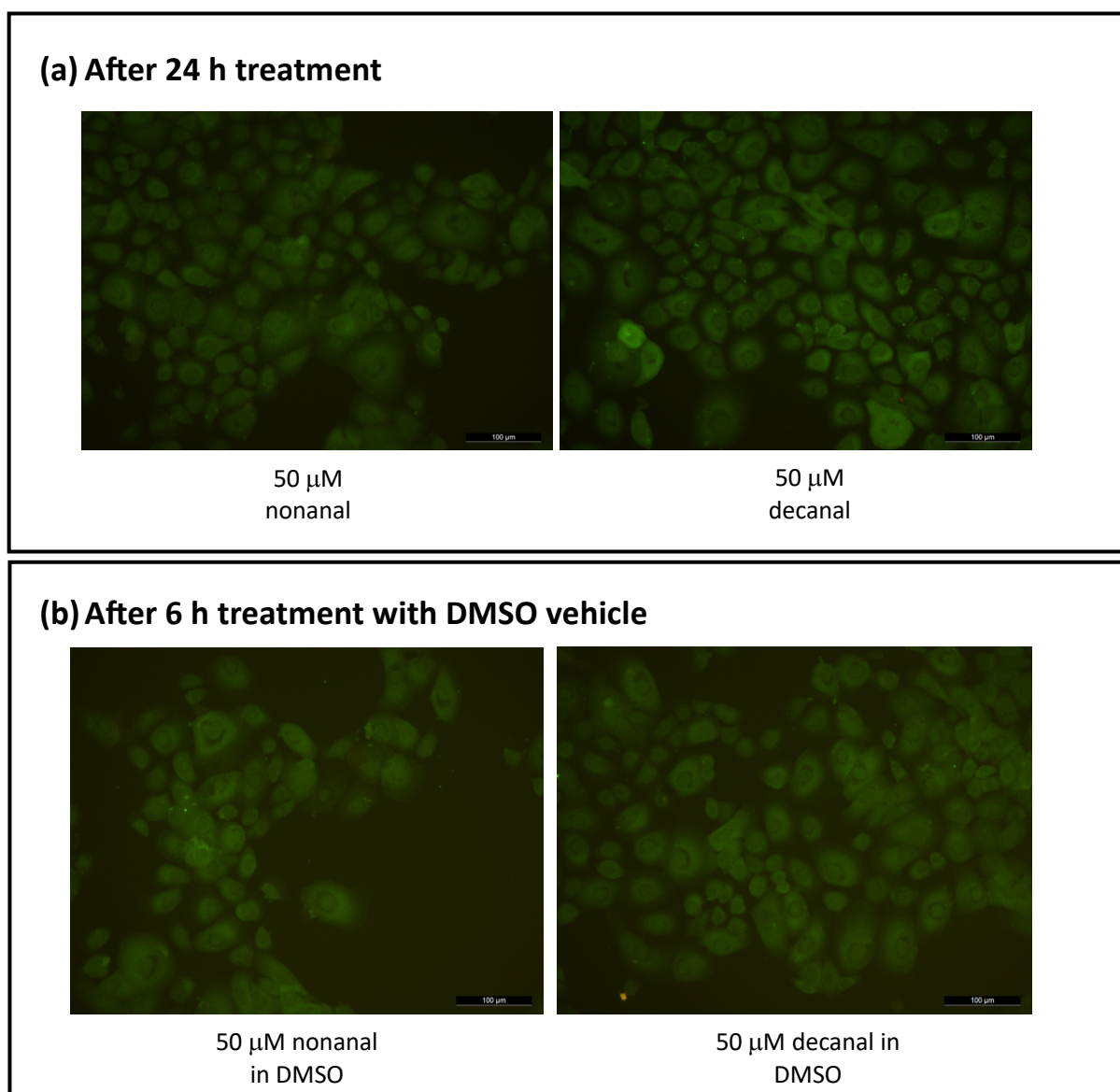


Figure 4.8. Nuclear translocation of Nrf2 protein visualised by immunofluorescent staining after treatment with (a) 50 μ M nonanal and decanal in cell media for 24 h and (b) 50 μ M nonanal and decanal in DMSO vehicle for 6 h. Images taken at 20X magnification. Scale bars = 100 μ m.

4.3.4. Elucidation of the mechanism of Nrf2 induction

4.3.4.1. Investigation of ROS generation induced by compounds in liquid phase

Following confirmation of the Nrf2 proteins translocation to the nucleus of NHEK cells following treatment with the saturated aldehydes, nonanal and decanal, the mechanism by which this translocation is activated by was investigated. Previous studies have shown that tBHQ, the positive control employed here induces intracellular oxidative stress thus leading to

the activation of the Nrf2-keap1 cell signalling pathway [36]. A recent study by Ron-Doitch et al partially outlines the mechanism of pathway activation by the saturated aldehydes nonanal and decanal and shows an increase in mitochondrial membrane potential which indicates increased ROS production by these compounds and thus indirect activation [27].

Here, ROS production by NHEK cells following exposure in the liquid phase to nonanal, decanal, 6-methyl-5-hepten-2-one and the positive Nrf2 inducer, tBHQ was monitored via the fluorescent probe, DCFDA in order to further elucidate the mechanism by which these saturated aldehydes induce the Nrf2-keap1 cellular defence mechanism. Given that Nrf2 translocation was induced by nonanal, decanal and tBHQ, ROS production following their exposure was monitored for both 2 h and 24 h whereas ROS generation by 6-methyl-5-hepten-2-one was only monitored for 2 h. All compounds here were dissolved in DMF (final concentration = 0.1%) (no ROS elevation observed) as DMSO is known to be a free radical scavenger, thus limiting ROS production within the cells.

Figure 4.9 (a) shows ROS generation after 2 h exposure to nonanal, decanal, 6-methyl-5-hepten-2-one and tBHQ. Exposure to nonanal and decanal show significant elevation in ROS for all concentrations (0.05 – 100 μ M) while exposure to the ketone, 6-methyl-5-hepten-2-one showed no significant elevation in ROS after treatment and may be linked to ketones abilities to decrease oxidative stress through the scavenging of free radicals. Further work is needed to characterise and understand the response of keratinocyte cells toward ketones such as 6-methyl-5-hepten-2-one. ROS generation by tBHQ was also monitored after 2 h in order to elucidate the mechanism by which it activates the Nrf2 pathway and a significant increase in ROS production was observed ($p < 0.001$). Studies are conflicting around the mechanism by which tBHQ activates the Nrf2 pathway with some studies showing indirect activation through an augmentation of mitochondrial ROS while others have shown direct activation by interacting with thiol groups of cysteine molecules on the keap1 protein thus inhibiting its ability to repress Nrf2 [37].

After treatment for 24 h, a significant elevation in ROS generation is only observed for nonanal at 100 μ M while, albeit lower than for 2 h treatment, a significant generation is observed for decanal between 0.5 – 100 μ M. tBHQ also shows significant elevation in ROS levels after treatment for 24 h. Comparing 2 h treatment with 24 h treatment shows that ROS generation has decreased after 24 h which may be linked to the instability of ROS within the cell. The significant increase in ROS production within the cells suggest that the mechanism by which the Nrf2-Keap1 pathway is activated by is indirect due to an augmentation of ROS

species. It could be hypothesised that nonanal and decanal provide an adaptive response, in a similar way to HNE, albeit by an indirect mechanism, that causes the production of phase II enzymes following translocation of Nrf2 to the nucleus which may provide cells with protection against further oxidative stress.

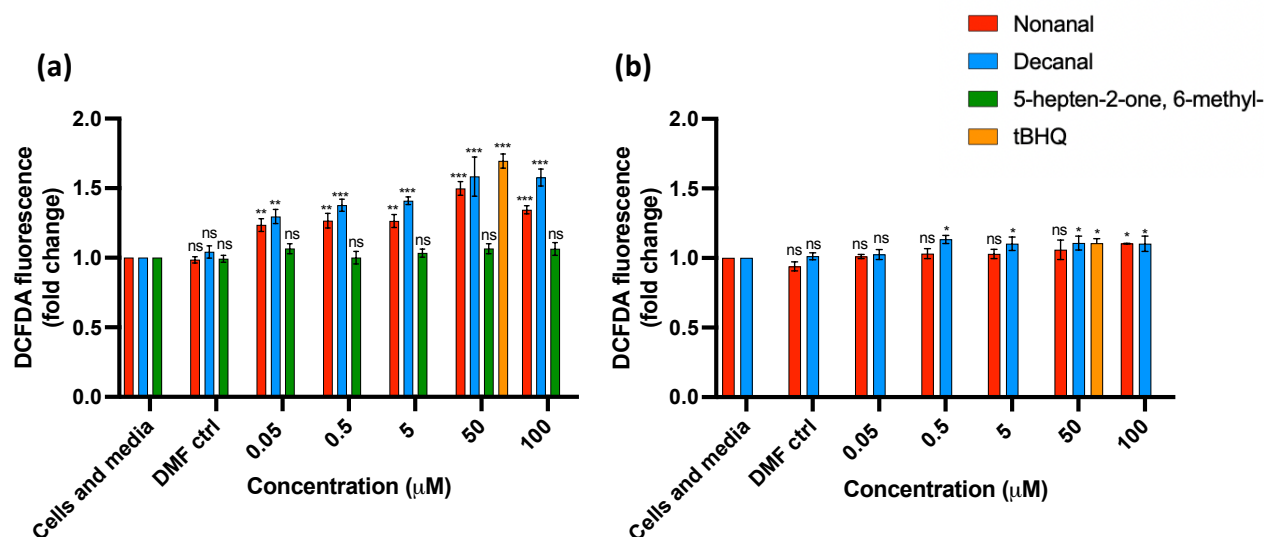


Figure 4.9. Endogenous ROS production after treatment of NHEK cells with (a) nonanal, decanal, 6-methyl-5-hepten-2-one and tBHQ for 2 h and (b) nonanal, decanal and tBHQ for 24 h. All values shown are the mean of n=4 technical replicates \pm standard error of mean (SEM). Student's t-test (two tailed with unequal variances) was performed to test significance of ROS generation between cells and media (control) and treatments (nonanal, decanal, 6-methyl-5-hepten-2-one and tBHQ), (ns = not significant, * $p < 0.05$, ** = $p < 0.01$ and *** = $p < 0.001$).

4.3.4.2. Investigation of ROS generation induced by nonanal in gas phase

Following analysis of the compounds in the liquid phase and their ability to generate ROS, the ability of nonanal in the volatile phase to generate intracellular ROS was investigated. This work aims to understand if nonanal, in the volatile phase, generates ROS within NHEK cells which in turn may lead to the activation the Nrf2 pathway. As discussed in Chapter 3, nonanal is emitted from skin in the volatile phase in a concentration range from 0.625-20 ppb, with average emission from a healthy population being 2.42 ppb. This work aims to understand if nonanal, in the volatile phase, generates ROS within NHEK cells which in turn may lead to the activation the Nrf2 pathway. Cells were treated with 0.1 μ l and 0.5 μ l of nonanal in an 850 ml headspace which equate to 16,500 ppbv and 82,600 ppbv, where headspace concentration was calculated using the ideal gas law [38]. Concentrations much higher than the physiological range were employed in order to initially to try and show proof of concept of the ability of

volatile nonanal to generate ROS within cells. Figure 4.3 above outlines the protocol followed for ROS generation assessment in the volatile phase. Figure 4.10 below shows the set-up of the 96-well plate for these experiments where n=27 wells have cells with 20 μL of media on them and n=27 well have cells with residual media on them for the duration of the exposure to nonanal in gas phase. Columns are labelled 1-9 for ease of analysing results.

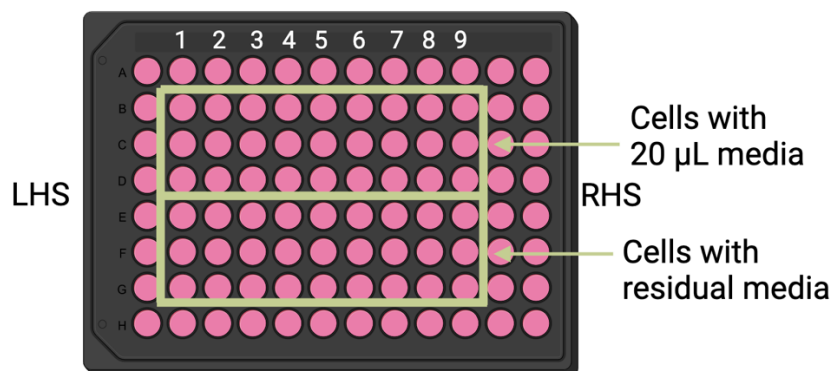


Figure 4.10. Layout of 96-well plate for ROS volatile assay where n=27 wells have cells with 20 μL and n=27 well have cells with residual media on them. 0.1 μL or 0.5 μL of nonanal was pipetted either on the LHS or RHS of well plate as shown here. Columns are labelled 1-9 for easy interpretation of results.

ROS generation within cells was assessed both with 20 μL and with residual media. Cells with residual media attempt to mimic skin whereby skin is generally a relatively dry environment. Another reason for assessing the response of cells with residual media is that nonanal has low solubility in water thus indicating that it would not fully dissolve in cell media which is primarily aqueous-based and so the use of media may limit ROS generation within cells due to the low partition coefficient between nonanal in the gas phase and cell media.

A major limitation associated with using cells with residual media is that the lack of media itself can cause stress on the cells which may lead to increase in ROS generation. Controls whereby the cells were exposed to a headspace of the same volume without nonanal were employed to understand the effect residual media on the cells has with regard to ROS generation. The DCFDA fluorescence fold change between cells with media and cells with residual media showed that the lack of media on cells showed a significant increase in ROS production ($p < 0.01$) indicating that they are under stress (Fig 4.11). This increase in ROS showed the need for a control to be run each time in order to understand generation of ROS by cells themselves without the presence of nonanal. Such controls proved crucial in the data

processing where each well number had its own control for each condition and this was used to calculate DCFDA fluorescence fold change against.

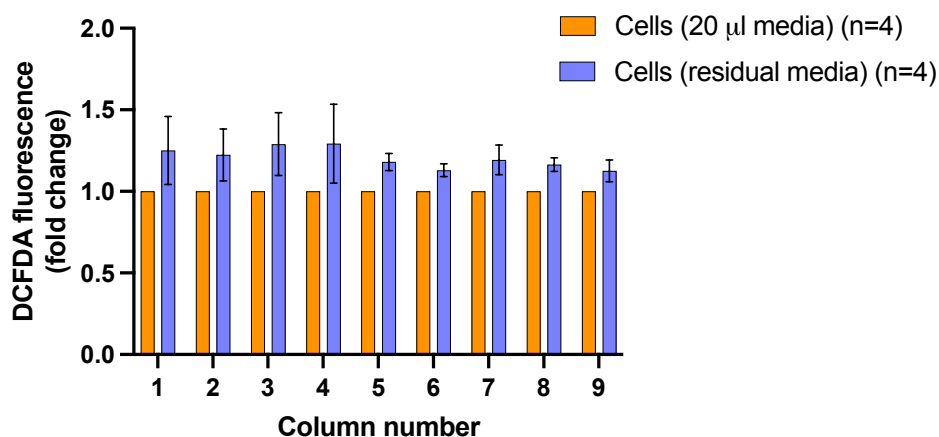


Figure 4.11. Control for ROS production in NHEK cells with residual media. All values shown are the mean of n=4 replicates \pm standard error of mean (SEM). Student's t-test (two tailed with unequal variances) was performed to test significance between ROS generation in cells with 20 μ l media (control) and cells with residual media, (ns = not significant, * $p < 0.05$, ** = $p < 0.01$ and *** = $p < 0.001$).

Results show no significant ROS generation by cells with media across all columns when exposed to a headspace concentration of 16,517 ppbv nonanal (Figure 4.12 (a-b)). Some significance ($p < 0.05$) was observed when cells with media were exposed to the same headspace concentration. A gradient effect was observed where when nonanal was pipetted on the LHS of the plate, columns 1-3 showed significant ROS generation whereas columns further away from the source of nonanal in gas phase showed no or limited significant increase in ROS indicating that the gaseous nonanal may have not reached those columns within the 2 h exposure time.

Exposure of cells with media to a headspace concentration of 82,585 ppbv nonanal showed significantly higher production of intracellular ROS within NHEK cells ($p < 0.01$) (Figure 4.12 (c-d)). This may indicate an increased dissolution of nonanal in cell media due to the higher concentration present in the headspace. Cells with residual media in a headspace concentration of 82,585 ppbv nonanal again showed a higher production of ROS when compared with exposure to the lower concentration of 16,517 ppbv ($p < 0.001$). A similar gradient effect was observed in cells with residual media and was not in cells with media whereby cells/columns closest to the nonanal source exhibited increased ROS generation. This

leads to further hypothesis that nonanal produced in keratinocyte cells may trigger ROS generation in neighbouring cells and provides initial proof of concept that nonanal in the volatile phase can cause significant increase in ROS production which in turn may lead to the activation of the Nrf2-Keap1 protective pathway.

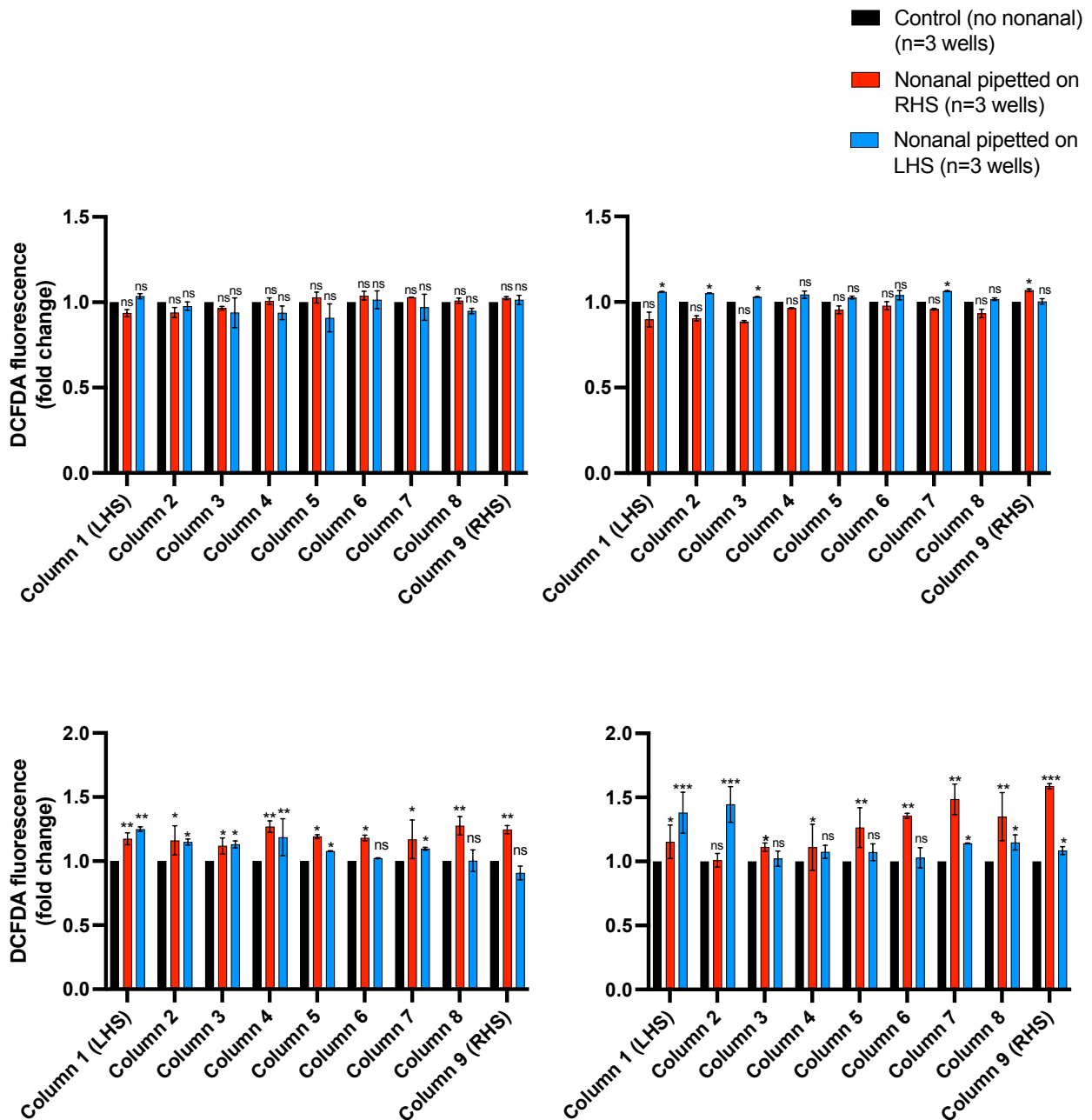


Figure 4.12. Endogenous ROS production after treatment of NHEK cells with (a) 0.1 μ l nonanal in gas phase in the presence of 20 μ l media on cells, (b) 0.1 μ l nonanal with residual media on cells, (c) 0.5 μ l nonanal with 20 μ l media on cells and (d) 0.5 μ l nonanal with residual

media on cells. All values shown are the mean of n=3 technical replicates \pm standard error of mean (SEM). (ns = not significant, * p<0.05, ** = p<0.01 and *** = p<0.001).

4.4. Conclusion

In summary, the results of this work show that the saturated aldehydes, nonanal and decanal activate the Nrf2-Keap1 protective mechanism in NHEK cells. Augmentation of ROS species was observed when NHEK cells were treated with varying concentrations of nonanal and decanal in the liquid phase thus elucidating a mechanism of indirect activation of Nrf2 translocation to the nucleus. The ketone, 6-methyl-5-hepten-2-one, did not cause activation of the Nrf2 pathway in human keratinocyte cells and this may be linked to no significant elevation in ROS generation observed upon exposure. It is speculated that this may be linked to ketones ability to scavenge free radical however, more work is needed to understand this response.

A proof of concept study also showed an increase in ROS production when cells were exposed to varying concentrations of nonanal in gas phase. To the best of our knowledge, this is the first study that investigates the effect of treatment of cells with nonanal in the volatile phase and leads to hypothesis that nonanal in the gas phase produced by the skin may lead to ROS generation in cells and neighbouring cells which may lead to the activation of the Nrf2-Keap1 pathway through indirect activation. While this study is novel, it does provide initial proof of concept with some limitations. For example, cells were only exposed to a headspace of nonanal in gas phase. It would be more beneficial to expose cells to an artificial skin VOC mix, comprising common skin emitted compounds and physiological relevant concentrations. Furthermore, monolayer cultures only allow limited inference about response to external stimuli such as volatile emissions and their ability to trigger cell-signalling pathways. A move toward an organ on a chip model with the integration of an ALI culture would further enhance assessment of volatile compounds abilities to induce signalling pathways within cells.

Despite these challenges, we hypothesise that, in a similar way to HNE, nonanal and decanal, which are frequently emitted volatiles from skin, at lower concentrations (0.625 ppb – 20 ppb; Chapter 3) cause moderate stress on the skin which in turn generates a low concentration of ROS and triggers activation of the Nrf2-Keap1 pathway to keep the skin alert, thus protecting it from further oxidative stress that may occur.

4.5. References

- [1] Drabińska N, Flynn C, Ratcliffe N, Belluomo I, Myridakis A, Gould O, Fois M, Smart A, Devine T and Costello B D L 2021 A literature survey of all volatiles from healthy human breath and bodily fluids: the human volatilome *Journal of Breath Research* **15** 034001
- [2] Shirasu M and Touhara K 2011 The scent of disease: volatile organic compounds of the human body related to disease and disorder *J Biochem* **150** 257–66
- [3] Grice E A and Segre J A 2011 The skin microbiome *Nat Rev Microbiol* **9** 244–53
- [4] Samaras S and Hoptroff M 2020 The Microbiome of Healthy Skin *Skin Microbiome Handbook* (John Wiley & Sons, Ltd) pp 1–32
- [5] Byrd A L, Belkaid Y and Segre J A 2018 The human skin microbiome *Nature Reviews Microbiology* **16** 143–55
- [6] Chen J, Liu Y, Zhao Z and Qiu J 2021 Oxidative stress in the skin: Impact and related protection *International Journal of Cosmetic Science* **43** 495–509
- [7] Shin M H, Rhie G, Kim Y K, Park C-H, Cho K H, Kim K H, Eun H C and Chung J H 2005 H₂O₂ Accumulation by Catalase Reduction Changes MAP Kinase Signaling in Aged Human Skin In Vivo *Journal of Investigative Dermatology* **125** 221–9
- [8] Papaccio F, D'Arino A, Caputo S and Bellei B 2022 Focus on the Contribution of Oxidative Stress in Skin Aging *Antioxidants* **11** 1121
- [9] Schäfer M and Werner S 2015 Nrf2—A regulator of keratinocyte redox signaling *Free Radical Biology and Medicine* **88** 243–52
- [10] Kohen R and Nyska A 2002 Invited Review: Oxidation of Biological Systems: Oxidative Stress Phenomena, Antioxidants, Redox Reactions, and Methods for Their Quantification *Toxicol Pathol* **30** 620–50
- [11] Halliwell B 1989 Free radicals, reactive oxygen species and human disease: a critical evaluation with special reference to atherosclerosis. *British Journal of Experimental Pathology* **70** 737–57
- [12] Gęgotek A and Skrzydlewska E 2015 The role of transcription factor Nrf2 in skin cells metabolism *Arch Dermatol Res* **307** 385–96
- [13] Ben-Yehuda Greenwald M, Ben-Sasson S, Bianco-Peled H and Kohen R 2016 Skin Redox Balance Maintenance: The Need for an Nrf2-Activator Delivery System *Cosmetics* **3** 1
- [14] Ron-Doitch S and Kohen R 2020 The Cutaneous Physiological Redox: Essential to Maintain but Difficult to Define *Antioxidants (Basel)* **9** 942

- [15] Beyer T A, auf dem Keller U, Braun S, Schäfer M and Werner S 2007 Roles and mechanisms of action of the Nrf2 transcription factor in skin morphogenesis, wound repair and skin cancer *Cell Death & Differentiation* **14** 1250–4
- [16] Giudice A, Arra C and Turco M C 2010 Review of Molecular Mechanisms Involved in the Activation of the Nrf2-ARE Signaling Pathway by Chemopreventive Agents *Transcription Factors: Methods and Protocols* Methods in Molecular Biology ed P J Higgins (Totowa, NJ: Humana Press) pp 37–74
- [17] Tkachev V O, Menshchikova E B and Zenkov N K 2011 Mechanism of the Nrf2/Keap1/ARE signaling system *Biochemistry Moscow* **76** 407–22
- [18] Sirota R, Gibson D and Kohen R 2015 The role of the catecholic and the electrophilic moieties of caffeic acid in Nrf2/Keap1 pathway activation in ovarian carcinoma cell lines *Redox Biology* **4** 48–59
- [19] Ursini F, Maiorino M and Forman H J 2016 Redox homeostasis: The Golden Mean of healthy living *Redox Biology* **8** 205–15
- [20] Siow R C M, Ishii T and Mann G E 2007 Modulation of antioxidant gene expression by 4-hydroxynonenal: atheroprotective role of the Nrf2/ARE transcription pathway *Redox Report* **12** 11–5
- [21] Ishikado A, Nishio Y, Morino K, Ugi S, Kondo H, Makino T, Kashiwagi A and Maegawa H 2010 Low concentration of 4-hydroxy hexenal increases heme oxygenase-1 expression through activation of Nrf2 and antioxidative activity in vascular endothelial cells *Biochemical and Biophysical Research Communications* **402** 99–104
- [22] Zhang H and Forman H J 2009 Signaling pathways involved in phase II gene induction by α , β -unsaturated aldehydes *Toxicol Ind Health* **25** 269–78
- [23] Chen Z-H, Saito Y, Yoshida Y, Sekine A, Noguchi N and Niki E 2005 4-Hydroxynonenal Induces Adaptive Response and Enhances PC12 Cell Tolerance Primarily through Induction of Thioredoxin Reductase 1 via Activation of Nrf2 * *Journal of Biological Chemistry* **280** 41921–7
- [24] Mochalski P, Wiesenhofer H, Allers M, Zimmermann S, Güntner A T, Pineau N J, Lederer W, Agapiou A, Mayhew C A and Ruzsanyi V 2018 Monitoring of selected skin- and breath-borne volatile organic compounds emitted from the human body using gas chromatography ion mobility spectrometry (GC-IMS) *Journal of Chromatography B* **1076** 29–34
- [25] Rankin-Turner S and McMeniman C 2022 A headspace collection chamber for whole body volatilomics
- [26] Niki E 2015 Lipid oxidation in the skin *Free Radical Research* **49** 827–34
- [27] Ron-Doitch S, Soroka Y, Frusic-Zlotkin M, Barasch D, Steinberg D and Kohen R 2021 Saturated and aromatic aldehydes originating from skin and cutaneous bacteria activate the Nrf2-keap1 pathway in human keratinocytes *Experimental Dermatology* **30** 1381–7

- [28] Low L A, Mummery C, Berridge B R, Austin C P and Tagle D A 2021 Organs-on-chips: into the next decade *Nat Rev Drug Discov* **20** 345–61
- [29] Leung C M, de Haan P, Ronaldson-Bouchard K, Kim G-A, Ko J, Rho H S, Chen Z, Habibovic P, Jeon N L, Takayama S, Shuler M L, Vunjak-Novakovic G, Frey O, Verpoorte E and Toh Y-C 2022 A guide to the organ-on-a-chip *Nat Rev Methods Primers* **2** 1–29
- [30] Feaugas T and Sauvonnnet N 2021 Organ-on-chip to investigate host-pathogens interactions *Cellular Microbiology* **23** e13336
- [31] Serasanambati M, Broza Y Y and Haick H 2019 Volatile Compounds Are Involved in Cellular Crosstalk and Upregulation *Advanced Biosystems* **3** 1900131
- [32] Barkal L J, Procknow C L, Álvarez-García Y R, Niu M, Jiménez-Torres J A, Brockman-Schneider R A, Gern J E, Denlinger L C, Theberge A B, Keller N P, Berthier E and Beebe D J 2017 Microbial volatile communication in human organotypic lung models *Nat Commun* **8** 1770
- [33] Chen S and Schoen J 2019 Air-liquid interface cell culture: From airway epithelium to the female reproductive tract *Reproduction in Domestic Animals* **54** 38–45
- [34] Mochalski P, King J, Unterkofler K, Hinterhuber H and Amann A 2014 Emission rates of selected volatile organic compounds from skin of healthy volunteers *Journal of Chromatography B* **959** 62–70
- [35] Ouahiba E, Chabani M, Assadi A A, Abdeltif A, Florence F and Souad B 2023 Mineralization and photodegradation of oxytetracycline by UV/H₂O₂/Fe²⁺ and UV/PS/Fe²⁺ process: quantification of radicals *Res Chem Intermed* **49** 1–21
- [36] Imhoff B R and Hansen J M 2010 Tert-butylhydroquinone induces mitochondrial oxidative stress causing Nrf2 activation *Cell Biol Toxicol* **26** 541–51
- [37] Li W and Kong A-N 2009 Molecular mechanisms of Nrf2-mediated antioxidant response *Molecular Carcinogenesis* **48** 91–104
- [38] Müller-Wirtz L M, Kiefer D, Ruffing S, Brausch T, Hüppe T, Sessler D I, Volk T, Fink T, Kreuer S and Maurer F 2021 Quantification of Volatile Aldehydes Deriving from In Vitro Lipid Peroxidation in the Breath of Ventilated Patients *Molecules* **26** 3089

**Chapter 5: The determination of skin surface pH via skin
volatile emission using colorimetric sensors**

Abstract

Biodiagnostic sensors in the form of wearables have become of widespread interest in both the scientific and clinical communities in recent years due to their potential for monitoring human health, well-being and physical performance. However, collecting biofluids from the skin to enable biochemical analysis using wearables has proved challenging to date. This research seeks to overcome the need for fluid collection by designing a wearable sensing platform capable of monitoring the volatile emission from skin with the aim of collecting biodiagnostic information from the body. We investigate the use of a simple wearable colorimetric sensing platform incorporating sensor spots comprising encapsulated bromocresol green pH indicator dye in an enclosed headspace above the skin. The sensor spots change from yellow to blue as a response to basic volatile nitrogen compounds such as ammonia and volatile amines being emitted from skin. By deploying this wearable in a healthy participant study, a strong correlation between sensor ED response and skin surface pH was demonstrated, despite a high inter-individual variability being noted. Sensor response was observed to be highly dependent on gender as well as body site, and attributed to factors such as gland and microbial composition differences. Finally, skin surface pH and wearable sensor responses were measured following various skin treatments and showed the wearable's ability to detect changes in skin surface pH in response to topical skin treatments. Overall, this work demonstrates a novel and simple approach to wearable biodiagnostics that exploits the skin volatile emission to monitor skin physiology without the need for microneedles or the requirement to harvest fluid from the skin.

5.1. Introduction

The skin is the largest organ of the human body with a high surface area of 1.5-2 m² [1], making it readily accessible as an organ to perform diagnostics on and as such, has been exploited as a matrix for a range of wearable sensing approaches to date [2]. The stratum corneum (SC) is the outer layer of the epidermis of the skin hosting a rich set of biomarkers and a high metabolic activity [3]. Quantifying levels of various biomarkers present in skin fluid matrices [4] such as interstitial fluid (ISF) [5] and sweat [6] can provide valuable insights into the health of an individual. Indeed, these opportunistic fluid matrices within skin have given rise to the fabrication and development of epidermal platforms [7] engineered to extract these biofluids from skin for detection of many biomarkers including the hydrogen ion [8], glucose [9][10], lactate [11][12], sodium [12][13], potassium [13], ammonia [14] and urea [15].

ISF, for example, is considered as an alternative to blood for accessing systemic biomarkers of disease. Small molecules such as lactate, glucose, cortisol and urea are present in ISF and measuring their concentrations and flow patterns can provide information on specific diseases [16]. There are many extraction methods used to extract ISF from skin including suction blister, iontophoresis, sonophoresis and microdialysis, none of which are immediately straight-forward [17]. Most recently microneedles (MNs) have been developed to extract and collect ISF from skin. Goud et al have recently developed a wearable microneedle device for the continuous sensing of levodopa in ISF which is a drug used to treat Parkinson's disease [18]. A microneedle electrode array which penetrates the skin and allows for dual-mode sensing involving both redox and biocatalytic processes. However, this approach is far from being clinically available as trials were only carried out on mice and human participant testing remains to be done. In addition to this, MNs have the drawback of damaging the skin by puncturing and thus can induce immunological responses that can give rise to localised skin irritation and even infection.

Sweat is a more accessible skin matrix that can be sampled non-invasively. In a similar manner to ISF, it can provide information about human health by analysis of the biomarkers it contains. The SWEATCH wearable platform is an exciting example of this and was developed to harvest and analyse sodium concentration in sweat in real-time [19]. This electrochemical approach is comprised of a pod-like design which incorporates an ion-selective electrode for sodium detection. It also integrates a fluidic system, driven by capillary forces, to collect sweat from the skin, directing its flow over the electrodes for detection. Recently, the SWEATCH platform has been further developed, facilitating the detection of sodium and

potassium ions simultaneously [20]. The detection of the hydrogen ion in sweat has also been targeted with wearable sensing devices. A recent demonstration of a single-use colorimetric wearable sensor integrating detection of several analytes including sweat pH was recently reported by the group of Rogers using a skin-interfaced microfluidic/electronic system [21]. This colorimetric approach uses pH-responsive universal indicator dye dip-coated on filter paper to determine sweat fluid pH. As with the SWEATCH, participants were asked to exercise to induce sweating. Produced sweat is then manipulated through hollow microfluidic channels, again by capillary force action, and routed to the pH sensor for detection. A smartphone was used to image the colour sensor after sampling, and images were compared to reference markers to determine sweat pH. Approaches to sweat diagnostics such as these, rely on microfluidic architecture to guide the sweat to the sensing interface for analysis which can lead to complexities. Furthermore as these approaches, along with many others [22] require the generation of sweat, they are thus suited more to sports applications than routine health diagnostics.

The analysis of volatile compounds emanating from the skin is emerging as an interesting source of information regarding subcutaneous and even systemic biochemistry [3]. These volatiles are derived from glandular secretions and their interactions with the microflora of the skin. Over 500 compounds have been reported to be emitted as volatiles from skin [23][24]. Skin volatiles are sampled non-invasively [25][26] without the need to puncture skin as often required for ISF collection for example. Compared to sweat, volatile emissions are a more accessible skin matrix as the volatiles are passively emitted and can be collected easily [27][28]. Our group has been studying the skin volatile emission for several years [3][29][30] using gas-chromatography mass-spectrometry (GC-MS) workflows and we have recently established evidence for a correlation between the emission rate of volatile fatty acids (VFAs) from skin and skin surface pH [31]. Skin surface pH is a parameter of interest as changes in skin surface pH can indicate dysregulation of the skin barrier function and alterations in skin surface pH can play a role in the pathogenesis of skin conditions such as atopic dermatitis [32][33]. Healthy human skin has an acidic surface pH of between 4.0 and 6.0 [1]. The acidic nature of the SC is important both for permeability barrier function and cutaneous antimicrobial defence. The acidic pH of the skin surface is established by several key mechanisms [34]: the breakdown of the filaggrin gene to produce trans-urocanic acid, the sodium proton exchanger - a transporter protein which transports H⁺ ions to the SC, and the hydrolyzation of free fatty acids (FFAs) from phospholipids by phospholipases.

Ammonia in the human body stems primarily from the bacterial breakdown of proteins within cells and the intestine. It is transported by blood to the liver where it is converted to urea and ultimately washed out in urine. Ammonia remaining in the blood can diffuse through the SC [35] or be emitted in eccrine sweat [15]. Total ammonia consists of two principal forms, the ammonium ion (NH_4^+) and un-ionised free ammonia (NH_3), with relative concentrations being pH- (and temperature-) dependent. Within the SC, ammonia production is probably not high enough to affect large pH changes in the skin. However, NH_4^+ is present in eccrine sweat gland secretions [15] and converts to gaseous NH_3 in a pH-dependent manner. Ammonia may also be produced microbially on the skin surface, for example from the action of microbial urease enzyme on urea substrate (present in sweat [36][37]). Volatile amines such as triethylamine and ethanolamine are also emitted from skin, and are likely again microbially-derived [38]. Longer chain amines in the skin volatile emission have also been reported but their origin is not yet elucidated [39][29]. Overall, it is ammonia that is thought to contribute most significantly as a basic volatile nitrogen compound to the skin emission and this has been studied by several groups [35][40][41]. However, interestingly, none of the studies published to date consider the implication of skin surface pH on the emission flux.

Colorimetric dyes as wearable sensors such as those measuring skin pH have up to now been typically limited to sweat analysis [42][43][44][45] and so require sweat-promoting stimulation as well as intricate microfluidics to guide sweat to the localised sensing chemistries for detection. This work proposes measuring of the skin surface pH via the volatile ammonia emission in a simple colorimetric sensor format. It is based on the principle that the $\text{NH}_4^+/\text{NH}_3$ equilibrium in skin is pH dependent. Thus, it could be expected that by monitoring the flux of gaseous ammonia from skin, it would provide a measure of skin surface pH. To this end, a simple sensor comprising spots of encapsulated pH-responsive dye, bromocresol green (BCG) was used in both indirect and direct methods for the colorimetric sensing of skin volatiles. The colour changes observed were consistent with dye deprotonation and are attributed principally to the pH-dependent skin volatile ammonia emission. Given the observed correlation of sensor response to the underlying skin surface pH, this offers an interesting sensing approach that has advantages over other methods measuring skin pH that require sweat fluid extraction and collection. It opens up the possibility of this volatile compound emission sensing approach as a way to detect other biomarkers that may have diagnostic value. This work deepens our understanding of the initial concept reported earlier [31], and investigates the wearable sensor,

employed for the direct colorimetric sensing of skin's, ability to accurately measure skin surface pH and the various factors that influence the measurement including gender, body site, measurement time and topical treatment of skin. The outcome of this work provides an understanding of some of the key factors and challenges impacting the sensor's response behaviour when worn on the body, while also highlighting the potential of monitoring other components of the volatile emission using selective encapsulated colour chemistries as a non-invasive and facile approach to skin diagnostics.

5.2 Materials and Methods

5.2.1. Preparation of colorimetric sol-gel

Colorimetric sol-gel solution was prepared according to previously published protocol [46]. Briefly, sol-gel was prepared by mixing 126 μL triethoxy(octyl)silane, 40 μL methyltriethoxysilane, 304 μL hydrochloric acid (0.1 M), 384 μL 2-methoxyethanol and 272 μL propylene glycol monomethyl ether acetate in a reaction vessel and stirring overnight. 4 mg bromocresol green (BCG) was then dissolved in the sol-gel (1 mL).

5.2.2. Solution-based pH study

20 μL of the BCG sol-gel solution was added to vials containing bulk solutions (2800 μL) of varying pHs (3.2-7.0) prepared using 0.01 M HCl and 0.01 M NaOH stock solutions. A calibrated HI-1131B pH electrode (Hanna Instruments) was used to determine the pH of each vial solution. A reference solution (pH 2.50), containing 20 μL BCG sol-gel diluted in 2800 μL 2-methoxyethanol, was also prepared. Imaging of the vials was done using an iPhone 11 Pro Max and images processed as described below. $n=3$ replicates were carried out for each pH solution.

5.2.3. Preparation of colorimetric sensor spots

0.5 μL of the BCG sol-gel solution was drop-cast as a single spot onto an unmodified cellulose thin layer chromatography (TLC) plate or a 10 % acetate cellulose TLC plate (Macherey-Nagel, Fischer Scientific, Ireland) (3 x 2 cm) and allowed to dry in a vacuum desiccator before use. 6 spots, approx. 1 cm apart, were drop-cast onto each cellulose substrate to form a 3 x 2 colorimetric sensor array of replicate spots.

5.2.4. Indirect colorimetric sensing of skin volatiles

One healthy female volunteer (aged 23) was recruited for this aspect of the study (See Consort Diagram, Scheme 1). No special dietary regimes were applied, however, the participant was asked not to apply perfumes or cosmetics on the day of sample volatile collection. Participant was informed on the aim and purpose of the study, and asked to provide written informed consent. The local ethics committee (Dublin City University Research Ethics Committee) approved the study on skin volatiles (Reference: DCUREC/2016/053) prior to commencement of the work, and the study was performed according to the Declaration of Helsinki.

Sensors comprised of BCG colorimetric solution drop-cast onto cellulose TLC plates were used for this study. An image of the replicate BCG sensor spots, before exposure to skin volatiles, was taken using an Epson XP-322 flatbed scanner. Prior to sampling, the gauze was sterilised using HPLC grade methanol and was baked at 100°C for 1 h to remove any contaminants [47]. The participant was then asked to hold a piece of sterile gauze (5 x 5 cm-8 ply, Propax, Amazon UK), between their palms for 15 min to collect volatiles emanating from skin. Following the collection of the volatiles from the skin using the gauze, the gauze was then placed in a headspace vial (22 ml, Sigma-Aldrich, Ireland) with the colorimetric sensor adhered to the inside of the vial using Blu-Tack. The lid was placed on the headspace vial and the sample was left overnight to equilibrate at 37°C. After 12 h the sensor was removed from the glass vial and the sensor spots were imaged again using the scanner (Fig 5.1 (a)). Multiple samples were collected over multiple days (see Consort Diagram, Scheme 5.1). Skin surface pH of each palm was taken before application of the wearable platform using a wireless HALO flat glass probe (HI14142) (Hanna Instruments) and Hanna Lab App (v3.0) for iPhone.

5.2.4.1 Control for indirect study

A piece of gauze that had not been exposed to volatile skin emission was placed in the vial, along with the colorimetric sensor which was adhered to the inside of the vial using Blu-Tack. The vial was again left to equilibrate overnight at 37°C. Imaging was carried out as outlined above (Figure A5.1(a)).

5.2.5. Colorimetric sensor response to ammonia

The colorimetric sensor was prepared (comprising 6 replicate BCG spots drop-cast on 10% acetate TLC plates as described above), scanned and the RGB values of the individual spots quantified using ImageJ. In order to measure the response of the sensor spots to ammonia, the sensor was adhered to the lid of a plastic petri dish (0.04 L) using Blu-Tack. A piece of filter paper (Whatman, diameter: 4.70 cm) was placed in the bottom of the petri dish and a precise volume of neat ammonia solution (0.1-10 μL) was dropped directly onto the filter paper. The lid was placed on top of the petri dish and sealed with parafilm. After 3 h, the sensor was removed from the petri dish and scanned. Processing of the sensor image before and after exposure to ammonia was carried out using ImageJ as described below.

5.2.6. Direct colorimetric sensing of skin volatiles - preparation of wearable platform

The wearable platform comprised a stainless steel woven wire mesh (Inoxia Ltd, UK) to define the headspace (4 x 3 cm), on top of which was the cellulose substrate comprising of 6 replicate BCG sensor spots. Sensors comprised of BCG colorimetric solution drop-cast onto 10% acetate TLC plates were used for this study. The sensor spots were covered with a polyethylene terephthalate (PET) film (5 x 4 cm) and the complete platform was enclosed (Fig 5.1(a)) and secured to a body site using Leukosilk surgical tape (BSN Medical GmbH, Hamburg, Germany).

5.2.7. Direct colorimetric sensing of skin volatiles (using a wearable sensor)

Ten healthy volunteers (5 female and 5 male; aged 20-45) were recruited onto this wearable sensor study (see Consort Diagram, Scheme 5.1). Again, no special dietary regimes were applied, however, the participant was asked not to apply perfumes or cosmetics on the day of sample volatile collection. Participants were informed on the aim and purpose of the study, and asked to provide written informed consent. Again, the local ethics committee (Dublin City University Research Ethics Committee) approved the study on skin volatiles (Reference: DCUREC/2016/053).

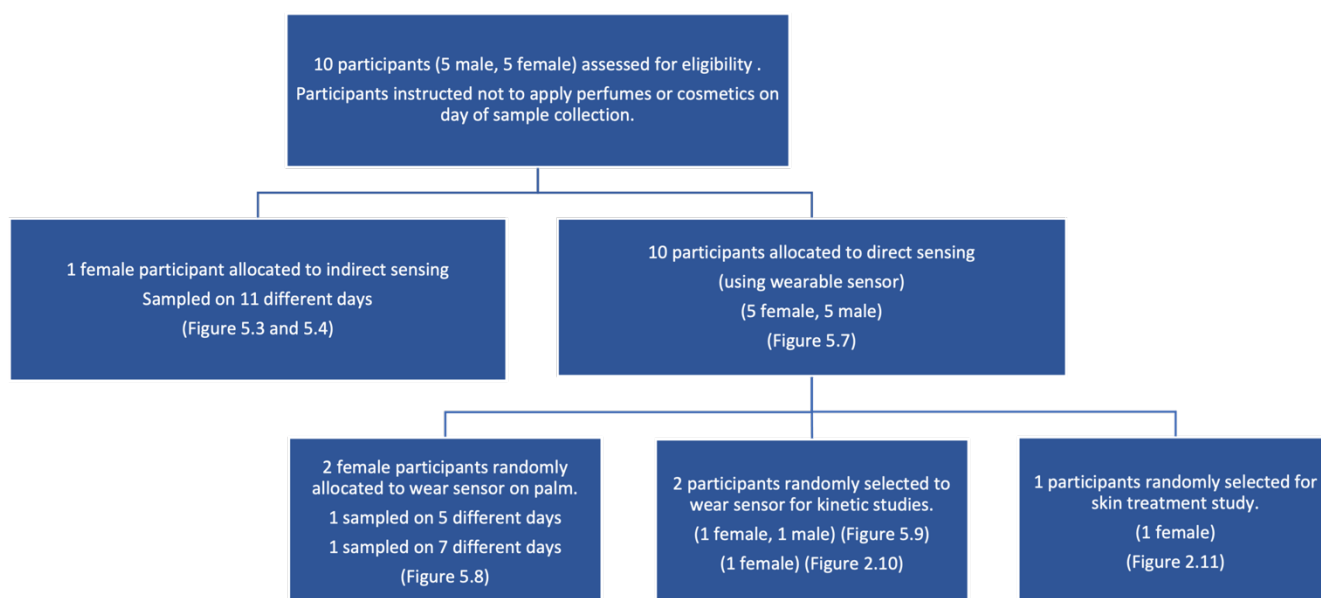
Prior to application of the wearable platform to participant's skin, in a similar manner to the indirect study, an image of the replicate BCG sensor spots was taken using an Epson XP-322 flatbed scanner. Participants were then asked to apply the wearable platform to a specific skin site (palm of hand, sole of foot, forehead or stomach) for up to 300 min while they went about their daily activities. After a fixed time, the wearable was removed from the skin and the

sensor spots imaged again using the scanner. Where specified, the wearable was removed from the skin periodically (i.e., every 15 min) and the sensor spots imaged using the scanner before being replaced on the skin.

Again, skin surface pH of each site was taken before application of the wearable platform using a wireless HALO flat glass probe (HI14142) (Hanna Instruments) and Hanna Lab App (v3.0) for iPhone.

5.2.7.1. Control for wearable colorimetric sensor study

A PET film was placed between the palm of the hand and the wearable in order to exclude skin volatile emission from the HS of the wearable and was worn for 5 h (Figure A5.1(b)). Imaging was carried out as outlined above.



Scheme 5.1. Consort Diagram showing the flowchart for the different aspects of the participant studies.

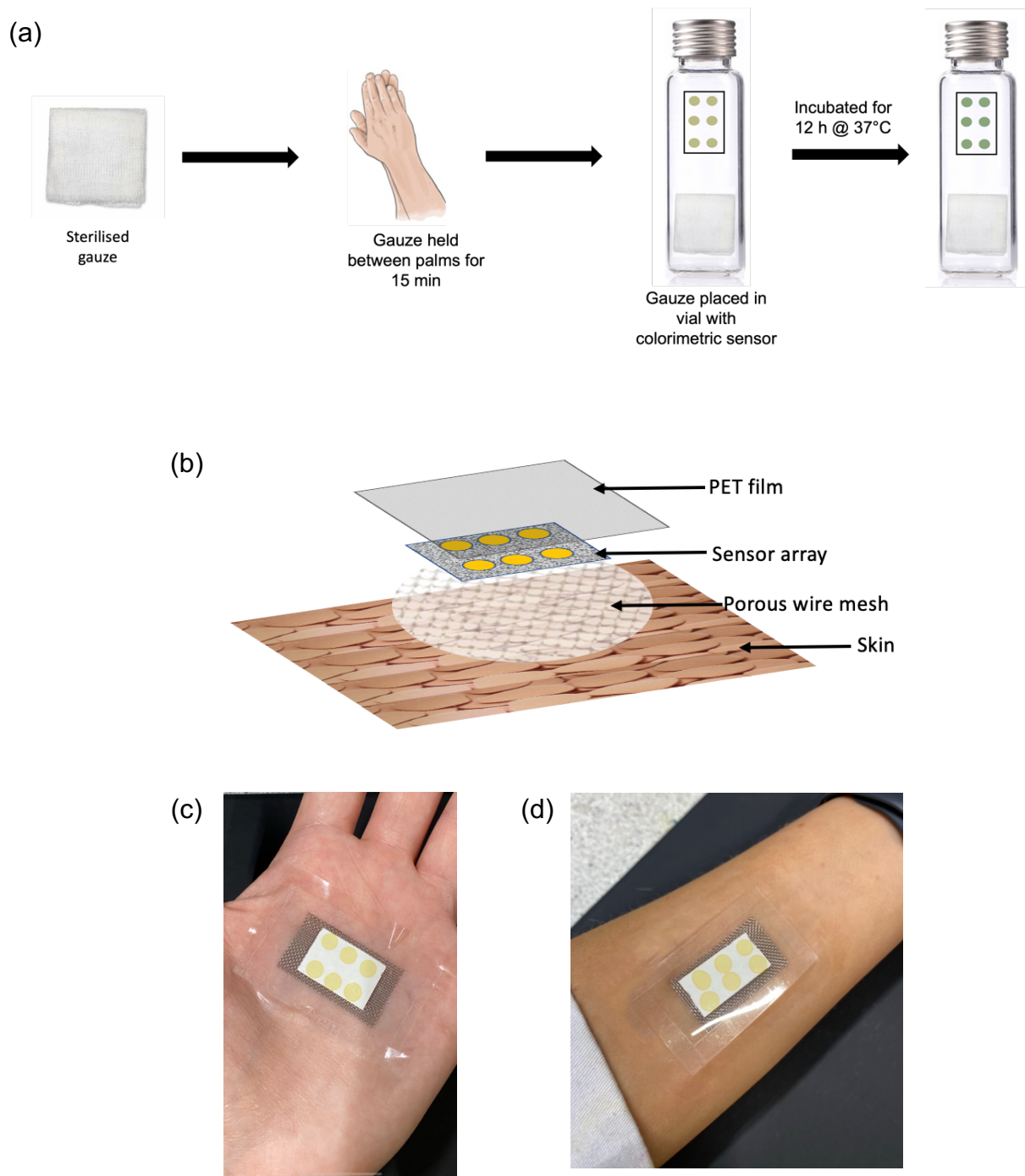


Figure 5.1. (a) Schematic showing the procedure for indirect colorimetric sensing of skin volatiles, (b) schematic of the different layers comprising the wearable platform applied to the skin surface for the direct colorimetric sensing of skin volatiles [31]; (b) image of wearable platform worn on palm and (c) on the forearm.

5.2.8. Skin treatment study

Four different skin treatments were carried out on the palm to investigate their impact on sensor colour response. The treatments were (a) washing the skin with soap (Dove Beauty Cream Bar), (b) applying a 2% salicylic acid (SA) solution (The Ordinary©), (b) wiping the skin with an isopropyl alcohol (IPA) (Qualicare Products) wipe and (d) tape-stripping of the SC using Leukosilk surgical tape (1.25 cm wide) where the skin was tape stripped 10 times as a single treatment. Following each treatment, the wearable sensor was applied for 120 min and imaged in the usual manner before and after wearing. Skin surface pH was also taken at the site before the wearable was applied.

5.2.9. Image analysis

Images were analysed using ImageJ to measure absolute red (R), green (G) and blue (B) colour values for the sensor spots before (R_1, G_1, B_1) and after exposure (R_2, G_2, B_2) to skin. RGB absolute values were used to quantify response of the sensor spots. Sensor spot response was also quantified using a distance measurement called Euclidean distance (ED). The ED formula is given by:

$$ED = \sqrt{(R_2 - R_1)^2 + (G_2 - G_1)^2 + (B_2 - B_1)^2} \quad \text{Equation 5.1}$$

5.2.10. Data analysis

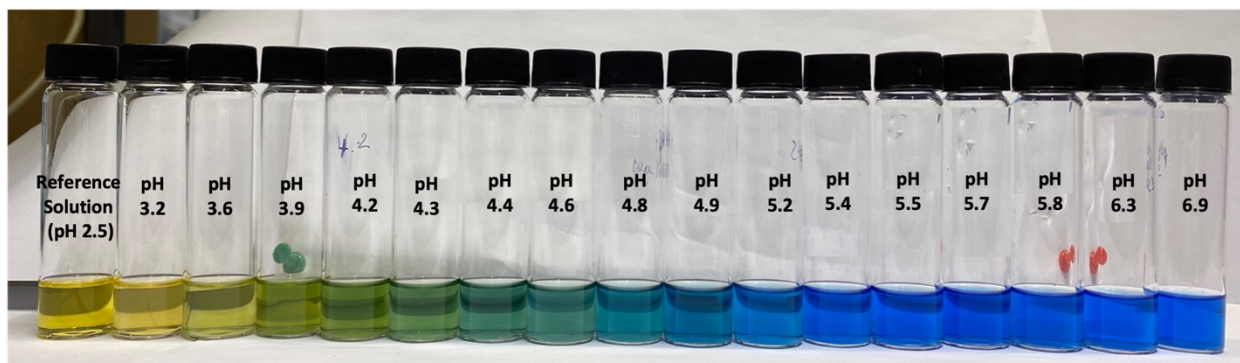
1-D linear regression analysis was used to investigate the association between sensor spot ED response and skin surface pH. The correlation coefficient, R, was used to quantify association between sensor response and skin surface pH as it is suited to participant studies where variables including age, ethnicity, etc are not controlled [48].

5.3. Results and discussion

5.3.1. Solution-based response of BCG sol-gel solution

Prior to any skin-based studies, work was carried out to investigate the response behaviour of the dye, BCG ($pK_a=4.7$). A study of the colorimetric response of prepared BCG sol-gel solutions was carried out in order to verify the dyes response to changes in pH over the relevant range (Fig 5.2 (a)). ED values obtained from the image processing step were plotted against solution pH to show dye sensitivity between pH 4 and 6 (Fig 5.2 (b)), which is within the typical pH range of the skin surface, thus making it a suitable dye for this application.

(a)



(b)

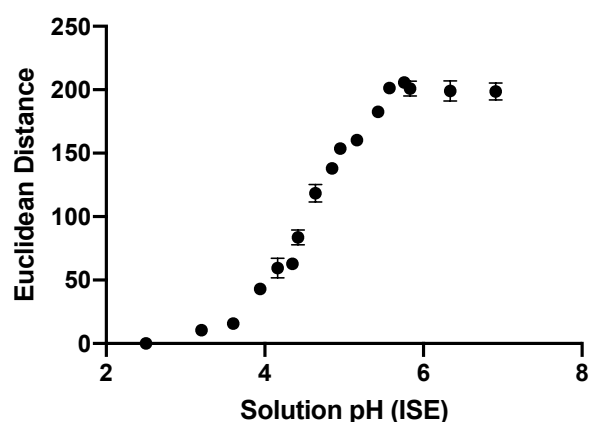


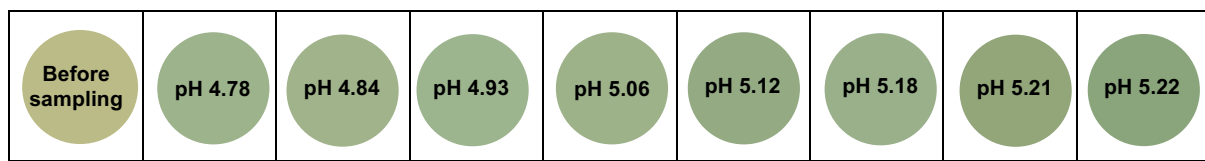
Figure 5.2. (a) Image of BCG sol-gel solutions across the pH range 2.5-6.9 and (b) Euclidean distance plotted against bulk solution pH measured using a calibrated ISE. Error bars represent $n=3$ replicates of each pH solution.

5.3.2. Indirect sensing of skin volatiles

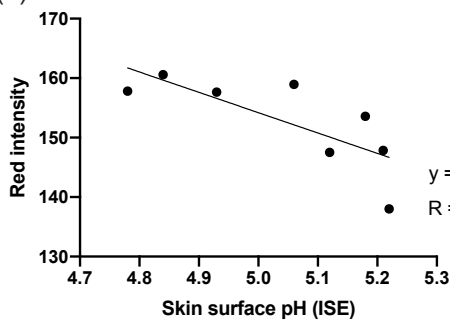
Initially, in order to assess how the BCG sensor spots responded to the volatile skin emission, a preliminary study using an indirect method of sampling was employed as outlined in the Materials and Methods section. Here, a piece of sterile gauze was held between the palm of the hands for 15 min in order to collect the volatiles emitted from skin. The gauze is then placed in a glass headspace vial with a colorimetric sensor adhered to the inside using Blu-Tack. Figure 5.3 (a) shows the reproduced colour of BCG sensor spots after exposure to skin volatiles collected using gauze. It can be seen that the colour intensity increases slightly as skin surface pH increases. However, the skin surface pH range investigated here is narrow at 0.44 pH units, which may account for the small colour change. For this data processing, the sensor spot response was quantified via absolute RGB values and also via a relative change using ED

(Equation 5.1). Correlation analysis was performed as outlined in section 5.2.10. Negative correlations were observed for RGB intensities (Fig 5.3 b-e) whereby the red, green and blue intensities showed strong correlation with skin surface pH. The red intensity showed the highest sensitivity (slope = -34.19). ED was also quantified and positive correlation shown ($R=0.711$). Overall, this data suggests that skin surface pH can be related linearly to the colour response of the sensor spots. ED quantification takes into account the absolute RGB intensities and thus, on this basis, ED was chosen to quantify sensor spot response for all further data processing.

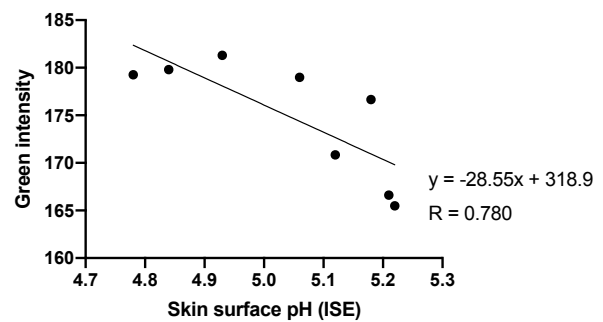
(a)



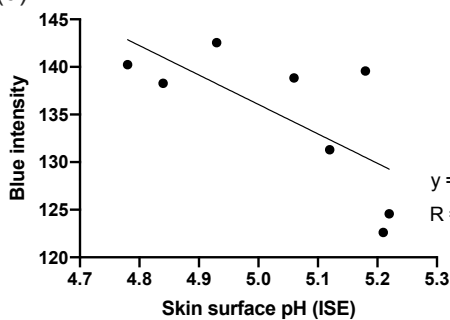
(b)



(c)



(d)



(e)

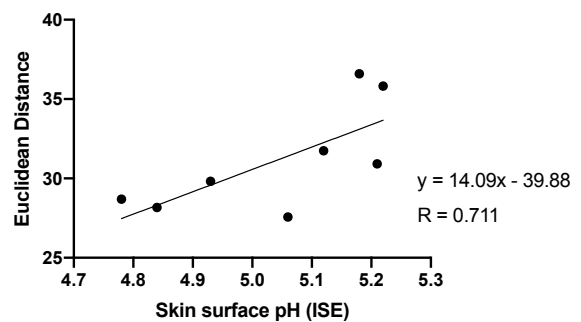


Figure 5.3. (a) Reproduced colour response from colorimetric sensor after exposure to gauze used to capture skin volatile emission for one female participant; the corresponding skin surface pHs as measured by a calibrated ISE (bold text), (b) red intensity, (c) green intensity, (d) blue intensity and (e) ED from (a) plotted as a function of skin surface pH.

As mentioned above the skin surface pH range investigated was limited between pH 4.78-5.22. In order to extend this skin surface pH range and also to understand the effects of topical treatment on both the skin surface pH and volatile emission, the palm of the participant was treated with a non-volatile salicylic acid solution prior to sampling. The application of the salicylic acid decreased both the skin surface pH which was correlated with a low ED sensor response, thus indicating that the salicylic acid treatment altered the skin volatile emission.

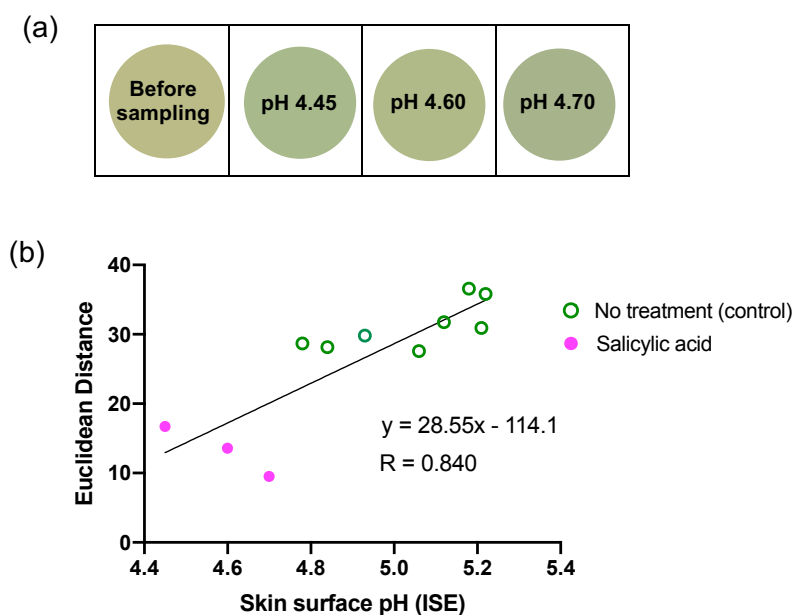


Figure 5.4. (a) Reproduced colour response from colorimetric sensor after exposure to gauze used to capture skin volatile emission following application of salicylic acid for one female participant; the corresponding skin surface pHs as measured by a calibrated ISE (bold text), (b) ED values from Fig 5.3 (a) and Fig 5.4 (a) plotted as a function of skin surface pH.

5.3.3. Effect of substrate on BCG sol-gel solution

From the indirect study, it was observed that the colour response to change in skin surface pH was low when the BCG colorimetric solution was drop-cast on unmodified cellulose TLC plates. This may be dependent on the surface pH of the substrate the BCG colorimetric solution was drop-cast on. The surface pH of the unmodified cellulose TLC plate affected the colour of the BCG sol-gel solution (Figure 5.5). Comparing this colour to the colour observed in the solution-based pH study (Figure 5.2), it was hypothesised that the surface pH of the unmodified cellulose TLC plate is approx. 4.2, which is supported by literature [49]. This surface pH is close to the pKa of the dye BCG (4.7) and also to normal skin surface pH thus no significant colour change upon interaction with skin volatile emission was observed.

Therefore, the use of other substrates including 10% acetate cellulose TLC plates, were explored. Acetylated TLC plates are prepared by the esterification of cellulose using acetic acid, thus making its overall surface pH lower. Again, comparing the colour of the BCG solution drop-cast on the 10% acetate TLC plate to the solution-based pH study, it was speculated that the surface pH of the modified TLC plate was approx. pH 3. The modification of the sensor in such a way allows skin surface pH values as low as 3.1 to be detected.

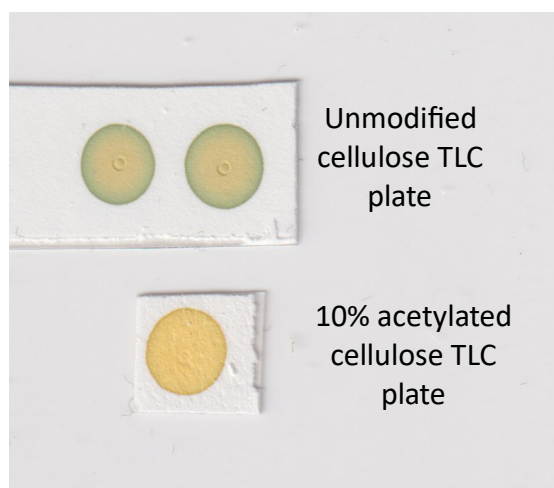


Figure 5.5. Scanned image showing BCG colorimetric sol-gel solution drop-cast on both unmodified cellulose TLC plate and 10% acetylated cellulose TLC plate.

5.3.4. Colorimetric response to volatile fatty acids and ammonia

In order to understand the sensor spots (drop-cast on 10% acetylated TLC plates) response to acidic and basic volatile species, the sensor was exposed to a headspace of a volatile fatty acid (VFA) mix in hexane (containing 4 VFAs (1000 ppm each) known to be present in the skin volatile emission: hexanoic acid, octanoic acid, decanoic acid and dodecanoic acid) and also a headspace of concentrated ammonia. 100 μ l of each solution (VFA mix or ammonia) was dropped onto filter paper which was placed inside a petri dish and the response monitored as outlined in the Materials and Methods section (Fig 5.6 (a)). Following this, a quantitative ammonia calibration plot was generated based on sensor ED response whereby correlation with ED response was observed up to a mass of approx. 2.5 mg ammonia (Fig 5.6 (b)). Beyond this, the sensor spots became saturated and no further increase in ED observed. In order to quantify the limit of detection (LOD) of the sensor spots, a narrower mass range of ammonia was used (0.0665 - 0.6650 mg; (Fig 5.6 (c)) and linear regression applied to the data to give a linear regression line of $y=74.1x+12.71$; $R=0.960$. Based on this regression, the LOD for the sensor was calculated to be 0.092 mg ammonia.

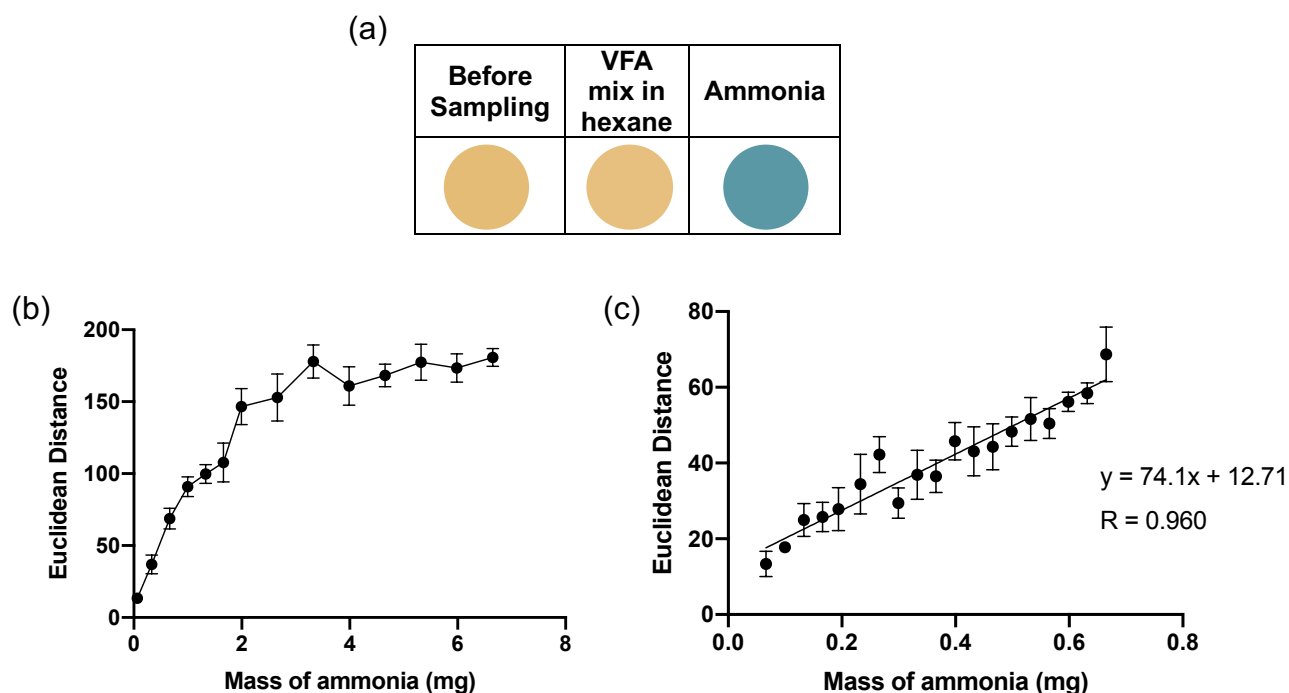


Figure 5.6. (a) Reproduced average colour from sensor (6 replicate BCG sensor spots) after exposure to the HSs of VFA mix and ammonia for 180 min, (b) graph showing average ED response as a function of mass of ammonia (mg) added to the HS that the sensor was exposed to and (c) Average ED as a function of a narrow mass range of ammonia (mg). Error bars in (b) and (c) represent standard deviation of $n=6$ replicate BCG sensor spots within a single platform. (Note: sensors comprised of BCG solution drop-cast on 10% acetate TLC plates were used for these calibration experiments.)

5.3.5. Direct sensing of skin volatiles using a wearable sensor platform

Following these calibration experiments, the BCG sensor spot substrate was integrated within a wearable platform (Figure 5.1), and applied to the palm of healthy participants skin for 5 h and the colour response monitored. Figure 5.7 (a) shows the average colour of the BCG sensor spots (based on 6 replicate spots from one wearable measurement) after wearing on skin by 5 female and 5 male participants with different skin surface pHs. For both genders, it can be seen that the ED response increases with increasing skin surface pH and despite likely inter-person variability, good correlation is seen. The correlated sensor response with respect to pH can be explained by the dependency of ammonia emission flux from the skin on skin surface pH.

Using the standard calibration plot (Fig 5.6 (c)) for ammonia, the ammonia flux ($\text{mg h}^{-1} \text{cm}^{-2}$) for each participant was estimated and the computed values corresponding to the measured pHs are given in Figure 5.7 (a). The emission fluxes calculated in this study are higher than previously reported skin ammonia fluxes [40][35][41]. For example, our work reports an average ammonia emission flux for female palm of $0.0198 \text{ mg h}^{-1} \text{cm}^{-2} (\pm 0.0113)$ (based on the average values measured in Fig 5.7) whereas Furukawa et al report an average ammonia flux of $0.0006 \text{ mg h}^{-1} \text{cm}^{-2}$ for the same site collected using a passive flux sampler with ion chromatographic analysis. A significant disparity arises here but our greater flux estimations may be due to the detection of some volatile amines as well as ammonia from skin. In addition, given the occlusion of the skin for our measurements, there is likely some sweat/water vapour being eliminated from the skin containing ammonia and interacting with the sensor spots that could also account for the higher than expected ammonia fluxes measured. No previous study to our knowledge relating to ammonia measurements from skin consider skin surface pH and yet our results show that the ammonia flux can vary by an order of magnitude over the healthy skin surface pH range.

As noted earlier, a strong gender effect on sensor response can be observed in Figure 5.7 where males and females with approximately matched skin surface pH values show different colour responses after exposure to the palm for equivalent times. Males elicited an increased colour response for comparable skin surface pHs compared to females. Although males and females are known to have equivalent numbers of eccrine glands on the palm, the size and volume of sweat produced by these glands is approx. 5 times greater in males compared to females [50]. This increased response in males may be due to higher fluxes of ammonia being emitted from the male eccrine sweat gland on account of the larger gland volumes, as well as potential microbial differences.

(a)

Female		pH 4.33 (0.0096)	pH 4.73 (0.0145)	pH 4.83 (0.0152)	pH 4.97 (0.0199)	pH 5.01 (0.0385)
Male		pH 4.32 (0.0181)	pH 4.48 (0.0256)	pH 4.57 (0.0471)	pH 4.72 (0.0584)	pH 5.21 (0.0562)

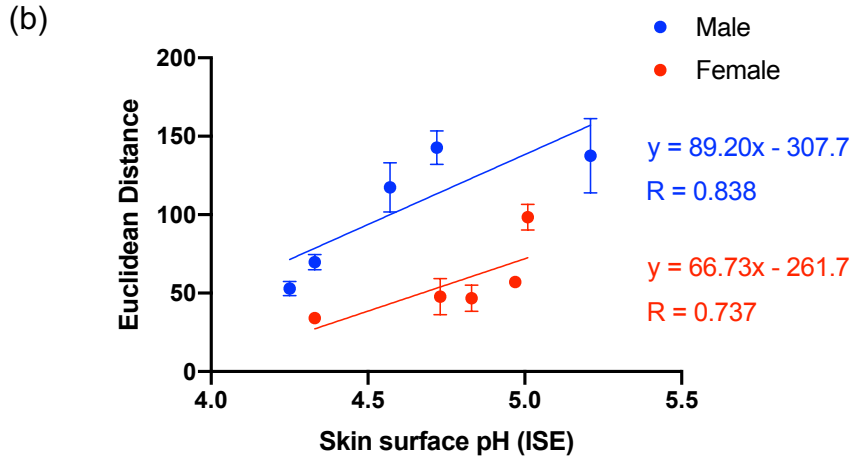


Figure 5.7. (a) Reproduced average ED colour response from wearable platform (6 replicate BCG sensor spots) after being worn on 5 females and 5 males (left palm, 5 h); the corresponding skin surface pHs as measured by a calibrated ISE (**bold text**) and estimated ammonia flux in $\text{mg h}^{-1} \text{cm}^{-2}$ (*italicised text in parenthesis*) also given. (b) ED value from (a) plotted as a function of skin surface pH. Error bars represent standard deviation in ED response from $n=6$ sensor spots within a single wearable platform. Note: Table A5.1 in Appendix for tabulated data.

In order to investigate the significance of the inter-person variability on sensor response, single participant data was collected on multiple days. For this, 2 participants were randomly selected to wear the sensor as before for fixed periods of time (5 h) on multiple days as outlined in the Consort Diagram (Scheme 5.1). Figure 5.8 demonstrates that the ED correlates with pH as expected and that there is significantly increased correlation between ED response and skin surface pH for a single participant compared to Figure 5.7 where data from multiple participants was plotted against skin surface pH. This confirms the relationship between sensor ED response and skin surface pH and highlights the inter-person variability as a challenge when designing such sensors. This inter-person variability observed complicates calibration of the sensor and means that sensor calibration would be required for each individual participant given the differences observed in response.

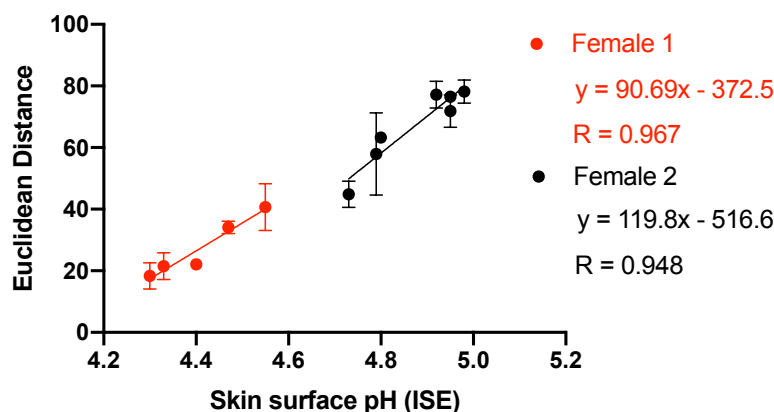


Figure 5.8. Average ED response from wearable platform (6 replicate BCG sensor spots) after being worn on Female 1 and Female 2 for 5 h (left palm used for sampling) (one sensor worn per day) plotted against skin surface pH (measured using a calibrated ISE). Error bars represent standard deviation in ED response from n=6 sensor spots within a single wearable platform. Note: See Table A5.2 and A5.3 in Appendix for tabulated data.

In order to investigate the kinetic response of the sensor spots, imaging of the sensor was done periodically during the measurement by removing the wearable from the skin every 15 min, imaging the sensor spots, and replacing on the skin immediately after. Corresponding skin surface pH measurements were also taken at these time points, while the wearable was off the skin. Kinetic data at four skin sites - palm, foot, abdomen and forehead – was collected. Skin surface pH data showed that pH did not fluctuate during the measurement period (Fig 5.9 a-d) indicating the emission flux of ammonia from the skin remained constant over the period investigated. In general, ED response was observed to increase over time, across all body sites. For all sites, the general trend was that ED continued to increase over time. However, the rate of change of ED differs across the sites, a consistent effect for both males and females. The response differences across the different sites is attributed to differences in skin surface pH but also the microflora and gland type and density present at a particular site. The palm elicited the highest ED response of the sites investigated. The foot resulted in significantly lower responses. However, both the palm and foot are known to have similar eccrine gland densities [51][52] and the measured skin surface pHs for both sites were similar (average measured pH over 300 min: female palm 4.81 ± 0.069 ; female foot 4.60 ± 0.063), indicating that the ED response for both sites would be expected to be similar. Thus, it is unclear as to why the ED response is lower for the foot compared to the palm and additional studies would be required to further understand this response difference. It may be related to different microbial environments on

account of the different exposures to ambient of the site. Interestingly the abdomen had significantly lower ED responses compared to the palm and foot sites despite having a comparable skin surface pH. The stomach has a much lower density of eccrine glands (~2-5 fold lower than that of the palm and foot) [51] likely resulting in lower amounts of ammonia being produced, resulting in a corresponding lower overall flux of ammonia, despite an inherent high skin surface pH, likely dictated by the SC acidity regulation mechanisms outlined earlier. The microflora on the skin surface may also influence the ED response. The forehead elicited the lowest ED sensor spot responses, indicating the lowest ammonia emission. This site contains the highest density of sebaceous glands and secretions as well as hair follicles (also on the stomach site) [53] which produce significant proportions of FFAs [54] heavily influencing the low skin surface pH (average measured pH over 300 min: female 4.50 ± 0.045 ; male 4.60 ± 0.054) observed at this site. Very low ED responses were observed likely on account of this low pH. It is important to note that, despite the different response behaviours across different sites, the correlation of sensor ED response with skin surface pH, (as seen in Figures 5.7 & 5.8 for the palm), is expected to be valid at each site, but sensitivity of response is highly site-dependent.

Finally, the gender effect observed in Figure 5.7 is also apparent in Figure 5.9. Skin surface pH measurements were consistently lower for males at the palm, foot and abdomen. Despite this lower pH, male sensor spot responses were greater than from females, consistent with what has already been observed. The gender effect was not observed at the forehead as both genders exhibited similar skin surface pH measurements for this site as outlined above.

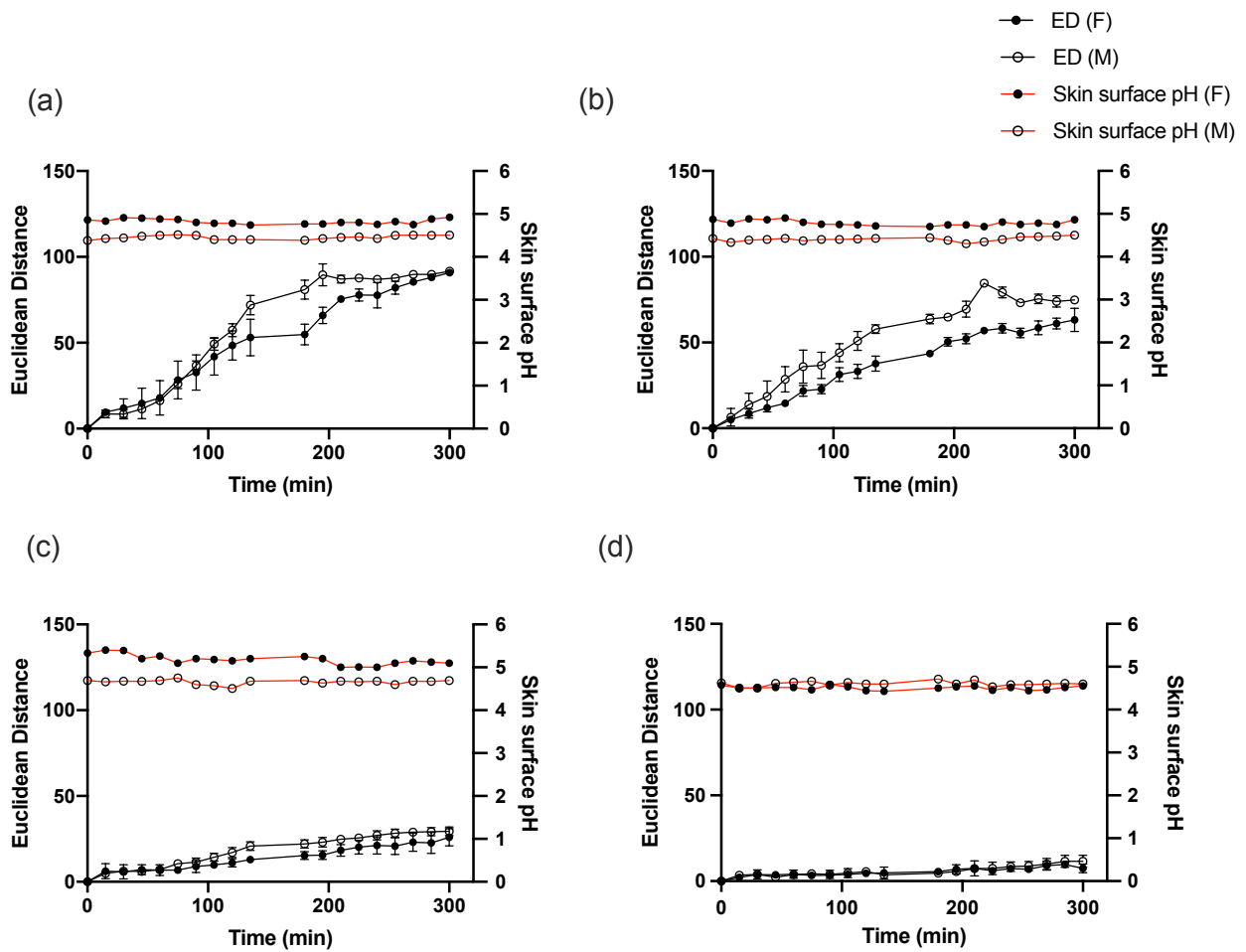


Figure 5.9. Average ED colour response from wearable platform (6 replicate BCG sensor spots) over time on one female and one male participant and corresponding skin surface pH values for (a) palm, (b) foot, (c) abdomen and (d) forehead. Error bars represent standard deviation in ED response from $n=6$ sensor spots within a single wearable platform. Note: See Table A5.4-11 in Appendix for tabulated data.

In order to investigate sensor spot response over time for periods of continuous wear, the wearable platform was worn continuously on the palm for different fixed periods of time up to 270 min (in contrast to the 15 min intervals used in the previous study) and the sensor spots scanned in the usual manner (Figure 5.10). This data confirms that the occlusion of the skin is not affecting the pH measurement or the sensor spot response and that the ammonia and volatile amine flux remains constant throughout the sampling period and an accumulative response, which is approximately linear, is observed.

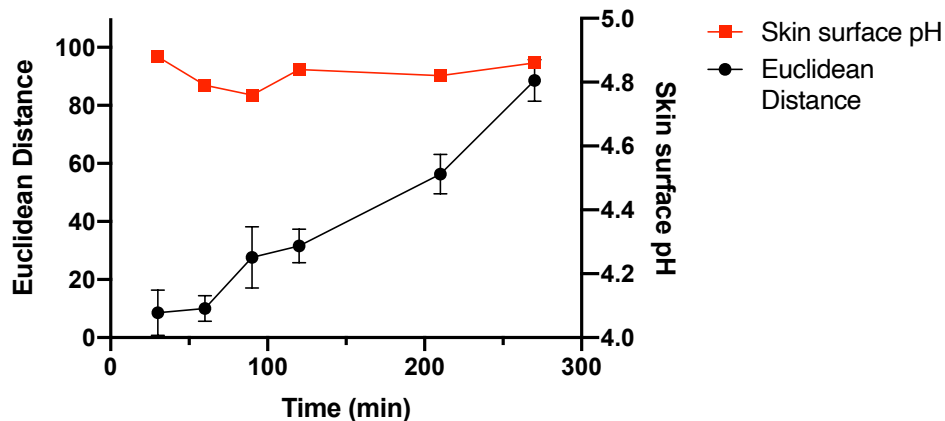


Figure 5.10. Average ED colour response from wearable platform (6 replicate BCG sensor spots) worn for different periods of time by a single participant, (female; left palm; average skin surface pH=4.82±0.05). Error bars represent standard deviation in ED response from n=6 sensor spots within a single wearable platform.







To investigate the time dependence on the sensor spot ED response further, a greater number of sensors were worn by a single participant over multiple days (a maximum of one sensor measurement taken per day) (one sensor worn per day for n=7 days) for different wear times to better understand both the sensitivity and correlation of sensor response with respect to skin surface pH values measured (Table 5.1). Sensor ED data (n=7) for each sampling time was plotted against pH and 1D linear regression applied (Figure A5.2 in Appendix) to quantify the slope and R. The results show that the ED response increased with wear time as expected and also that both sensitivity and correlation are low for short sampling times (< 60 min) but this increases with time. For example, the slope was observed to increase 4-fold from 90 min on compared to at 30 min. Correlation was also observed to improve with extended sampling times. These results show that the minimum wear time for these sensors in their current form is 90-120 min to obtain reliable pH data. Work is ongoing to reduce this wear time and/or enhance wearability of the sensor before this simple approach to wearable biodiagnostics becomes viable.

Table 5.1. 1-D linear regression parameters for regression lines fitted to ED colour response as a function of skin surface pH for wearable platforms (6 replicate BCG sensor spots) worn by a single participant collected for continuous sampling times between 30-270 min. Note: see Fig A5.2 in Appendix for ED data and 1-D linear regression analysis of data.

Time (min)	Skin surface pH range	No. of measurements	Average ED response	Slope (ED/pH unit)	y-intercept	R
30	4.78 - 5.09	7	8.72	20.63	-92.88	0.526
60	4.61 – 5.18	7	17.90	20.82	-85.00	0.689
90	4.67 – 4.85	7	29.57	84.14	-371.20	0.609
120	4.84 – 5.13	7	46.07	86.32	-381.70	0.814
210	4.67 – 5.31	7	83.01	93.75	-369.00	0.767
270	4.78 – 5.29	7	95.58	93.53	-375.00	0.849

In order to investigate how the sensor spots respond to externally applied skin treatments that can temporarily modulate skin pH, various treatments to the skin were investigated for their impact on both skin pH and sensor spot response. Soap, salicylic acid and IPA were all applied as topical treatments and tape-stripping (TS) of the skin to perturb the skin barrier was also carried out according to Methods. Skin surface pH was taken before and after all treatments. Figure 5.11 shows the colour changes of the sensor spots after each treatment and the ED response plotted as a function of skin surface pH following treatment. Following all treatments, it can be seen that the sensor underwent a colour change that correlated with change in skin surface pH. For example, the application of salicylic acid resulted in the lowest skin surface pH measurement which correlated with a low ED sensor response. In contrast, soap elevated the skin surface pH, again correlating with a high ED response. There is high variability noted in the ED response for the soap data in particular despite the study being carried out on a single participant. This may be due to the procedure for washing of the skin with soap where, e.g., the ratio of water:soap used for each treatment was not controlled and may have contributed variability to the sensor response. IPA application and tape-stripping both lowered the skin surface pH by small amounts relative to the control, resulting in a correlated small reduction in ED response. These experiments demonstrate that skin surface pH and the corresponding volatile profile is altered temporarily by these treatments and that these alterations can be tracked using our wearable colorimetric sensor spot platform.

(a)

Before Sampling	Salicylic acid	IPA	TS	No Treatment (control)	Soap
					

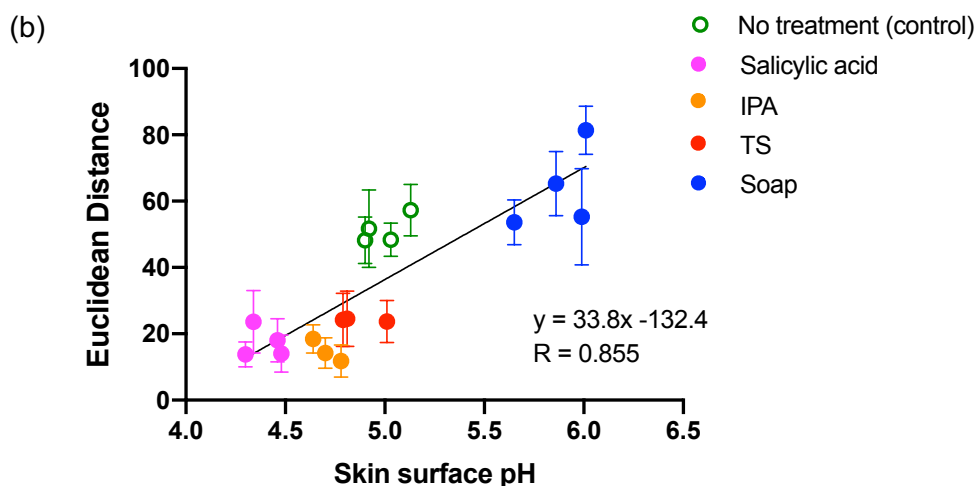


Figure 5.11. (a) Reproduced colour (average of 6 replicate BCG sensor spots) following 120 min sampling time on palm of a single female participant for untreated skin and following various treatments, and (b) average ED colour response from wearable platform as a function of skin surface pH. Error bars represent standard deviation in ED response from n=6 sensor spots within a single wearable platform.

5.4. Conclusion

The application of pH-responsive sensor spots for the measurement of skin surface pH via the volatile ammonia emission from skin in a healthy participant study was reported. Overall, this work demonstrates the potential use of the volatile emission from skin including the capabilities, the exciting opportunities as well as the challenges for such a sensing approach in wearable biodiagnostics. Our direct method for sensing skin volatile ammonia using a wearable sensor platform was investigated for healthy participant skin surface pH measurements, and gender and body site differences were attributed to gland type and distribution densities as well as potential microbial influences. Our findings demonstrate that such wearable colorimetric sensor platforms can be used to selectively monitor target components of the skin volatile emission and offers an alternative to skin fluid harvesting and analysis. This work also highlights challenges associated with the approach such as significant inter-person variability in the sensor ED response. Also, the impacts of skin occlusion need to be considered as it can trigger a sweat response from the skin. Ideally, sensors for these measurements require short response times or have a form factor that does not occlude the skin. Furthermore, an in-situ or even wearable imaging approach will further enhance these colour sensors deployability and potential use which is currently being developed in our group.

Despite these challenges, the development of this new wearable paves the way for demonstrating the concept of harnessing diagnostic information from the skin volatile emission as well as motivating the use of alternate colour chemistries for targeting other volatile biomarkers such as aldehydes for the monitoring of states including ketosis and oxidative stress for example. The development of such simple, colour-based wearable sensing approaches could prove useful in personalised monitoring of general health and also for self-management of chronic diseases associated with volatile biomarkers in the future.

5.5. References

- [1] Drislane C and Irvine A D 2020 The role of filaggrin in atopic dermatitis and allergic disease *Annals of Allergy, Asthma & Immunology* **124** 36–43
- [2] Piro B, Mattana G and Noël V 2019 Recent Advances in Skin Chemical Sensors *Sensors* **19** 4376
- [3] Duffy E and Morrin A 2019 Endogenous and microbial volatile organic compounds in cutaneous health and disease *TrAC Trends in Analytical Chemistry* **111** 163–72
- [4] Heikenfeld J, Jajack A, Feldman B, Granger S W, Gaitonde S, Begtrup G and Katchman B A 2019 Accessing analytes in biofluids for peripheral biochemical monitoring *Nat Biotechnol* **37** 407–19
- [5] Joseph J I 2021 Review of the Long-Term Implantable Senseonics Continuous Glucose Monitoring System and Other Continuous Glucose Monitoring Systems *J Diabetes Sci Technol* **15** 167–73
- [6] Ghaffari R, Rogers J A and Ray T R 2021 Recent progress, challenges, and opportunities for wearable biochemical sensors for sweat analysis *Sensors and Actuators B: Chemical* **332** 129447
- [7] Heikenfeld J, Jajack A, Rogers J, Gutruf P, Tian L, Pan T, Li R, Khine M, Kim J, Wang J and Kim J 2018 Wearable sensors: modalities, challenges, and prospects *Lab Chip* **18** 217–48
- [8] Escobedo P, Ramos-Lorente C E, Martínez-Olmos A, Carvajal M A, Ortega-Muñoz M, Orbe-Payá I de, Hernández-Mateo F, Santoyo-González F, Capitán-Vallvey L F, Palma A J and Erenas M M 2021 Wireless wearable wristband for continuous sweat pH monitoring *Sensors and Actuators B: Chemical* **327** 128948
- [9] Kim J, Campbell A S and Wang J 2018 Wearable non-invasive epidermal glucose sensors: A review *Talanta* **177** 163–70
- [10] Bandodkar A J, Jia W, Yardımcı C, Wang X, Ramirez J and Wang J 2015 Tattoo-Based Noninvasive Glucose Monitoring: A Proof-of-Concept Study *Anal. Chem.* **87** 394–8

- [11] Jia W, Bandodkar A J, Valdés-Ramírez G, Windmiller J R, Yang Z, Ramírez J, Chan G and Wang J 2013 Electrochemical Tattoo Biosensors for Real-Time Noninvasive Lactate Monitoring in Human Perspiration *Anal. Chem.* **85** 6553–60
- [12] Shitanda I, Mitsumoto M, Loew N, Yoshihara Y, Watanabe H, Mikawa T, Tsujimura S, Itagaki M and Motosuke M 2021 Continuous sweat lactate monitoring system with integrated screen-printed MgO-templated carbon-lactate oxidase biosensor and microfluidic sweat collector *Electrochimica Acta* **368** 137620
- [13] Sempionatto J R, Nakagawa T, Pavinatto A, Mensah S T, Imani S, Mercier P and Wang J 2017 Eyeglasses based wireless electrolyte and metabolite sensor platform *Lab Chip* **17** 1834–42
- [14] Bong Kim S, Koo J, Yoon J, Hourlier-Fargette A, Lee B, Chen S, Jo S, Choi J, Suk Oh Y, Lee G, Min Won S, J. Aranyosi A, P. Lee S, B. Model J, V. Braun P, Ghaffari R, Park C and A. Rogers J 2020 Soft, skin-interfaced microfluidic systems with integrated enzymatic assays for measuring the concentration of ammonia and ethanol in sweat *Lab on a Chip* **20** 84–92
- [15] Sonner Z, Wilder E, Heikenfeld J, Kasting G, Beyette F, Swaile D, Sherman F, Joyce J, Hagen J, Kelley-Loughnane N and Naik R 2015 The microfluidics of the eccrine sweat gland, including biomarker partitioning, transport, and biosensing implications *Biomicrofluidics* **9** 031301
- [16] Corrie S R, Coffey J W, Islam J, Markey K A and Kendall M a. F 2015 Blood, sweat, and tears: developing clinically relevant protein biosensors for integrated body fluid analysis *Analyst* **140** 4350–64
- [17] Kashaninejad N, Munaz A, Moghadas H, Yadav S, Umer M and Nguyen N-T 2021 Microneedle Arrays for Sampling and Sensing Skin Interstitial Fluid *Chemosensors* **9** 83
- [18] Goud K Y, Moonla C, Mishra R K, Yu C, Narayan R, Litvan I and Wang J 2019 Wearable Electrochemical Microneedle Sensor for Continuous Monitoring of Levodopa: Toward Parkinson Management *ACS Sens.* **4** 2196–204
- [19] Glennon T, O’Quigley C, McCaul M, Matzeu G, Beirne S, Wallace G G, Stroiescu F, O’Mahoney N, White P and Diamond D 2016 ‘SWEATCH’: A Wearable Platform for Harvesting and Analysing Sweat Sodium Content *Electroanalysis* **28** 1283–9
- [20] Pirovano P, Dorrian M, Shinde A, Donohoe A, Brady A J, Moyna N M, Wallace G, Diamond D and McCaul M 2020 A wearable sensor for the detection of sodium and potassium in human sweat during exercise *Talanta* **219** 121145
- [21] Bandodkar A J, Gutruf P, Choi J, Lee K, Sekine Y, Reeder J T, Jeang W J, Aranyosi A J, Lee S P, Model J B, Ghaffari R, Su C-J, Leshock J P, Ray T, Verrillo A, Thomas K, Krishnamurthi V, Han S, Kim J, Krishnan S, Hang T and Rogers J A 2019 Battery-free, skin-interfaced microfluidic/electronic systems for simultaneous electrochemical, colorimetric, and volumetric analysis of sweat *Sci. Adv.* **5** eaav3294

- [22] Martín A, Kim J, Kurniawan J F, Sempionatto J R, Moreto J R, Tang G, Campbell A S, Shin A, Lee M Y, Liu X and Wang J 2017 Epidermal Microfluidic Electrochemical Detection System: Enhanced Sweat Sampling and Metabolite Detection *ACS Sens.* **2** 1860–8
- [23] Dormont L, Bessière J-M and Cohuet A 2013 Human Skin Volatiles: A Review *J Chem Ecol* **39** 569–78
- [24] Drabińska N, Flynn C, Ratcliffe N, Belluomo I, Myridakis A, Gould O, Fois M, Smart A, Devine T and Costello B D L 2021 A literature survey of all volatiles from healthy human breath and bodily fluids: the human volatilome *J. Breath Res.* **15** 034001
- [25] Penn D J, Oberzaucher E, Grammer K, Fischer G, Soini H A, Wiesler D, Novotny M V, Dixon S J, Xu Y and Brereton R G 2007 Individual and gender fingerprints in human body odour *J R Soc Interface* **4** 331–40
- [26] Grabowska-Polanowska B, Miarka P, Skowron M, Sułowicz J, Wojtyna K, Moskal K and Śliwka I 2017 Development of sampling method and chromatographic analysis of volatile organic compounds emitted from human skin *Bioanalysis* **9** 1465–75
- [27] Roodt A P, Naudé Y, Stoltz A and Rohwer E 2018 Human skin volatiles: Passive sampling and GC × GC-ToFMS analysis as a tool to investigate the skin microbiome and interactions with anthropophilic mosquito disease vectors *Journal of Chromatography B* **1097–1098** 83–93
- [28] Zhang Z-M, Cai J-J, Ruan G-H and Li G-K 2005 The study of fingerprint characteristics of the emanations from human arm skin using the original sampling system by SPME-GC/MS *Journal of Chromatography B* **822** 244–52
- [29] Duffy E, Jacobs M R, Kirby B and Morrin A 2017 Probing skin physiology through the volatile footprint: Discriminating volatile emissions before and after acute barrier disruption *Exp. Dermatol.* **26** 919–25
- [30] Duffy E, Guzman K D, Wallace R, Murphy R and Morrin A 2017 Non-Invasive Assessment of Skin Barrier Properties: Investigating Emerging Tools for In Vitro and In Vivo Applications *Cosmetics* **4** 44
- [31] Shetewi T, Finnegan M, Fitzgerald S, Xu S, Duffy E and Morrin A 2021 Investigation of the relationship between skin-emitted volatile fatty acids and skin surface acidity in healthy participants – a pilot study *J. Breath Res.*
- [32] Danby S G and Cork M J 2018 pH in Atopic Dermatitis *pH of the Skin: Issues and Challenges* **54** 95–107
- [33] Knor T, Meholjić-Fetahović A and Mehmedagić A 2011 Stratum corneum hydration and skin surface pH in patients with atopic dermatitis *Acta Dermatovenerol Croat* **19** 242–7
- [34] Proksch E 2018 pH in nature, humans and skin *The Journal of Dermatology* **45** 1044–52

- [35] Nose K, Mizuno T, Yamane N, Kondo T, Ohtani H, Araki S and Tsuda T 2005 Identification of Ammonia in Gas Emanated from Human Skin and Its Correlation with That in Blood *Anal. Sci.* **21** 1471–4
- [36] Bulmer M G 1957 The concentration of urea in thermal sweat *The Journal of Physiology* **137** 261–6
- [37] Watabe A, Sugawara T, Kikuchi K, Yamasaki K, Sakai S and Aiba S 2013 Sweat constitutes several natural moisturizing factors, lactate, urea, sodium, and potassium *Journal of Dermatological Science* **72** 177–82
- [38] Martínez-Lozano P 2009 Mass spectrometric study of cutaneous volatiles by secondary electrospray ionization *International Journal of Mass Spectrometry* **282** 128–32
- [39] Bernier U R, Kline D L, Barnard D R, Schreck C E and Yost R A 2000 Analysis of Human Skin Emanations by Gas Chromatography/Mass Spectrometry. 2. Identification of Volatile Compounds That Are Candidate Attractants for the Yellow Fever Mosquito (*Aedes aegypti*) *Anal. Chem.* **72** 747–56
- [40] Furukawa S, Sekine Y, Kimura K, Umezawa K, Asai S and Miyachi H 2017 Simultaneous and multi-point measurement of ammonia emanating from human skin surface for the estimation of whole body dermal emission rate *Journal of Chromatography B* **1053** 60–4
- [41] Li M, Weschler C J, Bekö G, Wargocki P, Lucic G and Williams J 2020 Human Ammonia Emission Rates under Various Indoor Environmental Conditions *Environ. Sci. Technol.* 10
- [42] Xiao J, Liu Y, Su L, Zhao D, Zhao L and Zhang X 2019 Microfluidic Chip-Based Wearable Colorimetric Sensor for Simple and Facile Detection of Sweat Glucose *Anal. Chem.* **91** 14803–7
- [43] Choi J, Kang D, Han S, Kim S B and Rogers J A 2017 Thin, Soft, Skin-Mounted Microfluidic Networks with Capillary Bursting Valves for Chrono-Sampling of Sweat *Advanced Healthcare Materials* **6** 1601355
- [44] Koh A, Kang D, Xue Y, Lee S, Pielak R, Kim J, Hwang T, Min S, Banks A, Bastien P, Manco M, Wang L, Ammann K, Jang K-I, Won P, Han S, Ghaffari R, Paik U, Slepian M and Rogers J 2016 A soft, wearable microfluidic device for the capture, storage, and colorimetric sensing of sweat *Science Translational Medicine* **8** 366ra165-366ra165
- [45] Zhang Y, Guo H, Kim S B, Wu Y, Ostojich D, Park S H, Wang X, Weng Z, Li R, Bandodkar A J, Sekine Y, Choi J, Xu S, Quaggin S, Ghaffari R and Rogers J A 2019 Passive sweat collection and colorimetric analysis of biomarkers relevant to kidney disorders using a soft microfluidic system *Lab Chip* **19** 1545–55
- [46] Suslick K S, Rakow N A and Sen A 2004 Colorimetric sensor arrays for molecular recognition *Tetrahedron* **60** 11133–8

- [47] Curran A M, Rabin S I, Prada P A and Furton K G 2005 Comparison of the volatile organic compounds present in human odor using SPME-GC/MS *J. Chem. Ecol.* **31** 1607–19
- [48] Hamilton D F, Ghert M and Simpson A H R W 2015 Interpreting regression models in clinical outcome studies *Bone Joint Res* **4** 152–3
- [49] Cserhati T and Forgacs E 1997 Trends in Thin-Layer Chromatography: 1997 *Journal of Chromatographic Science* **35** 383–91
- [50] Low P A 2012 Chapter 51 - Sweating *Primer on the Autonomic Nervous System (Third Edition)* ed D Robertson, I Biaggioni, G Burnstock, P A Low and J F R Paton (San Diego: Academic Press) pp 249–51
- [51] Taylor N A and Machado-Moreira C A 2013 Regional variations in transepidermal water loss, eccrine sweat gland density, sweat secretion rates and electrolyte composition in resting and exercising humans *Extrem Physiol Med* **2** 4
- [52] Harker M 2013 Psychological Sweating: A Systematic Review Focused on Aetiology and Cutaneous Response *Skin pharmacology and physiology* **26** 92–100
- [53] SanMiguel A and Grice E A 2015 Interactions between host factors and the skin microbiome *Cell. Mol. Life Sci.* **72** 1499–515
- [54] Shamloul G and Khachemoune A 2021 An updated review of the sebaceous gland and its role in health and diseases Part 1: Embryology, evolution, structure, and function of sebaceous glands *Dermatologic Therapy* **34** e14695

Chapter 6: Conclusions and future work

6.1. Conclusions and future work

As discussed in Chapter 1, wearable sensing technology has recently and rapidly moved towards the development of many commercially available sensing devices that focus on physical measurements such as heart rate and blood oxygen levels. However, physical measurements such as these give limited insight into an individual's health. The skin offers great biodiagnostic potential through the analysis of biofluids such as interstitial fluid (ISF) and sweat. Many of these wearable sensors employ electrochemical transduction but recently sensors incorporating optical transduction have gained traction owing to their simplicity and low-cost. Wearable sensor development for biofluids such as ISF and sweat have thrown up many challenges with respect to generating and collecting sufficient volumes of such biofluids for reliable analyte detection.

The primary aim of this work was to overcome the need for collection and manipulation of biofluids from skin through the exploitation of the volatile emission from skin which is passively and continuously emitted from skin, known to contain biomarkers of metabolic and cellular processes within the body and can be sampled in a non-invasive manner. This work contributes to a greater understanding towards factors that can affect the skin volatile emission such as circadian rhythm, sampling site, gender, and age. An investigation into the effect of frequently emitted skin-derived compounds on primary human keratinocytes show that specific compounds afford protection against oxidative stress through the activation of the Nrf2-Keap1 pathway, a cellular defence mechanism. Finally, a simple, low-cost colorimetric sensor platform was fabricated in order to monitor volatile ammonia emission from skin. Here, the feasibility of measuring skin surface pH via the volatile ammonia emission from skin was assessed and highlights great potential of such simple wearable colorimetric sensors for personalised skin monitoring.

Chapter 2 employs a non-invasive, HS-SPME GC-MS workflow to investigate diurnal- and skin site-associated changes in the human skin volatile profile of a single healthy female participant. Results confirm significant diurnal variation in the skin volatile profile also with changes in the skin surface pH which were shown to have correlation with some of the acidic compounds emitted from skin. Interestingly, no diurnal change in TDC was observed even though changes in the volatile profile, such as increased ketone production, may suggest increased sebum secretion on the skin. TDC is a measure of skin-to-fat tissue water and measures at a depth of 0.5 mm below skin. A skin surface measurements such as TEWL may prove more insightful and may better help correlations between hydration of the skin and the

skin volatile profile. Future work, around this would involve obtaining volatile HS-SPME measurements along with TEWL surface hydration measurements and assessing for correlation between the two. Although, significant changes in TDC were observed across different skin sites, again TEWL may be able to give a better insight into the correlation between volatile emissions and skin surface hydration as volatile compounds are typically emitted from the surface of the skin [1]. Stratum corneum hydration (SCH) which measures the water content of the uppermost layers of the skin may also provide insight into the correlations between skin hydration and volatile compound emission [2]. Furthermore, it would be interesting to recruit a larger participant cohort for this study and assess inter-participant variability in diurnal- and site-specific changes in the volatile along with skin surface pH, TEWL and SCH.

Chapter 3 builds on chapter 2 and characterises the skin volatile emission from the volar forearm of a large healthy participant cohort (n=60) comprised of male and female participants, ages 18-80. Gender and age associated changes in the skin volatile emission from the volar was assessed across the participant cohort. Results confirmed significant gender influences on the skin volatile emission indicating that male and female data should be treated individually when investigating age-related changes in the skin volatile emission. Statistical analysis of the volatile profile with age showed that there were compound abundances that significantly changed with age (acetic acid, hexanal, nonanal, undecanal, benzyl alcohol and 2-ethyl-1-hexanol). Age-related changes in skin surface pH and TDC were also observed. Again, as mentioned above, TEWL and SCH measurements may also prove insightful here to understand skin surface hydration in a large participant cohort.

Chapter 4 investigates the effect that commonly skin-derived compounds, such as nonanal, decanal and 6-methyl-5-hepten-2-one, impact host skin cells' signalling pathways. Results show that nonanal and decanal trigger activation of the Nrf2-pathway in primary human keratinocytes while the ketone, 6-methyl-5-hepten-2-one, does not elicit activation. Elucidation of the mechanism by which this pathway is activated shows that an augmentation in ROS production in NHEK cells was caused by exposure to nonanal and decanal but not the ketone, indicating indirect activation of the cellular defence pathway. A proof of concept study also showed an increase in ROS production when cells were exposed to varying concentrations of nonanal in gas phase. To the best of our knowledge, this is the first study that investigates the effect of treatment of cells with nonanal in the volatile phase and leads to hypothesis that nonanal in gas phase produced by the skin may lead to ROS generation in cells and neighbouring cells which may lead to the activation of the Nrf2-Keap1 pathway through

indirect activation. While novel, this volatile work has some limitations. For example, cells were only exposed to a headspace of nonanal in gas phase. It would be more beneficial to expose cells to an artificial skin VOC mix, comprising common skin emitted compounds and physiological relevant concentrations. Furthermore, monolayer cultures only allow limited inference about response to external stimuli such as volatile emissions and their ability to trigger cell-signalling pathways. Future work would involve a move toward an organ on a chip model with the integration of an air-liquid interface (ALI) culture which could further enhance assessment of volatile compounds abilities to induce signalling pathways within cells (Fig 6.1) [3].

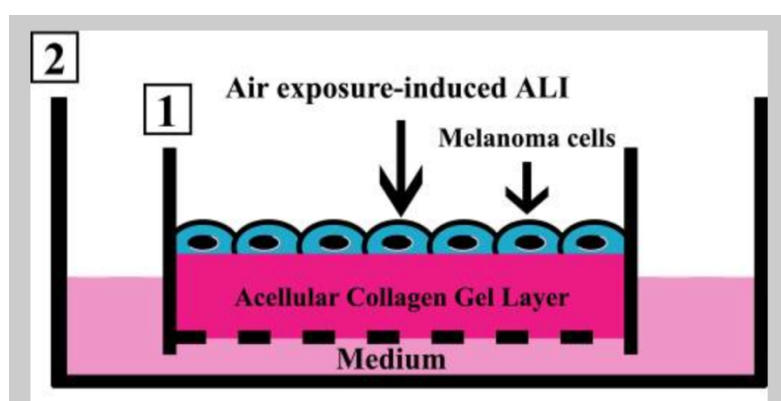


Figure 6.1. ALI cell culture set-up for melanoma cells. Cells here are kept moist and fed by the cell culture medium in the bottom of the assay that moves towards the cells by capillary action through collagen gel layer [4].

Chapter 5 investigated the use of a simple wearable colorimetric sensing platform incorporating sensor spots comprising encapsulated bromocresol green pH indicator dye in an enclosed headspace above the skin. The sensor spots change from yellow to blue as a response to basic volatile nitrogen compounds such as ammonia and volatile amines being emitted from skin. By deploying this wearable in a healthy participant study, a strong correlation between sensor Euclidean Distance (ED) response and skin surface pH was demonstrated, despite a high inter-individual variability being noted. Sensor response was observed to be highly dependent on gender as well as body site, and attributed to factors such as gland and microbial composition differences. Finally, skin surface pH and wearable sensor responses were measured following various skin treatments and showed the wearable's ability to detect changes in skin surface pH in response to topical skin treatments.

Recent work has involved investigating new targets, such as aldehydes, for colorimetric sensing of skin volatiles. Work in Chapter 3 has shown the aldehyde profile of skin changes with age and so a move toward a wearable sensor for aldehydes emission could allow for a low-cost way to assess aldehyde emission from skin. This work has briefly investigated the use of simple amine-containing dyes, pararosaniline and *N, N*-dimethyl 4,4'-azodianiline, incorporated into a wearable platform, as outlined in Chapter 5, to detect aldehyde emission from skin. Initial results have shown that this sensor may have shown the sensors sensitivity for aldehydes characteristic to human skin after exposure in-vitro to standard analytes. Furthermore, initial work has shown the ability of the sensor array to differentiate between the aldehyde emission from different skin sites (Figure 6.2). While this work is interesting, much more work is needed to correlate the response of the sensors with GC-MS data from different skin sites to understand the response of the sensor. Furthermore, preliminary results on different humidity conditions also suggest that sensor response may be affected by skin humidity. Further studies investigating other humidity conditions would be needed to confirm and understand this effect.

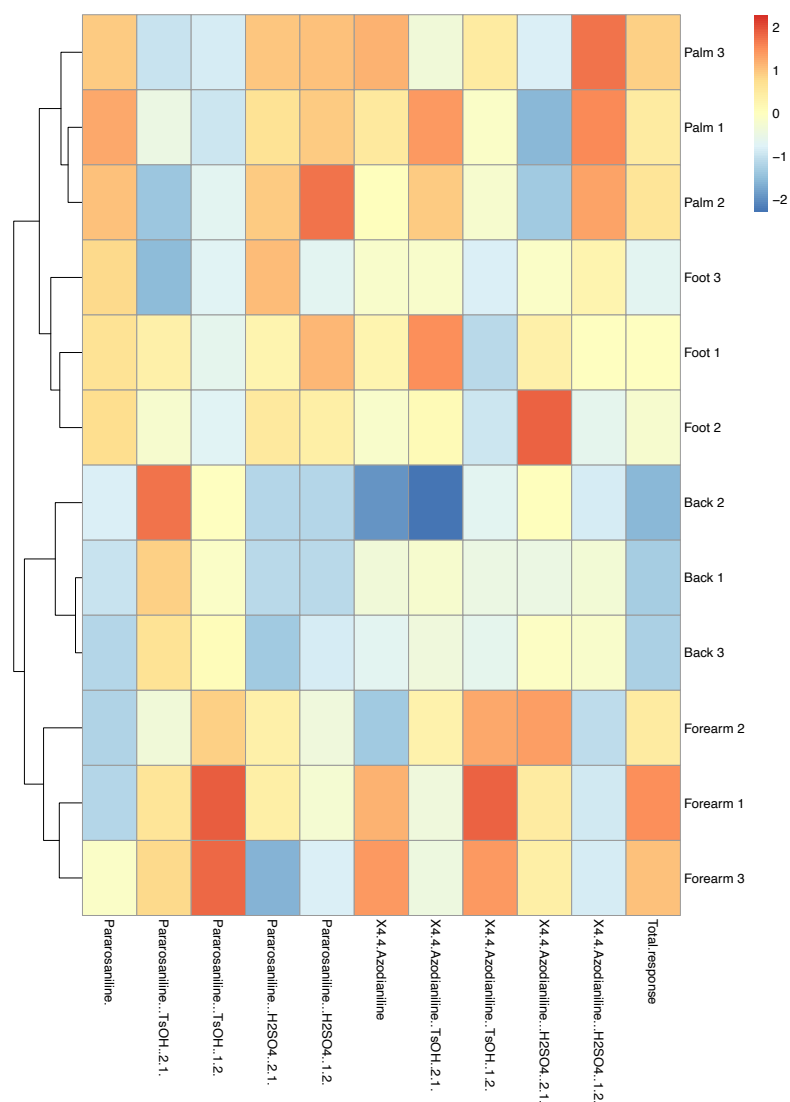


Figure 6.2. Heatmap with hierarchical clustering showing response for each sensor spot (columns) to each skin site (rows). Values were centred and scaled by their respective columns, with a high response being coloured as red and a low response being coloured as blue.

One major limitation of the sensors in their current form presented in Chapter 5 is the inability to continuously image/monitor sensor response throughout wear. Kinetic data was obtained in Chapter 5, where imaging of the sensor was done periodically during the measurement by removing the wearable from the skin every 15 min, imaging the sensor spots, and replacing on the skin immediately after. This removal of the sensor from the skin every 15 min for imaging may mean the equilibrium between the volatile ammonia emission and the sensor headspace is disturbed each time the sensor is removed, however no drop in signal was observed. Chapter 5 highlights the potential capabilities of a simple bromocresol green sensor to monitor skin surface pH via ammonia emission from skin, even being able to detect changes

after topical treatment applications but the imaging process limits the abilities and applications of the sensor. Chapter 5 shows one way to avoid the need for removal is to develop a real-time imaging method that can enable us to image the sensor while still on the skin. Preliminary real-time imaging experiments were carried out using an iPhone camera and a lightbox (CALISTOUK Mini Photo Studio Light Box, Amazon UK) to try and provide a constant, consistent light source for each image captured. The sensor was kept on the skin for 5 h without removal and was imaged every 15 min using this set-up. Figure 6.3 shows a comparison between the two different imaging methods and shows large error bars for the iPhone/lightbox imaging method which highlights inconsistencies in RGB values of each sensor spot and attributed to light artefacts in the image. The inconsistencies may also be attributed to the PET backing on the cellulose TLC plates used which may distort colour of sensor spots in the image. One of the main aims for future work in this project is to develop an in-situ imaging method that eliminates all these outlined effects and has the ability to continuously monitor the sensor response during wear on the skin.

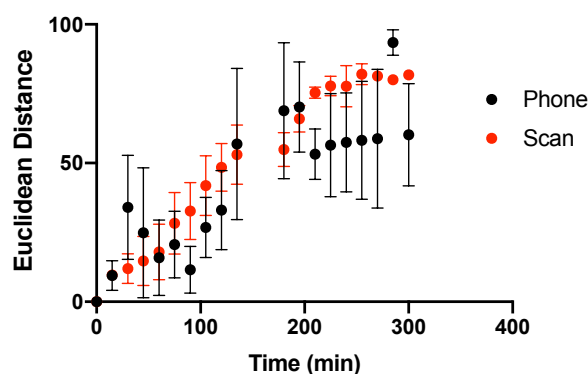


Figure 6.3. Shows comparison between removing the sensor from the skin to scan and imaging of the sensor on the skin with an iPhone. Error bars represent standard deviation in ED response from n=6 sensor spots within a single wearable platform.

More recently, we have been working with Dr. Nigel Kent's group in the School of Mechanical Engineering in DCU to development a continuous imaging wearable platform that incorporates a commercially available ESP32-CAM with a built-in LED that can allow for continuous on-skin imaging in a light-controlled environment. The device also has the capability to transmit images obtained via Wi-Fi which can allow for quick image analysis. Furthermore, response time from the sensor in Chapter 5 is 5 h and a 5.2 V battery was selected to allow enough power supply for that sampling time. Further work is needed to realize the full

potential of the continuous wearable platform, but it shows promise toward continuous imaging of the sensor on the skin.



Figure 6.4. Continuous imaging wearable platform with built-in ESP32-CAM worn on the forearm.

6.2. References

- [1] Alexander H, Brown S, Danby S and Flohr C 2018 Research Techniques Made Simple: Transepidermal Water Loss Measurement as a Research Tool *J Invest Dermatol* **138** 2295-2300.e1
- [2] Jansen van Rensburg S, Franken A and Du Plessis J L 2019 Measurement of transepidermal water loss, stratum corneum hydration and skin surface pH in occupational settings: A review *Skin Research and Technology* **25** 595–605
- [3] Leung C M, de Haan P, Ronaldson-Bouchard K, Kim G-A, Ko J, Rho H S, Chen Z, Habibovic P, Jeon N L, Takayama S, Shuler M L, Vunjak-Novakovic G, Frey O, Verpoorte E and Toh Y-C 2022 A guide to the organ-on-a-chip *Nat Rev Methods Primers* **2** 1–29
- [4] Hong Yee C, Aoki S, Uchihashi K, Matsunobu A, Yamasaki F, Misago N, Piao M, Tetsuji U, Yonemitsu N, Sugihara H and Toda S 2010 The Air Liquid-interface, a Skin Microenvironment, Promotes Growth of Melanoma Cells, but not Their Apoptosis and Invasion, through Activation of Mitogen-activated Protein Kinase *Acta Histochem Cytochem* **43** 1–7

Appendix

Chapter 2: Assessing diurnal and site-associated differences in the skin volatile emission, skin surface pH and tissue dielectric constant in healthy skin

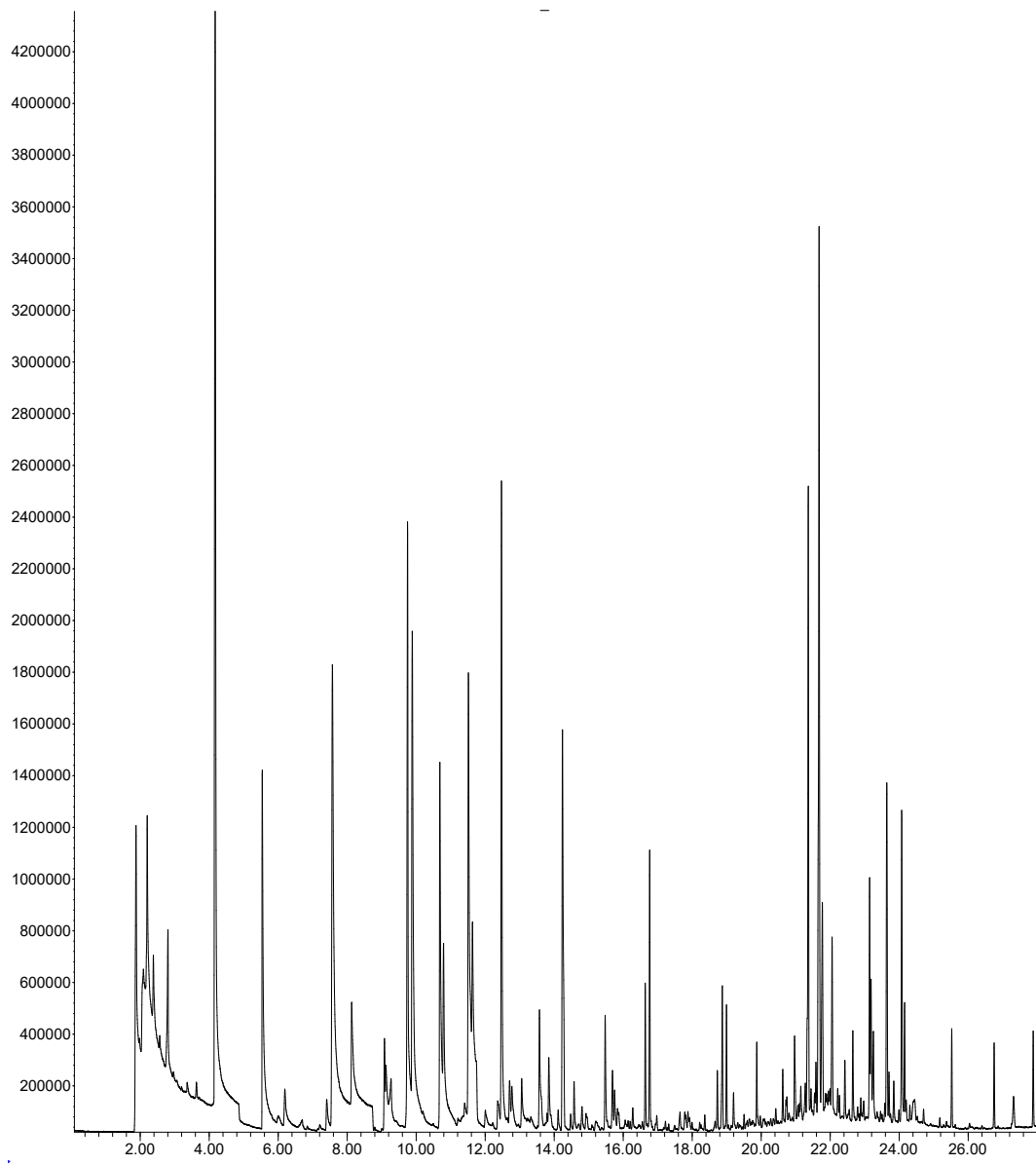


Figure A2.1. Typical chromatogram from the volar forearm of a single female participant.

Chapter 3: Skin volatile emission profiling of healthy participants – influence of gender and age

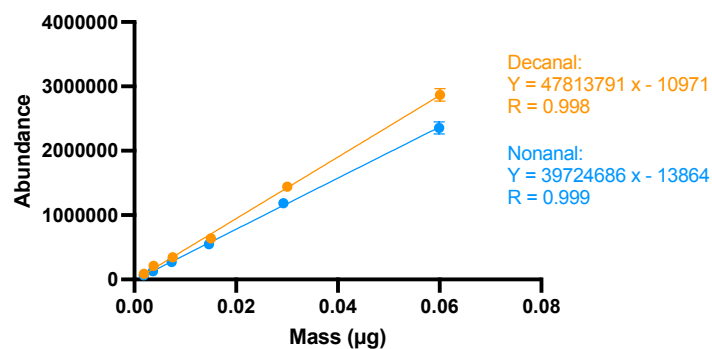


Figure A3.1. Graph showing calibration curves for nonanal and decanal of abundance vs mass (μg) present in 3 ml headspace funnel used to sample skin. Error bars represent standard deviation of $n=3$ replicates for each mass. Note: this data was used to calculate emission fluxes for nonanal and decanal.

**Chapter 5: The determination of skin surface pH via skin
volatile emission using colorimetric sensors**

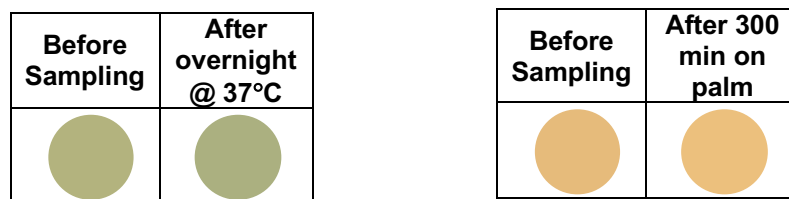


Figure A5.1. (a) Reproduced average colour response (6 replicate BCG sensor spots on unmodified cellulose TLC plate) from control study where sensor was placed in a vial along with gauze that had not been exposed to skin and (b) reproduced average colour response (6 replicate BCG sensor spots on 10% acetylated TLC plate) from control study where sensor was worn on the skin for 300 min with PET film between skin and sensor.

Table A5.1. Tabulated data from Figure 3 showing average red intensity, green intensity, blue intensity and corresponding ED response from wearable platform (6 replicate BCG sensor spots) for n=5 female and n=5 male participants. Calculated ammonia flux ($\text{mg h}^{-1} \text{cm}^{-2}$) and reproduced average colour after 5 h wear also shown.

Participant	Average Red intensity (RI)	Average Green intensity (GI)	Average Blue intensity (BI)	Average Euclidean distance (ED)	Skin surface pH (ISE)	Calculated ammonia emission flux ($\text{mg h}^{-1} \text{cm}^{-2}$)	Reproduced average colour after 5 h wear
F1	218.29	200.87	141.89	34.16	4.33	0.0096	
F2	192.42	187.61	137.60	47.68	4.73	0.0145	
F3	201.09	200.74	153.68	46.69	4.83	0.0152	
F4	168.97	178.11	137.42	57.14	4.97	0.0199	
F5	123.647	161.89	129.40	98.39	5.01	0.0385	
M1	178.15	188.03	1.26	52.95	4.25	0.0181	
M2	170.09	187.57	150.89	69.72	4.33	0.0256	
M3	122.49	171.92	160.59	117.43	4.57	0.0471	
M4	90.18	155.79	149.48	142.67	4.72	0.0584	
M5	83.26	137.51	148.79	137.64	5.21	0.0562	

Table A5.2. Tabulated data from Figure 4 showing average red intensity, green intensity, blue intensity and ED response from wearable platform (6 replicate BCG sensor spots) for female 1. Calculated ammonia flux ($\text{mg h}^{-1} \text{cm}^{-2}$) and reproduced average colour after 5 h wear also shown.

Sam ple no.	Red intensity (RI)	Green intensity (GI)	Blue intensity (BI)	Euclidean distance (ED)	Skin surface pH (ISE)	Calculated ammonia emission flux ($\text{mg h}^{-1} \text{cm}^{-2}$)	Reprod uced average colour after 5 h wear
1	218.24	200.009	141.41	18.33	4.3	0.0025	
2	216.82	202.04	143.63	21.54	4.33	0.0039	
3	215.05	197.111	138.496	22.14	4.4	0.0042	
4	204.29	197.877	144.89	34.16	4.47	0.0096	
5	197.06	194.76	144.99	40.74	4.55	0.0126	

Table A5.3. Tabulated data from Figure 4 showing average red intensity, green intensity, blue intensity and corresponding ED response from wearable platform (6 replicate BCG sensor spots) for female 2. Calculated ammonia flux ($\text{mg h}^{-1} \text{cm}^{-2}$) and reproduced average colour after 5 h wear also shown.

Sam ple no.	Red intensity (RI)	Green intensity (GI)	Blue intensity (BI)	Euclidean distance (ED)	Skin surface pH (ISE)	Calculated ammonia emission flux ($\text{mg h}^{-1} \text{cm}^{-2}$)	Reprod uced average colour after 5 h wear
1	197.31	196.41	149.36	44.89	4.73	0.0145	
2	174.82	178.94	123.38	57.99	4.79	0.0203	
3	172.52	178.97	131.41	63.26	4.8	0.0227	
4	150.24	178.68	149.49	77.21	4.92	0.0290	
5	167.53	182.65	140.11	71.86	4.95	0.0266	
6	159.23	177.73	137.35	76.53	4.95	0.0287	
7	158.14	173.91	130.65	78.21	4.98	0.0295	

Table A5.4. Tabulated data from Figure 5 showing average red intensity, green intensity, blue intensity and corresponding ED response from wearable platform (6 replicate BCG sensor spots) worn on the palm for a single female participant. Reproduced average colour after 5 h wear also shown.

Time (min)	Red intensity (RI)	Green intensity (GI)	Blue intensity (BI)	Euclidean distance (ED)	Skin surface pH (ISE)	Reproduced average colour after 5 h wear
0	233.35	193.52	123.13	0	4.85	
15	230.09	195.23	124.98	9.26	4.95	
30	224.14	194.27	126.29	8.54	4.88	
45	217.85	192.71	126.94	14.21	4.83	
60	208.65	190.69	129.20	18.65	4.76	
75	199.18	189.22	132.86	25.16	4.78	
90	189.65	187.33	134.61	32.12	4.76	
105	180.53	184.73	135.90	36.13	4.74	
120	179.86	184.93	136.86	44.85	4.70	
135	180.23	185.59	137.48	49.44	4.70	
180	175.86	184.34	138.21	69.02	4.86	
195	173.31	184.19	139.84	75.35	4.90	
210	172.45	184.08	140.41	79.32	4.78	
225	169.23	183.07	140.78	78.45	4.80	
240	170.57	183.86	140.72	81.06	4.86	
255	171.82	184.29	141.39	80.45	4.85	
270	169.82	184.22	142.17	86.68	4.80	
285	167.69	183.44	142.68	87.76	4.83	
300	167.87	183.59	143.34	90.92	4.90	

Table A5.5. Tabulated data from Figure 5 showing average red intensity, green intensity, blue intensity and corresponding ED response from wearable platform (6 replicate BCG sensor spots) worn on the palm for a single male participant. Reproduced average colour after 5 h wear also shown.

Time (min)	Red intensity (RI)	Green intensity (GI)	Blue intensity (BI)	Euclidean distance (ED)	Skin surface pH (ISE)	Reproduced average colour after 5 h wear
0	227.86	186.18	125.79	0	4.43	
15	225.66	192.60	130.74	8.50	4.44	
30	222.16	189.11	126.37	8.49	4.48	
45	219.76	189.76	120.92	11.37	4.50	
60	213.11	189.34	125.98	16.30	4.52	
75	202.06	186.09	126.00	26.08	4.50	
90	191.63	182.13	123.67	36.65	4.40	
105	179.22	179.75	129.77	49.26	4.40	
120	173.07	182.94	141.78	57.25	4.40	
135	158.03	175.36	136.23	71.89	4.39	
180	149.24	173.19	138.94	80.91	4.43	
195	141.47	171.92	144.07	89.61	4.45	
210	145.72	177.40	153.21	87.09	4.47	
225	145.31	177.12	153.68	87.63	4.43	
240	146.49	178.01	155.12	86.88	4.50	
255	149.26	178.05	153.18	87.69	4.51	
270	149.21	177.99	153.52	89.86	4.50	
285	150.85	177.96	151.92	89.79	4.50	
300	149.05	176.61	151.82	91.71	4.51	

Table A5.6. Tabulated data from Figure 5 showing average red intensity, green intensity, blue intensity and corresponding ED response from wearable platform (6 replicate BCG sensor spots) worn on the foot for a single female participant. Reproduced average colour after 5 h wear also shown.

Time (min)	Red intensity (RI)	Green intensity (GI)	Blue intensity (BI)	Euclidean distance (ED)	Skin surface pH (ISE)	Reproduced average colour after 5 h wear
0	234.38	190.31	114.68	0	4.87	
15	228.85	189.18	115.79	5.02	4.78	
30	225.23	189.11	117.33	8.56	4.88	
45	220.81	188.29	118.19	11.96	4.86	
60	216.55	189.12	121.15	14.50	4.90	
75	212.05	188.17	121.85	21.76	4.80	
90	203.44	185.09	123.10	22.78	4.76	
105	200.12	184.95	124.91	31.33	4.75	
120	195.20	184.67	126.51	33.17	4.74	
135	191.31	183.90	127.58	37.69	4.72	
180	193.51	184.31	128.78	43.56	4.70	
195	188.53	183.06	129.35	50.43	4.74	
210	185.53	182.64	130.84	52.18	4.74	
225	182.85	181.55	130.73	56.91	4.70	
240	181.12	182.23	132.02	58.28	4.81	
255	182.51	182.12	130.27	55.58	4.75	
270	180.54	181.78	132.00	58.50	4.78	
285	179.43	181.83	132.86	61.05	4.75	
300	177.66	181.42	133.19	63.15	4.86	

Table A5.7. Tabulated data from Figure 5 showing average red intensity, green intensity, blue intensity and corresponding ED response from wearable platform (6 replicate BCG sensor spots) worn on the foot for a single male participant. Reproduced average colour after 5 h wear also shown.

Time (min)	Red intensity (RI)	Green intensity (GI)	Blue intensity (BI)	Euclidean distance (ED)	Skin surface pH (ISE)	Reproduced average colour after 5 h wear
0	227.24	186.70	128.15	0	4.43	
15	223.57	186.83	125.57	6.47	4.33	
30	214.06	186.14	129.47	13.81	4.39	
45	209.27	184.93	128.82	18.51	4.40	
60	199.60	183.09	131.33	28.57	4.43	
75	192.19	181.93	132.31	35.95	4.37	
90	191.66	181.88	133.01	36.62	4.40	
105	184.22	180.56	134.37	44.02	4.40	
120	177.75	178.38	135.01	50.92	4.41	
135	170.97	176.80	136.32	57.84	4.43	
180	165.50	175.43	138.10	63.73	4.44	
195	164.41	176.42	139.81	64.84	4.38	
210	159.98	174.28	139.09	69.45	4.30	
225	145.80	171.30	143.80	84.54	4.35	
240	150.59	171.37	139.35	79.13	4.40	
255	156.53	173.39	141.18	73.20	4.46	
270	154.50	172.64	141.06	75.40	4.47	
285	155.89	173.62	141.36	73.93	4.48	
300	154.87	172.86	140.34	74.83	4.50	

Table A5.8. Tabulated data from Figure 5 showing average red intensity, green intensity, blue intensity and corresponding ED response from wearable platform (6 replicate BCG sensor spots) worn on the abdomen for a single female participant. Reproduced average colour after 5 h wear also shown.

Time (min)	Red intensity (RI)	Green intensity (GI)	Blue intensity (BI)	Euclidean distance (ED)	Skin surface pH (ISE)	Reproduced average colour after 5 h wear
0	229.49	188.33	128.43	0	5.33	
15	227.12	184.98	123.94	6.19	5.40	
30	227.42	185.02	124.48	5.75	5.39	
45	225.81	185.68	126.28	7.05	5.20	
60	224.84	185.76	126.19	6.76	5.26	
75	224.18	185.68	127.12	6.82	5.10	
90	222.73	184.92	125.22	8.91	5.20	
105	221.27	184.75	125.90	9.76	5.18	
120	219.57	184.91	127.11	11.07	5.15	
135	217.70	184.40	127.18	12.98	5.20	
180	215.31	184.02	126.94	15.27	5.25	
195	215.02	184.51	127.97	15.54	5.20	
210	212.06	183.90	128.70	18.32	5.00	
225	210.41	183.30	127.74	20.18	5.01	
240	209.48	183.30	128.19	21.12	5.00	
255	209.48	183.79	129.18	20.81	5.10	
270	207.96	183.20	129.26	23.04	5.15	
285	207.85	183.48	130.16	22.69	5.12	
300	204.55	182.13	129.38	25.91	5.10	

Table A5.9. Tabulated data from Figure 5 showing average red intensity, green intensity, blue intensity and corresponding ED response from wearable platform (6 replicate BCG sensor spots) worn on the abdomen for a single male participant. Reproduced average colour after 5 h wear also shown.

Time (min)	Red intensity (RI)	Green intensity (GI)	Blue intensity (BI)	Euclidean distance (ED)	Skin surface pH (ISE)	Reproduced average colour after 5 h wear
0	227.99	188.15	127.69	0	4.69	
15	223.57	187.37	129.40	4.98	4.66	
30	222.47	186.51	128.14	6.21	4.68	
45	222.68	187.70	129.27	6.00	4.67	
60	221.11	186.83	127.16	7.11	4.69	
75	217.72	185.71	127.28	10.57	4.75	
90	216.82	186.21	128.70	11.42	4.60	
105	214.08	186.07	129.87	14.26	4.57	
120	211.38	184.82	128.72	17.00	4.51	
135	208.01	184.93	131.51	20.78	4.68	
180	206.57	183.96	130.94	22.08	4.69	
195	205.94	184.36	132.54	23.06	4.63	
210	203.88	183.41	131.06	24.82	4.68	
225	203.17	183.53	131.56	25.55	4.66	
240	201.75	183.39	132.32	27.12	4.68	
255	200.58	183.29	133.00	28.36	4.60	
270	199.93	182.73	132.15	28.93	4.68	
285	199.84	183.32	133.38	29.13	4.67	
300	199.49	182.89	132.95	29.46	4.69	

Table A5.10. Tabulated data from Figure 5 showing average red intensity, green intensity, blue intensity and corresponding ED response from wearable platform (6 replicate BCG sensor spots) worn on the forehead for a single female participant. Reproduced average colour after 5 h wear also shown.

Time (min)	Red intensity (RI)	Green intensity (GI)	Blue intensity (BI)	Euclidean distance (ED)	Skin surface pH (ISE)	Reproduced average colour after 5 h wear
0	226.19	184.05	122.20	0	4.57	
15	227.95	183.85	122.53	2.16	4.50	
30	229.42	185.59	123.47	3.81	4.51	
45	229.26	185.46	123.05	3.65	4.52	
60	228.74	185.97	124.12	4.05	4.52	
75	227.91	185.53	123.60	3.29	4.46	
90	227.61	185.65	124.04	3.47	4.58	
105	227.72	186.17	124.98	3.90	4.53	
120	227.41	186.43	125.74	4.56	4.44	
135	227.22	186.26	125.49	4.79	4.43	
180	229.62	187.58	124.11	5.56	4.50	
195	229.17	188.35	126.47	6.89	4.53	
210	228.26	188.59	126.82	7.39	4.55	
225	227.42	188.17	126.19	6.09	4.45	
240	226.86	188.24	126.86	7.30	4.52	
255	225.81	187.68	126.68	6.94	4.44	
270	225.33	188.16	127.74	9.01	4.46	
285	224.43	188.62	129.34	9.64	4.52	
300	224.04	187.64	126.94	7.41	4.55	

Table A5.11. Tabulated data from Figure 5 showing average red intensity, green intensity, blue intensity and corresponding ED response from wearable platform (6 replicate BCG sensor spots) worn on the forehead for a single male participant. Reproduced average colour after 5 h wear also shown.

Time (min)	Red intensity (RI)	Green intensity (GI)	Blue intensity (BI)	Euclidean distance (ED)	Skin surface pH (ISE)	Reproduced average colour after 5 h wear
0	226.10	185.44	125.90	0	4.62	
15	226.10	186.78	126.80	3.48	4.50	
30	225.83	187.33	127.69	3.91	4.50	
45	224.87	186.17	125.98	2.37	4.61	
60	223.00	185.35	124.79	3.86	4.64	
75	222.59	185.34	125.20	4.25	4.66	
90	222.86	185.02	124.47	3.92	4.57	
105	222.11	185.61	124.90	4.67	4.63	
120	221.05	185.89	126.45	5.52	4.60	
135	223.87	187.02	126.52	3.63	4.60	
180	222.47	186.71	127.36	4.71	4.71	
195	221.16	186.23	127.24	5.56	4.60	
210	219.78	186.29	128.02	7.26	4.69	
225	218.99	185.52	126.43	7.49	4.53	
240	218.35	186.10	128.20	8.41	4.58	
255	218.35	186.41	129.00	8.79	4.58	
270	216.67	185.57	128.30	9.88	4.60	
285	215.53	185.65	129.37	11.59	4.61	
300	215.36	185.67	129.17	11.56	4.60	

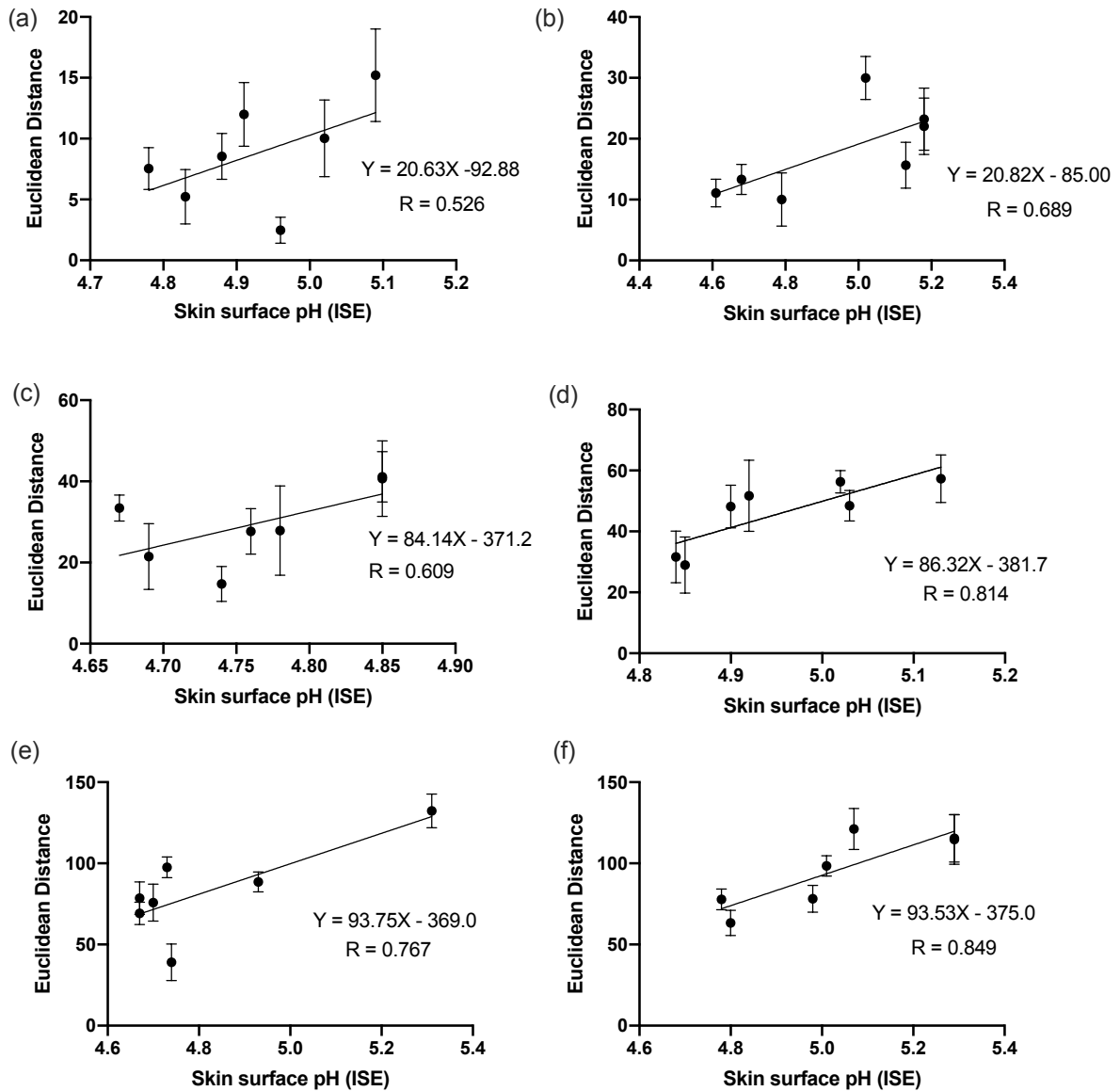


Figure A5.2. Average ED colour response from wearable platform (6 replicate BCG sensor spots) worn continuously on palm for a single female participant for (a) 30 min, (b) 60 min, (c) 90 min, (d) 120 min, (e) 210 min and (f) 270 min as a function of skin surface pH measured using a calibrated ISE.